Brushes and Particles

Promotor

Prof. dr. M.A. Cohen Stuart,
Hoogleraar fysische chemie en kolloïdkunde
Wageningen Universiteit

Copromotoren

Dr. A. de Keizer
Universitair hoofddocent, Laboratorium voor fysische chemie en kolloïdkunde
Wageningen Universiteit

Dr. ir. J. M. Kleijn
Universitair docent, Laboratorium voor fysische chemie en kolloïdkunde
Wageningen Universiteit

Promotiecommissie

Prof. dr. H. Zuilhof	(Wageningen Universiteit)
Prof. dr. A. Halperin	(Université Joseph Fourier, Grenoble, Frankrijk)
Dr. ir. A. A. van Well	(Technische Universiteit Delft)
Dr. A. Mckee	(Unilever R&D, Port Sunlight, Verenigd Koninkrijk)

Dit onderzoek is uitgevoerd binnen de onderzoeksschool VLAG

Brushes and Particles

Wiebe Matthijs de Vos

Proefschrift
ter verkrijging van de graad van doctor
op gezag van de rector magnificus
van Wageningen Universiteit
Prof. dr. M. J. Kropff
in het openbaar te verdedigen
op woensdag 16 september 2009
des namiddags te vier uur in de Aula

ISBN: 978-90-8585-452-4

Ter herinnering aan Evelien, mijn moeder.
Omdat ik precies weet hoe trots ze nu op me geweest zou zijn.

Contents

Chapter 1

Introduction

Motivation

Things get dirty, a common truth that everyone can relate to. It is the case for the clothes that we wear, for the car that we drive, and for the house that we live in. It is thus not surprising that we spend enormous amounts of time, effort and money on cleaning. On average a Dutch adult spends about 4.8 hours per week cleaning [1, 2]. This might seem quite a lot, but actually the time spend on cleaning has significantly decreased over the years. For example, in 1975 this was about 5.6 hours per person per weak [1, 2] and although no exact numbers are known, experts estimate that this number used to be much higher at the start of the 20^{th} century [3-5]. This reduction in time can be attributed mainly to technological advances [3-5]. Laundry machines, dishwashers, and vacuum cleaners have been improved and have become available for every household. In addition, the effectiveness of the soaps and detergents improved significantly. A third technological improvement is the use of materials that can be more easily cleaned. An example of this is the use of non-sticking surfaces in cookware (especially frying pans). Clearly, new technology, and the science that has led to the development of this technology, have great impact on everyday life.

New technologies are naturally not only useful for household applications; they are also very important for the improvement of many industrial processes or for biomedical applications. Filters that are used in water purification or in the treatment of dairy products can get clogged if matter in the filtered solution sticks to the filter surface. The use of non-sticking (antifouling) surfaces can prevent this and allows for much longer use of such filters. For biomedical applications it is of the utmost importance to work as hygienically as possible, and again antifouling surfaces are very useful as they prevent the adhesion of possible disease agents such as bacteria. Contact lenses can become cloudy when proteins accumulate at their surface, this can be prevented with special coatings. Antifouling coatings are even important for surfaces as large as the hulls of sea ships. By preventing the adhesion of proteins and cells these coatings also prevent the sticking of larger organisms like shells and see weeds. Such fouling would otherwise lead to increased drag and thus to a significant increase in the fuel consumption of the ship.

In this thesis we investigate one particular system that is believed to have a strong potential as an antifouling coating. This system consists of polymers that are end-attached to the interface that should be protected against fouling, and is called *polymer brush*.

Polymer brushes and their antifouling properties

A polymer brush can be defined as a dense layer of polymers that are end-attached to an interface and stretch out into the surrounding solution [6-11]. It is the high polymer density that causes the polymers to stretch and that gives the brush its very specific properties and its antifouling qualities. For polymers grafted to an interface there is a number of possible regimes that depend on the density and on the interaction of the polymer with the interface [6]. We schematically show these possible regimes in Figure 1. If only a few polymers are end-grafted to an interface and there is no attraction between the polymer and the surface, the polymer will adapt its preferred conformation and form a polymer coil (Figure 1a, mushroom regime). However, if the density of chains is increased, the polymer coils will come into contact and will start to overlap. To minimize contact between the polymer segments, the polymer chains will stretch away from the surface as shown in Figure 1b. This is the so-called brush regime.

It is also possible that there is an attraction between the polymer and the surface. For a low density of chains (and at high enough attraction) this may cause the polymer to adsorb on the surface (Figure 1c); this situation is called the pancake-regime. For higher densities (Figure 1d) the surface will be saturated with adsorbed polymer, and polymer coils as depicted in Figure 1a will appear. Further increase in the brush density will lead to overlap of the polymer coils and force the polymers to stretch away from the interface (Figure 1e). This is again the brush regime although in this case some polymer will still be adsorbed on the interface [12].

Thus, polymers in a brush stretch away from a surface due to the high polymer density or so-called high excluded volume. This high excluded volume is exactly the property of the brush that makes the brush suitable as an antifouling layer. If a fouling agent (for example a protein) penetrates into a polymer brush, this will lead to an increase in the local polymer density and thus to an increase in local osmotic pressure. This osmotic pressure will force the particle out of the brush and restore the brush equilibrium. We schematically show this effect in Figure 2a. The polymer brush thus forms a barrier between a solution containing fouling agents and the surface to which the fouling agents could adsorb.

These antifouling properties have been mostly investigated using polymer brushes made of the polymer poly(ethylene oxide) (PEO). This polymer is well soluble in water, is known to be non-toxic [13], very flexible [14], and compatible with living cells [15]. Indeed in many experiments brushes made of this material have been found to prevent or strongly reduce the adsorption of proteins to surfaces [16-18].

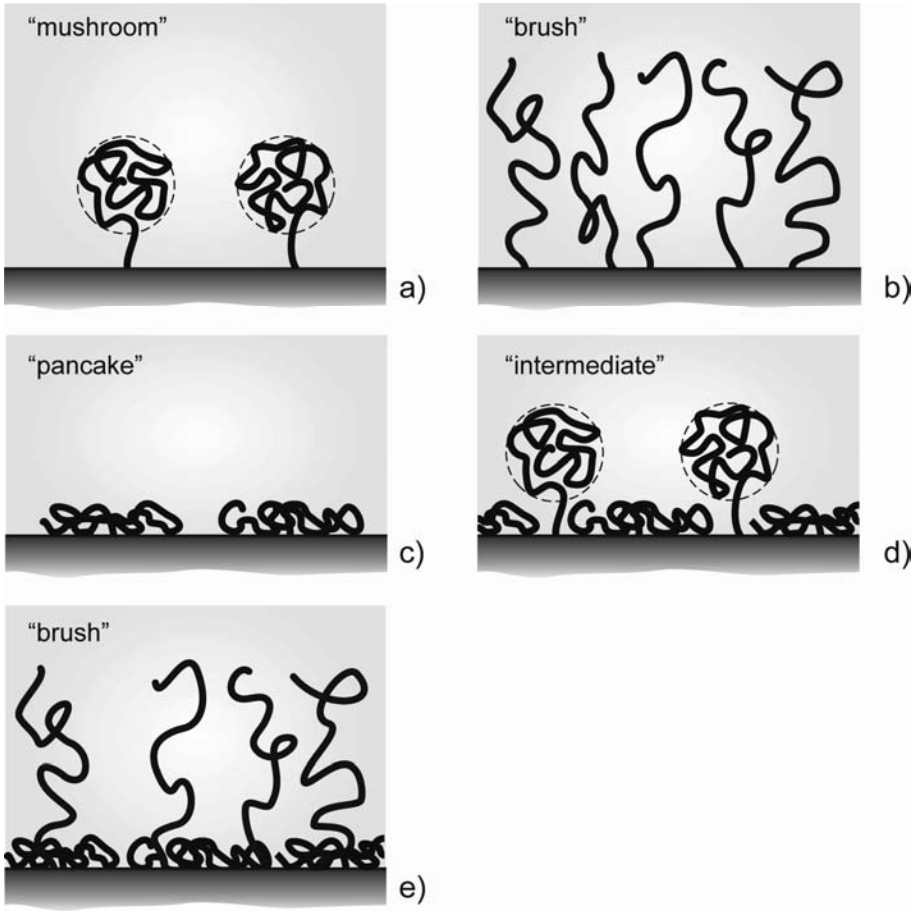

Figure 1. The different regimes for polymer chains end-grafted to an interface. The black lines represent polymer chains end-attached to the interface. The different regimes are discussed in the text.

Other applications for polymer brushes

Polymer brushes are not exclusively used for their antifouling properties. Clearly, the grafting of chains to a surface gives enormous possibilities of controlling the properties of that surface. In this section we discuss the major applications of polymer brushes apart from antifouling: particle stabilization, friction reduction, and protein transportation/stabilization.

We have seen that a polymer brush can form a barrier for adsorbing particles. Closely related is the use of a brush to stabilize a dispersion of colloidal particles [19-21]. Covering colloidal particles with a sufficiently dense layer of grafted polymer chains can prevent the aggregation of these particles. This is schematically shown in Figure 2b. When the brush-

coated particles come into contact, the brushes will partly overlap, leading to an osmotic pressure which forces the particles away from each other. This is, for example, useful when one needs to stabilize hydrophobic pigment particles in a water-based paint.

The frictional forces between two surfaces covered with polymer brushes can be very different from those between two bare surfaces (Figure 2c). It has been found that brushes in a good solvent can significantly (by orders of magnitude) reduce the frictional force relative to bare surfaces [22-23]. Even under moderate compression of the brush layers, there is almost no interpenetration of the brushes, leaving a low viscosity interfacial fluid layer were most of the shear occurs [23]. Brushes can thus successfully be used as lubricants, for example in artificial joints.

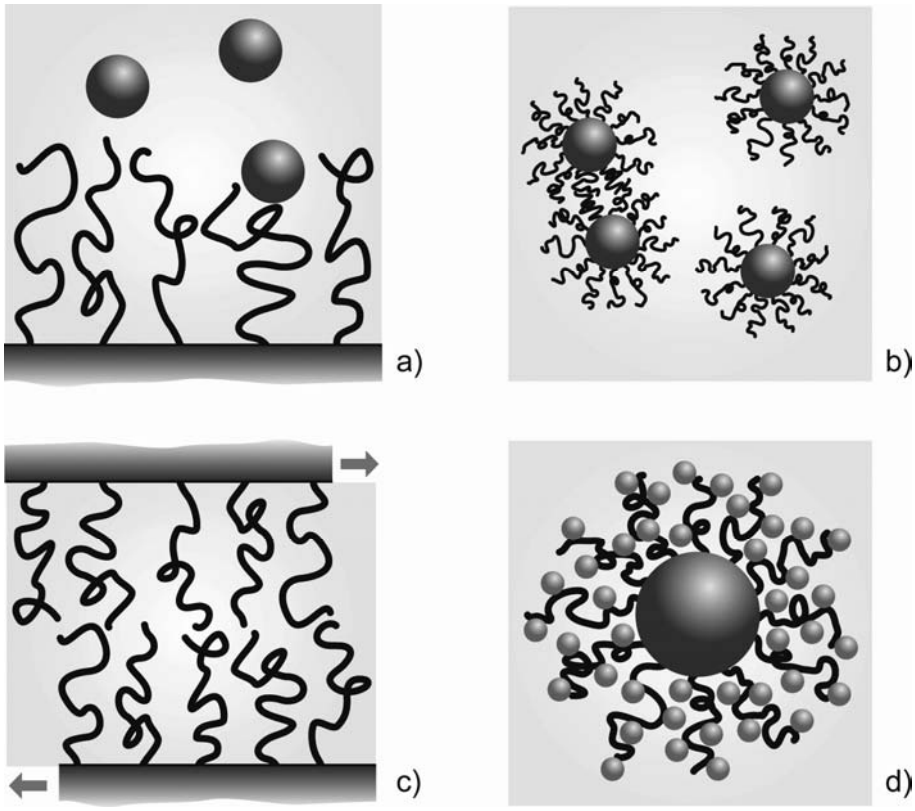

Figure 2. Applications for polymer brushes: a) antifouling, b) particle stabilization, c) friction reduction, d) protein carriers.

Polymer brushes are not only investigated as a means to prevent adsorption, but also for their capability to accommodate (immobilize) proteins or enzymes [24-26]. If there is sufficient attraction between a protein and a polymer brush to overcome excluded volume effects, much larger amounts of protein can accumulate inside a brush layer than can be adsorbed onto a flat solid surface. Here, attachment of polymer chains is used to strongly increase the available surface area. In addition, protein molecules immobilized by polymers are found to be relatively weakly bound and therefore they keep their conformation and (enzymatic) activity largely intact [27-28], whereas proteins adsorbing on a smooth, hard surface often change their conformation to adjust to the flat surface, resulting in a loss of enzymatic activity [29]. Protein uptake is best achieved with polyelectrolyte brushes as strong (electrostatic) interaction is necessary to overcome the excluded volume effects of the brush. In Figure 2d we schematically show a spherical polymer brush filled with adsorbed particles. By using colloidal particles covered by polymer brushes, the surface area is much larger than when using a macroscopic flat surface covered by a polymer brush.

The production of brushes

Over the years, quite a number of different methods have been developed to produce polymer brushes, each method having its own advantages and disadvantages [6,7,9]. In this section, we will shortly review these techniques, which are schematically depicted in Figure 3.

The most simple and earliest approach for the formation of polymer brushes is direct adsorption from solution (physisorption) [30-32] as shown in Figure 3a. For this, one uses a diblock copolymer, of which one block should adsorb to the grafting interface (anchor block) and the other block is preferably non-interacting with the grafting interface. This method has the big advantage that a polymer brush is formed spontaneously if one has the right combination of diblock copolymer, surface, and solvent, and thus can quickly and easily be used on surfaces of any size. However, the disadvantages of this technique are also significant. One is that a solvent is needed in which both blocks of the diblock copolymer are soluble, or else one will get micelle formation often leading to an inhomogeneous adsorption. The most serious disadvantage, however, is that this technique tends to form polymer brushes with low and ill-controlled grafting densities. During the adsorption process, the initial dilute polymer brush is formed and acts as a barrier, not only for fouling agents (such as proteins), but also for the adsorption of more diblock copolymer needed to form a denser polymer brush.

Another way to make polymer brushes is by covalently attaching chains to a surface (Figure 3b). In the ‘grafting to’ approach one uses polymers with a reactive chain end

which are connected to the surface using a suitable reaction [33-35]. High grafting densities can be achieved, especially when this reaction can be done without solvent (in melt) [35]. This approach is easier and more suitable for large surfaces than the "grafting from" approach that is described below. Disadvantages are that the grafting density is hard to control and that a reactive surface is needed.

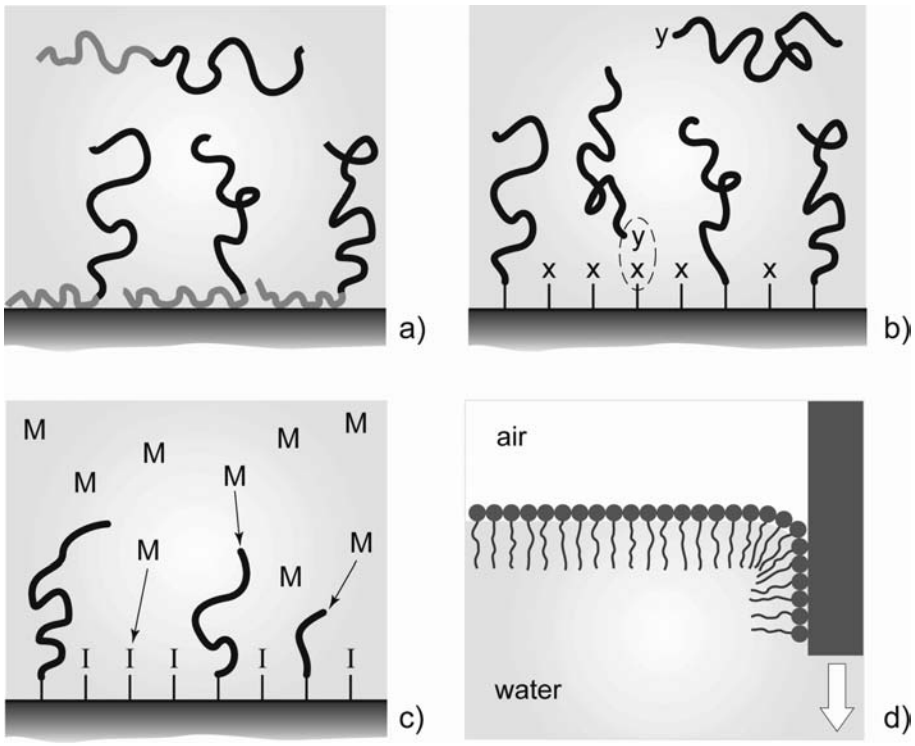

Figure 3. The main methods to produce polymer brushes: a) adsorption from solution, b) grafting to, c) grafting from, d) Langmuir-Blodgett transfer.

Instead of using pre-made polymers another approach is to polymerize (grow) the polymer chains from the grafting interface. This is called the "grafting from" approach [36-38] and is schematically shown in Figure 3c. For this, one first prepares a surface with (usually covalently) attached monomers from which polymerization is initiated with a suitable polymerization reaction. With this approach high degrees of polymerization and grafting densities [36] can be achieved. Polydispersity depends on the type of polymerization reaction. This approach also has the disadvantage that the grafting density is hard to control, and that it is even harder to determine brush properties such as polydispersity and chain length.

In Figure 3d we schematically show the so-called Langmuir-Blodgett approach [39-41]. For this technique, just as in the adsorption approach, we use a diblock copolymer consisting of one adsorbing (anchor) block and one block that is well soluble. However, the brush is first made at the air-water interface in a Langmuir trough, by carefully applying a known amount of diblock copolymer to the interface. After applying the diblock copolymer, the surface area of the trough can be changed to obtain the desired grafting density of the brush. The brush at the air-water interface can then be transferred to a solid surface by simply moving a hydrophobic surface very slowly through the air-water interface (see Figure 3d). The technique has the huge advantage of allowing complete control of both the grafting density and the chain length, and one can reach reasonably high grafting densities. The main disadvantage is that the technique can only be used with very specific surfaces (extremely flat, hydrophobic, relatively small).

Brushes and theory

Much work has been done to theoretically model the polymer brush [6, 11, 42, 43]. Over the years, this has contributed much to the understanding of the polymer brush. One of the first and certainly the most famous results of theoretical investigations comes from de Gennes [44]. From a scaling model, based on the earlier work of Alexander [45], he derived a simple scaling law for the brush thickness, H, depending on the polymer chain length N, and the grafting density σ:

$$H \sim N\sigma^{1/3} \qquad [1]$$

The main assumption in this scaling model, also called a box model, is that all polymers are equally stretched and thus that all chain ends are positioned at exactly the same distance H from the grafting interface. This also implies that the polymer density is constant throughout the brush. The assumption of equal stretching is a serious oversimplification and models were introduced in which it is possible for the chain ends to distribute throughout the brush. These so-called analytical self-consistent field (aSCF) models were pioneered by Semenov [46] by introducing the so-called strong stretching assumption. In this model one only takes into account the most probable polymer conformation for a given chain end position in the brush. As this approach excludes backfolding of the polymer chains, it is only valid for a brush in which the polymers are strongly stretched (in which the height of the brush is many times the Gaussian dimension of the chains). Semenov applied this theory to densely grafted chains without solvent; later the theory was generalized and applied to brushes in solvent [47,48].

Another method to model polymer brushes is the numerical self-consistent field (nSCF) approach [49-51]. In contrast to the aSCF approach, all possible chain conformations are taken into account and are weighed by their (Boltzmann) probability factor. In Figure 4 we compare brush density profiles (i.e. the polymer density in a brush as a function of distance z from the grafting interface), obtained from the three above mentioned theoretical approaches. As stated above, the polymer density in the box model is equal throughout the whole brush up to a labeled value of z (H) at which the density drops to zero. For both SCF approaches, on the other hand, the polymer density decreases gradually with increasing distance. The resulting density profile of the aSCF and the nSCF models are very similar, except in the tail region of the brush and close to the grafting interface. This is the result of two phenomena that are taken into account in nSCF and not in aSCF: i. close to the wall the nSCF model predicts a depletion zone for the polymer caused by a lower entropy of a polymer chain close to a hard wall; ii. the difference in the tail region is caused by the nSCF model taking into account fluctuations in the brush while the aSCF model only includes the most probable distributions.

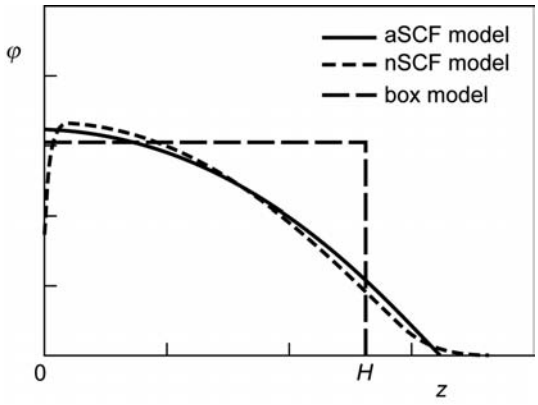

Figure 4. The polymer density (φ) as a function of distance from the grafting interface (z) for three different theoretical approaches as indicated.

Comparing the results of each of the above theories with those of, for instance, Monte Carlo simulations or molecular dynamics simulations, the best agreement is usually found with the results of the nSCF model [52-53]. Still, it is important to note that in the SCF models as well as in the simulations, the Alexander-de Gennes scaling law for the brush height (Eq. 1) was recovered [6]. Agreement with this scaling law was reported has been often reported by experimental investigations [54-55].

Outline of this thesis

This thesis comprises a broad investigation on the topic of polymer brushes and can be divided in four parts. In the first part (*Chapters 2 and 3*) we investigate the production of polymer brushes. In *Chapter 2* we revisit the Langmuir-Blodgett technique (Figure 4b) to produce PEO brushes. Although this method has been used before in a number of studies to prepare PEO brushes, the technique itself was never thoroughly investigated. It turns out that the efficiency at which the polymer is transferred from the liquid to the solid surface is a strong function of chain length and the polymers chemical nature. In *Chapter 3* we present a new method to produce very dense neutral polymer brushes through adsorption. By adsorbing a diblock copolymer (with a neutral block and a polyelectrolyte block) to an oppositely charged polyelectrolyte brush, a neutral polymer brush is formed on top of an almost neutral layer of complexed polyelectrolytes. Advantages of this method are that the brush formation is completely reversible, that very high grafting densities can be reached, and that the grafting density can be controlled. We also test the antifouling properties of this brush.

In the second part (*Chapters 4 to 7*) we investigate the interaction of polymer brushes with particles, using a combination of experiments and theory. In *Chapter 4* we present a simple model for the investigation of the adsorption of particles to a polymer brush. The goal of the chapter is to illustrate earlier theoretical work on polymer brushes and particles and to show some of the typical properties of a polymer brush that have been found over the years. In *Chapter 5* we consider the adsorption of surfactant (micelles) to a neutral polymer brush, and we investigate if we can use this surfactant adsorption to tune the antifouling properties of the PEO brush against silica particles. In *Chapters 6 and 7* we focus on the adsorption of protein to a poly(acrylic acid brush) as a function of pH and ionic strength. The focus is on the driving forces for this process, to explain the remarkable observation that for proteins it is possible to adsorb to a like-charged polyelectrolyte brush.

The third part (*Chapters 8 and 9*) focuses on a previously neglected property of the polymer brush: its polydispersity. In (almost) all theoretical papers on polymer brushes, the brush is assumed to be monodisperse, whereas in experiments polydispersity is unavoidable. In *Chapter 8* we focus on the effect of polydispersity on the structure of the brush and in *Chapter 9* we study the effect of polydispersity on the interaction with particles.

In part four, *Chapter 10*, we present a novel, simple idea to create a surface that is easy to clean. By applying a thin layer to a surface that can be removed by a given trigger (change in pH, salt concentration, or surfactants) it becomes possible to get rid of any adsorbed material by removal of the layer. We call such a layer a sacrificial layer. We

explore the idea experimentally and consider possibilities and limitations. For two different systems we show “proof of principle” that the sacrificial layer approach can indeed be used to remove adsorbed particles.

References

1. Breedveld K.; van den Broek, A.; de Haan, J.; Harms, L.; Huysmans, F.; van Ingen, E. *De tijd als spiegel*, **2006**, Sociaal en Cultureel Planbureau Nederland, Den Haag.
2. www.tijdsbesteding.nl
3. Groffen, M.; Hoitsma, S. *Het geluk van de huisvrouw* **2004**, Boom, Amsterdam.
4. Cowan, R. S. *Technology and Culture* **1976**, *17*, 1.
5. Tijdens, K. G. *Mens en Maatschappij* **1995**, *70*, 203.
6. Currie, E.P.K.; Norde, W.; Cohen Stuart, M.A. *Adv. Colloid Interface Sci.* **2003,** *100-102,* 205.
7. Zhao, B.; Brittain, W.J. *Prog. Polym. Sci.* **2000,** *25,* 677.
8. Milner, S.T. *Science* **1991,** *251,* 905.
9. Advincula, R.C.; Brittain, W.J.; Caster, K.C.; Rühe, J. *Polymer Brushes,* **2004,** Wiley-VHC, Weinheim.
10. Halperin, A. *Langmuir* **1999,** *15,* 2525.
11. Szleifer, I.; Carignano, M.A. *Advances in chemical physics, volume XCIV* **1996,** 165.
12. Chakrabarti, A. *J. Chem. Phys.* **1994,** *100,* 631.
13. Herold, D.A.; Keil, K.; Bruns, D.E. *Biochem. Pharmacol.* **1989,** *38,* 73.
14. Pattanayek, S.K.; Juvekar, V.A. *Macromolecules* **2002,** *35,* 9574.
15. Albertsson, P.-Å. *Partition of cell particles and macromolecules,* **1986,** Wiley, New York.
16. Halperin, A.; Leckband, D.E. *C. R. Acad. Sci. Paris* **2000,** *serie IV,* 1171.
17. Jönsson, M.; Johansson, H.-O. *Colloids and Surfaces B* **2004,** *37,* 71.
18. Mcpherson, T.; Kidane, A.; Szleifer, I.; Park, K. *Langmuir* **1998,** *14,* 176.
19. Napper, D.H. *Polymeric stabilisation of colloidal particles,* **1983,** Academic Press, London.
20. Ottewill, R. *J. Colloid Interface Sci.* **1977,** *58,* 357.
21. Pathmamanoharan, C. *J. Colloid Interface Sci.* **1998,** *205,* 340.
22. Klein, J.; Kumacheva, E.; Mahalu, D.; Perahla, D.; Fetters, L.J. *Nature* **1994,** *370,* 634.
23. Klein, J. *Annu. Rev. Mater. Sci.* **1996,** *26,* 581.
24. Wittemann, A.; Haupt, B.; Ballauff, M. *Phys. Chem. Chem. Phys.* **2003,** *5,* 1671.
25. Wittemann, A.; Ballauff, M. *Phys. Chem. Chem. Phys.* **2006,** *8,* 5269.
26. Wittemann, A.; Ballauff, M. *Analytical Chemistry* **2004,** *76,* 2813.
27. Xia, J.; Mattison, K.; Romano, V.; Dubin, P.L.; Muhoberac, B.B. *Biopolymers* **1997,** *41,* 359.
28. Caruso, F.; Schüler, C. *Langmuir* **2000,** *16,* 9595.
29. Norde, W.; Giacomelli, C.E. *Macromol. Symp.* **1999,** *145,* 125.
30. Marra, J.; Hair, M.L. *Colloids and Surfaces* **1988,** *34,* 215.
31. Watanabe, H.; Tirell, M. *Macromolecules* **1993,** *26,* 6455.
32. Maas, J.H.; Cohen Stuart, M.A.; Fleer, G.J. *Thin Solid Films* **2000,** *358,* 234.
33. Auroy, P.; Auvray, L.; Leger, L. *Macromolecules* **1991,** *24,* 2523.
34. Tran, Y.; Auroy, P.; Lee, L.-T. *Macromolecules* **1999,** *32,* 8952.
35. Maas, J.H.; Cohen Stuart, M.A.; Sieval, A.B.; Zuilhof, H.; Sudhölter, E.J.R. *Thin Solid Films* **2003,** *426,* 135.
36. Tsujii, Y.; Ohno, K.; Yamamoto, S.; Goto, A.; Fukuda, T. *Adv. Polym. Sci.* **2006,** *197,* 1.
37. Rühe, J.; Ballauff, M.; Biesalski, M.; Dziezok, P.; Gröhn, F.; Johannsmann, D.; Houbenov, N.; Hugenberg, N.; Konradi, R.; Minko, S.; Motornov, M.; Netz, R.R.; Schmidt, M.; Seidel, C.; Stamm, M.; Stephan, T.; Usov, D.; Zhang, H. *Adv. Polym. Sci.* **2004,** *165,* 79.
38. Edmondson, S.; Osborne, V.L.; Huck, W.T.S. *Chem. Soc. Rev.* **2004,** *33,* 14.
39. Currie, E.P.K.; van der Gucht, J; Borisov, O.V.; Cohen Stuart, M.A. *Pure Appl. Chem.* **1999,** *71,* 1227.
40. Currie, E.P.K.; Sieval, A.B.; Avena, M.; Zuilhof, H.; Sudhölter, E.J.R.; Cohen Stuart, M.A. *Langmuir* **1999,** *15,* 7116.
41. Kuhl, T.L.; Leckband, D.E.;Lasic, D.D.; Israelachvili, J.N. *Biophysical J.***1994,** *66,* 1479.
42. Birschtein, T.M.; Amoskov, V.M. *Polymer Science Ser. C* **2000,** *42,* 172.

43. Halperin, A.; Fragneto, G.; Schollier, A.; Sferrazza, M. *Langmuir* **2007,** *23*, 10603.
44. deGennes, P.G. *Macromolecules* **1980,** *13*, 1069.
45. Alexander, S. *J. Phys. (Paris)* **1977,** *38*, 983.
46. Semenov, A. N. *Sov. Phys. JETP* **1985**, *61*, 733.
47. Milner, S.T.; Witten, T.A.; Cates, M.E. *Macromolecules* **1988,** *21*, 2610.
48. Birschtein, T.M.; Liatskaya, Y.V.; Zhulina, E.B. *Polymer* **1990,** *31*, 2185.
49. Scheutjens, J.M.H.M.; Fleer, G.J.;Cohen Stuart, M.A.;Cosgrove, T.; Vincent, B. *Polymers at Interfaces*, *1993*, Chapman & Hall, London.
50. Cosgrove, T.; Heath, T.; van Lent, B.; Leermakers, F.A.M.; Scheutjens, J.M.H.M. *Macromolecules* **1987,** *20*, 1692.
51. Wijmans, C.M.; Scheutjens, J.M.H.M.; Zhulina, E.B. *Macromolecules* **1992,** *25*, 2657.
52. Lai, P.-Y.; Zhulina, E. B. *J. Phys. II* **1992,** *2*, 547.
53. Murat, M.; Greet, G. S. *Macromolecules* **1989**, *22*, 4054
54. Currie, E.P.K.; Wagenmaker, M.; Cohen Stuart, M.A.; van Well, A.A. *Physica B* **2000,** *283*, 17.
55. Auroy, P.; Auvray, L.; Leger, L. *Macromolecules* **1991,** *24*, 2523.

Part 1: Making Brushes

Chapter 2

The production of PEO polymer brushes via Langmuir-Blodgett and Langmuir-Schaeffer methods: incomplete transfer and its consequences.

Abstract

Using fixed-angle ellipsometry we investigate the degree of mass transfer upon vertically dipping a polystyrene surface through a layer of a polystyrene-poly(ethylene oxide) (PS-PEO) block copolymer at the air-water interface (Langmuir-Blodgett or LB transfer). The transferred mass is proportional to the PS-PEO grafting density at the air-water interface, but the transferred mass is not equal to the mass at the air-water interface. We find that depending on the chain length of the PEO block only a certain fraction of the polymers at the air-water interface is transferred to the solid surface. For the shortest PEO chain length (PS_{36}-PEO_{148}) the mass transfer amounts to 94%, while for longer chain lengths (PS_{36}-PEO_{370} and PS_{38}-PEO_{770}) a transfer of respectively 57% and 19% is obtained. We attribute this reduced mass transfer to a competition for the PS surface between the PEO block and the PS block. Atomic force microscopy shows that after transfer the material is evenly spread over the surface. However, upon a short heating of these transferred layers (95°C, 5 minutes) a dewetting of the PS-PEO layer takes place. These results have a significant impact on the interpretation of the results in a number of papers in which the above described transfer method was used to produce PEO polymer brushes, in a few cases in combination with heating. We shortly review these papers and discuss their main results in the light of this new information. Furthermore, we show that by using Langmuir-Schaeffer (LS, horizontal) dipping, much higher mass transfers can be reached than with the LB method. When the LB or LS methods are carefully applied, it is a very powerful technique to produce PEO brushes as it gives full control over both the grafting density and the chain length.

A manuscript based on this chapter was published as:

de Vos, W.M.; de Keizer, A.; Kleijn, J.M.; Cohen Stuart, M.A. *Langmuir* **2009**, *25*, 4490-4497.

Introduction

Poly(ethylene oxide) brushes have been widely investigated over the last three decades for their antifouling and particle stabilization properties [1,2,3]. The properties of these polymer brushes are strongly influenced by the chain length and the grafting density. Thus, to investigate the properties of such polymer brushes it would be ideal to have a method of preparation that gives complete control over both the grafting density and the chain length of the brush. However, especially control of the grafting density is quite a challenge in the production of polymer brushes.

In several reviews [1,4-8] the techniques to produce polymer brushes are extensively debated; a short summary is given here. For the major brush production techniques, we distinguish three different categories: adsorption, 'grafting to', and 'grafting from'. The adsorption approach is the earliest and most simple approach to produce polymer brushes [9-11]. For this a suitable surface is brought into contact with a solution of diblock copolymers. These diblock copolymers consist of one block capable of adsorption to the substrate (anchor block) and one block that is preferably non-interacting with the substrate. With the right choice of substrate, diblock copolymer and solvent, the adsorption of the anchor blocks leads to the formation of a brush consisting of the non-adsorbing block. The main advantage of this technique is its simplicity, but the disadvantages are large. The main disadvantage is that with this technique one can only produce brushes with low and ill-controlled grafting densities. During the adsorption process, the forming brush acts as barrier for the adsorption of more diblock copolymer thus stopping the brush formation at relatively low grafting densities. There is some control on the grafting density as with different block lengths one can achieve different grafting densities, however then one also changes the chain length of the brush polymer.

In the 'grafting to' approach polymers with a reactive chain end are used [12-14]. These polymers are then covalently connected to the surface by using a suitable reaction between surface groups and the chain end. High grafting densities can be achieved, especially when the reactions can be performed in a melt [14]. Still a relatively simple approach, but it is hard to control the grafting density and a reactive surface is needed.

In the 'grafting from' approach the polymers are grown from the surface. For this a surface is prepared with (usually covalently) attached monomers from which the polymerization is initiated. With this approach high degrees of polymerization and high grafting densities can be achieved [8]. But also with this approach it is hard to control the grafting density. An approach that has been used to control the grafting density is a method in which the monomers were attached to the surface via Langmuir Blodgett dipping [15].

With this approach one has full control over the density of initiators on the surface although one can never be sure that all of those initiators also result in a polymer chain.

An approach that does not neatly fit into any of the above categories also makes use of Langmuir Blodgett transfer to produce polymer brushes. In this approach a polymer brush is first prepared at the air-water interface and then transferred to a solid substrate. This approach has the big advantage that both the grafting density and chain length are completely controlled [1]. The technique was first used by Kuhl *et al* [16] who used a PEO chain connected to a lipid. A monolayer of a mixture of PEO-lipids and unconnected lipids is spread on the air-water interface to form a mixed lipid and PEO-lipid monolayer with PEO tails sticking into the water phase. At maximum compression a solid surface covered with a lipid monolayer is transferred through the monolayer at the air-water interface to form a lipid-bilayer with a connected PEO brush. The grafting density is determined by the ratio between PEO-lipids and unconnected lipids at the air-water interface. Until now only relative short PEO chain lengths (N) have been investigated using this method (N = 18, 45, 114) [17,18].

A different approach to produce polymer brushes via LB transfer was applied by Currie *et al* [19] who for the production of PEO brushes used a diblock copolymer consisting of a polystyrene (PS) block connected to a PEO block. A monolayer of this diblock copolymer is spread on the water surface to form a PEO brush at the air-water interface. The grafting density of this brush is completely controlled by changing the size of the interface. By then dipping a polystyrene surface through the air-water interface, the PEO brush is transferred to the polystyrene surface, strongly attached by the hydrophobic interaction between the PS surface and the PS block. In his investigation, Currie *et al* used relatively long PEO chains (N=148, 445, 700). Over the years this technique has been used to produce PEO brushes in seven different studies [19-25]. In all of these investigations, it was assumed that the transfer ratio upon LB dipping equals unity, thus the grafting density on the solid substrate is the same as the grafting density at the air-water interface. The validity of this assumption was however never thoroughly investigated.

In this chapter we carefully re-examine the LB transfer method to produce PEO brushes as proposed by Currie *et al*. Using ellipsometry we investigate the degree of mass transfer upon LB transfer of a monolayer of PS-PEO at the air-water interface to a polystyrene surface. Using atomic force microscopy (AFM) we investigate if the polymers are evenly spread over the surface. We discuss the previous work for which this technique was used taken into account the results of this study.

Materials and methods

Preparation of PEO brush layers

PEO brush layers of varying grafting density were prepared by means of a Langmuir-Blodgett (LB) method first described by Currie *et al* [19] with some modifications. As substrates, flat silicon wafers were used, coated with polystyrene.

Because polystyrene films spin-coated on clean silicon wafers are not stable, the coating of substrates with polystyrene (PS) was done in the following way. First, the silicon wafer (which has a natural SiO_2 layer with a 2-3 nm thickness) was cut into strips (4 cm x 1 cm), rinsed with alcohol and water, and further cleaned using a plasma-cleaner (10 minutes). The strips were covered with a solution of 11 g/l vinyl terminated PS_{200} (M_n=19000 g/mol, M_w/M_n=1.03, Polymer Source Inc. Montreal/Canada) in chloroform and, after evaporation of the solvent, were heated for 72 hours at 150 ºC under vacuum. In this way the vinyl-PS is covalently bound to the Si/SiO_2 surface [14]. Excess Vinyl-PS was washed off with chloroform. The PS surface films prepared in this way are stable in aqueous solutions and have a thickness of about 8 nm.

For the brush layer transfer, monolayers of PS-PEO block copolymers (PS_{36}-PEO_{148} M_w/M_n=1.05, $PS_{36}PEO_{370}$ M_w/M_n=1.03, $PS_{38}PEO_{770}$ M_w/M_n=1.05, Polymer Source Inc.) at the air-water interface, were prepared by dissolving the copolymers in chloroform and spreading these solutions very carefully on water in a Langmuir trough using a micro syringe. (For these systems, the surface pressure as a function of surface area per molecule was measured by Bijsterbosch *et al* [26].) Subsequently, the films were compressed to the appropriate surface density and transferred to the substrates in a single passage, Langmuir-Blodgett transfer, or in some cases the substrate was horizontally dipped through the interface (a variant of Langmuir-Schaeffer). To obtain a single passage transfer through the air-water interface a silica strip was slowly lowered through the monolayer and then pulled under the barrier and taken out of the water on the side of the Langmuir trough without a monolayer. The surfaces so prepared were carefully stored in clean water until use. For the ellipsometry and AFM measurements, the surfaces were dried at room temperature under a stream of nitrogen. All solvents used were of PA grade (Sigma-Aldrich). Water used was demineralized using a Barnstead Easypure UV and had a typical resistance of 18.3 $M\Omega cm^{-1}$.

Ellipsometry and atomic force microscopy

Thicknesses of (dry) layers on the silicon wafers were measured using an ellipsometer (SE 400, Sentech instruments GmbH, Germany) assuming the following refractive indices: $\tilde{n}_{silicon}$ = [3.85, 0.02], n_{silica} = 1.46, $n_{polystyrene}$ = 1.59, n_{H2O} = 1.33, n_{PEO} = 1.46. For the measurement of the PS-PEO layer a three layer model was used with on top of the silicon a silica layer of 2.5 nm thickness, a polystyrene layer of 8 nm thickness and a PS-PEO layer of unknown thickness. The thicknesses of the silica and polystyrene layer were determined beforehand with a one and a two layer model. The refractive indices of transferred layers were also measured and always found to be between 1.46 and 1.50 (thus showing that upon drying of a layer no large amounts of air or water are trapped in the layer). To further show that no large amounts of water were trapped in the PEO layer, we performed an additional experiment. The layer thickness of a single surface ($PS_{38}PEO_{770}$, σ_{AW} = 0.3 nm^{-2}) was measured before and immediately after it was heated in a vacuum oven at 50°C for approximately 60 minutes. The measured average layer thicknesses were almost identical.

For every data point (Figures 1,2 and 6), at least two separately prepared surfaces were investigated. For a single surface the thickness was measured at least three times at different positions. The average value of the minimum of six measurements is used, while the error bars give the standard deviation. The error bars thus represent a measure for the spread of the data points.

To check the validity of the chosen refractive indices (see above) for the determination of the layer thickness by ellipsometry, we checked, for some surfaces (only PS, and PS plus the transferred layers of PS_{36}-PEO_{148}, $PS_{36}PEO_{370}$ and $PS_{38}PEO_{770}$ at σ_{AW} = 0.3 nm^{-2}), the measured thicknesses by atomic force microscopy (Nanoscope III, Veeco instruments Inc, Plainview NY, USA). To measure polymer layer thicknesses with AFM, the surface was scratched by hand using a sharp needle. As the silicon and silica layers are much harder compared to the polymer layer, only the polymer is scratched away and the thickness of the layer can be measured by making a height image of the scratch and the surrounding area. The measured height corresponded in all cases with the height that was measured by ellipsometry within a 10% margin of error. All height images were made using the contact mode. In all cases we used Veeco V-shaped cantilevers with silicon nitride tips. In contact mode it is important to make sure that the scanning does not damage the surface. This was checked on a number of surfaces by repeatedly scanning a 1μm^2 area and then scanning a larger area, including the repeatedly scanned area. As no difference in height or in roughness was found between the previously scanned surface and the “fresh” surface, we conclude that the surface was not damaged during imaging.

Results and discussion

The preparation of PEO polymer brushes via Langmuir Blodgett transfer has many advantages compared to other brush preparation techniques. This relatively simple method allows control over the grafting density, chain length, and polydispersity. However, in none of the seven studies in which this method has been used [19-25], was it ever checked by independent techniques if the complete monolayer at the air-water interface was transferred using this method. In Figure 1 we show the results of ellipsometry experiments on the dry layer thickness after transfer as a function of the PS-PEO grafting density at the air-water interface. The dry layer thickness is a measure for the mass in the polymer brush.

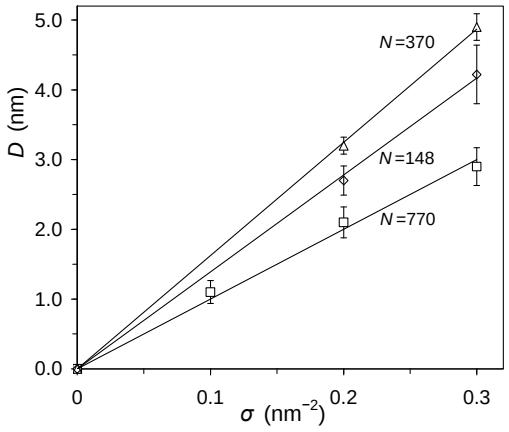

Figure 1. Layer thickness (D) as determined by ellipsometry of a PS_{36}-PEO_N layer on a polystyrene surface after LB transfer as a function of the grafting density (σ) at the air-water interface for different PEO chain lengths (N) as indicated. Points represent the average experimental values, error bars give the standard deviation, and lines give the best linear fits.

As can be clearly seen in Figure 1, for all different PEO block lengths, the data can well be described by a linear fit through the origin. Thus, when the grafting density at the air-water interface becomes twice as high, the thickness of the layer also becomes twice as thick. However, a very surprising finding is that the transfer of the longest PEO block length (N = 770) does not result in the thickest layer, in contrast it results in the lowest dry layer thickness. This is surprising as the thickness of the dry layer is a measure for the mass transferred from the air-water interface to the solid substrate. The mass in a polymer brush scales with σN and thus for a given grafting density, the mass should be much higher for a long chain than for a short chain. The only possible explanation for this finding is that the

degree of transfer from the air-water interface to the solid substrate is different for these diblock copolymers with different PEO block length. We can check this by calculating the expected layer thickness upon complete transfer of the layer. This is easily done by using Eq. 1:

$$D = \frac{\sigma M_W \times 10^{24}}{\rho N_{AV}} \qquad [1]$$

Here D is the thickness in nm, σ is the grafting density in nm^{-2}, M_W is the mass of the polymer in Dalton, ρ is the average density in kg/m^3, and N_{AV} is Avogadro's number. The average density ρ of the PS-PEO layer was calculated by taking the weight average of the density of PEO and of PS for a given PS-PEO diblock copolymer. Applying this to the case of PS_{38}-PEO_{770} for a σ of 0.3, a ρ_{PS} of 1040 kg/m^3 [27], and *a* ρ_{PEO} of 1130 kg/m^3 [28] we find a thickness of 16.2 nm. The experimentally measured thickness for this system is 2.9 nm; thus the transferred mass is only a small fraction of the mass per surface area at the air-water interface. To investigate this further, we have recalculated all the measured thicknesses to grafting densities. In Figure 2 we show a comparison between the grafting density at the air-water interface and the resulting grafting density after transfer to the solid substrate.

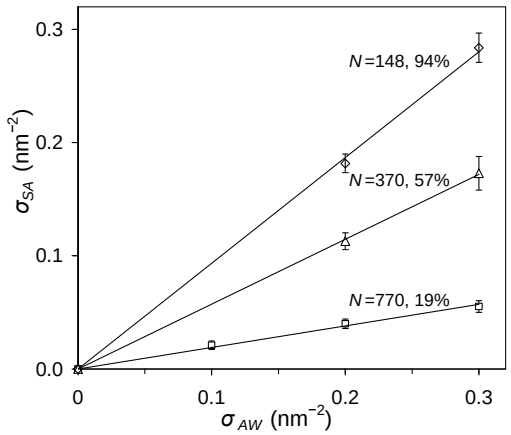

Figure 2. Brush grafting density on the solid substrate (σ_{SA}) after LB transfer as a function of the grafting density at the air-water interface (σ_{AW}) for different PEO chain lengths (N) as indicated. Points represent the average experimental values, error bars represent the standard deviation, lines represent best linear fits, and percentages represent the transfer ratio σ_{SA}/σ_{AW}.

From Figure 2, we can clearly observe that a longer PEO chain leads to a lower transfer ratio. Of the short PEO chain (N = 148) almost 100% of the mass at the air-water interface is transferred to the solid substrate while of the longest polymer chain (N = 770), only 19% of the mass at the air-water interface is transferred to the solid substrate. Still, even though only part of the mass at the air-water interface is transferred, the transferred amount is proportional to the increasing grafting density.

These results have a significant impact on the results of a number of papers [19-25] in which LB transfer was used with similar diblock copolymers to produce PEO brushes. In these papers full-transfer was always assumed. Full transfer was however not assumed without any experimental proof. In a number of papers [19, 22, 23, 24] the authors report to have measured a transfer ratio of 1 using surface pressure measurements. The transfer ratio is determined by dividing the change in surface area due to a decrease in mass as a result of the transfer by the surface area of the dipped substrate. For this it was assumed that the PS-PEO was only transferred to the PS surface and not to the other side of the slide, a rough silica surface. We repeated this experiment for $PS_{38}PEO_{770}$ and indeed found a transfer ratio of approximately 1, when assuming only adsorption to the polystyrene side of the slide. However, to check if no adsorption takes place at the rough silica side, two slides were simply glued together creating a slide with a polystyrene surface on both sides; upon LB dipping we then found a transfer ratio of approximately 0.2, thus in complete agreement with the 19% transfer for this polymer measured by ellipsometry (Figure 2). Two slides glued with the polystyrene sides together to give a new slide with rough silica on both sides was also dipped and a transfer ratio of approximately 0.8 was found. Thus, the transfer ratio of unity that was reported by the authors stems from a combination of about a 20% transfer on the polystyrene side of the slide and 80% transfer to the rough silica surface.

To explain the reduced transfer of PS-PEO, especially for the longer PEO chains, it is important to realize that although the polystyrene block in an aqueous environment will strongly attach to a polystyrene surface, PEO is also well-known to adsorb to polystyrene surfaces [29]. This is especially important for the PS-PEO polymers that we use, as the length of the PEO chain is much higher than the polystyrene chain length. Chain length is known to play an important role in competitive adsorption. However, in the case that PS and PEO would compete for adsorption, one would expect gradual desorption of polymer from the interface, especially at high grafting densities. A more likely idea is that although a PEO block is unable to displace a PS block, an adsorbed PEO block might be able to prevent the adsorption of a PS block, especially in the short time span that the LB transfer takes place. In other words, we believe that the PS and PEO blocks adsorb simultaneously to the polystyrene substrate. The PEO blocks, then act as a kinetic barrier for the adsorption

of the PS block. The chance that a PS block adsorbs to the surface depends on chain lengths of both the PS and the PEO block, the longer the PEO compared to the PS chain, the less change the PS block has of strongly attaching to the PS interface. This idea is supported by the research of Pagac *et al* [29], who compared the adsorption to a polystyrene interface of a PEO homopolymer (PEO_{9545}) from aqueous solution, to the adsorption of PS-PEO diblock copolymers ($PS_{73}PEO_{1368}$, $PS_{287}PEO_{7841}$, $PS_{458}PEO_{9798}$). They find that it is impossible in this way to create a PEO polymer brush, and find no difference in adsorbed amount between the adsorption of the homopolymer and the diblock copolymers. They state that apparently the surface affinity of the PEO presents a large kinetic barrier for the PS block, thus preventing displacement of the water soluble PEO block by the insoluble PS block. This is off course hard to compare to the effects we find during LB transfer but it does show that if during transfer PEO would adsorb to the polystyrene surface before the PS block that it can prevent the adsorption of the PS block. As stated above we believe that the chance that PEO connects with the PS substrate during LB transfer before the PS block does depends strongly on the chain lengths of these two blocks. In Figure 2 we have only investigated the effect of the PEO chain length but we have also tested the transfer of a $PS_{120}PEO_{700}$ diblock copolymer. This yielded a transfer ratio of about 40%. This is very high compared to $PS_{38}PEO_{770}$ which has a similar PEO chain length but a much shorter PS block length. This shows that as expected the PS chain length also plays an important role in the transfer process.

It is also interesting to compare the transfer of PS-PEO to the transfer of PS-Poly(acrylic acid) (PAA). The LB transfer method has also been used to produce PAA brush layers [30], and in a recent paper on the adsorption of protein to a PAA brush [31 (Chapter 6)], the authors checked the transfer ratio of $PS_{40}PAA_{270}$ with ellipsometry. For this polymer the transfer ratio was found to be even slightly higher than 1. While PEO is known to strongly adsorb to PS, PAA shows almost no adsorption to PS. This is again an indication that the reduced transfer ratio of PS-PEO is because of the adsorption of the PEO polymer to the polystyrene substrate.

It is important to realize that the adsorption of PEO to the PS surface will probably also have a strong effect on the structure of the transferred PS-PEO layer in aqueous solution. Especially at low grafting densities (before the brush regime), one would expect most of the PEO to be adsorbed to the PS surface (the so-called pancake regime). At higher grafting densities (in the brush regime) one would expect that most of the PEO is stretching away from the surface as part of the brush, but that part of the PEO is still adsorbed to the PS surface. In the work of Chakrabarti [32], the author showed using Monte Carlo simulations

that in the brush regime, the brush chains can indeed be adsorbed to the surface, effectively reducing the polymer density in the brush.

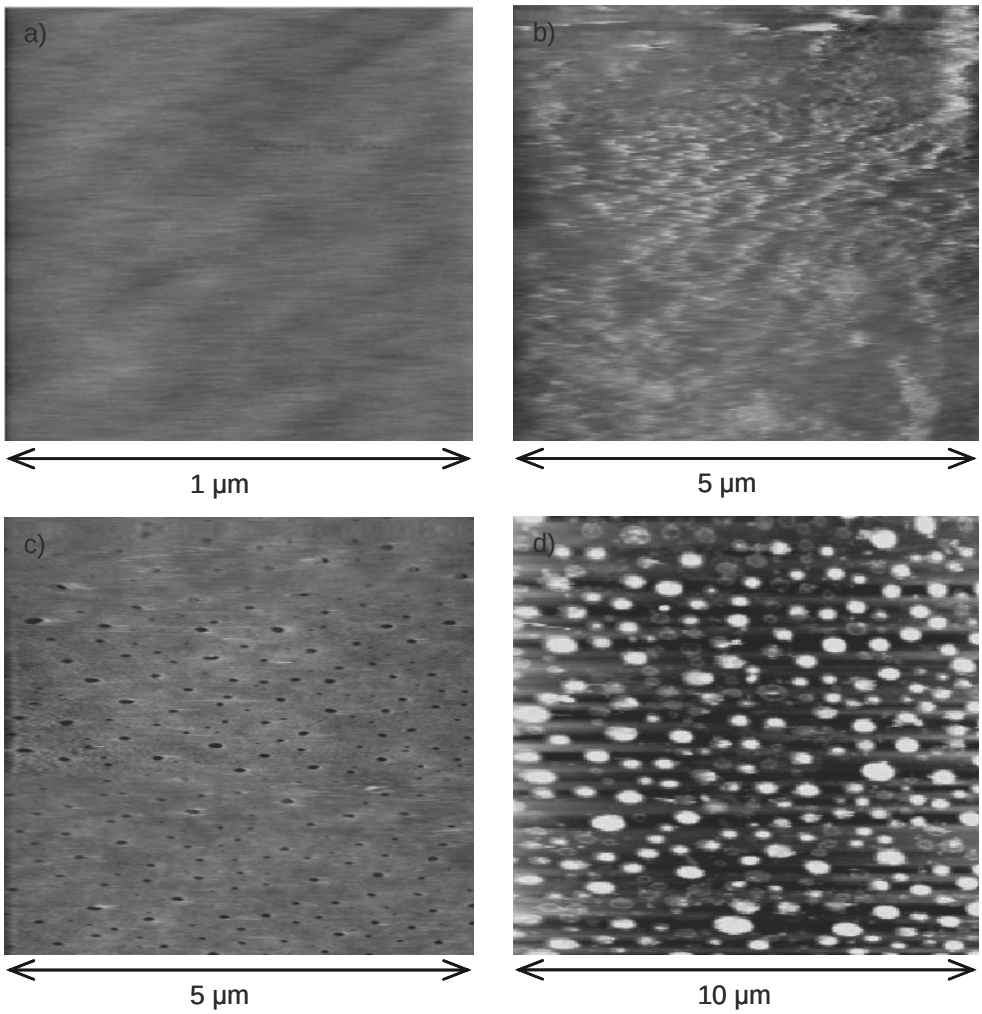

Figure 3. Atomic force microscopy height images (contact mode) of dried layers of PS_{38}-PEO_{770} (σ_{SA} = 0.04 nm^{-2}). a) without further treatment ; b) with on top of it a second layer of PS_{38}-PEO_{770} (σ_{SA} = 0.20 nm^{-2}) due to a second passage through the copolymer monolayer at the air-water interface (see text) ; c) as in a, after heating to 95°C for 5 minutes ; d) as in b, after heating to 95°C for 5 minutes.

In the above investigations the preparation of the polymer brush slightly differs from the way the PEO brushes were prepared in most of the other work in which this technique was used. In this work, after Langmuir Blodgett transfer of the polymer, the surface was taken out of the water on the side of the barrier were no polymer was present. Thus, the produced layer is a monolayer of PS-PEO. In other investigations [19-24] the surface was always taken out on the side of the barrier containing a polymer layer at the air-water interface. It was assumed that this second layer could simply be removed by rinsing with water. We checked this assumption for $PS_{38}PEO_{770}$ (σ_{AW} = 0.2) and found the following: by measuring the change in surface area during the second passage through the monolayer at the air-water interface, we obtained a transfer ratio approximately 1 (using two surfaces glued together as above). The thickness of the resulting layer was about 12 nm, corresponding well to a first layer of $PS_{38}PEO_{770}$ of 2 nm thickness (19% transfer) and a second layer of 10 nm thickness (close to 100% transfer). After thorough rinsing with water, the thickness was again measured and we found a layer thickness of 2 nm. Thus, one can indeed create a PS-PEO double layer by dipping and taking out of the substrate through the air-water interface with the PS-PEO monolayer, and the second layer can indeed be removed by thorough rinsing with water.

In the preparation of the PEO brushes, not only the transferred mass is important. It is also important that the polymers are evenly spread over the surface. This can be checked with atomic force microscopy. By making a topographic image of the surface, we can determine if the surface is flat, indicating an homogeneous transfer of polymer. In Figure 3 we show the results of an AFM investigation of $PS_{38}PEO_{770}$ layers transferred to a polystyrene substrate by the LB method.

In Figure 3a, we show the surface topography of a dry layer of transferred PS_{38}-PEO_{770} (σ_{SA} = 0.02 nm^{-2}). The polymers are evenly spread over the surface, and there is only a small surface roughness of approximately 0.5 nm. This shows that the LB method is indeed suitable to produce polymer brushes. In Figure 3b we show the results for the case that the surface was double dipped (as described above), thus on top of the brush layer, an extra layer of PS-PEO was transferred to the substrate. Also here the polymer is evenly spread over the surface, but on this surface the roughness (3 to 4 nm) is much larger than in Figure 3a. This is not strange as the layer thickness of the polymer layer in Figure 3a is only about 2 nm thick, while the polymer layer in Figure 3b is about 12 nm thick. In a number of papers [22-24], the surface was heated after transfer. The goal of this heating was to allow diffusion of the PS block into the PS substrate by heating the polymers above the glass temperature of PS. Usually the polymers were heated for 5 minutes at 95°C. In Figure 3c and Figure 3d we show the effect of this heating on a layer PS-PEO. From the AFM

pictures, we see clear signs of dewetting. This may be explained as a temperature of 95°C is also above the glass temperature of PEO and heating allows the polymers to move. Thus, heating these surfaces has the opposite effect of what was tried to achieve. In Figure 3d, the degree of dewetting seems to be much larger than in Figure 3c, which is obviously related to the extra amount of polymer available on the surface in Figure 3d (6 times that of Figure 3c).

Thus by heating a layer of PS_{38}-PEO_{770}, one induces dewetting. This must have significant effects on the results of the investigations in which such layers have been heated before use [22-24]. However, it is very hard to Figure out exactly what this effect was. In Figure 3c, one can observe the formation of holes that have the depth of the PS_{38}-PEO_{770} layer (about 2 nm), although it is also clear that a significant part of the surface is unaffected by the heating. One could thus conclude that part of the surface consists of the intended PEO brush, and the rest of the surface consists of the polystyrene substrate. However, AFM investigations of higher grafting densities (results not shown) showed that the effect of dewetting is more pronounced for higher grafting densities. Also the dewetting is strongly dependent on the exact temperature and duration of heating.

Re-examination of old data

As stated before, this method to produce PEO brushes has already been used in a total of seven previous studies. However, the results presented above show that the PS-PEO transfer ratio is very different from the transfer ratio of 1 that was assumed in these previous studies. In this section we give a short overview and also reinterpret the data and discuss what effect these new insights have on the main conclusions. We stress that the best way to reinvestigate these previous studies would be to redo some or even all of the experiments. As there are small differences between all these papers in for example: the method to prepare the PS surface, the exact length and polydispersities of the PS-PEO diblock copolymers, we cannot be completely sure that the transfer ratios discussed above are correct.

Stuffed brushes

Currie *et al* [19] present a mean-field analytical model for the interactions between grafted chains and particles. The title “stuffed brushes” refers to the adsorption of particles to the chains within a polymer brush (also called ternary adsorption). Among other things the authors predict a maximum in the adsorbed amount of particles as a function of grafting density under certain conditions. This was experimentally studied with PEO brushes produced using the LB technique. For three different PEO chain lengths, (PEO_{148}, PEO_{445},

and PEO_{700} (PS_{40} in all cases)) the adsorption of the protein bovine serum albumin (BSA) was studied as a function of grafting density. Their results (Figure 4a) indeed show a maximum in the adsorption but only for the two longest PEO chain lengths. Apart from that difference between the three chain lengths, the authors did not discuss the effect of chain length on the reduction of protein adsorption. In Figure 4b we show the data from Currie *et al* again but now corrected for the non-ideal transfer of PS_{40}-PEO_N that was discussed above. As the PEO chain lengths slightly differ from our investigated chain lengths, their transfer ratio was estimated based on the data in Figure 2 (For N = 700, 445 and 148 the transfer ratios were estimated as 0.25, 0.42 and 0.94 respectively). In this reinterpretation of the data, the maximum as a function of grafting density is of course retained, it is only shifted to significantly lower grafting densities. This means that the main conclusion of the experimental work by Currie *et al* is not changed by this correction of the data. However, the results after correction are very interesting as they now show a very pronounced effect of the PEO chain length on the antifouling properties of the brush. For longer chain lengths, much lower grafting densities are necessary to go to very low values of protein adsorption. This is a very interesting result as in recent theoretical publications on this subject [19,33], the most important parameter for the reduction of protein adsorption is found to be a sufficiently high grafting density. At a high grafting density, it is hard for particles to reach and adsorb onto the surface, but it is also harder for particles to adsorb to the polymer chains inside of the brush. A long chain length can make it harder for a particle to reach the interface, however it does not contribute to a denser brush and thus to a reduction in particle adsorption to the polymer chains in the brush. What could play an important role in this case is the adsorption of PEO to the PS surface. As discussed above this could have a strong influence on the structure of the brush. If part of the PEO chains is adsorbed to the PS surface, the formed PEO brush will be less dense than in the case that the polymers do not adsorb and thus that all polymers “participate” in the brush. This effect is smaller for long PEO chains, as for long chains a smaller number will adsorb to the surface than for small chains and the effect on the effective grafting density (the grafting density without the adsorbed polymers) will thus be less for the long chains than for the short chains.

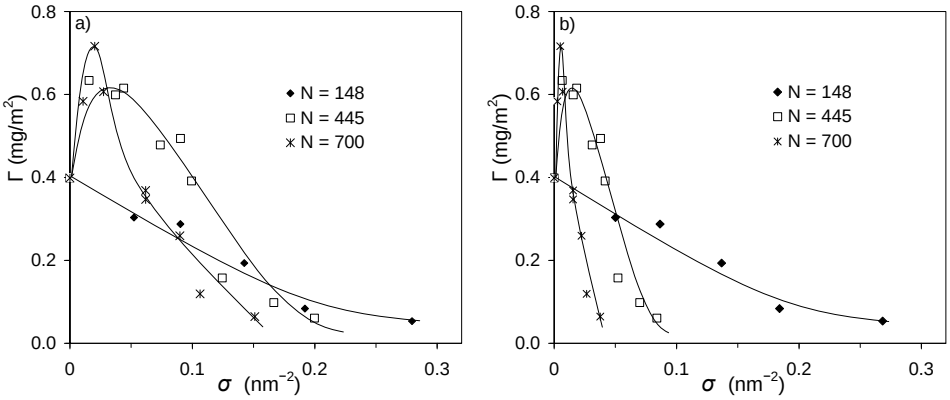

Figure 4. Adsorption of BSA to a PEO brush covered polystyrene surface as a function of PEO grafting density for different PEO chain lengths as indicated a) Data as presented by Currie et al [19] ; b) Same data, corrected for the lower transfer ratio than assumed in the original work. It is noted here that the guide for the eye lines for the data of ref. 19 are not identical to the guide for the eye lines as drawn in the original paper.

Another explanation comes from the work of Szleifer [34], who argues, that because of the attraction between the polymer and the surface, there will be a competition between the particle and polymer for the surface. The length of the polymer will thus be an important parameter in the repulsion of particles. The model of Szleifer indeed predicts that in case of attraction between the polymers in the brush and the surface, the chain length strongly affects the particle adsorption. Longer chain lengths result in lower adsorbed amounts.

We would again like to stress that we cannot be completely sure that the data can be corrected in this way due to small differences in the manner of preparation of these brushes and the brushes in our investigation. This exercise shows how important it would be to redo at least some experiments in the near future to find if a high polymer chain length will indeed lead to a low grafting density at which only low amounts of protein adsorption are found.

Adsorption of nanocolloidal SiO_2 particles on PEO brushes.

Gage *et al* [20] present a study on the adsorption of silica particles to a PEO brush as a function of grafting density for a number of different pH's. The PEO brush is produced with LB transfer of $PS_{48}PEO_{700}$. The authors find very high adsorptions (upto 20 mg/m^2) that are strongly dependent on the pH: a higher pH leads to lower adsorption. Silica particles and PEO chains interact by forming hydrogen bonds between the oxygen in the

PEO and OH groups at the silica surface. At high pH, silica is highly charged, an thus has only few OH groups on the surface. When the pH is lowered, the number of OH groups and thus also the adsorbed amount increases. The authors also find a broad maximum in the adsorbed amount as a function of grafting density. The maximum is explained as follows: the increasing adsorbed amount at low grafting density stems from the increase of PEO chains (and thus adsorption sites). At higher grafting densities, however the osmotic pressure in the brush strongly increases and the SiO_2 particles are excluded from the inner part of the brush and can only adsorb on the outside of the brush. They report the maximum to be situated around a grafting density of 0.2 nm^{-2}. With the information we now have on the transfer ratios of $PS_{38}PEO_N$, we estimate the actual value of that maximum to be 0.05 nm^{-2}. Clearly, much lower grafting densities are needed to exclude the silica particles from the inner part of the brush. Apart from that, no conclusions of the authors are affected.

Protein adsorption at polymer grafted surfaces: comparison between a mixture of saliva proteins and some well-defined model proteins.

Kawasaki *et al* [21] investigated the adsorption and the zeta-potential during adsorption of four proteins (lysozyme, human serum albumin, β-lactoglobulin, and ovalbumin) and a mixture of saliva proteins on polystyrene and on PEO brushes ($PS_{40}PEO_{772}$) of different grafting densities (σ = 0.08, 0.18 and 0.25 nm^{-2}). They focus on the antifouling properties of the PEO brush. Compared to the adsorption on pure PS, they find for all proteins a reduction in the adsorbed amount at high grafting density (50 to 90% reduction, depending on the protein). For lysozyme, the smallest of the proteins, they find no reduction in the adsorbed amount at the lowest grafting density (σ = 0.08 nm^{-2}), while for all others they do find a reduction in adsorption. The authors explain this by proposing that a single lysozyme molecule (4.6 * 3 * 3 nm^3) fits between two grafted chains at this grafting density (distance approximately 3 - 4 nm) and thus the grafted chains do not prevent adsorption. However, with the knowledge we now have on the transfer ratio of $PS_{38}PEO_{770}$, we believe that the actual grafting densities where σ = 0.015, 0.035 and 0.048 nm^{-2}. Thus, much lower grafting densities already give the measured 50 to 90% reduction in protein adsorption. Also, it is clear that comparing the distance between the grafted chains at the interface and the size of the protein does not give a clear indication when reduction of protein adsorption begins.

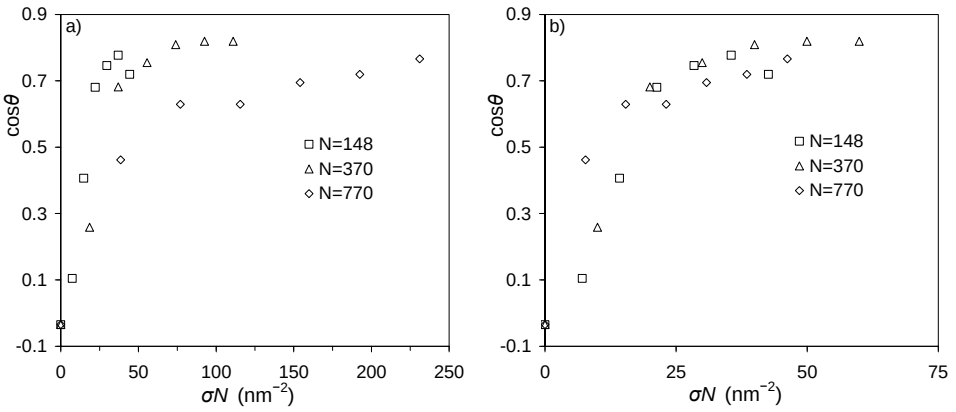

Figure 5. Cosine of the contact angles θ of a captive air bubble under a polystyrene surface covered by a PEO brush (N as indicated) measured as a function of grafted amount σN nm^{-2} for different PEO chain lengths as indicated. a) Data as presented by Cohen Stuart et al [25]; b) same data, corrected for the lower transfer ratio than assumed in the original work.

Why surfaces modified by flexible polymers often have a finite contact angle for good solvents

Cohen Stuart *et al* [25] present a self-consistent field analysis in which they show that it is expected that the contact angle between a good solvent and a polymer brush is finite. This stems from the fact that most polymers in a good solvent are able to significantly adsorb to the solution-vapor interface. Therefore, in a very thin solvent layer (as thick as the brush), the grafted chains will bridge from the solid surface to the solvent vapor interface. If now a drop of water is added on top of such a surface, the droplet will not completely spread out over the surface, as the further the droplet spreads, the more of these bridges would have to be broken. How far the droplet spreads (thus determining its contact angle) depends on how strong the polymers adsorb to the solvent vapor interface. For a PEO brush of sufficient grafting density and chain length, the authors predicted a contact angle of approximately 40° ($\cos\theta$ = 0.77). Experimental data on the contact angle of air bubbles in water with PEO brushes ($PS_{36}PEO_{148}$, $PS_{36}PEO_{370}$, $PS_{38}PEO_{770}$) was presented that underpinned the self-consistent field data. These experimental results are shown in Figure 5a. Indeed, at high enough σN for the air-water interface to be saturated by adsorbed polymer, a contact angle of approximately $\cos\theta$ = 0.77 is found. However, another prediction was that the transition from the contact angle at the ungrafted interface to that contact angle goes linear with increasing total polymer mass in the brush (σN), and is thus

independent on how the polymer is distributed in the brush. This was however not found in the original data; in Figure 5a a definite dependence of chain length is observed on the contact angle as a function of σN. In Figure 5b we present the corrected data based on the transfer ratios in Figure 2. In this corrected data we do not find the dependence of the contact angle as a function of σN of the chain length. Thus, the corrected data compares much better to the predictions of the nSCF model. In contrast to the other papers discussed in this section, the brushes in these experiments (Figure 5) were produced in exactly the same way and with exactly the same polymers as the brushes that were used to measure the transfer ratios of these polymers (Figure 2). Therefore, we are sure that the data in Figure 5b are corrected with the right transfer ratios.

Improving the brush preparation method

The low transfer ratio for $PS_{36}PEO_{370}$ and $PS_{38}PEO_{770}$ severely limits the grafting densities that can be reached using the LB technique. As the maximum grafting density that can be reached at the air-water interface before a collapse of the layer is about σ_{AW} = 0.35 nm^{-2}, the maximum grafting density that can be transferred to the solid substrate is thus a fraction of that (for $PS_{36}PEO_{370}$ σ_{max} = 57% × 0.35 = 0.20 nm^{-2}, for $PS_{38}PEO_{770}$ σ_{max} = 19% × 0.35 = 0.067 nm^{-2}). Above, we already reported that increasing the length of the PS block ($PS_{120}PEO_{800}$) leads to a higher transfer ratio (40%). However, a longer PS block also leads to a lower grafting density that can be reached at the air-water interface before a collapse of the layer. Therefore, increasing the length of the PS block does not lead to an increased maximum grafting density. A better approach would be to try to change and influence the transfer ratio without changing any block lengths. Therefore, we decided to dip the surfaces in a different way. First, we changed the speed with which the substrate is moved through the air-water interface. However, we found that this has no effect. A more successful change is shown in Figure 6. In Langmuir-Blodgett dipping the substrate is always moved vertically through the air-water interface. A different approach, called Langmuir-Schaeffer (LS), is to move the substrate horizontally onto the air-water interface and then retract the substrate. We used a variant of this technique in which the surface is horizontally moved through the air-water interface. In Figure 6 we compare the transferred amounts after LB and LS transfer for $PS_{36}PEO_{370}$ and $PS_{38}PEO_{770}$.

From Figure 6 we observe that just as with the Langmuir-Blodgett technique, with the Langmuir-Schaeffer dipping method the transferred mass is also proportional to the grafting density at the air-water interface. The main difference is that with the LS technique the transfer ratio is significantly higher; for $PS_{38}PEO_{770}$ the transfer ratio with LB was 19%, with LS the transfer ratio is 42%. For $PS_{36}PEO_{370}$ the transfer ratio with LB is 57% and

with LS the transfer ratio is 91%. This implies that the maximum grafting density that can be reached with the LS technique is significantly higher, for $PS_{38}PEO_{770}$ using LS σ_{max} = 0.15 nm^{-2}, for $PS_{36}PEO_{370}$ using LS σ_{max} = 0.32 nm^{-2}. Apparently, horizontal dipping somehow increases the chance that a PS block connects with the surface before the PEO block does. We speculate that this has to do with a different dynamic contact angle during dipping, as a result of the different dipping method. We did however find that the layers produced in this way are somewhat less stable than the layers produced with the LB method, strong rinsing with water reduced the layer thickness by 10-15%. Thus, we believe that some polymer is only loosely bound to the PS substrate.

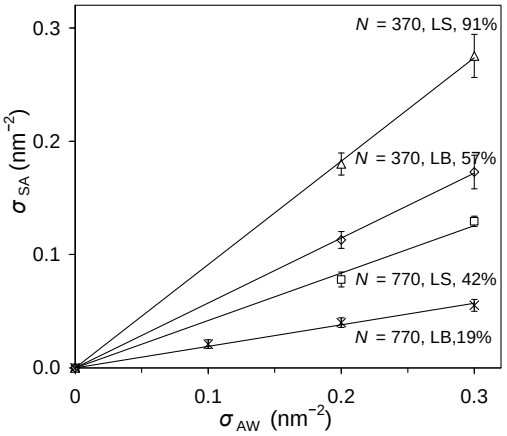

Figure 6. Brush grafting density on the solid substrate (σ_{SA}) after LB and LS transfer as a function of the grafting density at the air-water interface (σ_{AW}) for different PEO chain lengths (N) and transfer methods as indicated (LB = Langmuir Blodgett, LS = Langmuir-Schaeffer). Points represent the average experimental values, error bars represent the standard deviation, lines represent best linear fits, and percentages represent the transfer ratio σ_{SA}/σ_{AW}.

Conclusions

In this chapter we have investigated the transfer of mass upon vertically dipping a polystyrene surface through a layer of a polystyrene-poly(ethylene oxide) at the air-water interface. The transferred mass is proportional to the PS-PEO grafting density at the air-water interface, but the transfer ratio is significantly lower than 1. Depending on the chain length of the PEO block a certain fraction of the polymers at the air-water interface is transferred to the solid surface. For the shortest PEO chain length (PS_{36}-PEO_{148}) we find a transfer of 94% of the mass, while for longer chain lengths (PS_{36}-PEO_{370} and PS_{38}-PEO_{770}) we find a transfer of respectively 57% and 19%. We believe that an important part of the explanation of this phenomenon is that both PEO and PS can adsorb on the PS substrate. During the transfer both polymer blocks adsorb and adsorbed PEO prevents PS adsorption at that position. This hypothesis is strengthened by the finding that a polymer with a longer PS block (PS_{120}-PEO_{800}) has a much larger transfer ratio (40%) compared to the corresponding polymer (PS_{38}-PEO_{770}). These findings have a significant impact on the results of a number of papers in which the above described transfer has been used to produce PEO polymer brushes. We shortly reviewed these papers and discussed the main results in the light of this new information. Although some data are strongly affected by this new information, the main conclusions are not affected. In a number of these papers however the authors have used a heating step in the production of PEO brushes via Langmuir-Blodgett transfer. Using atomic force microscopy, we have found that after LB transfer the material is evenly spread over the surface, however upon a short heating (5 minutes) of the layers (95°C) the surface shows signs of dewetting. It is not clear what effect this dewetting could have had on the results of studies that included this heating step in PEO brush preparation. Furthermore, we show that by using Langmuir-Schaeffer (LS, horizontal) dipping, much higher mass transfers can be reached than with LB transfer.

Finally, we would like to stress that these new insights, especially on the reduced transfer ratio of PS-PEO, do not diminish the strength of this method to produce PEO brushes. When the transfer ratio has been established for a certain PS_NPEO_M diblock copolymer, brush layers can be prepared with full control over the grafting density. By dipping via the Langmuir-Schaeffer approach it is possible to reach higher grafting densities with the longer PEO chains.

References

1. Currie, E.P.K.; Norde, W.; Cohen Stuart, M.A. *Adv. Colloid Interface Sci.***2003,** *100-102,* 205.
2. Milner, S.T. *Science* **1991,** *251,* 905.
3. Halperin, A.; Leckband, D.E. *C. R. Acad. Sci. Paris* **2000,** *serie IV,* 1171.
4. Zhao, B.; Brittain, W.J. *Prog. Polym. Sci.* **2000,** *25,* 677.
5. Advincula, R.C.; Brittain, W.J.; Caster, K.C.; Rühe, J. *Polymer Brushes,* **2004,** Wiley-VHC, Weinheim.
6. Rühe, J.; Ballauff, M.; Biesalski, M.; Dziezok, P.; Gröhn, F.; Johannsmann, D.; Houbenov, N.; Hugenberg, N.; Konradi, R.; Minko, S.; Motornov, M.; Netz, R.R.; Schmidt, M.; Seidel, C.; Stamm, M.; Stephan, T.; Usov, D.; Zhang, H. *Adv.Polym. Sci.* **2004,** *165,* 79.
7. Edmondson, S.; Osborne, V.L.; Huck, W.T.S. *Chem. Soc. Rev.* **2004,** *33,* 14.
8. Tsujii, Y.; Ohno, K.; Yamamoto, S.; Goto, A.; Fukuda, T. *Adv. Polym. Sci.* **2006,** *197,* 1.
9. Marra, J.; Hair, M.L. *Colloids and Surfaces* **1988,** *34,* 215.
10. Watanabe, H.; Tirell, M. *Macromolecules* **1993,** *26,* 6455.
11. Maas, J.H.; Cohen Stuart, M.A.; Fleer, G.J. *Thin Solid Films* **2000,** *358,* 234.
12. Auroy, P.; Auvray, L.; Leger, L. *Macromolecules* **1991,** *24,* 2523.
13. Tran, Y.; Auroy, P.; Lee, L.-T. *Macromolecules* **1999,** *32,* 8952.
14. Maas, J.H.; Cohen Stuart, M.A.; Sieval, A.B.; Zuilhof, H.; Sudhölter, E.J.R. *Thin Solid Films* **2003,** *426,* 135.
15. Devaux, C.; Chapel, J.P.; Beyou, E.; Chaumont, P. *Eur. Phys. J. E* **2002,** *7,* 345.
16. Kuhl, T.L.; Leckband, D.E.; Lasic, D.D.; Israelachvili, J.N. *Biophysical J.* **1994,** *66,* 1479.
17. Efremova, N.V.; Sheth, S.R.; Leckband, D.E. *Langmuir* **2001,** *17,* 7628.
18. Bianco-Peled H.; Dori Y.; Schneider J.; Sung L.; Satija S.; Tirrell M. *Langmuir*, **2001,** *17,* 6931.
19. Currie, E.P.K.; van der Gucht, J.; Borisov, O.V.; Cohen Stuart, M.A. *Pure Appl. Chem.* **1999,** *71,* 1227.
20. Gage, R.A.; Currie, E.P.K.; Cohen Stuart, M.A. *Macromolecules* **2001,** *34,* 5078.
21. Kawasaki, K.; Kambara, M.; Matsumura, H.; Norde, W. *Biofouling* **2003,** *19,* 355.
22. Bosker, W.T.E.; Iakovlev, P.A.; Norde, W.; Cohen Stuart, M.A. *J. Colloid Interface Sci.* **2005,** *286,* 496.
23. Norde, W.; Gage, R.A. *Langmuir* **2004,** *20,* 4162.
24. Zimmermann, R.; Norde, W.; Cohen Stuart, M.A.; Werner, C. *Langmuir* **2005,** *21,* 5108.
25. Cohen Stuart, M.A.; de Vos, W.M.; Leermakers, F.A.M. *Langmuir* **2006,** *22,* 1722.
26. Bijsterbosch, H. D.; de Haan, V. O.; de Graaf, A. W.; Mellema, M.; Leermakers, F. A. M.; Cohen Stuart, M. A.; van Well, A. A. *Langmuir* **1995,** *11, 4467.*
27. Brandrup, J.; Immergut E.H. *Polymer Handbook* **1993,** John Wiley and Sons, New York.
28. Mark J.E., Polymer Data Handbook **1999**, Oxford University Press, New York.
29. Pagac, E.S.; Prieve, D.C.; Solomentsev, Y.; Tilton, R.D. *Langmuir* **1997,** *13,* 2993.
30. Currie, E.P.K.; Sieval, A.B.; Avena, M.; Zuilhof, H.; Sudhölter, E.J.R.; Cohen Stuart, M.A. *Langmuir* **1999**, *15,* 7116.
31. de Vos, W.M.; Biesheuvel, P.M.; de Keizer, A.; Kleijn, J.M.; Cohen Stuart, M.A. *Langmuir* **2008,** *24,* 6575-6584.
32. Chakrabarti, A. *J. Chem. Phys.*, **1994**, *100,* 631.
33. Halperin, A.; Fragneto, G.; Schollier, A.; Sferrazza, M. *Langmuir*, **1997**, *23*, 10603.
34. Szleifer, I. *Biophysical J.*, **1997**, *72*, 595.

Chapter 3

Zipper brushes: ultra dense brushes through adsorption.

Abstract

We investigated a new type of polymer brushes: the zipper brush. By adsorbing a diblock copolymer with one charged block and one neutral block to an oppositely charged polyelectrolyte brush, a neutral polymer brush is formed on top of an almost neutral layer of complexed polyelectrolytes. This neutral brush can be adsorbed in minutes and desorbed in seconds to restore the original polyelectrolyte brush. The zipper brush can be used, for example, as an antifouling layer to prevent protein adsorption. These characteristics are shown by fixed-angle optical reflectometry for the system of poly(N-methyl-2-vinyl pyridinium)-block-poly(ethylene oxide) (P2MVP-PEO) adsorbed to a poly(acrylic acid) (PAA) brush. After the diblock copolymer has adsorbed (at pH 6), the charges of the PAA brush are almost completely compensated by the charges of the P2MVP block. The grafting density of the formed neutral brush can be controlled by the chain length and grafting density of the PAA brush, and by the chain length of P2MVP block. As the P2MVP blocks used in this study are much smaller than the PAA chains in the brush, the grafting density of the PEO brushes are found to be a multiplication of that of the PAA brush, and much higher grafting densities (up to 1.59 chains per nm^2) can be obtained than have previously been reported for polymer brushes prepared by adsorption. At low pH, when the PAA is uncharged only a few mg/m^2 adsorb, probably because of hydrogen bonding between uncharged PAA and PEO. As the pH increases the PAA becomes more charged and the adsorbed amount of diblock copolymer increases strongly until pH 6 and then levels off.

The adsorption of poly(N,N-dimethyl amino ethyl methacrylate)-block-PEO (PDMAEMA-PEO) to the PAA brush shows the same pH dependence as P2MVP-PEO with the difference that above pH 9 the adsorption quickly drops to zero due to discharging of the PDMAEMA block. Therefore, PDMAEMA-PEO can be easily desorbed by rinsing with a pH 10 solution. Thus, by using a diblock copolymer with a different chemistry, we can change the conditions at which the diblock copolymer adsorbs or desorbs.

A letter based on this chapter was published as: De Vos, W.M.; Kleijn J.M.; de Keizer A.; Cohen Stuart M. A. *Angew. Chem. Int. Ed.* **2009**, *48*, 5369-5371.

A full manuscript based on this chapter has been submitted.

Introduction

Polymer brushes, i.e., densely packed arrays of polymer chains end-attached to an interface, have been investigated and used for many years for their antifouling properties [1,2,3]. A brush layer in a good or theta solvent is swollen because of excluded volume interactions. Any deformation from its equilibrium, for example due to insertion of a protein, gives rise to a restoring force. Thus, as long as there is no attraction between the protein and the polymer, and this restoring force is large enough to prevent the protein from reaching the substrate, the brush layer prevents fouling.

There are several methods to produce polymer brushes, all of which have their own advantages and disadvantages. In a number of good reviews these techniques have already been extensively discussed [1,4-8], a short summary is given here. The major techniques to produce polymer brushes can be divided into three different categories: adsorption, 'grafting to', and 'grafting from'. In the 'grafting from' approach, polymer chains are polymerized from the grafting interface. For this, one first prepares a surface with (usually covalently) attached monomers from which polymerization is initiated. With this approach high degrees of polymerization and grafting densities [8] can be achieved, typically up to 0.8 nm^{-2}. Polydispersity depends on the type of polymerization reaction. This approach has the disadvantage that the grafting density is hard to control, and that it is difficult to separately determine grafting density and chain length.

In the 'grafting to' approach and the 'adsorption' approach preformed polymers are used. An obvious advantage of this is that one can beforehand determine properties such as the chain length and the polydispersity. The 'grafting to' approach uses polymers with a reactive chain end which are connected to the surface using a suitable reaction [9,10,11]. High grafting densities can be achieved, provided this reaction can be carried out without solvent (in melt) [11]. This approach is easier and more suitable for large surfaces than the 'grafting from' approach. Disadvantages are that the grafting density is hard to control and that a reactive surface is needed.

The most simple and earliest approach for the formation of polymer brushes is adsorption [12,13,14]. For this one needs a diblock copolymer, of which one block needs to be capable of adsorbing to the grafting interface (anchor block) and the other block is preferably non-interacting with the grafting interface. This method has the major advantage that a polymer brush is spontaneously formed if one has the right combination of diblock copolymer, surface, and solvent, and can thus quickly and easily be used on large surfaces. However, the disadvantages of this technique are also large. One is that a solvent is needed in which both blocks of the diblock copolymer are soluble or else one will get micelle formation, usually leading to an inhomogeneous adsorption. The most serious disadvantage,

however, is that this technique can only form polymer brushes with low and ill-controlled grafting densities. During the adsorption process the polymer brush which is formed acts as a barrier not only for fouling agents (such as proteins) but also for the adsorption of additional diblock copolymers attempting to enter the polymer brush. In an equilibrium situation, the brush formation stops when the energy gained by adsorbing an anchor block to the interface is equal to the energy that is lost when an extra chain is inserted into the polymer brush. To get a high grafting density one thus needs a very strong attraction between anchor block and surface which is hard to achieve in a solvent in which both blocks are soluble. In aqueous solution, one option is to use electrostatic interaction, if one adsorbs a diblock copolymer with one charged block and one neutral block to an oppositely charged surface. The electrostatic interaction between the anchor block and the surface can be very large. However, as a flat surface can only accommodate a limited number of charges this does not lead to high grafting densities.

In this chapter we propose a new method to produce polymer brushes in aqueous solution using adsorption. As stated above, a flat surface can only accommodate a limited number of charges. However, a surface covered with attached polyelectrolyte, for example a poly(acrylic acid) brush layer, can accommodate many more charges. Adsorbing a diblock copolymer with one neutral block and one charged block to a surface covered with attached oppositely charged polyelectrolyte should lead to the formation of a neutral brush. Because of the strong attraction between the oppositely charged polyelectrolytes and the large number of charges in the polyelectrolyte brush a large amount of diblock copolymer is expected to adsorb, implying that the formed neutral brush can have a very high grafting density. Another expected effect of the strong attraction between oppositely charged polyelectrolytes would be that the adsorbed number of diblock copolymers is determined by full charge compensation between the charges in the brush and the charge of the adsorbed diblock copolymer. As a consequence, it should be possible to tune the grafting density of the formed neutral brush by choosing the density and degree of polymerization of the polyelectrolyte brush and the degree of polymerization of the charged block of the diblock copolymer. Another advantage of this method is that complexes of oppositely charged polyelectrolytes can usually be broken by adding salt or changing the pH. Thus, in such a system a neutral brush could not only be formed due to adsorption, but could also be desorbed again. Therefore, we have named this new procedure to form neutral polymer brushes the “zipper brush” approach. The proposed method is depicted in Figure 1.

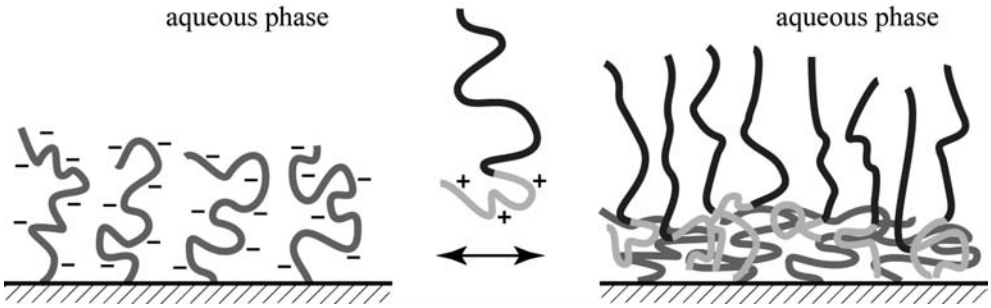

Figure 1. Schematic depiction of the formation of a neutral zipper brush: a system where the adsorption of a diblock copolymer to a polyelectrolyte brush layer leads to a new neutral brush layer. Desorption of the diblock copolymer restores the original brush layer. In this picture the polyelectrolyte block has half the degree of polymerization of the polyelectrolytes in the brush. Thus, the grafting density of the formed neutral brush is twice that of the original polyelectrolyte brush.

A system that resembles this approach is the formation of neutral polymer brushes by adsorption of so-called complex coacervate core micelles (C3M's) [15,16]. These micelles are formed by mixing a diblock copolymer with a charged block and a neutral block with an oppositely charged polyelectrolyte. Upon complexation of the oppositely charged polyelectrolytes, they form a separate (complex coacervate) phase [17] that forms the core of these micelles. The growth of the complex coacervate phase is stopped by the neutral blocks forming a corona surrounding the complex coacervate core. It has been found that these micelles adsorb to different types of surfaces, strongly reducing subsequent protein adsorption to that surface. The proposed, and for a specific system confirmed [18] structure resembles very strongly the structure proposed for the zipper brush in Figure 1: adsorbed to the interface a complex coacervate layer with on top of that a neutral polymer brush. The only difference is that the polyelectrolyte is not connected to the interface. Thus, the driving force for the formation of the neutral brush is very different. In the case of the zipper brush the driving force is the attraction between oppositely charged polyelectrolytes, in the C3M system the driving force is the phase separation of the complex coacervate.

In this chapter our investigation concerns the adsorption of P2MVP-PEO and PDMAEMA-PEO to a PAA brush, and the subsequent desorption. Adsorption and desorption are followed as a function of time by using fixed-angle optical flow cell reflectometry. Adsorption is studied as a function of pH, for different PAA grafting densities, PAA chain lengths and salt concentrations. In addition, the chain length of the neutral- and the charged block of the diblock copolymer are varied. The antifouling properties of the formed PEO brushes are tested by exposure different proteins.

Materials and methods

Polymers, proteins and solvents

Poly(N-methyl-2-vinyl pyridinium)-block-poly(ethylene oxide) diblock copolymers ($P2MVP_{41}$-PEO_{205}, M_w/M_n = 1.05; $P2MVP_{42}$-PEO_{446}, M_w/M_n = 1.02; $P2MVP_{71}$-PEO_{454}, M_w/M_n = 1.02) and poly(N-methyl-2-vinyl pyridinium) ($P2MVP_{43}$, M_w/M_n = 1.10) were formed by quaternization with methyl iodide from their precursors poly(2-vinyl pyridine) ($P2VP_{43}$, Polymer standards service Mainz, Germany) and poly(2-vinyl pyridine)-block-poly(ethylene oxide) ($P2VP_{41}$-PEO_{205}, Polymer Source Inc, Montreal, Canada; $P2VP_{42}$-PEO_{446} and $P2VP_{71}$-PEO_{454} synthesized as described in ref. 19). The quaternization reaction is described by Voets *et al* [19]. The degree of quaternization was found to be 91%.

Poly(N,N-dimethyl amino ethyl methacrylate)-block-poly(ethylene oxide) ($PDMAEMA_{35}PEO_{120}$, M_w/M_n = 1.3 and $PDMAEMA_{77}PEO_{120}$, M_w/M_n = 1.3 Polymer Source inc, Montreal, Canada) was used as received. Lysozyme, bovine serum albumin (BSA), α-lactoglobulin, and fibrinogen were ordered from Sigma and used as received, cytochrome c was ordered form Aldrich.

All solvents used were of PA grade (Sigma-Aldrich). Water used was demineralized using a Barnstead Easypure UV and has a typical resistance of 18.3 MΩ/cm.

Preparation of PAA brush layers

PAA brush layers of varying grafting density and length were prepared by means of a Langmuir-Blodgett (LB) method described by Currie *et al* [20] with a few adjustments. As substrates, flat silicon wafers were used, coated with polystyrene.

Because polystyrene films spin-coated on clean silicon wafers are not stable, the coating of substrates with polystyrene (PS) was done in the following way. First, the silicon wafer (which has a natural SiO_2 layer of a 2-3 nm thickness) was cut into strips (4 x 1 cm^2), rinsed with alcohol and water, and further cleaned using a plasma-cleaner (10 minutes). The strips were covered with a solution of 11 g/l vinyl-PS20 (M_n = 1.9 kg/mol, M_w/M_n = 1.03, Polymer Source Inc. Montreal, Canada) in chloroform and, after evaporation of the solvent, were heated overnight at 150ºC under vacuum. In this way the vinyl-PS20 is covalently bound to the Si/SiO_2 surface [11]. Excess vinyl-PS20 was washed off with chloroform. Subsequently, the strips were spin-coated using a solution of 11 g/l PS (M_n = 870 kg/mol, M_w/M_n = 1.05, Polymer Source Inc.) in toluene at 2000 rpm for 30 seconds in order to obtain a thicker PS layer (about 70 nm). The PS surface films prepared in this way are stable in aqueous solutions.

For the brush layer transfer, monolayers of PS-PAA block copolymers (PS_{36}-PAA_{270}, M_w/M_n = 1.09, $PS_{41}PAA_{120}$, M_w/M_n = 1.10, Polymer Source Inc. Montreal, Canada) at the air-water interface, were prepared by dissolving the copolymers in a 60%/40% 1,4-dioxane/toluene mixture and spreading these solutions very carefully on water in a Langmuir trough using a micro syringe. The water phase had been slightly acidified with HCl to pH 4 (for the grafting densities σ = 0.05 nm^{-2} and 0.1 nm^{-2}) or pH 4.7 (for σ = 0.2 nm^{-2} and 0.3 nm^{-2}). Subsequently, the films were compressed to the appropriate surface density and transferred to the substrates. For the transfer we used a variant of the Langmuir-Schaefer method [21] in which the substrate is held horizontally and dipped through the air-water interface at a speed of 1 mm/s. The substrate was then pulled under the barrier and taken out of the water on the side of the Langmuir trough without the monolayer. De Vos *et al* [22 (chapter 6)] showed with ellipsometry measurements that this technique indeed transfers the right amount of polymer for a given grafting density and showed by AFM that the material is evenly spread over the surface. The surfaces so prepared were carefully stored in clean water until use.

Ellipsometry and atomic force microscopy

Thicknesses of (dry) layers before and after adsorption were measured using an ellipsometer (SE 400, Sentech instruments GmbH, Germany). For this we assumed the following refractive indices: $\tilde{n}_{silicon}$ = [3.85, 0.02], n_{silica} = 1.46, $n_{polystyrene}$ = 1.59, n_{H2O} = 1.33. The refractive indices of adsorbed layers were also measured and always found to be between 1.48 and 1.52 (thus showing that upon drying of a layer no large amounts of air or water are trapped in the layer). For a single surface the thickness was measured a minimum of three times at different positions and the average value was used. For some surfaces, thicknesses measured with ellipsometry were also checked and confirmed by atomic force microscopy (Nanoscope III, Veeco instruments Inc, Plainview NY, USA). To measure thickness with AFM, the surface was scratched by hand using a sharp needle. As the silicon and silica layers are much harder compared to the polymer layer, only the polymer is scratched away, and the thickness of the layer can be measured.

Reflectometry

The adsorption of P2MVP-PEO onto PAA brush layers was followed with fixed-angle optical reflectometry. A detailed description of the reflectometer setup is provided by Dijt *et al* [23]. It contains a He-Ne laser (λ = 632.8 nm) with linearly polarized light. The change in polarization as a result of adsorption or desorption is measured by simultaneously detecting the parallel (R_P) and the perpendicular (R_S) reflectance and dividing R_P by R_S to

give signal *S*. Before each measurement, the system was calibrated by flowing with a blank solution to get a stable baseline signal (S_0). The measurement is started by introducing a polymer solution into the cell. All solutions are introduced into the cell using a stagnation point flow. The change in signal is measured ($\Delta S = S\text{-}S_0$) with a sampling time of 2 s. The adsorbed amount can be calculated from the change in signal and a sensitivity factor (Q), which depends on the angle of incidence of the laser (θ), the (complex) refractive indices ($\tilde{n}$ or n) and thicknesses (d) of the layers on the silicon wafer, and the refractive index increment (dn/dc) of the adsorbate: $\Gamma = Q(\Delta S/S_0)$. For relatively simple cases, such as the adsorption of polymer or protein to a hard surface, the Q factor is usually calculated from known refractive indices. However, we are dealing with a polyelectrolyte brush complexing with a diblock copolymer and this complexation can result into a large release of counterions. As this release also affects the reflectometry signal, our system is too complicated to calculate the Q factor. A better method is then to calibrate the Q factor of the system by measuring the absolute adsorbed amount with a different method. This was done by measuring the dry layer thickness (*Th*) of P2MVP-PEO adsorbed to a number of PAA brushes (N = 270, σ = 0.1, 0.2) with ellipsometry (see above). Thicknesses measured with ellipsometry are in line with the results obtained with AFM thickness measurements. The adsorbed amount can then be calculated from the known or estimated bulk density of the polymer (ρ) by $\Gamma(mg/m^2) = Th\ (nm) \times \rho\ (kg/m^3) \times 10^{-3}$. We have estimated the bulk density of P2MVP-PEO to be around 1200 kg/m^3. By combining the data on adsorbed amount with the measured signal ($\Delta S/S_0$) for the same system the Q factor can be determined by a best fit of this data. Results and fit are shown in Figure 2.

Unless otherwise stated, the polymer concentrations used for reflectometry were 0.1 g/l and the background electrolyte was 10 mM KNO_3. Flow speed was about 1 ml per minute. All experiments were performed at room temperature (approximately 20 ºC). Concentrated solutions of NaOH and HNO_3 were used to bring solutions to the desired pH. No buffer was used in these experiments. To minimize the effect of CO_2 uptake from the air or any other drifts in the pH, the pH of the solutions was adjusted just before the measurement. Also, pH values were used that are known to be not strongly influenced by drift (pH 10 and pH 6 and lower). After the measurements, the pH of the solutions was checked, results were always within 0.2 pH unit from the original pH.

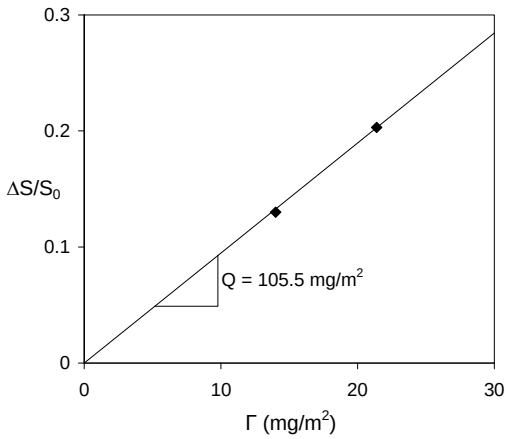

Figure 2. The reflectometer signal as a function of the adsorbed amount (Γ). Data points are experimental values determined by a combination of ellipsometry and reflectometry (see text). Line is a fit resulting in the sensitivity factor Q of the reflectometer for this system.

Results and discussion

Adsorption and desorption of P2MVP-PEO to a PAA brush

In the introduction and in Figure 1 we proposed a new method to produce a dense neutral polymer brush through adsorption: the 'zipper brush' method. To investigate this proposed method we have chosen to use a diblock copolymer consisting of poly(ethylene oxide) (PEO, a neutral polymer) block and a poly(N-methyl-2-vinyl pyridinium) (P2MVP, a strong positively charged polyelectrolyte) block in combination with a brush consisting of poly(acrylic acid) (PAA, a weak negatively charged polyelectrolyte).

The kinetics and reversibility of the formation of a zipper brush have been investigated using fixed-angle optical reflectometry. In Figure 3 a typical reflectometry experiment of the adsorption and desorption of P2MVP-PEO (N_{P2MVP} = 42, N_{PEO} = 205) to a PAA brush (N = 270, σ = 0.1) is shown. Different solutions are applied to the surface while the adsorbed amount is measured real-time. First, a solution of pH 6 (in all solutions c_{KNO3} = 10 mM) is added, after which the flow is switched to a 0.1 g/l P2MVP-PEO solution (P) of pH 6. As can be seen this leads to a strong adsorption of about 16 mg/m^2, the plateau value is reached after about 300 seconds. After the adsorption step, the surface is flushed again with the pH 6 solution (R), which does not result in desorption, showing that the diblock copolymer is strongly bound to the brush. To desorb the diblock copolymer, two approaches are used. In the first, the surface is flushed with a solution of pH 2, resulting in

a desorption of about 85% of the diblock copolymer. After flushing with pH 2, the surface is flushed again with solvent (R) resulting in a small increase in the signal. We emphasize that this is not due to adsorption but due to a change of the refractive index of the brush layer. With decreasing pH, the degree of dissociation of the polyelectrolyte decreases, leading to a decrease in the refractive index. This effect has already been described by Currie *et al* [20].

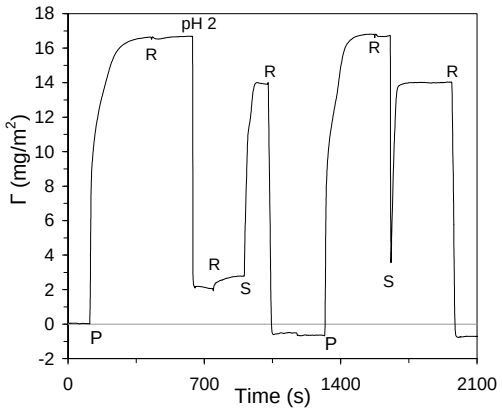

Figure 3. Adsorption of P2MVP-PEO (0.1 g/l) to a PAA brush (N = 270, σ = 0.1 nm^{-2}) and subsequent desorption measured as a function of time by fixed-angle optical reflectometry. P means addition of polymer, R rinsing with a pH 6 solution, pH 2 rinsing with a 0.01M HNO_3 solution, and S rinsing with of a nonionic surfactant solution ($C_{12}EO_5$, 3×CMC) of pH 2 (0.01M HNO_3).

To desorb the 15% of diblock copolymer remaining after rinsing with solvent (pH 6), the surface is exposed to a solution of nonionic surfactant ($C_{12}EO_5$) of a concentration of 0.2 mM (i.e., three times the critical micelle concentration, CMC) and pH 2 (S). As can be seen this leads to a strong and fast adsorption of the surfactant to the surface. However, when rinsed again with a pH 6 solution all surfactant is washed away with a resulting value slightly below the original starting point. Thus, rinsing with a nonionic surfactant solution of pH 2 completely removes all adsorbed diblock copolymer. This is most clearly seen in the second adsorption cycle in which directly after adsorption of the diblock copolymer (P) and rinsing with solvent (R) the surfactant solution (S) is used and after rinsing (R) the base line comes to the same value as before the adsorption. Probably, the resulting value is slightly lower than the starting value because the nonionic surfactant causes a very slight desorption (a few percent of the total amount) of the PS-PAA that makes up the brush. To

avoid this effect, all further experiments were started by first rinsing the surface with the surfactant solution.

As stated the plateau value for the adsorbed amount at pH 6 is 16 mg/m^2, much higher than any reported values for adsorption of P2MVP-PEO to a negatively charged flat surface. Assuming that the diblock copolymer indeed adsorbs as depicted in Figure 1, this adsorbed amount is equal to a grafting density of 0.7 PEO chains per nm^{-2}. This is much larger than any published grafting density of a polymer brush with long chains formed by adsorption.

Unexpectedly, not all P2MVP-PEO is desorbed when rinsing with pH 2. At pH2 PAA, which has a known pK value of 4.2, is almost completely uncharged. Still about 15 percent of the adsorbed diblock copolymer is retained. Since there is no expected ionic interaction, this remaining adsorption would be based on other interactions, presumably between the neutral block of the diblock copolymer and the PAA brush which is neutral at pH 2. Adsorption experiments (not shown) revealed that PEO (20 kg/mol) indeed adsorbs to a PAA brush, both at pH 2 (~ 1.5 mg/m^2) and at pH 4 (~ 1 mg/m^2), but only very little at pH 6 (0.1 mg/m^2). It is well known that PEO and PAA interact due to hydrogen bond formation at low pH [24]. This is also an explanation for the strong adsorption of the nonionic surfactant to the PAA brush (at pH 2) that is observed.

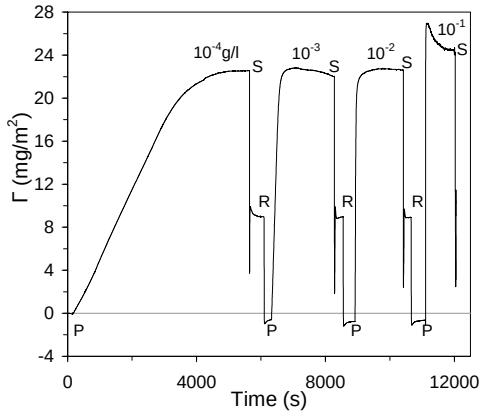

Figure 4. Adsorption of P2MVP-PEO to a PAA brush (N = 270, σ = 0.2 nm^{-2} (pH 6, c_{KNO3} = 10 mM)) for different diblock copolymer concentrations as indicated and subsequent desorption measured by fixed-angle optical reflectometry. P means addition of polymer solution, R rinsing with solvent, and S rinsing with of a nonionic surfactant solution ($C_{12}EO_5$, 3×CMC) of pH 2 (0.01M HNO_3).

In Figure 4 the adsorption of P2MVP-PEO to a PAA brush is shown as a function of time at different polymer concentrations. For all concentrations the initial adsorption is almost linear and near saturation the curves level off to a plateau value (except for the highest concentration, which shows an overshoot). A large increase in the initial adsorption rate is observed with increasing concentration. The initial adsorption rates from low concentration to high concentration are respectively 0.0064 mg/m^{2}s, 0.087 mg/m^{2}s, 0.77 mg/m^{2}s and 7.6 mg/m^{2}s (estimated error about 20%). Thus, with every tenfold increase in adsorption, the initial adsorption rate also increases by approximately a factor of 10. This is a strong indication that the rate of adsorption is limited by the rate of diffusion of the polymer to the surface (in the stagnant layer flow-cell of the reflectometer). The adsorbed amount in the plateau is the same for all concentrations (except the highest) which shows the pronounced high-affinity character of the adsorption of the block-copolymers. This is in agreement with the observation in Figure 3 that upon rinsing with solvent no polymer desorption is observed. At the highest concentration there is an overshoot in the adsorption, after which a slow desorption takes place and after 10 minutes a plateau value is reached. The total adsorbed amount at this plateau value is about 10% higher than the adsorbed amount at other polymer concentrations. We attribute this higher adsorption to kinetic trapping.

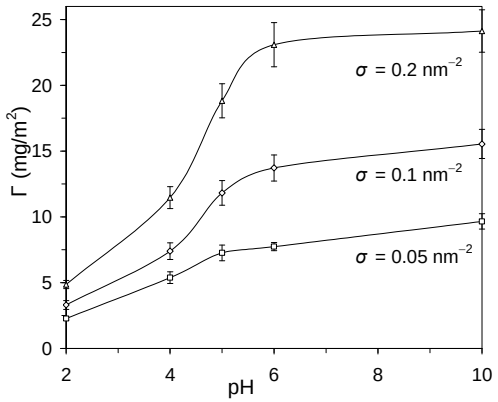

Figure 5. The adsorbed amount of P2MVP$_{42}$-PEO$_{205}$ (c_{KNO3} = 10 mM) to PAA brushes (N = 270) of different grafting density as indicated as a function of pH. Points are averages based on a minimum of 3 experiments, error bars show the standard deviation in the average, lines are used as guide for the eye.

In Figure 5 the adsorption of P2MVP-PEO to PAA brushes of different grafting density is shown as a function of pH. With increasing grafting density the adsorbed amount strongly increases. For the three grafting densities the adsorption as a function of pH shows the same behavior. At pH 2, when the PAA brush is almost uncharged, there is only a small adsorbed amount which is mainly because of hydrogen bonding between PEO and the uncharged PAA. At higher pH the adsorbed amount rises as the PAA becomes more charged. From pH 2 to pH 6 the adsorption increases strongly while between pH 6 and pH 10 there is only a small increase in adsorption. The increased adsorption with increasing pH is as expected as the PAA becomes more charged and thus more P2MVP can complex with the polyelectrolyte brush. It may seem somewhat surprising that between pH 6 and 10 there is only a small increase in the adsorbed amount. From potentiometric titrations, it is known that in a 10 mM NaCl aqueous solution at pH 6, PAA has a degree of dissociation of about 50%. The pH has to be increased to pH 10 before the degree of dissociation to reach about 100% [20]. In a polyelectrolyte brush, the degree of dissociation is expected to be lower than in bulk solution because of the high negative potential of the polyelectrolyte brush. However, it is also well established that in the case of weak polyelectrolytes, complexation with an oppositely charged polyelectrolyte will lead to a large increase in the degree of dissociation. We therefore conclude that due to complexation with P2MVP, the PAA brush at pH 6 already has a high degree of dissociation (we estimate about 90%, based on the difference of adsorbed amount between pH 6 and pH 10) due to charge regulation and that, therefore, increasing the pH to 10 gives only a small increase in the adsorbed amount.

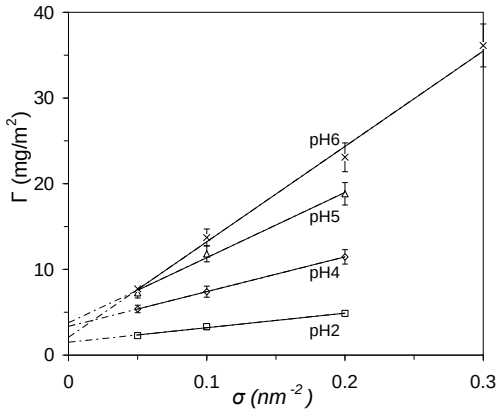

Figure 6. Adsorption of P2MVP-PEO (c_{KNO3} = 10 mM) to PAA brushes (N = 270) as a function of grafting density at different pH values as indicated. Points are averages based on a minimum of 3 experiments, error bars show the standard in the average, lines are linear fits of the data.

In Figure 6 we have replotted the data of Figure 5 to more clearly show the effect of grafting density on the adsorbed amount. In addition, an extra data point has been added for pH 6 at high grafting density (σ = 0.3 nm^{-2}). The data can be well described by a linear fit. Extrapolation of the adsorption at different pH values to σ = 0 gives an adsorbed amount of P2MVP-PEO of roughly 3 mg/m^2. This adsorption, which is independent of the grafting density (and pH), can probably be attributed to the adsorption of the P2MVP-PEO diblock copolymer to the polystyrene substrate to which the PAA chains are grafted. Although the experimental value for the bare surface is of the same order of magnitude, this explanation is however somewhat speculative given the experimental errors.

From the linear dependence of adsorbed amount on the grafting density, and thus on the total amount of polyelectrolyte on the surface, we can derive much about the stopping mechanism of the adsorption. As stated in the introduction, brush formation due to the adsorption of a diblock copolymer stops when the energy gained by adsorbing an anchor block to the interface is equal to the energy that is lost when an extra chain is inserted in the polymer brush. However, with an increase in the grafting density the energy that is gained when adsorbing a P2MVP chain to the PAA brush would not change very much, whereas the adsorbed amount of diblock copolymer does increase (and thus pressure in the formed neutral brush also increases). Therefore, such an energy balance cannot not explain the data. This must mean that there is a different stopping mechanism. Further analysis shows that the adsorption stops when (almost) all charges of the PAA brush are neutralized by the P2MVP. In Table 1 we have calculated the fraction of charges in the PAA brush that have been compensated by the adsorption of P2MVP-PEO at pH 6. For this we have assumed complete dissociation of PAA as well as P2MVP.

σ PAA_{270} (nm^{-2})	0.05	0.1	0.2	0.3
Γ $P2MVP_{42}$-PEO_{205} (mg/m^2)	7.73	13.70	23.09	36.13
σ $P2MVP_{42}$-PEO_{205} (nm^{-2})	0.34	0.60	1.01	1.59
Charge compensation	1.02	0.90	0.76	0.79

Table 1. Adsorbed amount of P2MVP-PEO to PAA brushes with different grafting densities (σ), and the resulting PEO grafting densities and charge compensation (defined as the total amount of positive charges divided by the total amount of negative charges assuming complete dissociation).

As follows from Table 1 the adsorption of P2MVP-PEO to a PAA brush leads to a fairly complete charge compensation for all PAA grafting densities. Most calculations show a somewhat smaller charge compensation than one, but this is in line with the expectation that at pH 6 the PAA is not completely charged after complexation with P2MVP (see above).

The PEO grafting density that results from the adsorption of P2MVP-PEO to the PAA brush is strongly enhanced with respect to the grafting density of the PAA brush. As for full charge compensation the number of positive and negative charges must be equal, the number of adsorbed diblock copolymers can be easily calculated by dividing the total number of negative charges by the block length of the P2MVP block. As the number of adsorbed diblock copolymers per surface area is equal to the grafting density of the formed PEO brush we can calculate it in the following way:

$$\sigma_{\mathrm{PEO}} = \sigma_{\mathrm{PAA}} \times \frac{N_{\mathrm{PAA}}}{N_{\mathrm{P2MVP}}} \qquad [1]$$

Interestingly, the grafting density of the neutral brush is thus given by the grafting density of the PAA brush, enhanced by a factor equal to the ratio between the degrees of polymerization of the PAA chain and that of the P2MVP chain. In the present system, this multiplication factor is 270 / 41 = 6.6. Thus, for a PAA brush of given length and grafting density, the resulting PEO grafting density can be completely controlled if one can control the length of the P2MVP chain. The maximum PEO grafting density that is reached here is 1.59 nm^{-2}. To our knowledge such a high grafting density for long neutral polymer chains has never been reported, although Zdyrko *et al* [26] reports similarly high grafting densities for somewhat shorter PEO chains (N = 113) produced using a ‘grafting to’ approach.

In Figure 7 we show the adsorption as a function of pH for two different PAA chain lengths. The same dependence on pH is observed as was discussed above and the larger the chain length the higher the adsorbed amount. Again, when we assume a linear fit to the data, extrapolation to N = 0 gives an adsorbed amount of P2MVP-PEO of 2-3 mg/m^2. That this value for a PAA-independent adsorption (e.g. because of adsorption of the diblock copolymer to the polystyrene substrate) is the same as found from Figure 6, suggests that the linear fits applied here are probably justified. More PAA chain lengths should be measured to underpin this assumption. Still, the probable linear dependence of adsorbed amount on the PAA chain length is completely in line with Eq. 1.

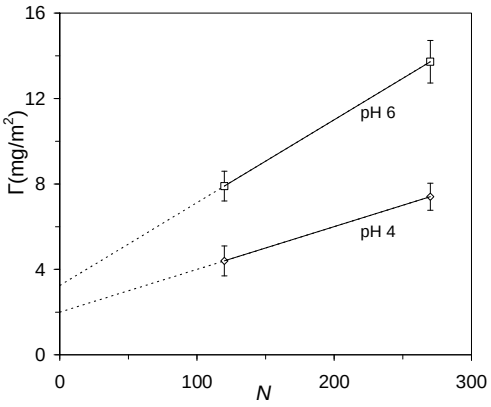

Figure 7. The adsorbed amount of P2MVP$_{41}$-PEO$_{205}$ (c_{KNO3} = 10 mM) as a function of pH to PAA brushes (σ = 0.1 nm^{-2}) of different length as indicated. Points are averages based on a minimum of three experiments, error bars show the standard in the average, lines are linear fits of the data.

In Figure 8 the adsorption is shown as a function of salt concentration for three different pH values. Very similar behavior is observed for pH 6 and 10, i.e., at low salt concentration there is a large adsorption which remains fairly constant up to a salt concentration of 250 mM. Above this, the adsorption decreases to only a few mg/m^2 at 500 mM and almost zero at 1 M. This shows how strong the attraction is between the oppositely charged polyelectrolytes: high salt concentrations are needed to significantly reduce this interaction.

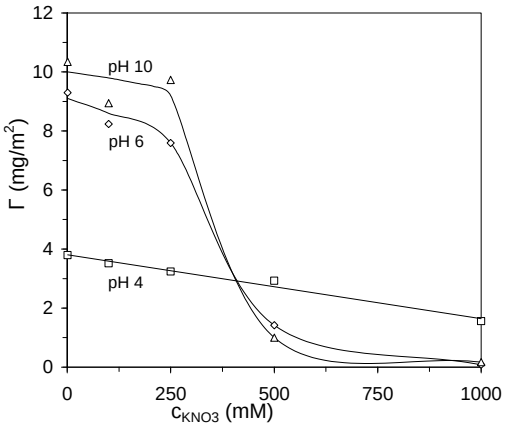

Figure 8. Adsorption of P2MVP$_{41}$-PEO$_{205}$ (c_{KNO3} = 10 mM) to a PAA brush (N = 270, σ = 0.2 nm^{-2}) as a function of KNO_3 concentration at different pH values as indicated. Lines are used as a guide to the eye.

At pH 4 a different dependence on the salt concentration is observed. The adsorption decreases almost linearly from about 8 mg/m^2 at low salt concentration to 4 mg/m^2 at 1M of salt. This indicates a reduced contribution of electrostatic interactions. As discussed above, at low pH, when the PAA is for a large part uncharged, hydrogen bonds are probably formed between the PEO and the PAA. This is in line with the observation that even at very high salt concentrations when all electrostatic interactions are screened, there is still an adsorption of about 2 mg/m^2 of the diblock copolymer.

Tuning the diblock copolymer properties

In the above adsorption experiments we have focused on the adsorption to a PAA brush of only one diblock copolymer, P2MVP$_{42}$-PEO$_{205}$. In this section we show a number of examples that illustrate how the properties of a zipper brush can be changed by varying the structure of the block-copolymer. The first example is given in Figure 9 and shows the adsorption of the block-copolymer PDMAEMA-PEO to a PAA brush. In contrast to the quaternized P2MVP, PDMAEMA is a weak polycation. This means that at high pH PDMAEMA becomes uncharged. Thus, at high pH one would expect no attraction between the diblock copolymer and the PAA brush.

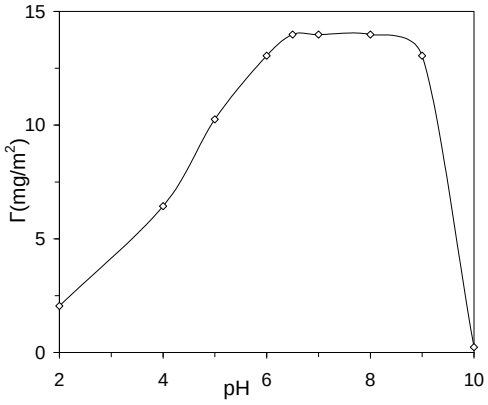

Figure 9. The adsorbed amount of PDMAEMA$_{35}$-PEO$_{120}$ (c_{KNO3} = 10 mM) as a function of pH to a PAA brush (N = 270 σ = 0.2). Points are data, lines are used as guide for the eye.

When we compare the adsorption of PDMAEMA-PEO to a PAA brush as a function of PAA (Figure 9) with that of P2MVP-PEO (Figure 5) strong similarities are observed. At low pH, when the PAA is uncharged, there is a small amount of adsorption, probably

because of hydrogen bonds between PEO and the uncharged PAA. With increasing pH, the PAA charges up and more diblock copolymer is adsorbed until a maximum is reached. For PDMAEMA-PEO this is at pH 6.5. The pronounced difference between the adsorption of PDMAEMA-PEO and P2MVP-PEO is that for PDMAEMA-PEO adsorption abruptly drops to zero between pH 9 and 10. At this pH, PDMAEMA becomes uncharged and as there is no electrostatic interaction anymore, no diblock copolymer adsorbs anymore. As shown in Figure 3, for P2MVP-PEO, the combination of low pH and nonionic surfactants could be used to rinse off all adsorbed polymer. For PDMAEMA-PEO this is also the case. In addition, a solution of pH 10 or higher also removes all adsorbed polymer. Thus, by using a diblock copolymer with a different chemistry, we can change the conditions at which the diblock copolymer adsorbs or desorbs. In addition, one could use diblock copolymers with (water soluble) neutral blocks of different chemistry. In that way, and provided there is no strong attraction between the neutral block and the polyelectrolyte brush (which is the usual case), one could use the zipper brush procedure to produce any neutral polymer brush. For example, provided the corresponding diblock copolymers are available, one can make not only PEO brushes but also brushes of poly(acryl amide), PolyNIPAM, PVA etc. The needed polymers can now be readily made using controlled radical polymerization.

As follows from Eq. 1, the PEO brush density can be tuned by the choice of the length of the surface-attached polyelectrolyte, its grafting density, or the length of the charged block of the diblock copolymer. The latter is probably the most flexible approach. In Table 2 we give the results of adsorption experiments of two kinds of diblock copolymers with different block lengths. We compare the adsorption of polymers with the same PEO length and a different cationic block length, i.e. $P2MVP_{42}$-PEO_{450} and $P2MVP_{72}$-PEO_{450}, and $PDAEMA_{35}$-PEO_{120} and $PDAEMA_{77}$-PEO_{120}. In both cases a longer cationic block leads to a reduction in the adsorbed amount while the degree of charge compensation is almost unchanged. As predicted by Eq. 1 the grafting density of the neutral block is inversely proportional to the length of the cationic block. Within experimental error, our results definitely support this.

	Ads. Amount (mg/m^2)	Charge compensation (-)	σ_{PEO} (nm^{-2})
$P2MVP_{42}$	18.4	1.50	-
$P2MVP_{42}$-PEO_{205}	25.9	0.90	1.16
$P2MVP_{42}$-PEO_{450}	33.0	0.63	0.81
$P2MVP_{72}$-PEO_{450}	26.2	0.74	0.56
$PDAEMA_{35}$-PEO_{120}	26.4	0.98	1.51
$PDAEMA_{77}$-PEO_{120}	21.6	1.09	0.76

Table 2. Adsorbed amount of indicated diblock copolymer to PAA brushes ($N = 270$, $\sigma = 0.2$ nm^{-2}, pH 6, $c_{KNO3} = 10$ mM) and the resulting PEO grafting density and amount of charge compensation ($\sigma_+N_+ / \sigma_-N_-$). Results are an average of two experiments on two surfaces.

It is also interesting to compare $P2MVP_{42}$, $P2MVP_{42}$-PEO_{205} and $P2MVP_{42}$-PEO_{450}, as in this series of copolymers the size of the neutral block is varied while that of the cationic block is kept the same. In the case of the cationic polymer without neutral block, a degree of charge compensation ($\sigma_+N_+ / \sigma_-N_-$) is found that is much larger than 1. It is known from experiments on polyelectrolyte multilayers [25, specifically for the PAA and P2MVP system] that the adsorption of a polyelectrolyte to a layer of oppositely charged polyelectrolyte usually leads to overcompensation. When a neutral block is attached to the cationic block ($P2MVP_{42}$-PEO_{205}) the degree of charge compensation is reduced to close to 1. However, when the PEO length becomes longer ($P2MVP_{42}$-PEO_{450}) the degree of charge compensation becomes significantly lower. We believe that for such a long chain, the very high pressure in the thick and dense neutral polymer brush is the reason that adsorption of diblock copolymer stops before all charges in the brush have been compensated. This shows that there are limits to how far we can go in multiplying the grafting density of the PAA brush by diblock copolymer adsorption, and that the stoichiometric condition (Eq. 1) is not accurate if the neutral brush density and degree of polymerization exceed a critical value.

Antifouling properties of the zipper brush

The results of antifouling experiments are shown in Table 3. We compare the adsorption of different proteins at pH 6 to a number of different surfaces: a polystyrene surface (PS), a polystyrene surface covered with complex coacervate core micelles (C3M), a polystyrene surface covered with a PAA brush (PAA brush, N = 270, σ = 0.2), and a polystyrene surface covered with an identical PAA brush and adsorbed $P2MVP_{42}$-PEO_{205} (zipper brush).

It is interesting to compare the antifouling properties of our zipper brush with the system described by Brzozowska *et al* [16] of an adsorbed layer of complex coacervate core micelles as this system has many similarities to our system. The used polymers are exactly the same, P2MVP-PEO and PAA, but in the system of Brzozowska *et al* the PAA chains are not grafted to a surface. When PAA and P2MVP complex in the right ratio (complete charge compensation), a polymer rich phase (a complex coacervate) is formed that phase separates. The PEO chain acts as a stop mechanism, thus forming a corona surrounding the complex coacervate core. It is known that when these micelles adsorb they spread over the surface where the polyelectrolyte complex core adsorbs to the surface to form a layer and the PEO chains form a polymer brush layer on top of the polyelectrolyte complex layer. The main difference between this system and ours is the PEO grafting density of the brush. The driving force for the brush formation in the C3M system is the phase separation of the polyelectrolyte complex which is much weaker than the driving force in our system, the formation of the polyelectrolyte complex with the PAA brush. The grafting density of PEO chains for the C3M system on polystyrene is approximately 0.05 nm^{-2} (as calculated from the measured adsorbed amount), thus much lower than the grafting densities reached with the zipper brush approach.

Adsorption of protein to a negatively charged PAA brush can reach very high adsorbed amounts [22 (chapter 6)]. For a number of proteins the adsorption was so high that it becomes hard to measure the exact amount. The only protein in this study that does not adsorb strongly to the PAA brush is β-lactoglobulin, which is negatively charged at pH 6. At this pH BSA is also negatively charged, however it is known to adsorb at the "wrong side" of its iso-electric point. This adsorption has been explained by charge regulation and patchiness.

When P2MVP-PEO is adsorbed to such a PAA brush, forming a high density PEO brush, the protein adsorption is reduced to practically zero for almost all investigated proteins. Of the investigated proteins only cytochrome c adsorbs weakly to the zipper brush. This shows that the zipper brush has very good antifouling properties.

In this investigation we have used a P2MVP-PEO diblock copolymer, thus forming a PEO polymer brush. We already pointed out that by using other neutral polymer blocks in the diblock copolymer one can make different polymer brushes such as poly(acrylamide) brushes or PNIPAM brushes. Thus, if the PEO zipper brush cannot prevent the adsorption of a certain protein, another type of zipper brush could be formed that might work to prevent the adsorption.

	PS [16] (mg/m^2)	C3M [16] (mg/m^2)	PAA brush (mg/m^2)	Zipper brush (mg/m^2)
β-lactoglobulin	0.91	0.45	0	0
BSA	1.21	0.37	25	0.03
Fibrinogen	8.37	3.11	>30	0
Lysozyme	0.47	0	>30	0
Cytochrome c		-	>30	0.8

Table 3. The adsorbed amount of various proteins on a number of different surfaces as indicated, at pH 6 and c_{KNO3} = 10 mM. For the PAA brush N = 270, σ = 0.2 nm^{-2}

Structure of the zipper brush

In Figure 1 we present a cartoon of the most likely structure of the neutral zipper brush: one dense collapsed layer of complex coacervate, covered with a swollen neutral brush. Although in this chapter we present no direct evidence, there is much indirect evidence that this is indeed the formed structure. The strongest indication is that very good antifouling properties are observed for this system. This can only be explained by the existence of a thick neutral polymer brush. Another strong indication is that we find almost complete charge compensation. Complexes of oppositely charged polyelectrolytes are well known to form separate polyelectrolyte-rich phases or even a precipitate close to charge compensation [16]. Thus, after adsorption of the diblock copolymer, the resulting filled PAA brush is definitely expected to collapse to form a dense phase of oppositely charged polyelectrolyte. Atomic force microscopy (AFM) experiments on a dry layer of $P2MVP_{41}$-PEO_{205} adsorbed to a PAA brush (experiments not shown, adsorption at pH 6, N = 270, σ = 0.2) showed a flat layer with a roughness of approximately 3 nm (on a total thickness of approximately 30 nm), thus proving that the polymer is evenly spread over the surface and indeed adsorbs as a flat layer.

Conclusions

In this chapter we present a novel method for the preparation of dense polymer brushes by adsorption. We show that by adsorbing a diblock copolymer of which one block is positively charged and one block is neutral (P2MVP-PEO), to a negatively charged polyelectrolyte brush (PAA) that a layer is formed with very good antifouling properties. Although the structure of this layer has not been investigated, the most likely structure of the layer is depicted in Figure 1: the oppositely charged polyelectrolytes complex to form a neutral layer adjacent to the grafting interface, while the PEO blocks form a dense neutral polymer brush on top of this layer. We have named this type of brush a zipper brush as the brush can easily be formed (zipped on) by adsorption in only a few minutes and can also easily be desorbed (zipped of) by rinsing with either a low pH nonionic surfactant solution, or a solution with high salt concentration.

The charges of the original polyelectrolyte brush are almost completely compensated by the charges of the adsorbed P2MVP. The number of adsorbed diblock copolymers, and thus also the grafting density of the PEO brush resulting from the adsorption, is to a good approximation determined by the ratio of negatively charged groups in the PAA brush divided by the number of charges of the cationic block. This implies that the grafting density of the PEO brush can be controlled by the chain length and grafting density of the PAA brush and by the length of the P2MVP block. In addition, there is a relatively small contribution (2-3 mg/nm^2) independent of these parameters, which is attributed to the adsorption of the diblock copolymer directly to the grafting substrate of the PAA brush. In our investigation the cationic block lengths were always shorter than the chain length of the PAA brush. This means that more than one cationic chain can adsorb per PAA chain, and that the resulting PEO grafting density is a multiplication (by up to a factor of approximately 6) of the original PAA grafting density. Thus, very high PEO grafting densities, up to 1.59 nm^{-2}, could be reached. To our knowledge such high PEO grafting densities have never been reported for such long PEO chains.

As PAA is a weak polyelectrolyte, the adsorption of P2MVP-PEO to such a brush depends strongly on the pH. At low pH when the PAA is uncharged, only a few mg/m^2 adsorb, presumably because of hydrogen bonding between uncharged PAA and PEO. As the pH increases the PAA becomes increasingly charged and the adsorbed amount of diblock copolymer grows strongly until pH 6. Between pH 6 and pH 10 there is only a small increase of adsorbed amount showing that at pH 6 the PAA is already almost completely dissociated after complexation with P2MVP. At pH 6 and 10 high salt concentrations (above 250 mM) are needed to significantly reduce the adsorbed amount. Adsorption of PDMAEMA-PEO shows exactly the same trend with pH as the adsorption of

P2MVP-PEO up to pH 9. Above pH 9 PDMAEMA, being a weak base, becomes uncharged and at pH 10 almost no adsorption is measured. PDMAEMA-PEO block copolymers that have been adsorbed at lower pH are almost completely washed away upon increasing the pH to 10.

In short, the zipper brush method allows to quickly switch between different types of brushes and to control the grafting density and chain length by choosing the right diblock copolymer. The conditions which trigger adsorption and desorption of the zipper brush can be varied by using chemically different polyelectrolytes. Very high grafting densities and very good antifouling properties can be achieved for a neutral (PEO) zipper brush.

References

1. Currie, E.P.K., Norde, W.; Cohen Stuart, M.A. *Adv. Colloid Interface Sci.***2003,** *100-102,* 205.
2. Milner, S.T. *Science* **1991,** *251,* 905.
3. Birschtein, T.M.; Amoskov, V.M. *Polymer Science Ser. C* **2000,** *42,* 172.
4. Zhao, B.; Brittain, W.J. *Prog. Polym. Sci.* **2000,** *25,* 677.
5. Advincula, R.C., Brittain, W.J., Caster, K.C.; Rühe, J. *Polymer Brushes,* **2004,** Wiley-VHC, Weinheim.
6. Rühe, J., Ballauff, M., Biesalski, M., Dziezok, P., Gröhn, F., Johannsmann, D., Houbenov, N., Hugenberg, N., Konradi, R., Minko, S., Motornov, M., Netz, R.R., Schmidt, M., Seidel, C., Stamm, M., Stephan, T., Usov, D.; Zhang, H. *Adv. polym. Sci.* **2004,** *165,* 79.
7. Edmondson, S., Osborne, V.L.; Huck, W.T.S. *Chem. Soc. Rev.* **2004,** *33,* 14.
8. Tsujii, Y., Ohno, K., Yamamoto, S., Goto, A.; Fukuda, T. *Adv. Polym. Sci.* **2006,** *197,* 1.
9. Auroy, P.; Auvray, L.; Leger, L. *Macromolecules* **1991,** *24,* 2523.
10. Tran, Y.; Auroy, P.; Lee, L.-T. *Macromolecules* **1999,** *32,* 8952.
11. Maas, J.H.; Cohen Stuart, M.A.; Sieval, A.B.; Zuilhof, H.; Sudhölter, E.J.R. *Thin Solid Films* **2003,** *426,* 135.
12. Marra, J.; Hair, M.L. *Colloids and Surfaces* **1988,** *34,* 215.
13. Watanabe, H.; Tirell, M. *Macromolecules* **1993,** *26,* 6455.
14. Maas, J.H.; Cohen Stuart, M.A.; Fleer, G.J. *Thin solid films* **2000,** *358,* 234.
15. van der Burgh, S.; Fokkink, R.; de Keizer, A.; Cohen Stuart, M.A.; *Coll. Surf. A.* **2004**, *242,* 167.
16. Brzozowska, A.M.; Hofs, B.; De Keizer, A.; Fokkink, R.; Cohen Stuart, M.A.; Norde W. *Coll. Surf. A. 2009*, doi:10.1016/j.colsurfa.2009.03.036.
17. Bungenberg de Jong, H.G.; In *Colloid Science volume II*, Elsevier, Amsterdam, **1949**.
18. Voets, I.K.; de Vos, W.M.; Hofs, B.; de Keizer, A.; Cohen Stuart, M.A. *J. Phys. Chem. B* **2008**, *112*, 6937.
19. Voets, I. K.; de Keizer A.; de Waard P; Frederik, P.M.; Bomans, P. H. H.; Schmalz, H.; Walther, A.; King, S. M.; Leermakers, F. A. M.; Cohen Stuart, M. A.; *Angew. Chem. Int. Ed.*, Supporting information, **2006,** *45*, 6673
20. Currie, E.P.K.; Sieval, A.B.; Avena, M.; Zuilhof, H.; Sudhölter, E.J.R.; Cohen Stuart, M.A. *Langmuir* 1999, *15,* 7116.
21. Gaines, G.L. *Insoluble monolayers at liquid gas interfaces* **1966,** Wiley-Interscience, New York.
22. de Vos, W.M.; Biesheuvel, P.M.; de Keizer, A.; Kleijn, J.M.; Cohen Stuart, M.A. *Langmuir* **2008**, *24*, 6575.
23. Dijt, J.C.; Cohen Stuart, M.A.; Hofman, J.E.; and Fleer, G.J. *Colloids and surfaces* **1990,** *51,* 141.
24. Lutkenhaus, J.L.; Mcennis, K.; Hammond, P.T. *Macromolecules* **2007,** *40,* 8367.
25. Kovacevic, D.; van der Burgh, S.; de Keizer, A.; Cohen Stuart, M.A. *J. Phys. Chem. B* **2003,** *107,* 7998.
26. Zdyrko, B.; Klep, V.; Luzinov, I. *Langmuir* **2003**, *19,* 10179.

Part 2: Brushes and Particles

Chapter 4

A simple model for particle adsorption in a polymer brush.

Abstract

This chapter acts as an introduction to the theoretical approaches found in this thesis. We present a simple model to describe particle adsorption in a polymer brush. The presented box-model combines a simple free energy description of a monodisperse brush, with a Langmuir-type model to describe adsorption of particles. When there is no attraction between the particle and the polymer chains, the brush acts as a barrier for the particles to reach the grafting interface. For the situation that there is an attraction between the polymeric brush chains and the particle, particles are found to adsorb. A maximum in the adsorbed amount is then predicted as a function of grafting density, while the adsorbed amount is predicted to be linearly dependent on the chain length. These model predictions are in full agreement with the results of experiments and more sophisticated models.

Introduction

Theoretical approaches have always played an important role in the investigation of polymer brushes [1-4]. This started with the work of Alexander [5], who was the first to use a so-called box model. A model for the polymer brush in which all chains are assumed to stretch exactly the same amount, up to a certain height (H) above the grafting interface. De Gennes [6] build upon this model and derived simple scaling laws for the brush height as a function of the main brush parameters: the grafting density (σ) and the chain length (N). For different solvent qualities, these scaling laws are:

$$\begin{aligned} H &\sim \sigma^{1/3} N \quad \text{(Good Solvent)} \\ H &\sim \sigma^{1/2} N \quad \text{(Theta Solvent)} \\ H &\sim \sigma N \quad \text{(Poor Solvent)} \end{aligned} \qquad [1]$$

In later years, the assumption of similarly stretched chains was found to be a serious oversimplification. More sophisticated models were introduced that allowed for the chain ends to distribute throughout the entire brush, in that way allowing the polymer chains to be unequally stretched. With these so-called self-consistent field models [7-9] it was shown that for a homodisperse polymer brush a parabolic density profile is expected (see for example Chapter 1, Figure 4). Still, these models as well as experimental results [10-11] recovered the Alexander-de Gennes scaling laws (eq. 1).

Many theoretical studies have focused on investigating the interaction between polymer brushes and particles. This is not surprising as these interactions are important for the main application of polymer brushes: antifouling. In an early study Jeon *et al* [12-13] predicted that for antifouling purposes, there are different optimal grafting densities depending on the size of the particle. That the size of the particle is important was also predicted by Subramanian *et al* [14] and Steels *et al* [15]. They showed that small particles (with respect to the grafting density) can penetrate a brush layer, whereas large particles can only compress the brush layer. These small penetrating particles can naturally also adsorb to the polymer chains in the brush, in case there is sufficient attraction between the two. Currie *et al* [16] and Halperin *et al* [17] investigated this type of brush-particle interactions, to find that a maximum in the adsorbed amount is to be expected as function of grafting density. At low grafting densities, an increase in the density leads to an increase in the number of binding sites and thus to a higher adsorbed amount. At high enough grafting densities the adsorption levels off because particles are pushed out of the polymer brush because of volume exclusion.

This chapter is intended to act as an introduction to the theoretical brush-particle investigations in this thesis (Chapters 5-7, 9). We build up a simple model to describe the

adsorption of small particles to the polymer chains in a brush. For the brush we use a simple description of the free energy, and assume all polymer chains to be equally stretched (a box model). The adsorption of particles to the polymer chains is described using a Langmuir-type approach. We show results for particles of different size, and for different polymer-particle interaction energies as a function of grafting density and chain length.

Theory and results

To illustrate the theoretical work that has been done with respect to polymer brushes we will introduce a simple model to describe the adsorption of particles to a polymer brush. The aim is to give some insight in the approximations commonly made in such models, to show which forces are believed to play a role in these systems, and to present some typical properties of the brush that have been found in theoretical investigations over the years. First, we will first describe a model for the polymer brush, then a model for adsorption to a solid surface, and next combine these two to describe particle adsorption in a polymer brush.

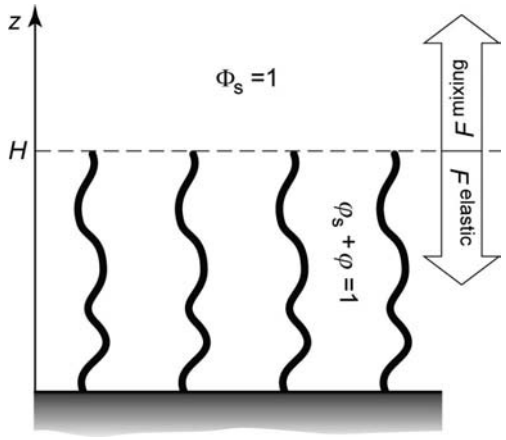

Figure 1. Schematic depiction of the so-called Alexander-de Gennes box model, or simply the box model for a polymer brush. All polymers in the brush stretch to exactly the same degree and thus all chain ends are found at the same distance from the grafting interface: the height of the brush (H). The height of the brush is determined by a balance between two opposing forces: the osmotic force and the elastic force.

The brush

We consider a polymer brush with a certain chain length N and grafting density σ grafted to a non-interacting surface and in contact with a bulk solution. In the bulk solution the volume fraction of solvent molecules is unity ($\Phi_s = 1$). In the brush, the volume fraction of polymer, φ, and of solvent, φ_s will always add up to 1:

$$\varphi_s + \varphi = 1 \qquad [2]$$

Furthermore, we use a so-called box model, meaning that we assume that all polymers stretch in exactly the same way and thus that all end-points are at a certain distance from the surface H. The starting point for the box model is the free energy F^{total} per chain (in units of k_BT). The equilibrium state of the system follows from the minimum in the free energy. F^{total} is given by

$$F^{total} = F^{elastic} + F^{mixing} + \left(F^{solvent}\right) \qquad [3]$$

The first term in Eq. 3 gives the free energy of stretching of the polymer chains in the brush. Here we use the Gaussian chain model

$$F^{elastic} = \frac{3}{2}\frac{H^2}{N} \qquad [4]$$

The Gaussian model treats the polymer chain as a spring. Any deviation from the equilibrium state of the polymer at very low grafting densities (a polymer coil, see also Chapter 1, Figure 1a) leads to an increase in the free energy, and thus to an elastic force (the derivative of the free energy with respect to the distance gives a force) counteracting the deviation.

The second contribution to the free energy corresponds to the mixing of the solvent with the polymer in the brush. This is calculated by taking the entropy of a solvent molecule in the brush and subtracting the entropy of a solvent molecule in bulk solution

$$F^{mixing} = \frac{H}{\sigma}\left[\varphi_s \ln \varphi_s - \varphi_s \ln \Phi_s\right] = \frac{H}{\sigma}\left[\varphi_s \ln \frac{\varphi_s}{\Phi_s}\right] \qquad [5]$$

Here the mixing entropies are multiplied by a factor of H/σ, which gives the volume of the brush per chain. Mixing is entropically favorable, hence, the more mixed the solvent and the brush are (the closer φ_s is to Φ_s) the lower the free energy will be. The derivative of Eq. 5 gives the osmotic force of the solvent. In Figure 1 we schematically show how F^{elastic} and F^{mixing} affect properties of the brush such as height and polymer density. F^{elastic} and F^{mixing} represent opposing contributions to the free energy (and thus opposing forces). It is

entropically favorable for the solvent to mix with the brush, leading to stretching of the polymers. On the other hand it is entropically unfavorable for the polymer chains to stretch. These opposing contributions to the free energy will lead to a certain equilibrium height and polymer density of the brush. We can find this equilibrium by finding the minimum in the free energy. A simple scaling law is obtained if we assume low polymer densities ($\ln(1-\varphi) \approx -\varphi$), when we realize that φ is directly related to H ($\varphi = N\sigma/H$), and (to find the minimum in the free energy) when we take the derivative of the free energy equation with respect to the height to be zero:

$$\frac{\delta F^{total}}{\delta H} = \frac{\delta(\frac{3}{2}\frac{H^2}{N} + \frac{H}{\sigma}(\varphi - \varphi^2))}{\delta H} = \frac{\delta(\frac{3}{2}\frac{H^2}{N} + N + \frac{\sigma N^2}{H})}{\delta H} = \frac{6}{2}\frac{H}{N} - \frac{N^2\sigma}{H^2} = 0$$

$$\longrightarrow \quad H \sim N\sigma^{1/3} \qquad [6]$$

As can be seen, for low polymer densities we recover the famous scaling law of Alexander and de Gennes (Eq. 1) for the height of a polymer brush in a good solvent.

The third (optional) term for the free energy equation is the quality of the solvent. The interaction between solvent and polymer are taken into account in the following way

$$F^{solvent} = \frac{H}{\sigma}\left[\varphi\varphi_s\chi\right] \qquad [7]$$

Here χ describes the net interaction between the solvent and the polymer. If $\chi < 0.5$ then contact between the polymer and solvent is favorable and we say that (for the polymer) the solvent is a good solvent. In the case that $\chi > 0.5$, the solvent is a bad solvent. At $\chi = 0.5$ we call the solvent a theta solvent. The $\varphi\varphi_s$ term is a measure for the probability of making a polymer-solvent contact. Just as in Eq. 5 we add the term H/σ, which gives the brush volume per polymer chain.

In Figure 2 we present results of our model. In Figure 2a we show the height of the brush as a function of the grafting density for different solvents. Here the effect of the solvent quality is clear: if the polymer is dissolved in a good solvent ($\chi < 0.5$) there will be an additional driving force for the polymer chain to mix with the solvent, thus leading to an increase in H. If we have a poor solvent for the polymers ($\chi > 0.5$), mixing is less favorable and H will decrease. In the case $\chi = 1$ this effect is so strong that the brush contains very little solvent. In Figure 2a we also show how well the results of the full model compare with the predictions of the Alexander-de Gennes scaling laws (Eq. 1) for the different solvent qualities. We observe that the scaling laws work well for low grafting densities, but

that at higher grafting densities (> 0.1) the full model deviates from the scaling laws. At these grafting densities, we can no longer assume low polymer densities (as in Eq. 6).

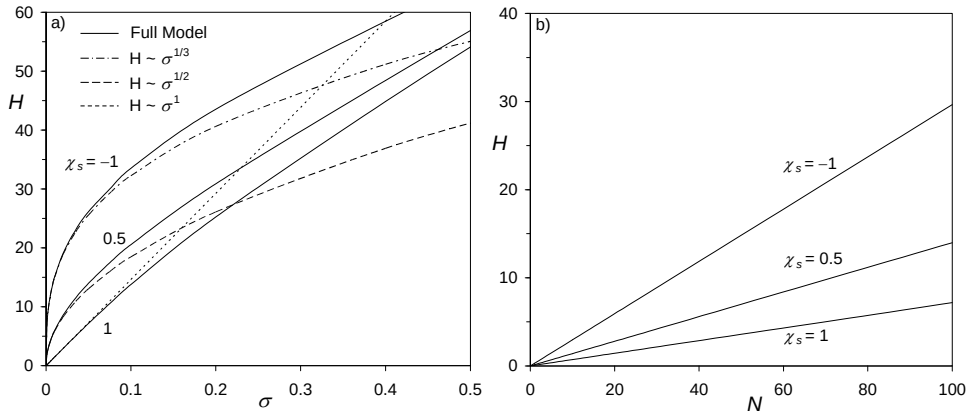

Figure 2. The height (H) of a polymer brush for different interactions between brush and solvent as indicated, a) as a function of grafting density (N=100), b) as a function of chain length (σ = 0.05).

In Figure 2b we show the height as a function of chain length for three different solvent qualities. Again a negative value of χ leads to an increase in brush height while a positive χ leads to a decrease in the brush height. The scaling law $H \sim N$ is valid for all conditions.

Langmuir adsorption

Adsorption from solution is an exchange process. In the case of a solution of particles, in contact with an interface, either the particle or solvent molecules will occupy a given adsorption site on the interface. Since there is only a limited number of adsorption sites, we can discuss adsorption as the fraction of sites occupied by a particle (segment), α, and the fraction of adsorption sites occupied by a solvent molecule, $1-\alpha$. The maximum adsorption, Γ^{max}, is reached when $\alpha = 1$. Γ^{max} is equal to the total number of adsorption sites per unit area and thus the adsorbed amount can be calculated from $\Gamma = \alpha\Gamma^{max}$. Here we model a surface in contact with a bulk solution containing a certain volume fraction of solvent molecules (Φ_s) and a volume fraction of particles (Φ_p, ($\Phi_s + \Phi_p = 1$)). The particles have a volume of N_P times the volume of a solvent molecule. We investigate the fraction of adsorption sites occupied by a particle segment (α). We will describe this adsorption by using a description of the free energy

$$F^{total} = F^{adsorption} + F^{mixing} \qquad [8]$$

The first term describes the energy gain upon adsorption per adsorption site

$$F^{adsorption} = \alpha U \qquad [9]$$

Here U is the net adsorption energy in units $k_B T$. Clearly, the maximum adsorption energy is reached when $\alpha = 1$, and thus when all adsorption sites are occupied by an adsorbed particle (segment).

Upon adsorption of a particle or a solvent molecule, it loses its mixing entropy in solution, but gains a mixing entropy on the interface. This is described by the second term in Eq. 8:

$$F^{mixing} = \frac{\alpha}{N_p} \ln \frac{\alpha}{\Phi_p} + (1-\alpha) \ln \frac{1-\alpha}{1-\Phi_p} \qquad [10]$$

Here N_P represents the size of the particle with respect to the size of a solvent molecules. Thus, if $N_P = 1$, the size of a particle is the same as that of a solvent molecule. We can now see that adsorption is a balance between F^{mixing} and $F^{adsorption}$. For F^{mixing} we find the minimum in the free energy for $\alpha = \Phi_P$, any deviation from ($\alpha > \Phi_P$ or $\alpha < \Phi_P$) leads to a decrease of entropy and is thus unfavorable. However, in the case that U is not 0, $F^{adsorption}$ will be minimal for deviations that are as large as possible (For U is negative $\alpha > \Phi_P$, For U is positive $\alpha < \Phi_P$).

Optimization of the free energy of Eq. 8 with respect to α gives a Langmuir-type adsorption equation:

$$\frac{\alpha}{(1-\alpha)^{N_p}} = \frac{\Phi_p}{\left(1-\Phi_p\right)^{N_p}} e^{-UN_p} \qquad [11]$$

For $N_p = 1$, this equation becomes the classical Langmuir equation which is easy to solve. In Figure 3a we show the results for a number of different adsorption energies (U). At two points all curves coincide, at $\Phi_P = 0$ and at $\Phi_P = 1$. Clearly, if there are no particles in solution, the fraction of occupied surface sites can only be zero while if there are only particles in solution, the fraction of occupied surface sites must be 1. For the case that there is no net attraction or repulsion between the interface and the particles ($U = 0$), there is no preference for either the solvent or the particles to adsorb and the fraction of occupied surface sites will simply be equal to the fraction of particles in solution. In case of attraction (negative U), α will be higher than the volume fraction in solution while for repulsion it is the other way around. For higher values of U (plus or minus) this effect is more pronounced.

There are two concentration regimes which are important to discuss here: the Henry regime, and the high-affinity regime. The Henry regime is the concentration regime at which α is proportional to the particle concentration in solution (thus, $\alpha = K\Phi_p$, where K is a constant). The size of this concentration regime strongly depends on the value of U and is especially small for strong attraction. The second regime, the high-affinity regime is only found in case of strong attraction (In Figure 3a for $U = -5$). In this concentration regime the value of α, and thus the adsorbed amount becomes almost independent of Φ_p, as even at low particle concentrations nearly all adsorption sites are occupied by adsorbed particles.

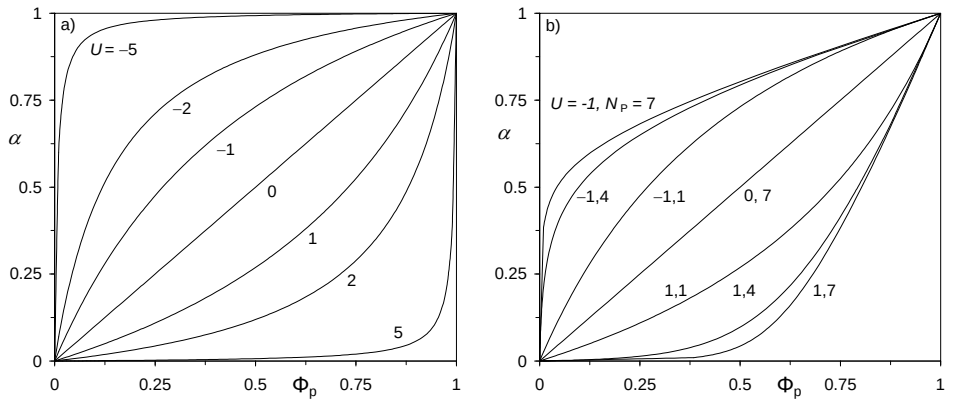

Figure 3. The fraction of adsorbed particles (α) as a function of the bulk particle concentration (Φ_P) a) for different adsorption energies (U), and b) for particle sizes (N_P) and adsorption energies (U) as indicated.

In Figure 3b, we look at the effect of the particle size. For $U = 0$ we again find that $\alpha = \Phi_p$, independent of the particle size (N_P). However, in the case of either a net attraction or repulsion, a larger particle size leads to an enhanced effect in the adsorption. This is a matter of entropy: for a particle larger than $N_P = 1$, the adsorption energy (attraction or repulsion) will be similarly larger, while the (translation) entropy of the particle (in solution and at the interface) does not depend on its size.

Adsorption in a brush

By combining the above model for the polymer brush with the described model for adsorption to a flat surface, we can now make a model to describe the adsorption of particles in a polymer brush. A bulk solution containing particles and solvent ($\Phi_s + \Phi_p$) is in contact with a polymer brush. Each polymer segment provides one adsorption site for a particle (or particle segment). The volume of a polymer segment is equal to that of a solvent molecule, while the volume of the particle is N_P times that of a solvent molecule. In the brush there is a volume fraction of polymer, φ, of solvent φ_s, of non-adsorbed particles φ_p and a fraction of adsorbed particles α, of which the volume fraction is $\alpha\varphi$. The incompressibility constraint in the brush thus becomes

$$\varphi + \varphi_s + \varphi_p + \varphi\alpha = 1 \qquad [12]$$

We now write for the free energy of one polymer chain

$$G = F^{elastic} + F^{adsorption} + F^{mixing} \qquad [13]$$

Here we leave out (for the sake of simplicity) the solvent quality expression (Eq. 7) and thus we assume that there is no interaction between polymer and solvent apart from the excluded volume interaction ($\chi = 0$).

For the first term we use the Gaussian elasticity term as given in Eq. 5. For the second term we use a modification of Eq. 10, as we now express the adsorption energy per polymer chain (instead of per binding site). We write:

$$F^{adsorption} = \alpha UN \qquad [14]$$

The third term, describing all the mixing entropies in the system becomes a combination of Eqs. 5 and 10. With respect to Eq. 10, a similar adjustment is needed as for Eq. 9. In addition we do not only take into account the mixing entropy of the solvent (Eq. 5) but also that of the particles. The mixing term is then given by:

$$F^{mixing} = N\left[\frac{\alpha}{N_p}\ln\frac{\alpha}{\varphi_p} + (1-\alpha)\ln\frac{1-\alpha}{1-\varphi_p}\right] + \frac{H}{\sigma}\left[\frac{\varphi_p}{N_p}\ln\frac{\varphi_p}{\Phi_p} + \varphi_s\ln\frac{\varphi_s}{\Phi_s}\right] \qquad [15]$$

This model is sufficient to describe the adsorption of particles to a polymer brush. We use the so-called excess adsorption which gives the number of particle segments in the brush per unit surface area in excess of the bulk contribution:

$$\Gamma = H\left[\varphi_p + \alpha\varphi - \Phi_p\right] \qquad [16]$$

Thus, a positive excess adsorption means that the particle density inside the brush (adsorbed and non-adsorbed particles) is larger than the density in bulk solution. Accordingly, a negative Γ means that the particle density inside the brush is lower than outside the brush; in that case the brush acts as a depletion layer for the particles.

In Figure 4 we show results of our model for the adsorption as a function of grafting density and as a function of chain length for different values of *U*. For $U = 0$ only negative adsorption is found, showing that the polymer brush indeed keeps away particles from the surface due to excluded-volume effects. However, if there is an attraction between the brush polymers and the particles this effect can be lost and for sufficiently negative values of *U* accumulation of particles in the brush is expected. In Figure 4a we show that this is strongly dependent on the grafting density of the brush. In case of attraction ($U = -0.5, -1$) we find that there is a maximum in the adsorbed amount as a function of grafting density. At low grafting densities, a higher density leads to more available adsorption sites and thus to an increase in the adsorbed amount. However, the increasing polymer density also leads to more excluded volume and at higher grafting densities, the particles are forced out of the brush. This maximum in the adsorbed amount as a function of grafting density is a result that has been theoretically predicted [16,17] and has also been found experimentally [16,18].

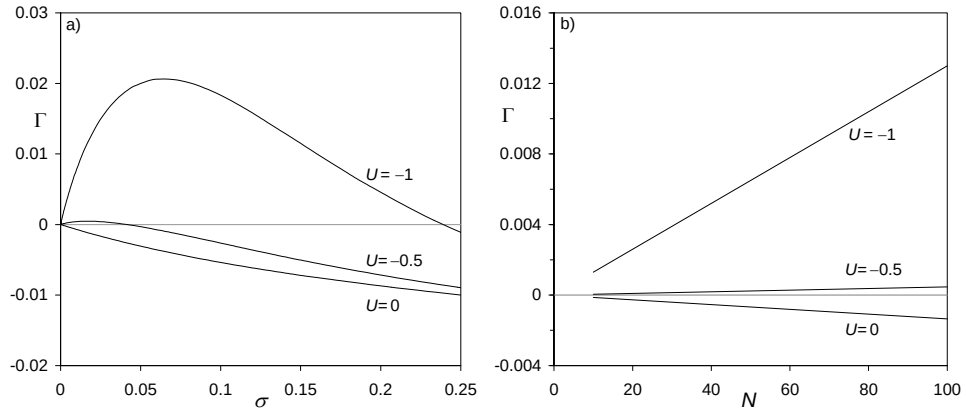

Figure 4. The adsorbed amount (Γ, in particle segments per unit surface area) for different adsorption energies as indicated ($\Phi_P = 0.001$). a) As a function of grafting density ($N = 100$). b) As a function of chain length ($\sigma = 0.025$).

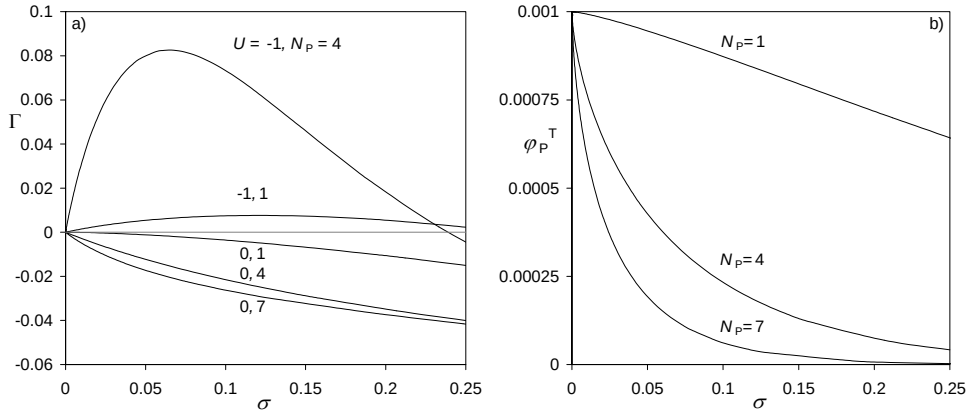

Figure 5. a) The adsorbed amount as a function of grafting density for different particle sizes and adsorption energies as indicated (N = 100, Φ_P = 0.001). b) The total particle density as a function of grafting density for different particle sizes as indicated (N = 100, Φ_P = 0.001).

In Figure 4b it is shown that the adsorption increases or decreases linearly with chain length (N) depending on U. In this model the height of the brush is proportional to the chain length ($H \sim N$). This means that while the chain length strongly affects the height of the brush, all other parameters (α, φ, φ_P) remain the same. In a brush with a higher chain length, the brush height will be equally higher and thus the adsorbed amount will proportionally change ($\Gamma \sim N$).

In Figure 5a we show the effect of the particle size on the adsorbed amount. Similar to the results of Figure 3b we see that for larger particles we find more extreme results. In the case of $U = -1$ a larger particle size leads to far more adsorption, but at high grafting densities this is no longer the case and the adsorbed amount actually becomes smaller. Thus, larger particles are more affected by the grafting density of the brush. This we can clearly see for the case of $U = 0$: the larger the particle the more negative the adsorbed amount becomes. Thus, the antifouling properties of a brush, in the case of no attraction between particle and polymer, are much better for larger particles. This is further illustrated by Figure 5b in which we show the total volume fraction of particles in the brush (adsorbed and non-adsorbed particles, $\varphi_P^T = \varphi_P + \alpha\varphi$) as a function of grafting density. At very low grafting densities φ_P^T is almost equal to the bulk volume fraction of particles ($\Phi_P = 0.001$), but with increasing grafting density φ_P^T decreases. For larger N_P this effect is much stronger and for $N_P = 7$, the particle concentration decreases to almost 0. For $N_P = 7$, at $\sigma = 0.25$ the

total particle concentration in the brush is a factor of 10^4 lower than the particle concentration in bulk.

Conclusions

The adsorption of small particles to the polymer chains in a brush is described by a simple model. For a particle solution in contact with a polymer brush we expect, if there is no attraction between particles and polymers, that the brush acts as a barrier for the particles to reach the grafting interface. Because of the excluded volume in the brush, the particle concentration in the brush will be lower than the particle concentration in bulk. This effect is stronger for larger particles and higher grafting densities. In the case that there is an attraction between polymer and particle, accumulation of particles in the brush becomes possible and a maximum in the adsorbed amount will be found as a function of grafting density. At low grafting densities, increasing σ leads to a higher adsorbed amount due to an increase in the number of adsorption sites. However, at higher grafting densities the adsorbed amount decreases again due to the increasing excluded volume in the brush. The adsorbed amount is expected to be linearly dependent on the chain length, as the chain length affects only the height of a brush and no other parameters.

References

1. Currie, E.P.K.; Norde, W.; Cohen Stuart, M.A. *Adv. Colloid Interface Sci.* **2003**, *100-102*, 205.
2. Szleifer, I.; Carignano, M.A. *Adv. Chem. Phys, volume XCIV* **1996**, *94*, 165.
3. Birschtein, T.M.; Amoskov, V.M. *Polymer Science Ser. C* **2000**, *42*, 172.
4. Milner, S.T. *Science* **1991**, *251*, 905.
5. Alexander, S. *J. Phys. (Paris)* **1977**, *38*, 983.
6. de Gennes, P.G. *Macromolecules* **1980**, *13*, 1069.
7. Semenov, A. N. *Sov. Phys. JETP* **1985**, *61*, 733.
8. Milner, S.T.; Witten, T.A.; Cates, M.E. *Macromolecules* **1988**, *21*, 2610.
9. Zhulina, E.B.; Priamitsyn, V.A.; Borisov, O.V. *Polymer Science USSR* **1989**, *31*, 205.
10. Currie, E.P.K.; Wagenmaker, M.; Cohen Stuart, M.A.; van Well, A.A. *Physica B* **2000**, *283*, 17.
11. Auroy, P.; Auvray, L.; Leger, L. *Macromolecules* **1991**, *24*, 2523.
12. Jeon, S.I.; Lee, J.H.; Andrade, J.D.; de Gennes, P.G. *J. Coll. Int. Sci.* **1991**, *142*, 149.
13. Jeon, S.I.; Andrade, J.D. *J. Coll. Int. Sci.* **1991**, *142*, 159-166.
14. Subramanian, G.; Williams, D.R.M.; Pincus, P.A. *Macromolecules* **1996**, *29*, 4045.
15. Steels, B.M.; Koska, J.; Haynes, C.A. *J. Chromatography B* **2000**, *743*, 41.
16. Currie, E.P.K.; van der Gucht, J.; Borisov, O.V.; Cohen Stuart, M.A. *Pure Appl. Chem.* **1999**, *71*, 1227.
17. Halperin, A.; Fragneto, G.; Schollier, A.; Sferrazza, M. *Langmuir* **2007**, *23*, 10603.
18. Gage, R.A.; Currie, E.P.K.; Cohen Stuart, M.A. *Macromolecules* **2001,** *34*, 5078.

Chapter 5

Adsorption of anionic surfactants in a nonionic polymer brush: experiments, comparison with mean-field theory and implications for brush-particle interaction.

Abstract

The adsorption of the anionic surfactants sodium dodecyl sulphate (SDS) and sodium dodecyl benzene sulphonate (SDBS) in poly(ethylene oxide) (PEO) brushes was studied using a fixed-angle optical flow-cell reflectometer. We show that just as in solution there is a critical association concentration (CAC) for the surfactants at which adsorption in the PEO brush starts. Above the critical micelle concentration (CMC) the adsorption is found to be completely reversible. At low brush density the adsorption per PEO monomer is equal to the adsorption of these surfactants in bulk solution. However, with increasing brush density the number of adsorbed surfactant molecules per PEO monomer decreases rapidly. This decrease is explained in terms of excluded volume interactions plus electrostatic repulsion between the negatively charged surfactant micelles. Experimentally, a plateau value in the total adsorption is observed as a function of grafting density. The experimental results were compared to the results of an analytical self-consistent field (aSCF) model and we find quantitative agreement. Additionally, the model predicts that the plateau value found is in fact a maximum. Both experiments and model calculations show that the adsorption scales directly with the polymerization degree of the polymers in the brush. They also show that an increase in the ionic strength leads to an increase in the adsorbed amount, which is explained as being due to a decrease in the electrostatic penalty for the adsorption of the SDS micelles. The adsorption of SDS micelles changes the interactions of the PEO brush with a silica particle. This is illustrated by AFM measurements of the pull-off force of a silica particle from a PEO brush: at high enough PEO densities, the addition of SDS leads to a very strong reduction in the force necessary to detach the colloidal silica particle from the PEO brush. We attribute this effect to the large amount of negative charge incorporated in the PEO brush due to SDS adsorption.

A manuscript based on this Chapter has been accepted for publication in Langmuir.

Introduction

The interaction between polymers and surfactants is a phenomenon which has been widely investigated for many decades [1-5]. It is a very interesting phenomenon, not only from a fundamental point of view, but also because of the wide range of applications in cosmetics, paints, detergents, foods, and formulations of drugs and pesticides [1]. The polymer most investigated is polyethylene oxide (PEO), and over the years its interaction with anionic, nonionic, and cationic surfactants has been thoroughly examined [1-5]. A general conclusion is that anionic surfactants such as sodium dodecyl sulphate (SDS) and sodium dodecyl benzene sulphonate (SDBS) interact strongly with the polymer. They bind to PEO only in the form of micelles, while association takes place beyond a concentration known as the critical association concentration (CAC). Above the CAC the polymer provides a nucleation site for micelle formation [2] and thus the CAC is always lower than the critical micellar concentration (CMC). In contrast, cationic surfactants and nonionic surfactants show very little interaction with PEO except at elevated temperatures [6].

For many of the applications mentioned above the interfacial aspects are very important. Therefore, many studies have been devoted to investigating the polymer-surfactant interactions on and with interfaces [1,7,8]. Non-interacting polymers and surfactants such as PEO and nonionic surfactants are often found to be competitive in their adsorption to an interface [9]. In contrast, strongly interacting polymer-surfactant systems such as PEO and SDS are often found to adsorb to a surface cooperatively [8].

Limited work has been performed on the interaction between surfactants and polymers in very constrained environments such as a dense gel or a polymer brush. A polymer brush can be described as a dense array of polymer chains end-attached to an interface. Alexander and de Gennes [10,11] showed in the late seventies that the chains in these brushes tend to be strongly stretched because of excluded volume interactions between the chains. These excluded volume interactions not only cause the chains to stretch but also oppose penetration into the brush of particles and polymers. A polymer brush that is compressed or otherwise deformed from its equilibrium structure responds with a restoring force [12]. This property has given the polymer brush applications as a steric stabilizer and as an antifouling agent [12,13].

One of the few publications on the interaction between surfactants and polymer brushes comes from Pyshkina *et al* [14]. These authors studied the adsorption of cationic surfactants in anionic polymer brushes. They showed that the adsorption is completely reversible and that the grafting density of the brush has a large influence on the adsorption of the surfactants. At high grafting densities, only about 40% of the counter-ions of the brush are exchanged for surfactant ions. At lower grafting densities, the surfactant adsorption

increases up to a complete exchange. These observations are explained in terms of the bulkiness of surfactant ions and the high excluded volume interactions in these dense brushes.

In a similar study, Konradi and Rühe [15] showed that cationic surfactants bind cooperatively to an anionic polymer brush. Furthermore, they found that the polymer brush shrinks drastically at low surfactant concentration and even collapses at high surfactant concentration. The polymer used for the brush was more hydrophobic than the polymer used by Pyshkina *et al* [14].

Currie *et al* [16] performed a theoretical study on the adsorption of anionic surfactant micelles in a nonionic polymer brush. In their model surfactant micelles are treated as nanoparticles that, upon binding, change the excluded volume properties of the polymer chains. The model predicts a maximum in the adsorbed amount as a function of the grafting density. With increasing grafting density, the amount of polymer to which the surfactants can bind increases, and thus the surfactant adsorption increases as well. At higher grafting densities however, the excluded volume becomes so large that surfactant micelles are pushed out of the brush layer, thus decreasing the adsorption. Some experimental evidence in this direction was found for the case of adsorption of protein molecules [17] and for adsorption of silica nanoparticles [18] in a PEO brush.

In this chapter we present to our knowledge the first experimental results on the interaction between anionic surfactants (SDS and SDBS) and a planar nonionic polymer brush (PEO). Adsorption and desorption are studied real-time as a function of grafting density for three different values of the polymerization degree using a fixed-angle optical flow-cell reflectometer. We compare the experimental results with predictions of a model that includes volume interactions of the surfactant micelles in an analytical self-consistent field theory for brush conformations. We present brush density profiles and density profiles of surfactants adsorbed in the brush layer, and we investigate the influence of salt concentration on the adsorption. As a result of the adsorption of charged surfactants in a neutral polymer brush, the brush acquires a large number of charges and develops polyelectrolyte brush-like properties. We hypothesize that this charging of the brush through surfactant adsorption will have a significant impact on brush-particle interactions. Therefore, we also present results of an investigation of the interaction between a negatively charged silica particle and a PEO brush as a function of SDS concentration by using atomic force microscopy (AFM) force measurements.

Theory

In this section we present the mean-field theory which self-consistently describes brush density profiles as well as the adsorption of micelles in the brush. To describe the brush profile we use the self-consistent-field model in the strong-stretching limit (SCF-SS). Here we use a modification of the more traditional SCF-SS models by using an excess function for volume exclusion effects that is not based on the assumption of a lattice (regular solution theory, Flory-Huggins theory), but on the use of an equation-of-state (EOS) from liquid-state theory that is derived for mixtures of hard spheres of different sizes [19,20], which from comparison with simulations and experiment is known to be very exact [21-25]. This approach has the advantage that the Kuhn length can be varied independently of the monomer size and that it is easy to incorporate the adsorption of particles with sizes that are different from the size of the brush monomers.

In previous work, this approach was successfully applied to describe the adsorption of BSA protein in polyacrylic acid brushes, as a function of pH, ionic strength, and grafting density [26]. More recently it was shown that the same theory could also quantitatively describe results from molecular dynamics simulations for the total polymer density profile and the end-density profiles, for uncharged brushes in the very high grafting density limit, without using any adjustable parameter [27].

To describe the data we require numerical values for: 1. the Kuhn length of the chain, 2. the volume per chain "bead" (the concept of virtual chain 'beads' will be explained below), 3. an attractive nonelectrostatic (e.g., hydrophobic, enthalpic) interaction term χ_{mb} between micelles and chains, and 4. values for SDS micelle size, aggregation number N_{agg}, and charge Z. The latter are taken from literature values for SDS micelles in solution, see section *parameter settings*. We assume that the same values for N_{agg}, Z, and micelle size in solution can also be used in the brush. A nonelectrostatic hydrophobic interaction between brush segments is neglected, as well as between micelles; i.e., only an attraction between brush and micelle is assumed.

Brush conformations

In the following we assume that the brush is monodisperse. In this case the SCF-SS [31,27] model predicts that the polymer segment potential between the edge of the brush and the grafting interface increases in the same way as the stretching potential V. For the stretching potential (per unit chain length) we use the empirical expression [27]

$$V(\mathrm{x}) = 2 \cdot \frac{x^2}{k} \cdot \frac{2 - \frac{4}{5}x^2}{1 - x^2} \qquad [1]$$

which simplifies to the Gaussian expression for low stretching degrees x (x being the height above the grafting interface divided by chain contour length L) [27] which in the limit of a low brush density gives the well-known parabolic brush density profile [31]. Eq. 1 is an empirical expression which very accurately describes full numerical calculations from the SCF-SS model in the finite-stretching limit [27] (i.e. stretching is limited to the contour length [32]). Note that all potentials are scaled to the thermal energy k_BT.

To describe the volumetric interactions between the polymer chains in the brush (and in case of adsorption also between the other species in the brush) we use an expression from liquid-state theory, namely the Boublik-Mansoori-Carnahan-Starling-Leland (BMCSL) equation-of-state [19,20] which accurately describes volumetric and entropic interactions between mixtures of hard spheres of different sizes. This contribution is given by [26,33]

$$\mu_{i,BMCSL}^{ex} = -\left(1+\frac{2\xi_2^3 D_i^3}{\phi^3}-\frac{3\xi_2^2 D_i^2}{\phi^2}\right)\ln(1-\phi)+\frac{3\xi_2 D_i+3\xi_1 D_i^2+\xi_0 D_i^3}{1-\phi} + \frac{3\xi_2 D_i^2}{(1-\phi)^2}\left(\frac{\xi_2}{\phi}+\xi_1 D_i\right)-\xi_2^3 D_i^3\frac{\phi^2-5\phi+2}{\phi^2(1-\phi)^3} \quad [2]$$

where diameters are denoted by D_i, and the parameters ξ_1 and ξ_2 are given by

$$\xi_\alpha = \frac{\pi}{6}\sum_i \frac{\phi_i}{v_i} D_i^\alpha = \sum_i \phi_i D_i^{\alpha-3} \quad , \quad [3]$$

where ϕ is the total volume fraction of all species combined (brush monomers, micelles, ions), v_i the volume of species I, and ϕ_i volume fractions of the individual species. To use this expression for a polymer chain we have shown previously [26,27,35] that an approach in which the brush is considered as a 'chain-of-touching-beads' (beads being spheres) works well. To give this chain the same volume as the 'real' cylindrical polymer chain, the bead size D_b used in the theory must be larger by a factor of $\sqrt{1.5}$ to the cylindrical size of the chain.

Now, one modification must be made to the BMCSL equation because it treats each sphere as a separate object, thus also the virtual beads of the polymer chains. In reality the beads of a polymer chain are connected to one another. To correct for this effect (similar to the neglecting of the ideal entropic contribution of polymer segments for long chains in the Flory-Huggins theory) we exclude the chain beads from the entropic term in the equation-of-state on which μ_{BMCSL}^{ex} is based. (This is done by excluding the 'brush beads' from the term ξ_0, which then only has contributions from ions and micelles. All higher terms, ξ_1 etc., do contain the brush beads.) Making this modification at the level of the expression for the

excess free energy density f (e.g., Eq. A4 in ref.33) results with $\mu_i^{ex}=v_i \cdot df^{ex}/d\phi_i$ in the fact that μ_{BMCSL}^{ex} of Eq. 2 needs to be corrected for mixtures containing polymer chains.

The corrected equation for the brush beads becomes

$$\mu_b^{ex} = \mu_{b,BMCSL}^{ex} - \frac{\phi_b}{1-\phi} + \ln(1-\phi) \qquad [4]$$

and the corrected equation for species other than the brush beads (micelles and ions) becomes

$$\mu_i^{ex} = \mu_{i,BMCSL}^{ex} - \frac{\phi_b}{1-\phi}\alpha_{ib}^3 \qquad [5]$$

where ϕ_b is the brush volume fraction and α_{ib} the size ratio of the inclusion (micelle, ion) over that of the brush beads, $\alpha_{ib} = D_i/D_b$.

At equilibrium, the summation $V(x) + \mu_{brush}(x)$ is independent of height, thus with V increasing with x, the chemical potential of the brush segments, μ_{brush} must decrease. The chemical potential, μ_{brush} has two contributions: μ_b^{ex} and (in case of adsorbing particles) the term μ_b^{att}, which describes the nonelectrostatic attraction between chains and micelles given by

$$\mu_b^{att} \cdot D_b = -v_b \chi_{mb} \phi_m \qquad [6]$$

Note that though the bare brush is uncharged, it is due to the interaction with the charged micelles, that the brush develops a polyelectrolyte character and for instance its profile becomes a function of ionic strength.

Ions and micelles in the brush

For the small ions and the micelles we use equality of chemical potential between each position in the brush and the solution phase where we set the electrostatic potential y to zero. For the ions, chemical equilibrium between the brush (left-hand side) and solution (right-hand side) is given by

$$\ln c_i + z_i y + \mu_i^{ex} = \ln c_{i,sol} + \mu_{i,sol}^{ex} \qquad [7]$$

where c_i is the ion concentration in the brush (in numbers per volume), z_i the charge number of the ion (+1 or –1) and y the dimensionless electrostatic potential in the brush. To describe the entropic and volumetric interactions of ions (and also of the SDS micelles in and outside the brush) we use the BMCSL equation (Eq. 5).

For the SDS micelles, we likewise take chemical equilibrium between each position in the brush phase (left-hand side of Eq. 8) and the solution phase (right-hand side) and we can use

$$\ln \phi_m + Z_m y + \mu_m^{ex} + \mu_{att} = \ln \phi_{m,sol} + \mu_m^{ex} \quad [8]$$

where we have added an attractive term, μ_{att}, namely because of an attractive interaction of micelles with the brush chains, given by

$$\mu_{att} = -v_m \chi_{mb} \phi_b \,. \quad [9]$$

Here v_m is the volume of a micelle, and ϕ_b is the volume fraction of brush segments. We define χ_{mb} as a positive number when we describe an attraction.

To calculate the dimensionless electrostatic potential y at each position x in the brush we assume that local electroneutrality is maintained:

$$Z_m c_m + c_+ - c_- = 0 \quad [10]$$

where $c_m = \phi_m / v_m$ and c_+ and c_- represent the concentration of free cations and anions, respectively.

Overall balances

The dimensionless excess adsorbed amount of SDS (in adsorbed volume per unit surface area) can now be calculated from

$$\Gamma = \int_0^H \left(\phi_m - \phi_{m,sol} \right) dx \quad [11]$$

where $\phi_{m,sol}$ is the SDS volume fraction in free solution, x the dimensionless coordinate perpendicular to the interface, and H the location where the chain ends are located. To obtain the dimensional SDS adsorption in mass/area, Γ is multiplied by the brush chain contour length and by the SDS mass density. The overall brush volume balance is given by

$$\sigma \cdot \frac{v_b}{D_b} = \int_0^H \phi_b \, dx \quad [12]$$

where σ is the grafting density.

Parameter settings

All input parameters, with the exception of the χmb-parameter representing the nonelectrostatic interaction between SDS and PEO, are directly or indirectly based on experimental values as described in literature, and on our experimental conditions. For a

description of the SDS micelles at different salt concentrations we use a fit of data from ref. 36 (for CMC, aggregation number, size), and ref. 37 (charge per micelle). For the frequently used condition of a concentration of added salt $c_{salt,added}$ of 50 mM, the fit-functions result in: N_{agg} = 88.3, Z = 47.1, R = 2.42 nm and CMC = 0.69 g/l. The method that was used to fit these data is described in detail in Appendix A. PEO has a segment length of 0.37 nm (as calculated from known bond angles and lengths) and a hydrated volume per monomer segment of 0.22 nm^3 [38] which translates, together with the segment length, into a cylindrical hydrated diameter of the chain of 0.87 nm. To describe the polymer brush as chains of touching beads [26,27,33,35] we need to multiply the cylinder radius by $\sqrt{1.5}$ resulting in a 'chain of touching beads' of the same volume as the original cylinder. In this way, we arrive at a diameter D_b = 1.066 nm for the polymer chain beads. The Kuhn length of PEO is reported in ref. 39 as k = 0.7 nm; we will use this value in the theory. For the ions in the brush we use the hydrated radius, just as for the brush, which for Na^+, the typical counter-ion in our experiments, is given by D_{ion} = 0.72 nm [40]. The polymerization degree varies in the range N = 148-770, and thus the contour length L is in the range of 55-285 nm. Experimental grafting densities, σ, range from 0.01 to 0.30 nm^{-2}. As it is almost impossible to determine the χ_{mb}-parameter by measurement, this parameter was used as a fitting parameter, taken to be independent of the added salt concentration. Adding charged surfactants to a solution will also influence the salt concentration of the solution. To calculate the solution concentration of anions, $c_{-,sol}$ and cations, $c_{+,sol}$, we include 1. the added monovalent salt, 2. the surfactant molecules which are not micellized (namely, the CMC recalculated to concentration; note that these surfactant molecules are considered as simple anions and included in $c_{-,sol}$, while the counterions are included in $c_{+,sol}$), and finally, 3. the free counterions of the micelles, which are Z free cations per micelle. For the typical condition of $c_{salt,added}$ = 50 mM and 5 g/l overall concentration of SDS, we obtain an anion concentration of $c_{-,sol}$ = 52.4 mM and a cation concentration of 60.3 mM, which together with Z = 47.1 and $c_{micelles}$ = 0.169 mM, closes the charge balance in solution.

Experimental

Preparation of PEO brush layers

PEO brush layers of varying grafting density were prepared by means of a Langmuir-Blodgett (LB) method first described by Currie *et al* [41] and later modified by De Vos *et al* [42 (chapter 2)]. As substrates, flat silicon wafers were used, coated with polystyrene.

The coating of substrates with polystyrene (PS) was done in the following way. First, the silicon wafer (which has a natural SiO_2 layer with a 2-3 nm thickness) was cut into strips (4

cm × 1 cm), rinsed with alcohol and water, and further cleaned using a plasma-cleaner (10 minutes). The strips were covered with a solution of 11 g/l vinyl-PS_{200} (M_n = 19100, M_w/M_n = 1.03, Polymer Source Inc. Montreal/Canada) in chloroform and, after evaporation of the solvent, heated overnight at 150ºC under vacuum. In this way the vinyl-PS_{200} is covalently bound to the Si/SiO_2 surface [42]. Excess vinyl-PS_{200} was washed off with chloroform. The strips were spin-coated using a solution of 13 g/l PS (M_n = 876 kg/mol, M_w/M_n = 1.05, Polymer Source Inc.) in toluene at 2000 rpm for 30 seconds in order to obtain a thicker PS layer (about 90 nm).

For the brush layer transfer, monolayers of PS-PEO block copolymers (PS_{36}-PEO_{148} M_w/M_n = 1.05, $PS_{36}PEO_{377}$ M_w/M_n = 1.03, $PS_{38}PEO_{773}$ M_w/M_n = 1.05, Polymer Source Inc.) at the air-water interface were prepared by dissolving the copolymers in chloroform and spreading these solutions very carefully on water in a Langmuir-trough using a micro syringe. After evaporation of the chloroform, a quick compression-decompression cycle is performed to make sure that any PEO not connected to a PS block is pushed out of the air-water interface and into the solution. Subsequently, the films were compressed to the appropriate surface density and the films were transferred to the substrates in a single passage Langmuir-Blodgett transfer. To obtain a single passage Langmuir-Blodgett transfer a silica strip was slowly transferred through the monolayer and then pulled under the barrier and taken out of the water on the side of the Langmuir-through without a monolayer. For this transfer it was found by De Vos *et al* [42] that only a certain fraction of the PS-PEO polymers is transferred. In other words, the grafting density of PS-PEO on the solid substrate can be quite a bit lower than the PS-PEO grafting density at the air-water interface through which the solid substrate was dipped. The transfer ratio from the air-water interface to the solid substrate depends on the length of the PS block and the length of the PEO block. For the polymers used in this investigation De Vos *et al* [42] found transfer ratio's of 19%, 54%, and 96%, for $PS_{38}PEO_{770}$, $PS_{36}PEO_{377}$, and PS_{36}-PEO_{148} respectively. These transfer ratio's were taken into account to calculate the final grafting densities. The surfaces so prepared were carefully stored in clean water until use. All solvents used were of PA grade (Sigma-Aldrich). All water used was demineralized using a Barnstead Easypure UV and has a typical resistance of 18.3 MΩ/cm.

Reflectometry

The adsorption of surfactants in the PEO brush layers was followed with fixed-angle optical reflectometry using an impinging jet flowcell. A detailed description of the reflectometer setup is provided by Dijt *et al* [44]. It contains a He-Ne laser (monochromatic light, λ = 632.8 nm) with linearly polarized light. Change in polarization is measured by

simultaneously detecting the parallel (R_p) and the perpendicular (R_s) reflectivity and dividing R_p by R_s to give signal S. Before each measurement, the system was calibrated by flushing with solvent to get a stable baseline (S_0) signal. The measurement is started by introducing a surfactant solution into the cell. The change in signal is measured ($\Delta S = S - S_0$) with a sample time of 2 s. The adsorbed amount can be calculated from the normalized ΔS: $\Gamma = Q(\Delta S/S_0)$. Here Q is a sensitivity factor, which depends on the angle of incidence of the laser (θ), the refractive indices (n), the thicknesses (d) of the layers on the silicon wafer, and the refractive index increment (dn/dc) of the adsorbate. To calculate the Q-factor the following values where used: $\theta = 71^{\circ}$, $n_{silica} = 1.46$, $n_{polystyrene} = 1.59$, $\tilde{n}_{silicon,} = (3.85, 0.02)$, $n_{H2O} = 1.33$, $dn/dc_{surfactants} = 0.126$ [45,46], $d_{silica} = 2.0$ nm, $d_{PS} = 90$ nm, $d_{adsorbed\ layer} = 5$ nm. The thickness and refractive index of the polymer brush layer was calculated using an estimate of brush length and average PEO weight density from neutron reflection experiments on brush layers by Currie *et al* [47]. For a grafting density of 0.166 nm^{-2} and a polymerization degree of 700 the brush height was found to be 50 nm. We recalculated this to other grafting densities and polymerization degrees using the well known equation: ($H \sim N\sigma^{1/3}$). This yielded, for all brush densities, a Q-factor close to 71 mg/m^2, and this number was used for all brush densities.

Adsorption experiments (except in Figure 2) of the anionic surfactants were performed well above the CMC (At $c_{NaNO3} = 50$ mM: $CMC_{SDS} = 2.4$ mM, $C_{SDS} = 5$ g/l = 17 mM. At $c_{NaNO3} = 0$ mM: $CMC_{SDBS} = 1.75$ mM. At $c_{NaNO3} = 171$ mM: $CMC_{SDBS} = 0.15$ mM, $C_{SDBS} = 1$ g/l = 2.86 mM. CMC_{SDBS} at 50 mM $NaNO_3$ is not known; from the above numbers we estimate it to be between 0.4 and 0.8 mM.) SDS concentrations used were typically 5 g/l; all SDBS solutions had a concentration of 1 g/l. Salt concentration was typically 50mM of $NaNO_3$. All experiments were performed at room temperature.

Results and Discussion

Adsorption of SDS and SDBS in a PEO brush

Over the years many studies have been devoted to investigate the complexation of anionic surfactants, such as SDS and SDBS, with PEO chains. Similarly much works has been done to investigate the properties of PEO polymer brushes. In this section we combine these two systems and study the adsorption of these anionic surfactants to the polymer chains in a PEO brush. We study the adsorption as a function of surfactant concentration and as a function of typical brush properties such as the grafting density and the chain length.

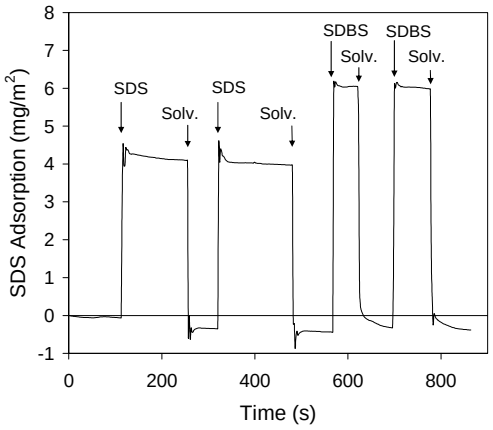

Figure 1. Reflectometry experiment showing the adsorption of SDS (C_{SDS} = 5 g/l) and SDBS (C_{SDBS} = 1 g/l) in a polymer brush (c_{NaNO3} = 50 mM, N = 770, σ = 0.05 nm^{-2}).

In Figure 1 we show a typical (real time) reflectometer result for the adsorption of SDS and SDBS in a PEO brush layer. Different solutions are brought in contact with a PEO grafted polystyrene surface while the adsorbed amount is measured continuously. At the start of the measurement, an electrolyte solution (c_{NaNO3} = 50 mM, pH = 5.8) is applied after which we switch to an SDS solution (C_{SDS} = 5 g/l, c_{NaNO3} = 50 mM, pH = 5.8). After reaching an adsorption plateau, the reversibility of the adsorption is tested by rinsing the interface with the electrolyte solution. This procedure is repeated for SDS and for an SDBS solution (C_{SBDS} = 1 g/l, c_{NaNO3} = 50 mM, pH = 5.8). As can be observed the adsorption and the desorption are both very fast. The adsorption of SDS even shows an overshoot, indicating a relaxation process taking place after adsorption. The adsorption appears (almost) completely reversible. After the first desorption step, the signal reaches a level

below the base-line suggesting a small desorption of PEO chains from the brush layer. However, after the first cycle no further desorption of brush molecules takes place.

In Figure 2 we present results on the adsorption of SDS in a PEO brush with a grafting density of 0.04 nm^{-2} as a function of SDS concentration. At low SDS concentrations (0.1 to 0.3 g/l) only a small amount of SDS adsorbs. This small amount, about 0.5 mg/m^2, is equal to the adsorption that is found on pure PS and thus we expect that at these low concentrations the measured adsorption is purely due to adsorption on the polystyrene substrate and not in the PEO brush. However, when changing from 0.3 g/l to 0.4 g/l we observe a strong increase in the adsorbed amount to about 3 mg/m^2. Thus, just as is found for PEO and SDS in bulk solution [2], there is a critical association concentration (CAC) somewhere between 0.3 and 0.4 g/l. Only beyond this CAC, complexation between SDS and the PEO chains in the brush is found. This CAC is lower than the critical micelle concentration (CMC) which at this salt concentration is approximately 0.7 g/l. As can be seen, for the two concentrations above the CAC and below the CMC (0.4 g/l and 0.5 g/l) the adsorption rate is very slow compared to the adsorption rate observed above the CMC (at 1 g/l, 2.5 g/l and 5 g/l, and also for the data presented in Figure 4). The crucial difference is that below the CMC, the association of monomers has to take place on the PEO chains which can be a slow process, whereas above the CMC micelles are already present in solution. Another difference is that for the SDS adsorption between the CAC and the CMC, the adsorption is not fully reversible. After rinsing with solvent, a residual adsorption of about 0.5 mg/m^2 remains. Above the CMC the SDS adsorption is fully reversible. Furthermore, the residual adsorption that we find after SDS adsorption between the CAC and the CMC and subsequent rinsing with solvent, can be washed away by rinsing with an SDS solution above the CMC (here 1 g/l). We believe that this irreversible adsorption is connected to the observation of Cosgrove *et al* [8], who showed by light scattering experiments that an array of PEO chains, grafted to a silica sphere, decreased significantly in height upon exposure to a SDS solution above the CAC but below the CMC. A collapse of an SDS filled brush, especially on a hydrophobic surface, could well lead to some irreversible behavior.

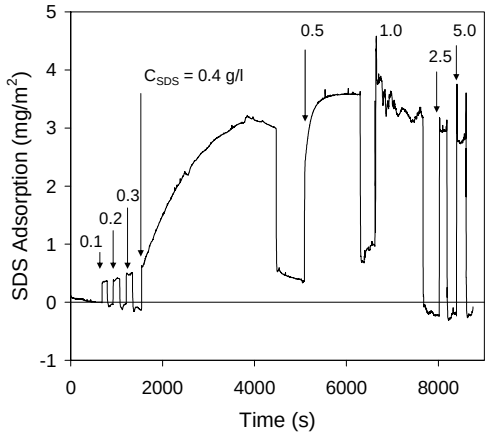

Figure 2. Reflectometry experiment showing the adsorption of SDS (at different SDS bulk concentrations as indicated) in a polymer brush (c_{NaNO3} = 50 mM, N = 770, σ = 0.04 nm^{-2}).

As stated above, at concentrations lower than the CAC (0.1 to 0.3 g/l), a small adsorption of about 0.5 mg/m^2 is observed, which we attribute to adsorption to the polystyrene surface. This means, that for higher SDS concentrations the adsorption of the surfactants onto the surface can be attributed to the sum of adsorption in the PEO polymer brush and adsorption onto the polystyrene surface. For the adsorption of SDBS we found the same effect, and also the same amount of adsorption to the PS surface (0.5 mg/m^2). As we are only interested in the adsorption of SDS and SDBS in the PEO polymer brush, we have corrected our adsorption data in the remainder of the chapter (Figures 3, 4, and 6) by subtracting 0.5 mg/m^2 from the measured values.

In Figure 3 we present results for the equilibrium adsorbed amount of SDS in PEO brushes of different polymerization degrees, *N*, and different grafting densities, σ. At low σ, the adsorption strongly increases with increasing grafting density and polymerization degree. We can expect that the height of the brush increases proportionally with *N*, which then leads to a proportionally larger volume in which SDS adsorption in the PEO brush can take place. As Figure 3b shows, this expectation is borne out by the experiment. With increasing grafting density the brush segment density ϕ_b increases and, as a result, the attractive force for a micelle to enter the brush, see Eq. 9. This increase however, is not proportional with the grafting density. Instead, with increasing grafting density a plateau in adsorbed amount is reached at grafting densities around σ = 0.1 nm^{-2}. For *N* = 148 for which we reach the largest grafting densities, this plateau value remains constant, up until our maximum grafting density of σ = 0.3 nm^{-2}.

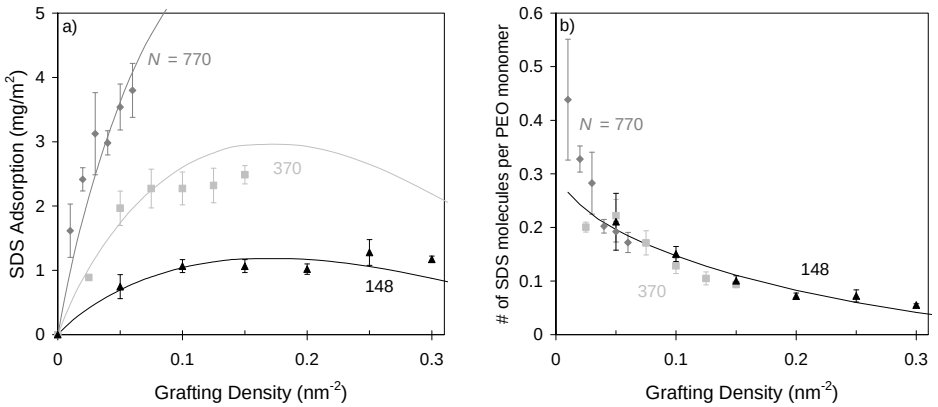

Figure 3. SDS adsorption in PEO brushes for different polymerization degrees, N, as function of grafting density, σ (C_{SDS} = 5 g/l, c_{NaNO3} = 50 mM). (a) Adsorbed amount per unit surface area. (b) Adsorption in number of surfactant molecules per brush monomer. Points show experimental data, curves are results from the aSCF model (χ_{mb} = 13 nm^{-3}).

For all three polymerization degrees, the model lines (shown as solid curves) fit well with the experimental data (Figure 3). First of all, the model properly describes the initial sharp increase in the adsorption (at low grafting densities). Secondly, where the experiments show a plateau value, the model results show a very broad maximum. The prediction of a maximum in adsorption is in agreement with the theoretical work of Currie *et al* [16]: first the adsorption increases since, with increasing grafting density, the number of binding sites for the surfactant micelles increases. At high enough grafting densities the adsorption levels off because surfactant micelles are pushed out of the polymer brush due to volume exclusion. Thus, we indeed expect that if we experimentally could go to higher PEO grafting densities that we would find a reduction in adsorbed amount. Such experimental maxima in the adsorbed amount as function of grafting density do not yet show up here, but have been found for the adsorption of BSA [17] and small silica particles [18] in PEO brushes.

In Figure 3b we rescaled the data for the increasing amount of polymer by expressing the adsorption as the amount of surfactants adsorbed per PEO monomer. What can be observed is that the adsorption per PEO monomer decreases strongly with increasing grafting density. The highest value is about 44% and the lowest one is about 6%. The value of 44% is very close to what can be reached by the complexation between PEO polymers and SDS surfactants in solution. For that case, (and at a NaCl concentration of 50 mM,) a ratio of surfactant molecules to monomers of approximately 42% could be calculated from the data of Minatti and Zanette [49] (See next section for details on the calculation.). The

large difference between the amount of adsorption in bulk solution and in the PEO brush at higher grafting density must therefore be related to the fact that we are dealing here with a brush layer. In solution, a polymer coil floats freely so there is no large excluded volume. Furthermore, a polymer with attached surfactant micelles in solution, is not surrounded by other polymers with likewise attached surfactant micelles, and thus the electrostatic repulsion between the micelles is much lower in that case than in a dense polymer brush.

In Figure 4 we present the adsorbed amount of SDBS in PEO brushes of different polymerization degrees as a function of grafting density. The results for SDBS are very similar to the results for SDS, except that the adsorption of SDBS in the PEO brush is somewhat larger than for SDS (see also Figure 1). Still, the same trends as for SDS adsorption in a brush layer are observed here, namely that with increasing grafting density the adsorption in mg/m^2 reaches a plateau, and that the adsorption per monomer is independent of the polymerization degree. In Figure 4b we see that the adsorption per monomer has a maximum of approximately 40-50%, thus very similar to the results that we obtained with SDS. From literature we know that SDBS and PEO in bulk behave very similar to SDS and PEO. The main differences are that for the SDBS-PEO system, the CAC (and CMC) and the adsorption per PEO monomer are both much lower [49]. Hence, the finding that in a brush SDBS adsorbs in the same surfactant-to-monomer ratio as SDS, while in bulk it adsorbs less, is an interesting and surprising one.

In both Figure 3b (for SDS) and in Figure 4b (for SDBS) we find that the rescaled data for the number of adsorbed surfactant molecules per PEO monomer for the different polymerization degrees collapse to a common master curve. Thus, the number of SDS and SDBS molecules per PEO-monomer does not depend on N, i.e. the adsorbed amount scales linearly with the polymerization degree. This is fully supported by the aSCF model, in which the adsorption per monomer is invariant with respect to polymerization degree.

The decrease in the adsorption per monomer as a function of the grafting density shows that by increasing the excluded volume, less surfactants adsorb per polymer. This effect was also shown by Pyshkina *et al* [14] for cationic surfactants in a poly(acrylic acid) brush. We illustrate this effect with a theoretical analysis in Figure 5. (Note that for the brush density profiles in Figure 5, the hydrated brush volume as used in the theory is recalculated to dry volume, namely by considering the volume of a hydrated segment ($0.22\ nm^3$) and a dry segment ($0.0609\ nm^3$), i.e., by dividing calculated hydrated brush volumes ϕ_b by a factor 3.6). In Figure 5 we show calculated aSCF results for the density profiles of a polymer brush with and without adsorbed SDS, for several grafting densities. We also present the density profile of the adsorbed SDS. From the latter, we see that at low grafting densities (Figure 5a) the maximum SDS volume fraction is located directly at the surface

where the polymer concentration is the highest. The maximum in polymer density ϕ is always located at the grafting interface $\phi(0)$, but when $\phi(0)$ exceeds approximately 4.5 % (Figure 5b) the maximum in SDS volume fraction starts to move away from the surface, into the brush. At even higher grafting densities (Figure 5c and 5d) the maximum becomes more pronounced and moves towards the periphery of the brush.

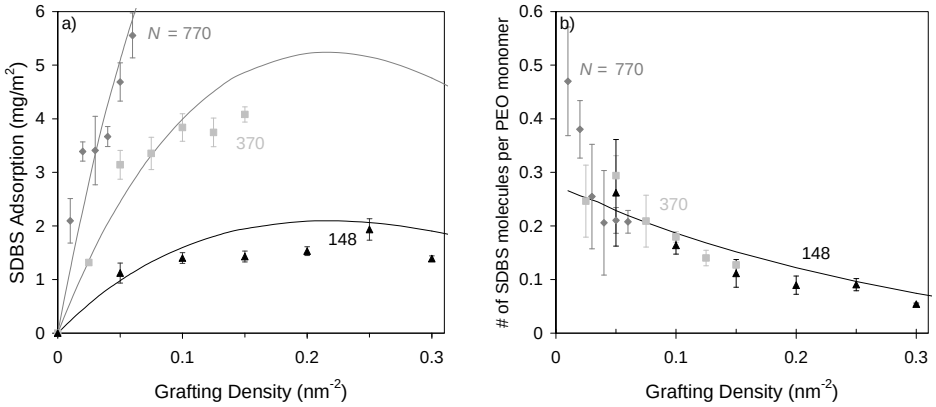

Figure 4. SDBS adsorption in PEO brushes for different polymerization degrees, N, as function of grafting density,σ (C_{SDBS} = 1 g/l, c_{NaNO3} = 50 mM). (a). Adsorbed amount per unit surface area. (b). Adsorption per brush monomer. Points are experimental data, lines are results from the aSCF model (χ_{mb}=18 nm^{-3}) with input parameters based on SDS and not on SDBS. Therefore, the theoretical curves should only be treated as a guide for the eye.

Interestingly, there is only a small difference between the brush density profiles with and without adsorbed SDS, even though the volume fraction of SDS can be as large as the volume fraction of polymer (at low grafting density). Intuitively, one would expect the brush to be stretched much further when such an amount of SDS adsorbs in the brush (namely to the length of an empty PEO brush in case of twice the grafting density, see Figure 5b). However, one important thing to realize is that for the stretching of the chains it is not the pure volume of the particles that is important, but the excluded volume of the particles. The radius of an SDS micelle is about three times that of a polymer bead (and hence its volume is ~27 times larger), and because (per unit volume) small objects contribute much more to the excluded volume than larger objects, the PEO beads contribute much more to the excluded volume than the SDS micelles. Furthermore, our theory predicts that by increasing the brush density, the brush increases the amount of contact with the SDS micelles leading to an increase in the nonelectrostatic interaction. In extreme cases this effect can even lead to a significant decrease or even a collapse of the polymer brush. In the

cases shown in Figure 5 however, our model results show a balance between, on the one hand the extra excluded volume that the adsorbed SDS micelles contribute and, on the other hand the extra attraction between the brush and the SDS micelles at high brush densities. In our calculations the consequence of this balance is that SDS adsorption hardly influences the brush density profile.

The shapes of the calculated brush density profiles without SDS are very similar to measured brush density profiles [47,48]. However, the predicted brush heights are almost a factor of two higher than experimentally determined. In, to our knowledge, the only other direct comparison between an experimental and theoretical (nSCF) PEO brush density profile, Currie *et al* [47] reproduced the experimentally determined density profiles using a value for the Kuhn length of k = 0.35 nm. In contrast, we use the experimentally determined Kuhn length of k = 0.7 nm [39], as we have attempted to use as realistic input parameters as possible (see section parameter settings). Furthermore, we would like to stress that the effect that the adsorbed SDS is pushed to edge of the brush with increasing grafting density (as shown in Figure 5) does not depend much on parameter choice, and it is this effect which causes the broad maximum in the adsorption that we predict in Figure 3a. Thus, it is expected, that introducing a fit parameter to adjust the height of the brush would not significantly change the predicted adsorptions in Figure 3 (although the value of χ_{mb} would change).

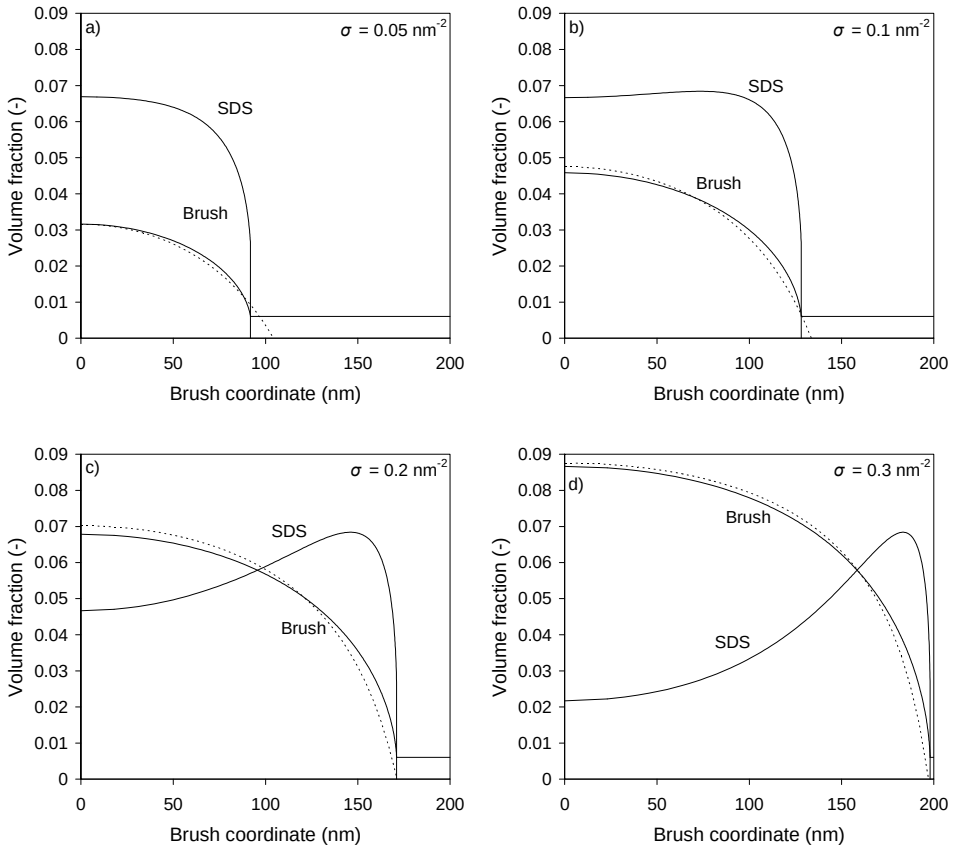

Figure 5. Brush and SDS density profiles as calculated by the mean-field model for different grafting densities as indicated (N=770, C_{SDS} = 5 g/l, c_{salt} = 50 mM). The dotted line is the brush profile for the given grafting density without adsorbed SDS.

The effect of ionic strength on the adsorption of SDS

As the surfactant micelles are charged, one would expect that the salt concentration is an important parameter in the adsorption of these micelles to the brush. Therefore, in this section we investigate the effect of the salt concentration on the adsorbed amount.

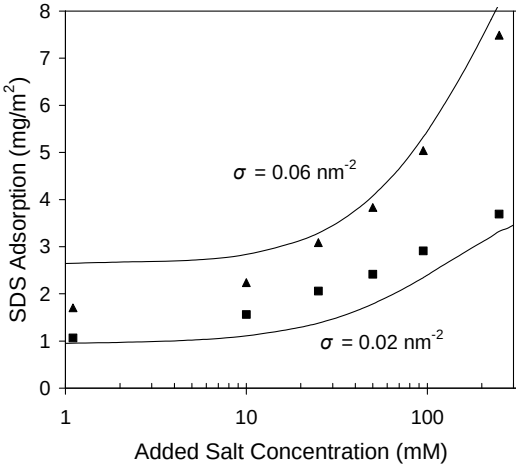

Figure 6. Adsorption of SDS in a PEO brush (N =770) as a function of added salt concentration ($NaNO_3$). Experimental results (dots) and aSCF calculations (lines) shown for two different grafting densities as indicated. (C_{SDS} = 5 g/l, χ_{mb} = 13 nm^{-3}).

Figure 6 shows that the adsorption of SDS in a PEO brush increases 3 to 4 fold when increasing the added salt concentration from 1 to 250 mM. This shows the importance of electrostatic effects in the adsorption of SDS micelles in the brush. Because of the adsorption of the charged micelles and their counterions in the brush, there will be a significant difference in the counterion concentration inside and outside of the brush. This leads to an osmotic pressure in the brush, which with more added salt decreases, allowing more SDS and accompanying counterions to adsorb. This effect is well reproduced by the model. The model also predicts that the stretching of the SDS containing brush changes with increasing salt concentration. At low salt concentration the brush is predicted to be stretched 37% (H/L = 0.37) while at a salt concentration of 250 mM the stretching is decreased to 0.29.

An estimate for the number of surfactant molecules complexed to a single PEO monomer can be estimated from the data of Minatti and Zanette [49]. They measured by conductivity experiments and for different salt (NaCl) concentrations the CMC for SDS and the so-called polymer saturation point (PSP) for SDS and PEO in solution. The PSP gives

the concentration at which a given amount of PEO is saturated with SDS. Subtracting the CMC from the PSP gives the total amount of SDS taken up by the PEO [52]. Dividing this by the PEO monomer concentration gives the number of complexed surfactant molecules per PEO monomer. From the data of Minatti and Zanette [49] we calculated the amount of complexed surfactant molecules per PEO monomer and find that between 0 mM and 50 mM of added salt, this number increases approximately increases by a factor of 2. This is very similar to the effect observed in Figure 6 (increase of a factor of 2.1 for σ = 0.02 nm^{-2} and 2.2 for σ = 0.06 nm^{-2} when we go from 1 to 50 mM of added salt), indicating that the effects of the ionic strength on the adsorption of SDS to a PEO brush are strongly related to effects observed for the complexation of PEO and SDS in solution.

Interaction between particles and SDS filled brushes

An interesting aspect is that because of the adsorption of charged objects in the PEO brush the neutral polymer brush gets properties typical for a weak polyelectrolyte brush. Because of the adsorbed SDS micelles the PEO brush becomes charged. With increasing salt concentration the adsorbed amount of micelles and thus the number of charges in the brush increases. Our model predicts that added salt leads to a reduction in swelling of the brush layer, also typically associated with polyelectrolyte brushes. This would imply that adsorption of SDS in a PEO brush can alter the interaction of the brush with charged particles. One may for instance expect that, because of their negative charge, silica particles which are known to strongly adsorb onto PEO brushes [18], are less likely to adsorb onto a PEO brush filled with adsorbed negatively charged SDS. On the other hand, a positively charged protein such as lysozyme against which PEO brushes have often shown good antifouling properties might be able to adsorb in an SDS-filled PEO brush.

To investigate the effect that SDS may have on the interaction of such particles with a PEO brush we have performed AFM force measurements. With these, we have measured the maximum force necessary to pull a silica colloidal probe from the surface (the so called pull-off force). The lower this pull-off force, the better the brush will be suited as an antifouling layer against these particles. For the longest PEO brush (N = 770) we measured the pull-off force for a number of different SDS concentrations and brush grafting densities. Results are shown in Figure 7a.

In Figure 7a we clearly see that there is a strong attraction between the bare PEO brush and the silica particle. In the absence of SDS, a force of more than 1 nN is necessary to pull the particle from the PEO brush, independent of the grafting density. For grafting densities of 0.02 nm^{-2} and higher, this strong attraction almost completely disappears above an SDS concentration of 0.3 g/l. As we know from Figure 2, this concentration is below the CAC

and therefore this effect must be attributed to the adsorption of SDS to the silica particle. At a concentration of 0.5 g/l SDS (above the CMC below the CAC), we expect the brush to be collapsed as described above, and at this concentration, there is also no measurable pull-off force. However, for dilute brushes $\sigma = 0.02$ nm^{-2} and $\sigma = 0.03$ nm^{-2}, we find that above 1 g/l SDS the pull-off force returns. Above the CMC, the brush likely consists of a swollen brush with adsorbed micelles. It is well known that a complex of PEO and SDS can adsorb to a silica surface [8]. We believe that at low brush densities, and above the CMC, this is exactly what happens. However, at higher grafting densities, the adsorbed amount of SDS and thus also the amount of negative charges in the brush is much larger. Indeed at the higher brush densities we find that there is only a very low pull-off force. In conclusion, adding SDS above the CMC to sufficiently dense PEO brushes results into good resistance against adsorption of silica particles. As this resistance most likely stems from the large amount of negative charge in the brush, we would expect that the same results can be achieved by using SDBS rather than SDS.

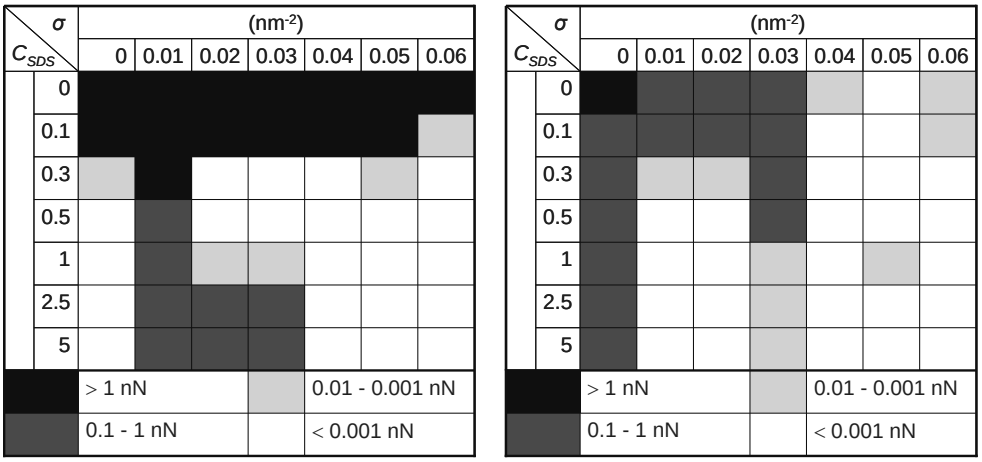

Figure 7. The pull-off force as measured by AFM for interaction between a PEO brush (N = 770, c_{NaNO3} = 50 mM, pH = 5.8) and a) a 6 μm Silica colloidal probe and b) a standard silicon nitride AFM tip. SDS concentration and brush grafting density have been varied as indicated. A grafting density of 0 means that a bare polystyrene surface was used.

These AFM pull-off force measurements as a function of SDS concentration and of grafting density were also performed for a standard silicon nitride AFM tip (Figure 7b). The silicon nitride surface is expected to be slightly positively charged at pH 5.8 [50] (Although in contact with an SDS solution, the slight positive charge might change to neutral or negative due to surfactant adsorption.). The contact area of such a tip is about 100 nm^2 and thus the contact area between brush and this tip is much smaller than the contact area

between the silica particle and the brush. This results, for the silicon nitride tip, in much lower pull-off forces for low grafting densities and low surfactant concentrations. The silicon nitride tip has a strong interaction with the bare polystyrene surface (σ = 0 nm^{-2}), and even high SDS concentrations do not lead to pull-off forces lower than 0.1 nN. In contrast, PEO grafting densities higher than 0.04 nm^{-2} reduce the pull-off force to values below 0.001 nN for almost any SDS concentration. For lower grafting densities (σ = 0.01 nm^{-2}, 0.02 nm^{-2}) a concentration of 0.5 g/l SDS is necessary to achieve the same reduction. For σ = 0.03 nm^{-2} however, there is always a significant pull-off force.

The AFM experiments show clearly that the adsorption of SDS to a PEO brush can lead to very different brush-particle interactions, and thus also to very different antifouling properties. For both investigated systems (silica colloidal probe and standard silicon nitride AFM tip) the combination of SDS and sufficiently dense PEO brushes leads to pull-off forces lower than 0.001 nN. We conclude that adsorbing SDS or SDBS in a PEO brush is a simple and reversible method to change the PEO brush from a neutral brush to a charged brush.

Conclusions

In this chapter we have systematically studied the adsorption of the anionic surfactants SDS and SDBS in PEO polymer brushes using reflectometry. We found that the adsorption of SDS in a PEO brush of any grafting density is completely reversible, while the adsorption of SDBS to a polymer brush is almost, but not completely, reversible. For the adsorption of SDS in a PEO brush a CAC is found between 0.3 and 0.4 g/l SDS (50 mM $NaNO_3$). Below this concentration only a small adsorbed amount is found, which is attributed to adsorption to the polystyrene surface on which the PEO is grafted. Above the CAC but below the CMC the adsorption is much higher, and the adsorption kinetics are found to be very slow, probably because of the time necessary for a micelle to form in the PEO brush. Above the CMC the adsorption is slightly higher and very fast adsorption kinetics are found.

At low grafting densities the normalized adsorption of SDS (i.e. per monomer unit of the polymer) is almost equal to the normalized adsorption to PEO in solution. However, the number of adsorbed surfactants per PEO monomer decreases rapidly with increasing grafting density. This is because of the effect that in a brush layer excluded volume interactions have a strong negative effect on adsorption and, in addition, the osmotic pressure in a brush (that stems from the high concentration of counterions in the brush) is also much higher than in (the neigbourhood of) a polymer coil in solution.

An aSCF model is presented to describe brush conformations and adsorption of micelles and ions, and the results of this model fit very well to the experimental data. Both experimentally and theoretically the adsorption is shown to scale directly with the polymerization degree of the polymers in the brush. Experiments and model calculations also show that the ionic strength significantly influences the adsorption of anionic surfactants in a PEO brush. The addition of salt decreases the osmotic pressure in the brush and leads to a three- to fourfold increase in adsorbed amount.

We also found that SDS significantly influences the interaction between a silica colloidal probe and a PEO brush. At high enough PEO densities, the addition of SDS leads to a very strong reduction in the measured force necessary to pull the colloidal silica particle from the PEO brush. This effect can be attributed to the large amount of negative charge incorporated in the PEO brush because of SDS adsorption. Adsorption of SDS in a PEO brush thus seems a simple and reversible method to change a neutral brush into a charged brush with all the corresponding effects on brush particle interactions.

References

1. Lindman, B. *Handbook of Applied Surface and Colloid Chemistry* **2001**, John Wiley, West Sussex, England.
2. Hansson, P. *Curr. Opin. Colloid Interface Sci*. **1996**, 1, 604.
3. Holmberg, K.; Jonsson, B.; Kronberg, B.; Lindman, B. *Surfactants and Polymers in Aqueous Solution* **2003**, John Wiley, West Sussex, England.
4. Lee, L.-T. *Curr. Opin. Colloid Interface Sci.* **1999**, 4, 205.
5. Pettersson, E.; Topgaard, D.; Stilbs, P.; Söderman, O. *Langmuir* **2004**, 20, 1138.
6. Anthony O.; Zana R. *Langmuir* **1994**, 10, 4048.
7. Goddard, E.D. *J. Colloid Interface Sci.* **2002,** 256, 228.
8. Cosgrove, T.; Mears, S.J.; Obey, T.; Thompson, L.; Wesley, R.D. *Colloids Surf. A* **1999,** 149, 329-338.
9. Ghodbane, J.; Denoyel, R. *Colloids Surf. A* **1997**, 127, 97.
10. Alexander, S. *J. Phys*. (Paris) **1977**, 38, 983.
11. de Gennes, P.G. *J. Phys*. (Paris) **1976**, 37, 1443.
12. Currie, E.P.K.; Norde, W.; Cohen Stuart, M.A. *Adv. Colloid Interface Sci.* **2003**, 100-102, 205.
13. Szleifer, I.; Carignano, M.A. *Advances in Chemical Physics*, Volume XCIV, John Wiley, Ontario, Canada, **1996**, 165.
14. Pyshkina, O.; Sergeyev, V.; Zezin, A.; Kabanov, V. *Langmuir* **2003**, 19, 2000.
15. Konradi, R.; Rühe, J. *Macromolecules* **2005**, 38, 6140.
16. Currie, E.P.K.; Fleer, G.J.; Cohen Stuart, M.A.; Borisov, O.V. *Eur. Phys. J. E* **2000**, 1, 27.
17. Currie, E.P.K.; van der Gucht, J.; Borisov, O.V.; Cohen Stuart, M.A. *Pure Appl. Chem.* **1999**, 71, 1227.
18. Gage, R.A.; Currie, E.P.K.; Cohen Stuart, M.A. *Macromolecules* **2001**, 34, 5078.
19. Boublik, T. J. *Chem. Phys*. **1970**, 53, 471.
20. Mansoori, G.A.; Carnahan, N.F.; Starling, K.E.; Leland, T.W. *J. Chem. Phys*. **1971**, 54, 1523.
21. Jackson G.; Rowlinson J.S.; Van Swol F. *J. Phys. Chem*. **1987**, 91, 4907.
22. Lue L.; Zoeller N.; Blankschtein D. *Langmuir* **1999**, 15, 3726.
23. Di Caprio D.; Borkowska Z.; Stafiej J. *J. Electroanal. Chem.* **2003**, 540, 17.
24. Dullens R.P.A.; Aarts D.G.A.L.; Kegel W.K. *Proc. Natl. Acad. Sci*. **2006**, 103, 529.
25. Patricaud P. *Phys. Rev. E* **2008**, 78, 021202.
26. de Vos, W.M.; Biesheuvel, P.M.; de Keizer, A.; Kleijn, J.M.; Cohen Stuart, M.A. *Langmuir* **2008**, 24, 6575.
27. Biesheuvel, P.M.; de Vos, W.M., and Amoskov, V.M. *Macromolecules* **2008,** 41, 6254.
28. Hill T.L. *Introduction to Statistical Thermodynamics*, Addison-Wesley, Reading, Massachusetts **1960**, p. 252.
29. Laidler K.J.; Meiser J.H. *Physical Chemistry*, Addison-Wesley, Reading, Massachusetts **1982**, p. 29.
30. Carnahan N.F.; Starling K.E. *AIChE J.* **1972**, 18, 1184.
31. Milner, S.T.; Witten, T.A.; Cates, M.E. *Macromolecules* **1988**, 21, 2610.
32. Amoskov, V. M.; Pryamitsyn, V. A. J. *Chem. Soc. Faraday Trans.***1994**, 90, 889.
33. Biesheuvel, P.M.; Leermakers, F.A.M.; Cohen Stuart, M.A. *Physical Review E* **2006**, 73, 011802.
34. Biesheuvel P.M.; Van Soestbergen M. *J. Colloid Interface Sci*., **2007**, 316, 490.
35. Zhou F.; Biesheuvel P. M.; Chol E.Y.; Shu W.; Poetes R.; Steiner U.; Huck W.T.S. *Nanoletters*, **2008**, 8, 725.
36. Van Os, N.M.; Haak, J.R.; Rupert, L.A.M. *Physico-chemical Properties of Selected Anionic, Cationic and Nonionic Surfactants*; Elsevier: Amsterdam, **1993**.
37. Healy, T.W.; Drummond C.J.; Grieser, F.; Murray, B.S. *Langmuir* **1990**, 6, 506.
38. Briganti G.; Bonincontro A. *Colloid Surf. A*. **1995**, 103, 105.

39. Pattanayek, S.K.; Juvekar, V.A. *Macromolecules* **2002**, 35, 9574.
40. Nightingale E.R. J. Phys. Chem. **1959**, 63, 1381.
41. Currie, E.P.K.; Sieval, A.B.; Avena, M.; Zuilhof, H.; Sudhölter, E.J.R.; Cohen Stuart, M.A. *Langmuir* **1999**, 15, 7116.
42. de Vos, W.M.; de Keizer, A.; Kleijn, J. M.; Cohen Stuart, M. A. *Langmuir* **2009**, 25, 4490.
43. Maas, J.H.; Cohen Stuart, M.A.; Sieval, A.B.; Zuilhof, H.; Sudhölter, E.J.R. *Thin solid films* **2003**, 426, 135.
44. Dijt, J.C.; Cohen Stuart, M.A.; Hofman, J.E.; Fleer, G.J. *Colloids and Surfaces* **1990**, 51, 141.
45. Rodenhiser A. P.; Kwak J. C. T. *Colloids Surf. A*, **1999**, 150, 191.
46. Wittgren B.; Stefansson M.; Porsch B. J. *Chromatography A* **2005**, 1082, 166.
47. Currie, E.P.K.; Wagenmaker, M.; Cohen Stuart, M.A.; van Well, A.A. *Physica B* **2000**, 283, 17.
48. Bianco-Peled H.; Dori Y.; Schneider J.; Sung L.; Satija S.; Tirrell M. *Langmuir* **2001**, 17, 6931.
49. Minatti, E.; Zanette, D. *Colloids Surf. A* **1996**, *113*, 237.
50. Hou, Z.; Li, Z. *J. Dispers. Sci. Technol.* **1999**, *20*, 1507.
51. Cerovic, L.S.; Milonjic, S.K.; Balhoul-Hourlier, D.; Doucey, B. *Colloids Surf. A* **2002**, 197, 147.
52. Froehner, S. J.; Belarmino A.; Zanette, D. *Colloids Surf. A* 1998, 137, 131.

Appendix A. Parameter settings for SDS micelles

For the aggregation number, N_{agg}, and charge, Z, of the SDS micelles as a function of the concentration of added salt (NaCl), we use data from refs. 36 and 37 and fit these to a function of the form

$$f(c) = a + b \cdot \left(1 - \exp\left(-\frac{c}{c^*}\right)\right) \qquad [A1]$$

where c is the salt concentration in mM, see Figure 8. For both parameters we use the same value for c^*, namely c^* = 60 mM. Best-fit values for a and b are as follows. For N_{agg}, a = 60 and b = 50; for Z, a = 20 and b = 48. Parameter a equals the value of y at zero added salt, while $a+b$ represents the value at infinite salt concentration. For the size D_m of the micelles (D_m = 2·R with R the micelle radius), we assume that the micelle mass density (mass/volume) is constant (independent of aggregation number), and thus we use a fit $D_m = \alpha \cdot N_{agg}^{1/3}$ with α = 1.0853 nm. The volume of an SDS micelle, v_m, is given by $v_m = \pi/6 \cdot \sigma_m^3 = \pi/6 \cdot \alpha^3 \cdot N_{agg}$. Figure 8 shows the data and the fitting functions. Though the data are derived for SDS micelles in solution, we will apply Eq. A1 also for the micelles in the brush, for lack of better data.

To obtain the value for Z, surface potential data were used from ref. 37. The surface charge Z follows from

$$Z = \frac{R}{\lambda_B} \cdot (1 + \kappa R)\, y \qquad [A2]$$

which is the low-potential solution of the Poisson-Boltzmann equation for a single sphere, where y is the dimensionless potential.

Experiments were done at 5 g/l SDS or 1g/l SDBS in solutions of various salt concentrations. The CMC of SDS as function of the concentration of added monovalent salt is given in Figure 9 where the full continuous line is an empirical fitting function given by: CMC (g/l) = $\alpha/c^{\beta \cdot \ln(c)}$ with c the concentration of added monovalent salt in mM, and where α = 2.0378 and β = 0.070682. Based on the fitting functions in Figure 8 a mass density of the micelles of 0.715 mg/ml follows. Thus, we can calculate the volume fraction of micelles in solution, $\phi_{m,sol}$; for example at 50 mM added salt, we obtain $\phi_{m,sol}$=0.6 %.

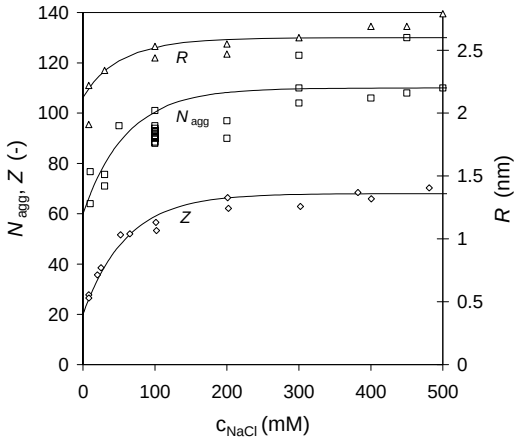

Figure 8. Input data for SDS micelles as a function of salt (NaCl) concentration. Z is the number of charges per micelle, N_{agg} the number of surfactant molecules per micelle and R the radius of a micelle. Points are experimental data from [N_{agg} and R; ref. 36, Z; ref. 37] while lines are given by Eq. A1.

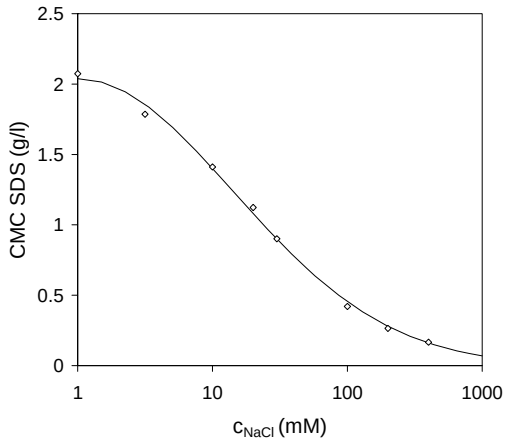

Figure. 9. Input data for the critical micelle concentration (CMC) of SDS as a function of salt (NaCl) concentration. Points are experimental data from ref. 36, the line is a fit (see text) used for the model.

Chapter 6

Adsorption of the protein bovine serum albumin in a planar polyacrylic acid brush layer as measured by optical reflectometry.

Summary

The adsorption of bovine serum albumin (BSA) in a planar poly(acrylic acid) (PAA) brush layer has been studied by fixed-angle optical reflectometry. The influence of polymer length, grafting density, and salt concentration is studied as a function of pH. The results are compared with predictions of an analytical polyelectrolyte brush model, which incorporates charge regulation and excluded volume interactions. A maximum in adsorption is found near the point of zero charge (pzc) of the protein. At the maximum, BSA accumulates in a PAA brush to at least 30 volume percent. Substantial adsorption continues above the pzc, i.e. in the pH range where a net negatively charged protein adsorbs into a negatively charged brush layer, up to a critical pH value. This critical pH value decreases with increasing ionic strength. The adsorbed amount increases strongly with both increasing PAA chain length and increasing grafting density. Experimental data compare well with the analytical model without having to include a non-homogeneous charge distribution on the protein surface. Instead, charge regulation, which implies that the protein adjusts its charge because of the negative electrostatic potential in the brush, plays an important role in the interpretation of the adsorbed amounts. Together with nonelectrostatic interactions, it explains the significant protein adsorption above the pzc.

A Manuscript based on this Chapter was published as:

De Vos, W.M.; Biesheuvel, P.M.; De Keizer, A.; Kleijn, J.M.; Cohen Stuart, M.A. *Langmuir* **2008**, *24*, 6575-6584.

Introduction

For many years now, polymer brushes, i.e., densely packed arrays of polymer chains end-attached to an interface, have been investigated and used to control the adsorption of proteins onto surfaces [1,2]. In most cases, uncharged polymer brushes are used to prevent the adsorption of proteins. The brush layer, which is swollen because of excluded volume interactions, responds to any deformation of the brush layer from its equilibrium (for example deu to insertion of a protein) with a restoring force. Due to this behavior polymer brushes can be applied as antifouling agents.

More recently, much attention has been given to the use of charged polymer brushes, not to prevent adsorption, but rather to accommodate (immobilize) proteins or enzymes [3-12]. If the attraction between protein and a polyelectrolyte brush is large enough to overcome steric effects, much larger amounts of protein can adsorb inside a brush layer than onto a solid surface. Also, protein molecules immobilized by polyelectrolytes are found to be weakly bound and therefore keep their conformation and (enzymatic) activity largely intact [13,14], whereas proteins adsorbing on a smooth hard surface often change conformation to adjust to the flat surface, resulting in a loss of enzymatic activity [14].

A very promising system for protein immobilization are colloidal particles with a densely packed array of end-attached polyelectrolytes [3-5,7-9,12]. In a specific example [16] these so-called spherical polyelectrolyte brushes (SPBs) consist of a polystyrene core of about 50 nm in radius covered with a poly(acrylic acid) (PAA) brush. Experiments have shown that at low salt concentration large amounts of bovine serum albumin (BSA) can adsorb onto these particles [3], that the BSA is evenly distributed throughout the brush [8], and that the secondary structure of the protein is almost completely retained [5]. The protein molecules can be released from the brush by exposure to a high pH or a high salt concentration [5]. Another study has shown that the enzymatic activity of glucoamylase was retained after being adsorbed to polyelectrolyte brushes [4].

All experiments [3-8,12] on the adsorption of BSA to spherical polyelectrolyte brushes have only been performed at or above the point of zero charge (pzc) of the protein using a serum replacement cell. To preclude flocculation of the dispersed particles, the region pH<pzc had to be avoided. The reported high adsorbed amounts were not only found at the pzc, where a net neutral protein adsorbs to a negatively charged polymer brush, but also above the pzc, where apparently a net negatively charged protein adsorbs into a negatively charged brush. This adsorption “on the wrong side” of the pzc of the protein was found to be highly dependent on salt concentration.

The interaction between BSA and PAA brushes has also been studied by Hollman and Czeslik [11] on planar surfaces with TIRF (total internal reflection fluorescence). Their

work shows the same trends that were found for the SPB, i.e., strong adsorption at and above the pzc and a strong dependence on salt concentration.

In a recent review of Wittemann and Ballauff [12], the driving forces behind adsorption "on the wrong side" of the pzc of the protein are discussed. They attribute the main driving force to the release of counterions related to the existence of distinct positively and negatively charged patches on the protein surface. As long as a protein molecule has patches of a sufficient size, the polyelectrolyte chain molecules will complex with oppositely charged patches and will evade similarly charged patches. The complexation of the polyelectrolyte with the oppositely charged patches releases counterions, which increases the entropy of the system and thus drives the adsorption. This explanation was theoretically elaborated by Leermakers *et al* using a two-dimensional self-consistent field method [17].

Complexation between polyelectrolyte and like-charged protein has been observed before in bulk solutions. Already in 1978 Kabanov *et al* [18] presented results on the complexation of BSA with three different polyelectrolytes. Complexation was found to depend on the pK_a of the polyelectrolyte. The lower the pK_a the higher above the pzc complexation was still observed. In later experiments polymer-protein interaction "on the wrong side" of the pzc of the protein was frequently found [19,20] and was also explained by the presence of charged patches on the protein surface [19-22].

In recent work, another contribution to complexation at the wrong side of the pzc was emphasized. For polyelectrolyte brushes, the possibility of charge regulation as a driving force for protein adsorption at a pH where the brush and protein have the same charge, was worked out by Biesheuvel *et al* [9,10]. They hypothesize that the concentration of protons inside the brush is different from that of the bulk solution due to the local negative potential in the brush. This difference in proton concentration might be enough to change the charge of the protein from net negative to net positive. However, experimental studies showed that the like-charge adsorption even occurs much further above the pzc than was theoretically predicted [9,10].

The aim of this work is two-fold. In the first place we show results of a thorough experimental study on the adsorption of BSA in planar PAA brush layers using real-time optical reflectometry. This technique measures the adsorbed amount as a function of time, thus also providing the adsorption kinetics. We study the effect of polymer length, grafting density, and salt concentration, all as a function of pH on both sides of the pzc. To our knowledge, we are the first to present experimental results on the adsorption of BSA in a PAA brush above and below the pzc. We revisit the question which driving forces contribute to adsorption at the "wrong side" of the pzc by emphasizing the importance of

contributions due to charge-regulation of protein and brush. To that end, we compare our experimental findings to an analytical model without considering the effect of discrete charged patches on the protein surface.

Theory

Introduction

To describe the measured adsorption isotherms theoretically we use a mean-field thermodynamic model including for all particles (ions, protein molecules, chain segments) the following contributions: entropy, volume exclusion, charge regulation, electrostatic interactions, and nonelectrostatic attraction terms. With charge regulation we imply the modification of the charge of a protein molecule and/or polyacid brush chain due to the nearby presence of other charged molecules, which leads to a different local electrostatic potential. When charge regulation is only due to proton ad-/desorption, one can state that the origin of charge regulation is the fact that proton concentration in the brush differs from that in bulk solution.

We model the ions and the protein molecules both as hard spheres (of different size), and the brush polymers as a “chain of touching beads”. This description of the brush chains was introduced by Biesheuvel *et al* [10] and will be discussed further on in more detail. To describe the conformational properties of the brush we use the well-known concept of a planar box model [24]. In a box model it is assumed that all chains have their free ends at the edge of the box and that the polymer density is constant throughout the brush. It was shown in ref. 10 that for protein adsorption, box models give predictions that are very similar to those of more refined models based on the Edwards, or polymer propagator, equation (at least for monodisperse brushes). The strong-stretching limit of the Edwards diffusion equation was used in ref. 10 in an off-lattice formalism combined with a full solution of a modified Poisson-Boltzmann equation. This approach has the advantage over box models that the decreasing polymer density with distance from the grafting interface is included and variations of protein density with height can be calculated. However, it is numerically a more complicated approach, and furthermore, to inhibit the brush to stretch beyond its contour length in the theory, which is very well possible for charged brushes (with Gaussian chain statistics), we need to include higher order corrections to the standard Gaussian form of the Edwards equation. Instead, the box model can deal with both low and high degrees of stretching without significant adjustments. In distinction with the box model of ref. 9 we now also include volumetric and nonelectrostatic attractive interactions

between brush segments and protein molecules as well as a more accurate titration model for BSA.

Recently, Leermakers *et al* [17] used a two-dimensional self-consistent field formalism, based on discretizing the Edwards equation onto a lattice with sites of the size of a solvent molecule, to study the interaction between an object with charged patches and a polyelectrolyte brush. The object was modeled as an infinitely long bar with a cross-section of 2×3 lattice sites of which the two (opposite) sides were highly oppositely charged. They convincingly showed that attraction between the brush and the object is possible by calculating the free energy changes upon entry of a single object in the brush. However, the model is not suitable to calculate the experimentally accessible property of equilibrium adsorbed amount of protein. That is possible in the previous self-consistent field model [10] as well as in the previous [9] and current box model. Also, the object used in the calculation in ref. 17 has very highly charged patches, with the charge density of the order of four charges per nm^2. These high charge densities are very unlikely to be found on protein molecules. When these high charge densities are lowered in the theory, the attraction between brush and object strongly decreases.

The box model that is presented here is a one-dimensional mean-field model that neglects the effect of patchiness on the protein molecule. Comparison with experiment -*vide infra*- shows that it is a good approximation, probably because the brush phase is rather dense and electrostatic potentials therefore do not fluctuate strongly on the scale of a protein molecule (i.e., a protein molecule cannot “shield” its negative patches from the negative-potential environment of the brush).

Box model

In the box model, at equilibrium the sum of forces on each brush segment (or chain) is zero. This force balance stems from the following three contributions. The first contribution is due to *chain stretching (elasticity)*. We use the Lyulin expression [25] that includes finite chain length, which results in

$$f^{\text{elastic}} = -\frac{1}{k}\left(3x - \frac{27}{20}x^2\ln(1-x) + \frac{9}{20}\frac{x^3}{1-x}\right) \qquad [1]$$

where k is the Kuhn length and x is the degree of stretching, $x=H/L$, with H the brush height, and L the contour length of the chain. Note that in this chapter all energies, pressures and forces are scaled to the thermal energy, kT. Eq. 1 simplifies to Gaussian stretching for weakly stretched chains and very accurately describes the chain elastic force at higher degrees of stretching.

The second contribution stems from *nonelectrostatic, short-range attractions* between brush, *b*, and protein, *p* (both homo- and hetero-interactions), which are described according to the free energy density function

$$\Im^{att} = -\tfrac{1}{2}\sum_i \sum_j \chi_{ij}\phi_i\phi_j \qquad [2]$$

where ϕ_i are volume fractions of components i. Here, χ-values are defined positive for attraction. To obtain the osmotic pressure, Π, required for the brush force balance (force $f=\Pi/\sigma$, where σ is grafting density), we make use of

$$\Pi = \phi^2 \frac{d}{d\phi}\frac{\Im}{\phi} \qquad [3]$$

where ϕ is the total volume fraction of all components combined, and the differentiation is made at a constant composition. For this case this results in $\Pi^{att} = \Im^{att}$, which in our specific case gives the following contribution to the force on a brush segment

$$f^{att} = -\frac{1}{2\sigma}\left(\chi_{pp}\phi_p^2 + 2\chi_{pb}\phi_p\phi_b + \chi_{bb}\phi_b^2\right) \qquad [4]$$

For comparison with the experimental results we will us χ_{bp} as a fitting parameter, while we keep χ_{pp} and χ_{bb} equal to zero.

Finally, the third contribution is due to *entropic and volumetric interactions* between the different species in the brush. We will assume that all species are spherical, also the segments of the brush. In this case it is possible to use an expression from liquid-state theory, namely the Boublik-Mansoori-Carnahan-Starling-Leland (BMCSL) equation-of-state [26,27] which accurately describes volumetric and entropic interactions between mixtures of hard spheres of different sizes. The osmotic pressure contribution is given by the BMCSL equation-of-state

$$\Pi^{BMCSL} = \frac{6}{\pi}\left[\frac{\xi_0}{1-\phi} + \frac{3\xi_1\xi_2}{(1-\phi)^2} + \frac{\xi_2^3(3-\phi)}{(1-\phi)^3}\right] \qquad [5]$$

where the interaction parameters ξ_α are given by

$$\xi_\alpha = \sum_i \phi_i D_i^{\alpha-3}\ , \qquad [6]$$

with D_i the diameters of all particles involved (polymer beads, ions, and protein molecules). Note that ξ_0 is independent of particle sizes, and is given by $\xi 0 = 1/6\pi c_{tot}$, with ctot the total local concentration of all species, while ξ_3 equals the total volume fraction, ϕ.

Π^{BMCSL} must also be evaluated in bulk solution and it is the difference between the brush and the bulk that adds as the net force to the force balance on the brush,

$$f^{BMCSL} = \left(\Pi^{BMCSL} - \Pi_{\infty}^{BMCSL}\right)/\sigma \qquad [7]$$

How do we describe the polymer chains in the BMCSL equation? The approach is to replace in the description the tube-like brush chain by a "string-of-touching-beads" each of a certain diameter D_b [10]. In a full chain we have L/D_b of these beads. The volume fraction ϕ_b of the brush (= volume fraction of the beads) follows from

$$\phi_b = \sigma v_b / D_b x \qquad [8]$$

in which $v_b = \frac{\pi}{6} D_b^3$ is the volume of the beads, and x is the stretching degree.

If each chain segment (with length a) carries an ionizable group we have D_b/a ionizable groups per bead. The advantage of this approach is that the polymer chains can be naturally included in the BMCSL expression. However, in the BMCSL equation correlations between connected chain beads are neglected and the equation is based on the assumption that the beads are distributed homogeneously over space. Besides, if the BMCSL formalism is applied directly to the chains, their entropic contribution is overestimated, as if each bead is a free particle. Instead, because the beads are connected to each other, we must omit their ideal entropy (or, ideal gas contribution) from the equation (which is in the spirit of Flory-Huggins polymer theory where this term is neglected as well for very long chains). This implies that the contribution of brush segments to ξ_0 must be omitted. (In ref. 10 the beads were erroneously included in the ξ_0 term and as a consequence the repulsion between brush segments and between brush and protein was overestimated).

A simplification can be made in the case that in bulk solution the protein concentration is very low, and the ions are point charges (no volume). In that case the contribution of the ions to $\Pi^{BMCL} - \Pi_{\infty}^{BMCL}$ of Eq. 5 can be split off. The osmotic pressure due to the ions, then becomes:

$$\Pi^{\mathrm{ions}} = 2n_{\infty}(\cosh y - 1) \qquad [9]$$

where y is the reduced electrostatic potential in the brush.

For each type of ion, we use equality of chemical potential, which results in

$$\ln \phi_{\mathrm{ion,b}} + z_i y + \mu_{\mathrm{ion,b}}^{\mathrm{ex}} = \ln \phi_{\mathrm{ion},\infty} + \mu_{\mathrm{ion},\infty}^{\mathrm{ex}} \qquad [10]$$

where subscript "b" describes the brush phase, and "∞" the bulk phase. The ion charge is z_i (−1 or +1) and the excess contribution to the chemical potential (because of volume effects, described by the BMCSL equation-of-state) is given by[10]

$$\mu_i^{ex} = -\left(1+\frac{2\xi_2^3 D_i^3}{\phi^3}-\frac{3\xi_2^2 D_i^2}{\phi^2}\right)\ln(1-\phi)+\frac{3\xi_2 D_i+3\xi_1 D_i^2+\xi_0 D_i^3}{1-\phi} + \frac{3\xi_2 D_i^2}{(1-\phi)^2}\left(\frac{\xi_2}{\phi}+\xi_1 D_i\right)-\xi_2^3 D_i^3\frac{\phi^2-5\phi+2}{\phi^2(1-\phi)^3} \quad [11]$$

Again we leave out the brush polymer beads from ξ_0. In bulk solution, we leave out both the protein molecules (dilute solution) and obviously the brush segments. Eq. 11 is also used as the excess term for the protein molecules (see below). In case the ions are infinitely small, the term $\mu_{ion,\infty}^{ex}$ is zero, and in the brush it is –ln(1-ϕ). This leads to a modified Boltzmann expression for the small ions which can be directly included in the electroneutrality balance (see below). For the protein molecules we similarly use equilibrium of chemical potential between brush and bulk phase as for the ions. We will first discuss volumetric and entropic contributions to the chemical potential of the protein molecule. When the ions are infinitely small, the excess contribution of the ions to the chemical potential of the protein molecules is [10]

$$\mu_p^{\text{ion pressure}} = 2v_p n_\infty (\cosh y - 1) \quad [12]$$

where v_p is the protein volume. Eq. 12 describes the difference in $\mu_p^{\text{ion pressure}}$ between brush and solution phase. For ions as point charges, there are no other contributions to $\mu_{p,\infty}^{ex}$ while in the brush the contribution of the interaction with other protein and brush beads to $\mu_{p,b}^{ex}$ is given by Eq. 11 with ions (like the chain beads) excluded from ξ_0.

To obtain the contribution to the chemical potential of the protein molecules of the nonelectrostatic attraction terms we must differentiate Eq. 2 according to $\mu_p = v_p \frac{d\Im^{att}}{d\phi_p}$ for constant ϕ_b, which results in

$$\mu_p^{att} = -v_p(\chi_{pp}\phi_p + \chi_{pb}\phi_b). \quad [13]$$

Electrostatics for protein molecules

As mentioned, for the protein molecules we use equality of chemical potential between the brush phase and the solution phase, $\mu_{p,b} = \mu_{p,\infty}$. Both in solution as well as in the brush a mean field environment is assumed, i.e. there is no explicit ion cloud around the individual protein molecules. Consequently, in solution we assume a zero electrostatic potential on the particle surface, in which case $\mu_{p,\infty}$ is given by [30]

$$\mu_{p,\infty} = \ln\phi_{p,\infty} + \sum_i q_i \ln(1-\alpha_{i,\infty}) + \mu_{p,\infty}^{ex} \quad [14]$$

where $\phi_{p,\infty}$ is the protein volume fraction in solution. In a dilute protein solution, and when the ions are assumed to have zero volume, the excess term $\mu_{p,\infty}^{ex}$ becomes zero. The summation runs over all types of ionizable groups on the protein surface (q_i their number and α_i their ionization degree). The ionization degree, α, represents the fractional charge ($0 < \alpha < 1$) which when multiplied by the charge sign, z, and the electron charge, e, gives the charge per group. To describe BSA, we use the Tanford model [31,32] which includes seven types of ionizable groups (of which four are cationic, i.e., positively charged, and three anionic). The anionic groups ($z_i = -1$) have $\{q_i, pK_i\}$ (where pK_i is the intrinsic pK-value of the respective ionizable group) as follows: {1, 3.75}; {99, 4.02}; {19, 10.35}, while for the cationic groups ($z_i = 1$) we have: {16, 6.9}; {1, 7.75}; {57, 9.8}; {22, 12}. This final group (guanidine, R) has such a high pK value that it is under all relevant experimental conditions almost fully charged ($\alpha_R \sim 1$) which in the numerical procedure is very problematic because of the ln(~0)-term. For guanidine we therefore assume $\alpha_G = 1$ and replace its contribution to the summation terms in Eq. 14 (and further on in Eq. 17) by $q_R.y_b$ and $q_R.y_\infty$ [9,10]. The ionization degrees are given by [30]

$$\alpha_i = \frac{1}{1+10^{z_i(\mathrm{pH}-\mathrm{pK}_i)}e^{z_i y}} \qquad [15]$$

where z_i is the charge sign (either +1 or –1), pH is that of the bulk solution, and pK_i the intrinsic pK-value of the respective ionizable group. The total protein charge is given by

$$Z_{p,\infty} = \sum_i z_i \alpha_i q_i \,. \qquad [16]$$

For protein in the brush the chemical potential is given by [10]

$$\mu_{p,b} = \ln \phi_p + \sum_i q_i \ln(1-\alpha_i) + \mu_p^{ex} + \mu_p^{att} \qquad [17]$$

where ϕ_p is the protein volume fraction in the brush, μ_p^{att} relates to nonelectrostatic attractive terms, and μ_p^{ex} relates to volumetric interactions. The ionization degrees, α_i, in the brush are again given by Eq. 15 with y the potential in the brush. To calculate y and α_i in the brush we use the brush electroneutrality condition,

$$-\alpha_A n_A + n_+ - n_- + Z_p n_p = 0 \qquad [18]$$

where n stands for concentration (in numbers per unit volume), subscript A for the brush segments, subscripts + and - for the small ions, while Z_p is the net charge per protein molecule, given by Eq. 16. The concentration of acrylic acid brush segments, n_A, relates to the brush volume fraction, ϕ_b, according to $n_A = \phi_b/v_b \cdot D_b/a$ where a is the segment length. The ionization degree of the brush segments follows from Eq. 15 with $z = -1$.

In case the ions are point charges, their balance for equality of chemical potential results in

$$\ln n_i + z_i y - \ln\left(1-\phi\right) = \ln n_\infty \qquad [19]$$

where the third term accounts for the volume of protein plus brush, $\phi = \phi_p+\phi_b$, which is excluded for the ions. Combining Eq. 19 with Eq. 18 results in

$$-\alpha_A n_A - 2n_\infty \left(1-\phi\right)\sinh y + Z_p n_p = 0 \qquad [20]$$

Parameter setting

All input parameters, with the exception of the χ-parameter describing the nonelectrostatic interaction between protein and polyelectrolyte, are directly or indirectly based on experimental values as described in literature, and our own experimental conditions. The polymer chain is described as a string of touching beads of diameter D_b and volume v_b. Based on the measured density of poly(acrylic acid) (1450 kg/m^3, Hiraoka *et al* [28]), and a molar mass per segment of 71 g/mol and a segment length of a = 0.25 nm we calculate a cylindrical chain diameter of 0.6 nm, a value which we will use in this work for the bead diameter, thus D_b = 0.6 nm. Each monomer, or segment, has a length of a = 0.25 nm (as calculated from known C-C bond length and angle), thus for a number of segments of N = 270 the chain has a contour length L of 67.5 nm. For the Kuhn length we use k = 1 nm as determined in ref. 9 by a fit of experimental values of the height of a PAA brush as a function of pH. The acrylic acid monomers have a well known intrinsic dissociation constant pK_A = 4.2. As the volume of one BSA molecule we used v_p = 85 nm^3, the specific volume of BSA as measured by Kadi *et al* [29]. For BSA pK values are used as described by Tanford [31] which is described in detail in the above section. As it is almost impossible to determine the χ-parameter by a direct measurement, this parameter was used as a fitting parameter and is obviously independent of pH and ionic strength. We set the size of the small ions to zero.

Materials and methods

Preparation of PAA brush layers

PAA brush layers of varying grafting density were prepared by means of a Langmuir-Blodgett (LB) method described by Currie *et al* [33] with a few adjustments. As substrates, flat silicon wafers were used, coated with polystyrene.

Because polystyrene films spin-coated on clean silicon wafers are not stable, the coating of substrates with polystyrene (PS) was done in the following way. First, the silicon wafer (which has a natural SiO_2 layer with a 2-3 nm thickness) was cut into strips (4 cm x 1 cm), rinsed with alcohol and water, and further cleaned using a plasma-cleaner (10 minutes). The strips were covered with a solution of 11 g/l vinyl-PS20 (M_N = 1.9 kg/mol, M_W/M_N = 1.11, Polymer Source Inc. Montreal, Canada) in chloroform and, after evaporation of the solvent, were heated overnight at 150ºC under vacuum. In this way the vinyl-PS20 is covalently bound to the Si/SiO_2 surface [34]. Excess vinyl-PS20 was washed off with chloroform. Subsequently the strips were spin-coated using a solution of 11 g/l PS (M_N= 870 kg/mol, M_W/M_N=1.05, Polymer Source Inc.) in toluene at 2000 rpm for 30 seconds in order to obtain a thicker PS layer (about 70 nm). The PS surface films prepared in this way are stable in aqueous solutions.

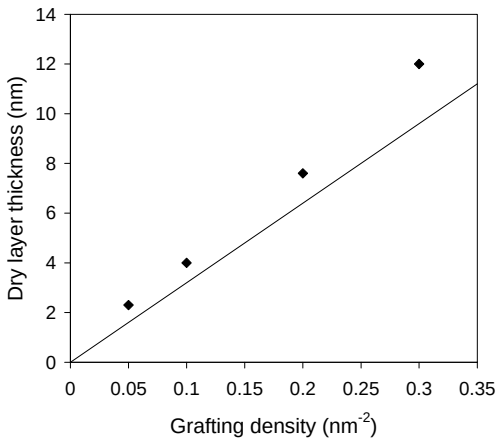

Figure 1. Dry layer thickness of $PS_{36}PAA_{270}$ measured by ellipsometry as a function of grafting density at the air-water interface before transfer. Points are experimental data, the solid line is the theoretical curve based on complete transfer (assumed density PAA 1450 kg/m^3 and PS 800 kg/m^3).

For the brush layer transfer, monolayers of PS-PAA block copolymers (PS_{36}-PAA_{270} M_W/M_N = 1.09, $PS_{41}PAA_{120}$ M_W/M_N = 1.10, Polymer Source Inc. Montreal/Canada) at the air-water interface, were prepared by dissolving the copolymers in chloroform and spreading these solutions very carefully on water in a Langmuir trough using a micro syringe. The water phase had been slightly acidified with HCl to pH 4 (for the grafting densities σ = 0.05 nm^{-2} and 0.1 nm^{-2}) or pH 4.7 (for σ = 0.2 nm^{-2} and 0.3 nm^{-2}). Subsequently, the films were compressed to the appropriate surface density and transferred to the substrates. For the transfer we used a variant of the Langmuir-Schaefer method [35] in which the substrate is held horizontally and dipped through the air-water interface at a speed of 1 mm/s. The substrate was then pulled under the barrier and taken out of the water on the side of the Langmuir trough without the monolayer. The transfer was checked by measuring the dry thickness of the transferred layer using ellipsometry (Figure 1). For some surfaces the transfer was also checked by AFM to see if the material was evenly spread over the surface. These experiments showed that a collapsed (dry) PAA brush is flat with height differences of 2 nm or less (comparable to the bare SiO_2 surface), indicating good transfer. The surfaces so prepared were carefully stored in clean water until use. All solvents used were of PA grade (Sigma-Aldrich). Water used was demineralized using a Barnstead Easypure UV and has a typical resistance of 18.3 MΩ/cm.

Bovine serum albumin (BSA)

BSA was obtained from Sigma (A3912, > 96%, M_w ~ 66 kg/mol, 0.02% fatty acids (approx. 0.1 per BSA molecule)). In most experiments the protein concentration in solution is 0.1 g/l which corresponding to a bulk concentration of 1.5 μM and a volume fraction $\phi_{p,\infty}$ = 90 ppm. The number of charges of BSA as function of ionic strength [31] (similar data in Wen and Dubin [36], and in Giacomelli *et al* [37]) are presented in Figure 2. These data can be satisfactorily described with the Debye-Hückel expression for the relation between surface charge and surface potential of a spherical particle and using Eqs. 15 and 16 for ionization degrees and total protein charge. According to Tanford seven ionizable groups (pK values) must be taken into account. The results suggest that smearing out the protein charge and assuming counterions to be point charges is an acceptable approximation, although a higher value for the effective protein diameter (10 nm) has to be applied to obtain a satisfactory fit. The point of zero charge (pzc) of BSA as calculated from the pK's of the ionizable groups amounts to 5.4 corresponding well to the experimental value of Tanford and is slightly higher than the experimental iso-electric point (iep) of 5.3 [38]. Compared to the titration model used in Ref. 9 a higher pzc (5.4 instead of 5.1) as well as a lower capacity at the pzc (slope in Figure 2) is found.

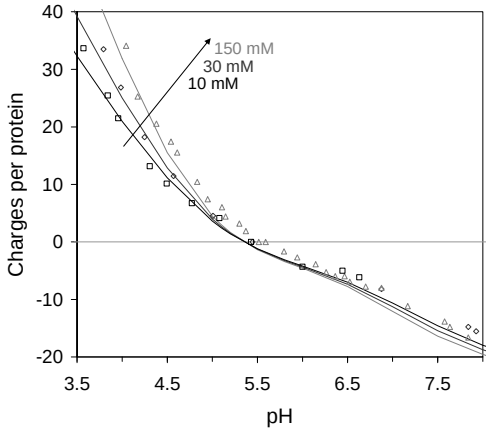

Figure 2. Number of charges per protein molecule as a function of pH. Points are experimental data as measured by Tanford et al [31] for different NaCl concentrations as indicated.. Lines are Debye- Hückel fits.

Reflectometry

The adsorption of BSA onto PAA brush layers was followed with fixed-angle optical reflectometry. A detailed description of the reflectometer setup is provided by Dijt *et al* [39]. It contains a He-Ne laser (λ=632.8 nm) with linearly polarized light. The change in polarization as a result of adsorption or desorption is measured by simultaneously detecting the parallel (R_P) and the perpendicular (R_S) reflectance and dividing R_P by R_S to give signal *S*. Before each measurement, the system was calibrated by flowing with a blank solution to get a stable baseline signal (S_0). The measurement is started by introducing a protein solution into the cell. All solutions are introduced into the cell using a stagnation point flow. The change in signal is measured ($\Delta S = S\text{-}S_0$) with a sampling time of 2 s. The adsorbed amount can be calculated from the change in signal and a sensitivity factor (Q), which depends on the angle of incidence of the laser (θ), the (complex) refractive index ($\tilde{n}$ or n) and thickness (d) of the layers on the silicon wafer, and the refractive index increment (dn/dc) of the adsorbate: $\Gamma = Q(\Delta S/S_0)$. The Q factor was calculated with the following values: $\theta = 71^{\circ}$, $n_{silica} = 1.46$, $n_{polystyrene}=1.59$, $\tilde{n}_{silicon} = [3.85,0.02]$, $n_{H2O} = 1.33$, $dn/dc_{BSA} = 0.185\ M^{-1}$, $d_{silica} = 2.0$ nm, $d_{PS} = 70$ nm, $d_{adsorbed\ layer} = 25$ nm.

The corresponding Q-factor was 40 mg/m^2. A slightly different approach of Q-factor calculation, in which we included the brush layer and increased the refractive index of the brush layer to simulate adsorption, yielded almost the same result.

All protein concentrations used for reflectometry were 0.1 g/l. The background electrolyte was always 10 mM KNO_3 unless stated otherwise. Flow speed was about 1 ml

per minute. All experiments were performed at room temperature (approximately 20 ºC). Because protein adsorption generally has the tendency to increase still slightly after 0.5-1 hour we have standardized the time for reading the protein adsorption value (about 2500 sec). Concentrated solutions of NaOH and HNO_3 were used to bring solutions to the desired pH. No buffer was used in these experiments, however the protein itself has a small buffering effect. To minimize the effect of CO_2 uptake from the air or any other drifts in the pH, the pH of the solutions was adjusted just before the measurement. After the measurements the pH of the solutions was checked, results were only used if the pH was within 0.1 pH unit from the original pH. Only a small number of results, all above pH 6, had to be discarded for this reason.

Results

Adsorption of BSA in a PAA brush

In Figure 3 a typical reflectometry experiment of the adsorption of BSA in a PAA brush (N = 120) is shown. Different solutions are applied to the surface while the adsorbed amount is measured real-time. First, a solution of pH 7 is added, after which the flow is switched to a protein solution (P) of pH 7. After each adsorption step, the surface is flushed with a pH 10 solution (R), resulting in desorption, and then flushed with a solution one pH unit lower than in the preceding adsorption step (S) starting the procedure again. We observe that upon going from the rinsing solution of pH 10 to solvent at (for example) pH 5 the signal shows a quick small decrease. We emphasize that this is not due to desorption but due to a change of the refractive index of the brush layer. With decreasing pH, the degree of dissociation of the polyelectrolyte decreases, leading to a decrease in the refractive index. This effect has already been described by Currie *et al* [33].

The adsorbed amount at pH 7 is comparable to the adsorption of BSA on a bare polystyrene surface (0.3 mg/m^2). At pH 6 the adsorption quickly increases (5 min) to about 7 mg/m^2 followed by a slow increase before adsorption levels off. For pH 6, the measurement in Figure 3 was stopped before a plateau value was reached. However, longer measurements have been done in which a plateau value was reached after approximately 2500 seconds. In those cases the adsorbed amount was only slightly higher (about 5%). Although at pH 6 both the (uncomplexed) protein and the brush layer are negatively charged, the adsorbed amount is substantial. Considering the kinetics of the adsorption, from the initial slopes at positions P in Figure 3 (50, 725, 850 μg m^{-2} s^{-1} at pH = 6, 5, 4 respectively) it follows that the lower the pH, the faster adsorption takes place. This trend was observed in all measurements. This might indicate the presence of an energy barrier for

the adsorption at higher pH values, especially for the adsorption at pH 6 ("wrong side" of the pzc).

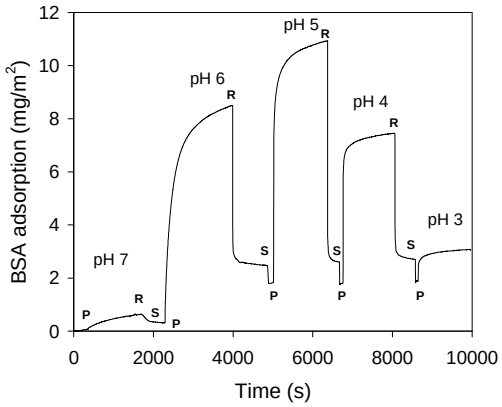

Figure 3. Adsorption of BSA (0.1 g/l) to a PAA brush (N = 120, σ = 0.1 nm^{-2}) at different pH values (10 mM KNO_3) measured as a function of time by fixed-angle optical reflectometry. P means addition of protein, R rinsing with a pH 10 solution, and S the addition of blank solution of the appropriate pH.

The adsorbed amounts in the range between pH 4 and 6 are very high compared to the adsorption on a bare polystyrene surface (1 mg/m^2 at pH 5). Although the height of the brush filled with BSA is unknown, we know that the maximum brush height that can be reached is the contour length of the polymer. In this case we estimate the contour length to be 30 nm (0.25 nm per monomer). In a layer of 30 nm thickness and an adsorbed amount of 11 mg/m^2 the volume fraction of protein will be approximately 30%. Of course this is a very rough estimate since we do not take into account that protein might also adsorb on top of the brush, that polydispersity might increase the effective maximum brush height, while it is also very unlikely that the brush is stretched to its full contour length. (For this system, the model predicts the brush to be stretched about 65% of its contour length, thus containing approximately 45% protein.)

After adsorption below pH 7, flushing with a solution of pH 10 does not lead to complete desorption but an irreversibly adsorbed amount of about 2 mg/m^2 seems present. We do not have enough information to comment on the reason for this; protein molecules might still be attached to the polyelectrolytes or they might have irreversibly adsorbed to the polystyrene surface. To check if the irreversible adsorption has any influence on the total adsorbed amount, we also checked the adsorption at each pH on freshly prepared brush surfaces. No significant difference in adsorption was found except for pH 3, where

adsorption is higher because of the irreversibly adsorbed part formed in preceding adsorption measurements. Therefore, all values for pH 3 were obtained on fresh surfaces.

In Figure 4 we show the effect of BSA concentration on the adsorption of BSA to a PAA brush (N = 270) for two different grafting densities. For both densities, we observe that the adsorption increases only ~20% by increasing the BSA concentration from 0.01 to 3 mg/ml.

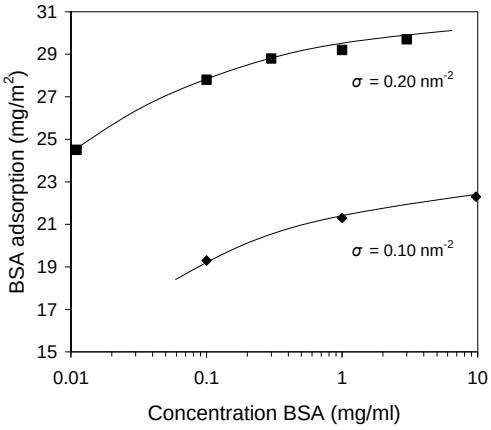

Figure 4. Adsorption of BSA to a PAA brush (pH 5, 10 mM KNO_3, N = 270) as a function of BSA concentration for two different grafting densities, lines are guide to the eye.

Effect of polymer length

In Figure 5a an overview is given of the plateau values for the adsorption of BSA to PAA polymer brushes of two polyacrylic chain lengths (N = 120 and N = 270) as a function of pH. For both brushes the same trends are observed: an increase in adsorption from pH 3 to 5, a broad maximum around pH 5 and also high adsorbed amounts above the pzc. Between pH 6 and 6.5 adsorption decreases sharply. The adsorbed amount is much higher for the longer polymer brush, which is obviously related to the larger amount of polymer to which the protein can adsorb.

When we compare the data to the model results (taking χ_{bp} as a fitting parameter) shown in Figure 5b, we see that there is good agreement. The model predicts the same large adsorbed amounts and also shows a maximum adsorption around pH 5. The sharp decrease in adsorption that was seen in experiments between pH 6 and 6.5 is predicted by the model to be at pH 6. Also the decrease of adsorption when the pH is decreased to below pH 5 is well described.

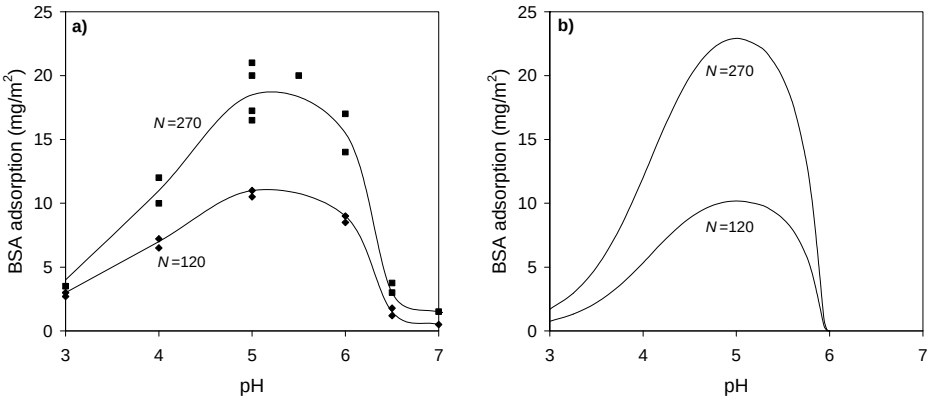

Figure 5. The adsorbed amount of BSA (0.1 g/l BSA, 10 mM KNO_3) as a function of pH to PAA brushes (σ = 0.1 nm^{-2}) of different length. (a). Experimental results, lines are guide to the eye. (b). Model results ($\chi_{pp}=\chi_{bb}=0$, χ_{bp} = 5 nm^{-3}).

In Figure 6 the adsorption data from Figure 5a are presented as a function of chain length, including the adsorption at the bare surface. From our box-model we expect that the adsorbed amount is proportional to the chain length. Extrapolation of the adsorption at different pH values to N=0 gives an adsorbed amount of BSA of roughly 3 mg/m^2 which is an additional adsorption independent of chain length. As the measured adsorption on the bare polystyrene surface is in the order of 1 mg/m^2 an additional amount of about 2 mg/m^2

also adsorbs independent of the thickness of the chain length and pH, most likely on top of the brush layer.

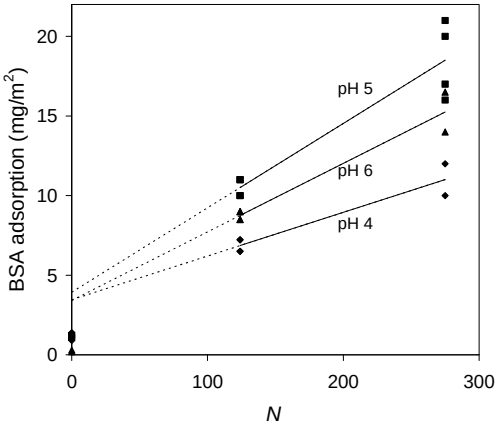

Figure 6. Adsorbed amounts of BSA (0.1 g/l BSA, 10 mM KNO_3) to PAA brushes (σ = 0.1 nm^{-2}) as a function of polymer length for different pH values. Adsorbed amounts at N = 0 were measured on bare polystyrene.

Effect of grafting density

In Figure 7a we show the effect of grafting density of the PAA brush on the adsorption of BSA. For all grafting densities, the adsorption has a maximum at about pH 5 and a sharp decrease in adsorption is observed between pH 6 and 7. The major effect of increasing the grafting density is that the adsorbed amount increases. This is to a large extent in line with expectations since more polyelectrolyte in the brush provides for more adsorption sites for the protein resulting in a higher adsorbed amount. Also, the denser the brush the more the proton concentration is increased compared to bulk solution, allowing for more BSA charge reversal. However, polymer brushes of high grafting densities are also expected to have large excluded volume effects. Therefore, at high grafting densities one might expect a decrease in adsorbed amount because at sufficiently high grafting density only a limited amount of protein can enter the brush.

The model well describes the shape of the experimental curves, the adsorption maximum, the critical pH, and adsorption behavior at low pH values quite well. However, the strong experimental increment of the maximal adsorbed amount with grafting density is not predicted by the model. This might be because of the fact that excluded volume effects are overestimated by the model and/or because of the fact that the decreasing brush density with distance (especially because of the brush polydispersity) is neglected in the model.

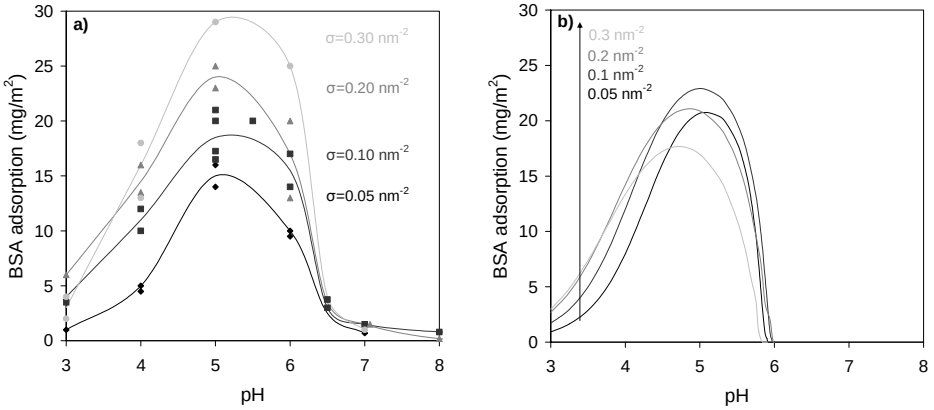

Figure 7. The adsorbed amount of BSA (0.1 g/l BSA, 10 mM KNO_3) as a function of pH to PAA brushes (N = 270) of different grafting densities. (a). Experimental results, lines are guide to the eye. (b). Model results.

In Figure 8 we more clearly show the effect of grafting density by replotting the adsorption data from Figure 7a as a function of the grafting density. Figure 8 shows that only at pH 4 a leveling off and a plateau state seems to be reached at high grafting densities. For both pH 6 and pH 5, the adsorbed amount still increases when going to high brush densities. That the proteins are not (yet) repelled from the brush with increasing grafting density is an indication that the interaction between the proteins and the brush is rather strong.

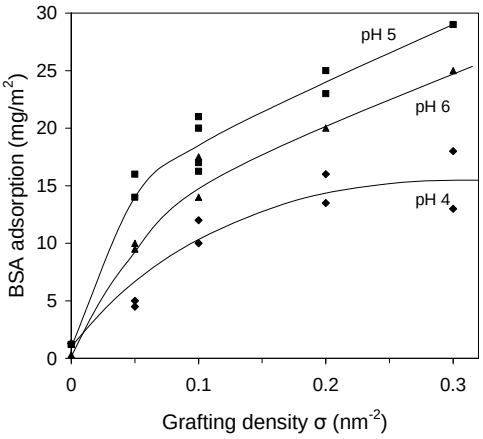

Figure 8. Adsorbed amount of BSA (0.1 g/l BSA, 10 mM KNO_3) as a function of grafting density in PAA brushes. Adsorbed amounts at N=0 were measured on a bare polystyrene surface. Lines are guide to the eye.

Effect of salt concentration

In Figure 9a we show the adsorption of BSA in a PAA polymer brush as a function of pH for different salt concentrations. For every salt concentration the maximum in adsorption is found around pH 5. At and below pH 5 the effect of salt concentration is moderate: going from a salt concentration of 100 to 1 mM, the adsorption decreases by 40% at the most. Instead, above the pzc of the protein we observe a very strong effect of the salt concentration. It can be clearly seen that the salt concentration strongly influences the critical pH (pH_c) at which the adsorbed amount abruptly decreases from large adsorptions between 13-22 mg/m^2 to only small values. The effect of salt on the pH_c is well described by the model (Figure 9b). Also the maximal adsorbed amounts are described well, but the salt effect on the adsorption around pH 4 is absent in the model. Also, the shift in pH at maximum adsorption in the experimental results is less pronounced than in the model. In Figure 10 the pH_c values are plotted separately against c_{salt}. This directly shows the large effect the salt concentration has on the pH_c, going from 1 to 100mM of salt shifts the pH_c from at the pzc to 1.5 pH units above the pzc. This effect is well described by our model results.

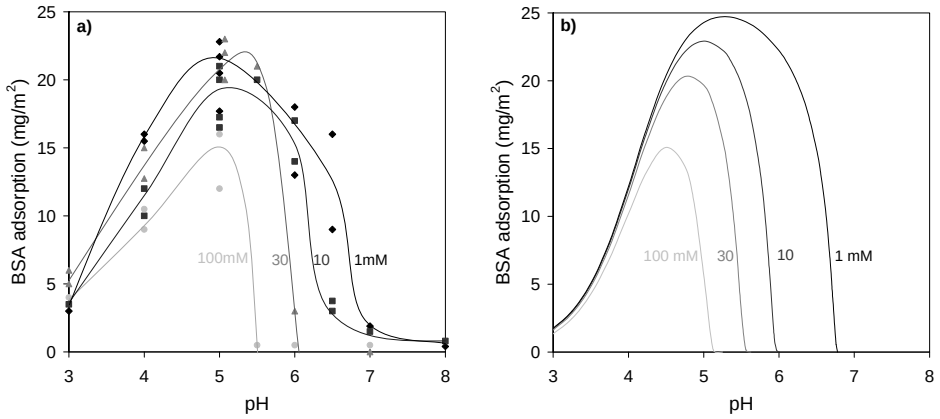

Figure 9. The adsorbed amount of BSA (0.1 g/l BSA) as a function of pH to PAA brushes (σ = 0.1 nm^{-2}, N = 270) at different ionic strength. (a). Experimental results, lines are guide to the eye. (b). Model results.

Discussion

At low salt concentration the protein BSA is able to adsorb in a negatively charged PAA brush up to a critical pH about 1.5 pH units above its pzc (and 2.4 units above its iep). At high salt concentration adsorption stops just a few tenths of a pH-point above the pzc. In the literature, one finds two arguments to rationalize adsorption of proteins 'at the wrong side of the pzc': (i) the 'correlation effect', which refers to the situation that a flexible polyelectrolyte can visit the attractive patches while avoiding the repelling ones, so that the overall free energy is negative; (ii) charge regulation of the participating macro-ions, so that an initially repulsive polymer/protein pair becomes attractive. Effect (i) is probably relatively weak but may well be dominant in the case of permanent charges; it will be very sensitive to the charge distribution. Effect (ii) requires weakly acidic or basic sites. In the latter case it is expected that the salt concentration has a large effect on the extent of adsorption. Since we have weak sites in the brush and the protein, and a mean field model including charge regulation agrees quite well with the data, we conclude that charge regulation is probably the dominant effect in the present system. The strong effect of salt concentration on the critical pH can then be explained in the following way: attraction above the pzc is due to the protein reversing its net charge, induced by the negative potential inside the polyelectrolyte brush. Although there is an energy penalty to these charge adjustments [10], complexation with the polyelectrolyte chains of the brush is very favorable as it allows the polyelectrolyte brush to increase its degree of dissociation, while small ions are released (ion release force). Note that ion release requires protein and brush to be oppositely charged in the brush. With increasing salt concentration, the entropy gain upon ion release decreases while the ionization of the empty brush is already much higher in the absence of protein adsorption. As a consequence the critical pH decreases with increasing salt concentration over the range 1 to 100mM from about pH 7 to pH 5.5. In solution charge regulation of BSA and PAA can be experimentally observed by pH stat titrations. We have added PAA to a BSA solution (1 g/l) at pH 6 (results not shown). About 10 protons per protein molecule are taken up during complexation, from which it can be derived that the charge of the protein is changed from net negative to net positive. Although charge regulation in the bulk and in a brush will be quantitatively different, this proton uptake is a clear indication of the relevance of charge regulation for the adsorption mechanism of BSA in a PAA brush.

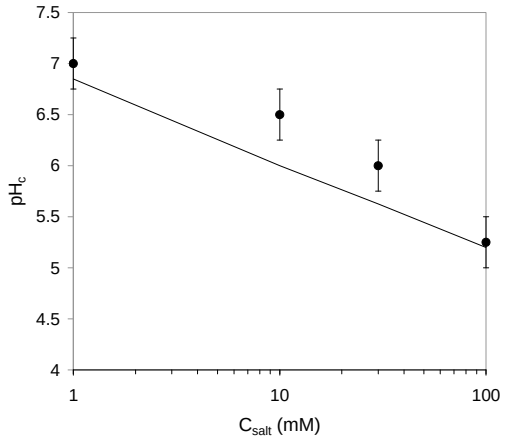

Figure 10. The pH_c (the pH at which the adsorption of BSA in the brush strongly decreases to zero) as a function of salt concentration. Points are experimental data, line is model prediction.

One characteristic experimental result is that the maximum in the adsorption is located near the pzc of the protein. The maximum can be explained as follows: with decreasing pH the negative charge of the brush decreases, and the positive charge of the protein increases. This lowers the adsorption capacity. At higher pH values the affinity decreases because charge regulation is not sufficient anymore in preventing repulsion. Therefore, there must be an optimal pH at which the charge of the polyelectrolyte is still high enough and the charge of the protein not too negative, which for this system is apparently around pH 5 and thus in between the iep and the pzc of BSA. This optimum will decrease with increasing salt concentration because charge regulation is suppressed.

It is interesting to compare our results with those for a brush on a spherical particle. Wittemann *et al*[3] have studied BSA adsorption on spherical polyelectrolyte brushes by depletion measurements. They report the adsorbed amount in milligram protein per gram of carrier particle. Since we know the size of the particles, the grafting density, and the molecular weight of the polyelectrolytes we can easily convert this to mg/m^2. We find that at pH 5.1 and a salt concentration of 12 mM, a grafting density of 0.13 nm^{-2} and a polymer length of 120 monomers, approximately 20 mg/m^2 has been adsorbed. This is almost twice the adsorbed amount of protein found in our experiment, but a direct comparison is hard because of the difference in grafting density and because the difference in geometry. Furthermore, there is a pronounced difference in polydispersity (M_W/M_N =1.05 for our polymer, M_W/M_N 1.7 for theirs). Our observation that the adsorption depends only weakly on the protein concentration (i.e. a high affinity character), differs from the results by

Wittemann *et al*[3]. At pH 5.1 and 10 mM buffer, they found that increasing the BSA concentration in the same range as in our study (from ~0.01 to ~3 g/l) resulted in a (gradual) increase of adsorbed amount by almost a factor of 10. Also, the decay of adsorption at a critical pH is found in our work at a lower pH than for the spherical brushes. (Note that this lower pH_c compares better to the predicted pH_C of previous models [9,10].) The conclusion that we can draw from the comparison is that in both cases very large adsorbed amounts are found compared to the adsorption of BSA to bare polystyrene surfaces, but the quantitative differences are difficult to explain from the difference in brush geometry and brush properties alone.

The model presented in this chapter describes our experimental data much better than comparable previous models[9,10] in which no adsorption took place above pH ~ 5.5. A major improvement in agreement was achieved by (i) the use of a more refined description of the charge of BSA as a function of pH using six ionizable groups as given by the Tanford model[31], and (ii) adding a nonelectrostatic attraction between the protein and the polyelectrolyte via the Flory-Huggins interaction parameter χ_{pb}. Furthermore, compared to ref. 10 we have improved the equation-of-state by no longer considering the "ideal gas" contribution of the chain segments in the brush (i.e. by excluding them from the overall particle concentration).

From our results, it follows that it is possible to explain the experimental protein adsorption data to a large extent on the basis of charge regulation of the protein and the brush. Using our model we are then able to separate the contributions of the protein and the brush to the total charge regulation. By way of illustration we analyse in Figure 11 the charge distributions in the filled and empty brush as well as the charge of the protein in the brush and in the bulk solution as a function of pH. The calculations are performed for a brush length of N=100, thus the 'absolute charge' for the brush chains equals the ionization degree per segment in percent. The protein charge is also expressed per chain taking into account the protein adsorption per chain, which is also presented in Figure 11. The dashed lines represent the situation before protein adsorption in the brush while the solid lines denote the situation after adsorption. Clearly, the absolute values of the charges of both protein and brush strongly increase upon protein adsorption in the brush. The difference in the charge of the protein and brush after adsorption is a measure for the charge compensation by the small ions. The role of small ions in charge neutralization is very pH dependent. Above pH 6 the charge of the brush is predominantly compensated by ions, while at pH 5 it is almost completely the protein that is responsible for charge neutrality. The role of protein in compensating the charge of the brush increases to 100% below pH 4. The protein charge per chain has a maximum of ~35 at pH around 5. With a maximum

protein adsorption (around that pH value) of 0.75 per chain, the charge of a BSA molecule in the brush is thus 46 at pH 5, a value that strongly increases with decreasing pH (85 at pH 3). Thus, it must be concluded that charge compensation is relatively high for both the protein and the brush, so that these effects cannot be neglected in any adsorption model for proteins on a surface carrying a weak polyelectrolyte brush.

From our model, we can also calculate the different contributions to the free energy change between the situation that the brush is empty and protein is in solution, and the situation in which the brush is in equilibrium with the protein solution. The results of this calculation are shown in Figure 12. The total free energy change has a minimum around pH 4.7, below the pzc of BSA. The main penalty that must be overcome is the modification of the charge of the protein molecules upon entry in the brush, which amounts to a maximum of +160 kT per chain (at pH 5.6; +100 kT per protein molecule at that pH). The driving force for this charge modification is the increase of ionization of the brush ($\Delta F_{\text{chem brush}}$) and the release of small ions. The latter is predominant at high pH (>5.7) while the first is predominant at low pH (<4). In the pH range of maximum protein adsorption both terms add significantly. The nonelectrostatic term added to the free energy balance in this chapter is most important at low pH (30% of the total driving force at pH 3, and decreasing rapidly to only about 8% above pH 5).

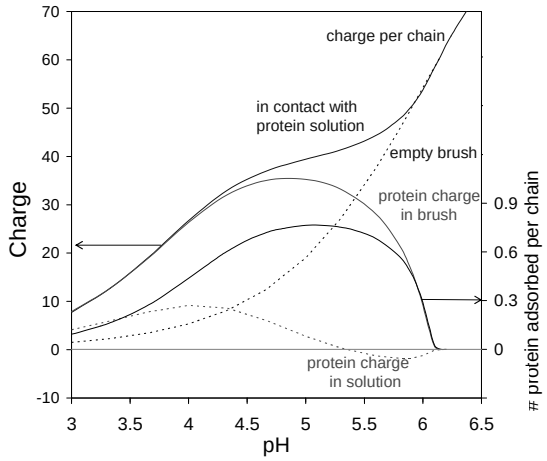

Figure 11. Model calculations of charge of the brush and protein, defined per chain (N=100) as a function of pH (c_∞ = 10 mM, σ = 0.1 nm^{-2}). The charge of the brush equals the fractional ionization degree, α, in percent (%). The dotted lines represent the charge of the empty brush and the charge of the equivalent amount of protein in solution; solid lines stand for equilibrium adsorption of protein in the brush.

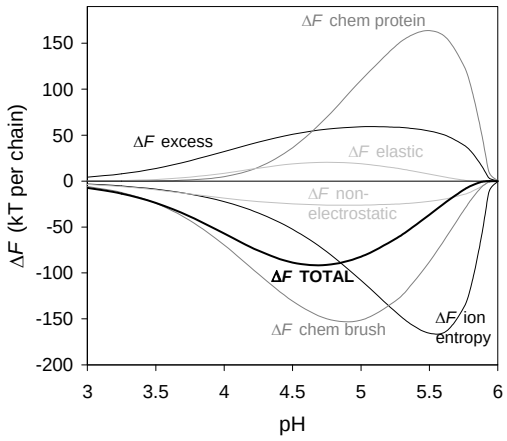

Figure 12. Contributions to the free energy change between a brush layer filled to equilibrium with protein molecules, and an empty brush (with protein in solution) as a function of pH (N = 100, c_∞ = 10 mM, σ = 0.1 nm^{-2}).

Conclusion

A detailed study of the adsorption of BSA to PAA brushes is presented in this chapter. Adsorption of BSA as a function of pH shows a broad maximum at about pH 5. Strong adsorption is also found above the pzc of the protein; thus, a net negatively charged protein adsorbs in a negatively charged PAA brush, up to a critical pH value. This critical pH value (pH_c) shifts to lower values with increasing ionic strength. The amount of adsorption is found to be very large, and we estimate that at least 30 volume percent inside the brush layer is occupied by protein molecules. In contrast to earlier studies, we find that there is almost no effect of protein concentration in solution on the adsorbed amount, which is in line with expectations for the high affinity system we investigate here. The adsorbed amount increases strongly with both increasing PAA chain length and increasing grafting density.

The experimental results compare satisfactorily to an analytical polyelectrolyte brush model, which incorporates charge regulation and volumetric interactions. Adsorption above the pzc of the protein is explained by charge regulation, which implies that the protein adjusts its charge because of the highly negative electrostatic potential in the brush. The strong effect of salt stems from an ion entropy effect and from the degree of dissociation of the polyelectrolyte. In a brush, polyanions have a much lower degree of dissociation than free monomers in solution because of the highly negative local potential. Charge reversed BSA molecules allow a highly favorable increase in the degree of dissociation of the polyanion. With increasing salt concentration, electrostatic potentials in the brush decrease in magnitude, and consequently, the degree of dissociation of the polyelectrolyte chains in the non-filled brush increases which results in a diminished driving force for subsequent protein adsorption.The model shows that nonelectrostatic attractive interactions (such as hydrogen bonds and Van der Waals forces) are required to satisfactorily describe the experimental results. The effect of charged patches, another explanation forwarded to describe the adsorption of BSA to PAA brushes at the wrong side of the pzc, is not required to describe the experimental data. Additional experimental evidence for charge regulation as a driving force derives from pH-stat measurements in solution. During complexation of PAA and BSA in solution at a pH that is at the “wrong” side of the pzc, enough protons are taken up to reverse the charge of the protein from net negative to net positive.

References

1. Currie, E.P.K.; Norde, W.; Cohen Stuart, M.A. *Adv. Colloid Interface Sci.* **2003**, *100*, 205.
2. Szleifer, I.; Carignano, M. A. *Macromolecular rapid communications* **2000**, *21*, 423.
3. Wittemann, A.; Haupt, B.; Ballauff, M. *Phys. Chem. Chem. Phys.* **2003**, *5*, 1671.
4. Neuman, T.; Haupt, B.; Ballauff, M. *Macromolecular Bioscience* **2004**, *4*, 13.
5. Wittemann, A.; Ballauff, M. *Analytical Chemistry* **2004**, *76*, 2813.
6. Czeslik, C.; Jackler, G.; Steitz, R.; Grünberg, H.-H. *J. Phys. Chem. B* **2004**, *108*, 13395.
7. Czeslik, C.; Jackler, G.; Hazlett, T.; Gratton, E.; Steitz, R.; Wittemann, A.; Ballauff, M. *Phys. Chem. Chem. Phys.* **2004**, *6*, 5557.
8. Rosenfeldt, S.; Wittemann, A.; Ballauff, M.; Breininger, E.; Bolze, J.; Dingenouts, N. *Phys. Rev. E* **2004**, *70*, 061403.
9. Biesheuvel, P.M.; Wittemann, A. *J. Phys. Chem. B* **2005**, *109*, 4209.
10. Biesheuvel, P.M.; Leermakers, F.A.M.; Cohen Stuart, M.A. *Phys. Rev. E* **2006**, *73*, 011802.
11. Hollmann, O.; Czeslik, C. *Langmuir* **2006**, *22*, 3300.
12. Wittemann, A.; Ballauff, M. *Phys. Chem. Chem. Phys.* **2006**, *8*, 5269.
13. Xia, J.; Mattison, K.; Romano, V.; Dubin, P.L.; Muhoberac, B.B. *Biopolymers* **1997**, *41*, 359.
14. Caruso, F.; Schüler, C. *Langmuir* **2000**, *16*, 9595.
15. Norde, W.; Giacomelli, C. E. *Macromol. Symp.* **1999**, *145*, 125.
16. Guo, X.; Ballauff, M. *Langmuir* **2000**, *16*, 8719.
17. Leermakers, F. A. M.; Ballauff, M.; Borisov, O. V. *Langmuir 2007*, *23*, 3937.
18. Kabanov, V. A.; Mustafaev, M. I.; Belova, V. V.; Evdakov, V. P. *Biofizika* **1978**, *23*, 789.
19. Seyrek, E.; Dubin, P. L.; Tribet, C.; Gamble, E. A. *Biomacromolecules* **2003**, *4*, 273.
20. Cooper, C. L.; Dubin, P. L.; Kayitmazer, A. B.; Turksen, S. *Curr. Op. Colloid Interface Sci.* **2005**, *10*, 52.
21. de Vries, R. *J. Chem. Phys.* **2004**, *120*, 2475.
22. de Kruif, C. G.; Weinbreck, F.; de Vries, R. *Curr. Op. Colloid Interface Sci.* **2004**, *9*, 340.
23. Biesheuvel, P. M.; Cohen Stuart, M. A. *Langmuir* **2004**, *20*, 2785.
24. Zhou F.; Biesheuvel, P.M.; Choi, E-Y.; Shu, W.; Poetes, R.; Steiner, U.; Huck, W.T.S., *Nano Letters*, **2008**, *8*, 725.
25. Lyulin, S.V.; Evers, L.J.; van der Schoot, P.; Darinskii, A.A.; Lyulin, A.V.; Michels, M.A.J. *Macromolecules* **2004,** 37, 3049.
26. Boublik T. *J. Chem. Phys*. **1970,** 53, 471.
27. Mansoori G.A.; Carnahan N.F.; Starling K.E.; Leland T.W. *J. Chem. Phys*. **1971**, 54, 1523.
28. Hiraoka, K.; Shin H.; Yokoyama, T. *Polymer Bulletin* **1982,** *8*, 303.
29. Kadi, N.E.; Taulier, N.; Le Huerou, J.Y.; Gindre, M.; Urbach, W.; Nwigwe, I.; Kahn, P.C.; and Waks, M. *Biophysical J.* **2006,** *91*, 3397.
30. Biesheuvel, P.M.; Lindhoud, S.; Cohen Stuart, M.A.; de Vries, R. *Phys. Rev. E* **2006**, *73*, 041408.
31. Tanford, C.; Swanson, S.A.; Shore, W.S. *J. Am. Chem. Soc.* **1955**, *77*, 6414.
32. Pujar, N.S.; Zydney, A.L. *J. Colloid Interface Sci.* **1997**, *192*, 338.
33. Currie, E.P.K.; Sieval, A.B.; Avena, M.; Zuilhof, H.; Sudhölter, E.J.R.; Cohen Stuart, M.A. *Langmuir* **1999**, *15*, 7116.
34. Maas, J. H.; Cohen Stuart, M. A.; Sieval, A. B.; Zuilhof, H.; Sudhölter, E. J. R. *Thin Solid films* **2003**, *426*, 135.
35. Gaines, G. L. *Insoluble monolayers at liquid-gas interfaces* **1966**, Wiley-Interscience, NY.
36. Wen, Y.-P.; Dubin, P. L. *Macromolecules* **1997**, *30*, 7856.
37. Giacomelli, C. E.; Avena, M. J.; De Pauli, C. P. *J. Colloid Interface Sci.* **1997**, *188*, 387.
38. Carter, D.C.; Ho, J.X. *Adv. Protein. Chem.* **1994**, *45*, 153.
39. Dijt, J.C.; Cohen Stuart, M.A.; Hofman, J.E.; Fleer, G.J. *Colloids and Surfaces* **1990**, *51*, 141.

Appendix A. Measuring charge regulation in solution

As discussed in the main text, we explain the adsorption of a like-charged-protein to a polyelectrolyte brush by assuming that under the influence of the negative electrostatic potential of the brush the protein adjusts its charge. Since charge adjustment takes place by uptake or release of protons, we can monitor the amount of charge regulation by pH measurements. Unfortunately such an experiment is not possible with our planar polyelectrolyte brushes. To measure a significant pH difference due to charge reversal, one would need a too large surface area covered with polyelectrolyte brushes. A different approach however, is to measure charge regulation for the bulk complexation between BSA and PAA. Here, we will first show the strong similarities between adsorption of protein molecules in a polyelectrolyte brush and protein-polyelectrolyte complexation in bulk. Thereafter we will show results of measured charge regulation.

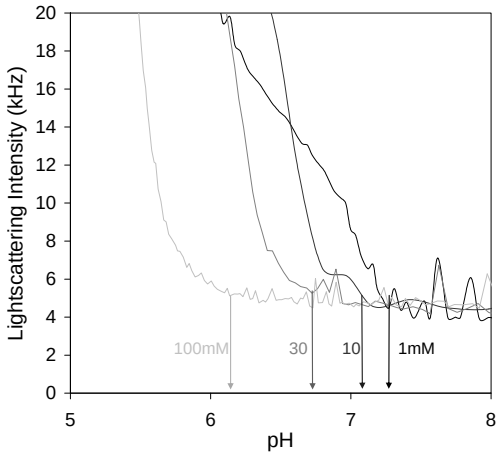

Figure A1. Light-scattering intensity as a function of pH for a mixture of 1 g/l BSA and 0.2 g/l PAA (M_N = 10 kg/mol) at different KNO_3 concentrations.

Both in adsorption in brush layers as well as in complexation in solution, proteins and polyelectrolytes are found to form complexes even when their (net) charges have the same sign. In Figure A1 we show light scattering results of a pH titration performed on a mixture of BSA and PAA in solution for different salt concentrations. Upon decreasing the pH, one passes a critical pH value below which significant complexation starts to take place. This critical pH decreases with increasing salt concentration. For all salt concentrations the pH_c is above the isoelectric point of BSA. Similar behavior has been reported for other protein-polyelectrolyte combinations [18-20]. This behavior in solution is completely in line with the adsorption behavior of BSA to a PAA brush as described above: a critical pH exists

below which adsorption strongly increases, and which shifts to lower values with increasing ionic strength. We conclude that it is very reasonable to assume that the driving forces for the adsorption of BSA to PAA brushes are the same as those for the complexation between BSA and PAA in solution. We note in passing that close to pH 5 the light scattering intensity becomes extremely high and the solution changes from clear to turbid indicating precipitation or phase separation of protein-polyelectrolyte complexes (data not shown). The exact pH for which this happens also decreases with increasing salt concentration.

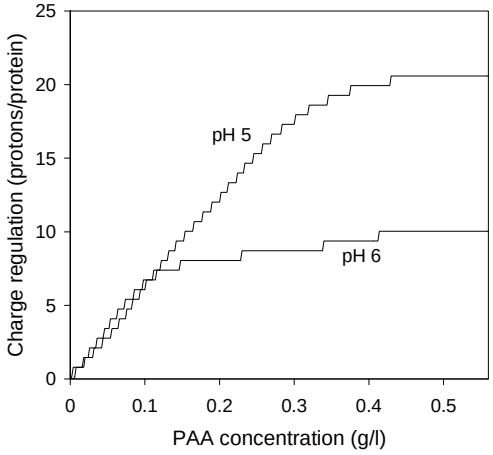

Figure A2. Number of protons taken up as a function of added PAA to a solution of 1 g/l BSA for different pH values at c_{KNO3} = 10mM. Measured by pH stat titration.

In Figure A2 we show the amount of charge regulation per BSA molecule, as a function of PAA concentration. The degree of charge adjustment was measured by adding PAA to a BSA solution of exactly the same pH in a so-called pH stat titration. The pH was kept constant by adding small amounts of concentrated acid whenever the pH became too high (i.e., more than 0.05 pH unit above the initial pH). pH changes are caused by uptake or release of protons from the protein or polyelectrolyte. Thus, the amount of protons required to keep the pH constant is a measure for the overall charge adjustment that takes place upon complexation. As can be seen for pH 6, per protein molecule complexed to PAA 10 protons are taken up. At pH 6, BSA has a net charge of –5 (Figure 1), and 10 protons would thus be enough to change its net charge from negative to positive. At pH 5, 21 protons were taken up per protein molecule complexed to PAA. These experiments show very clearly that upon complexation of BSA and PAA charge adjustment is taking place, enough for the protein molecule to reverse its charge. Note that the results shown here might even underestimate the exact amount of protons taken up by a single BSA molecule. Upon complexation of the

charge reversed BSA with PAA we expect that PAA will slightly charge up by taking up a few protons from solution. This would reduce the measured charge regulation in Figure A2.

One might wonder how we are certain that the protons are taken up by the protein molecule and not by the PAA. A simple argument for this is that charge reversal of the protein molecule can lead to attraction, while a reduced charge density of the PAA chains can only lead to a small reduction in repulsion. Furthermore, it has been well established by theory [39] and experiment [40, 41] that in case of charge reversal it is always the object that initially has the lowest potential relative to the bulk solution that adjusts the most.

Chapter 7

Field theoretical analysis of driving forces for the uptake of proteins by like charged polyelectrolyte brushes: effects of charge regulation and patchiness.

Abstract

At the moment two competing explanations exist for the experimental finding that net negatively charged proteins adsorb on or absorb in negatively charged polyelectrolyte brushes. One explanation is based on the possibility of charge regulation. The idea is that a protein can reverse its charge when it is in the presence of the high electrostatic potential of the brush and then can be inserted. The other explanation relies on the charge anisotropy of proteins, that is, that it carries positively charged and negatively charged patches. The positively charged region gains more energy from interacting with the negative brush than the negative charged patch looses, especially when the charge densities and electrostatic potentials are high, thus providing a net attraction. We present a model in which both mechanisms are combined. We confirm that both charge anisotropy- and charge regulation-effects on their own, can be responsible for protein uptake at the "wrong" side of the iso-electric point (IEP). In addition, we find that the respective effects are additive. Indeed, taking both effects into account results in a stronger attraction between a PE brush and protein at the IEP, and the attraction is found further above the IEP than the individual effects would have made possible. Still, for patchiness to have a strong contribution, the patches need very high charge densities. Therefore, we argue that for most types of protein charge reversal will be the main driving force for adsorption on the wrong side of the IEP, while patchiness will contribute less.

A manuscript based on this chapter has been accepted in *Langmuir*.

Introduction

For many applications, such as drug delivery, it is desired to have enzymes not free in solution, but encapsulated, e.g., through ad(b)sorption onto (into) a suitable carrier [1-8]. For example, one way to immobilize proteins is to adsorb the enzymes onto solid nano-particles [1] or absorb them into porous particles [2]. However, in many cases adsorption of enzymes to solid interfaces leads to conformational changes and an irreversible loss of activity [1]. A better way is then to immobilize enzymes by complexation with polymers/polyelectrolytes. Because polyelectrolytes are flexible and can adjust to the conformation of the enzymes, enzymes complexed with polyelectrolytes are typically found to retain their conformation and their enzymatic activity [3,4]. For this reason, much research has been devoted to incorporate enzymes inside gel particles [5] or into polymeric micelles [6,7]. Recently, it has been shown that charged polymer brushes are also a very promising system for enzyme immobilization [8,9].

The use of polyelectrolyte brushes to collect proteins was introduced in the work of Wittemann *et al* [8] who used so-called Spherical Polyelectrolyte Brushes (SPBs). These SPBs typically consist of a polystyrene nanoparticle (radius 50 nm) covered by a dense array of end-grafted poly(acrylic acid) (PAA) chains [10]. Because of the large space around the polystyrene core where the polyelectrolyte brush serves as the absorbent, and the strong attractive interactions between the polyelectrolyte and protein, very high adsorbed amounts were found. For example, for the protein bovine serum albumin (BSA), for which one usually finds adsorbed amounts of 1-2 mg/m^2 onto a solid interface [11], adsorption to polyelectrolyte brushes has been reported in the range 10-30 mg/m^2 [9,12 (chapter 6)]. Other investigations showed that the BSA is evenly distributed throughout the brush [13] and that the secondary structure of the protein was unaffected [14]. The protein is reversibly bound and can be released from the brush by imposing a high pH or a high salt concentration, showing that the binding is mainly electrostatic in nature. Also for the enzyme glucoamylase high adsorbed amounts and a retained enzymatic activity were found [15].

The research on SPBs as protein carriers has focused on the adsorption of proteins (especially BSA) at or above the iso-electric point (IEP) of the protein. Below the IEP, the adsorption of positively charged proteins to a negatively charged brush leads to neutralization of the brush layer. As the charges in the brush are needed to stabilize the particles against aggregation, this neutralization leads to a loss of colloidal stability. A remarkable finding is that above the IEP of the protein, that is where the (isolated) protein has a net negative charge, similar to the negatively charged brush, still a large uptake of protein into the brush is found [8-15]. At the same time the colloidal stability is retained.

De Vos *et al* [12 (chapter 6)] established that this adsorption above the IEP continues up to a critical pH (pH_c). This pH_c is a strong function of the salt concentration. More specifically, at low salt concentration (1 mM), adsorption was found up to 1.7 pH units above the IEP, at intermediate ionic strength this reduced to 1.2 pH units, whereas at high ionic strength (100 mM) no more adsorption is found above the IEP. The adsorption of proteins above their IEP onto a negatively charged brush is known as adsorption on the "wrong" side of the IEP.

The driving force for this phenomenon is currently under debate. In the recent literature, two viable options have been suggested. The first explanation is based on an inhomogeneous distribution of charges on the protein surface [9,16]. It is well known that a net negatively charged protein may still have surface patches with a net positive charge. Typically, the positive charges gain more energy from interacting with the negative brush than the negative charges loose, especially when the charge densities and electrostatic potentials are high, and hence an inhomogeneous charge distribution on the protein can explain the uptake at the wrong side of the IEP. This explanation was investigated by Leermakers *et al* using a 2-gradient SCF approach [16]. They computed changes in the free energy during the uptake of an (infinitely long) beam oriented parallel to a brush surface. The beam had two sides with equal but opposite charge density (that is the beam was overall electroneutral). The two charged sides had the same distance to the surface, so that a possible (free) energy gain due to a favorable orientation of the beam was avoided (the charge-dipole was oriented parallel to the brush surface). Both the brush and the charges on the patch had a quenched character (no pH dependence). At high charge density and sufficiently low salt concentration (high electrostatic potentials) the spontaneous uptake of the object in the brush was predicted, proving that patchiness is indeed a valid explanation for the adsorption on the wrong side of the IEP. This conclusion is supported by the work of Hu and Cao [17] who, using a coarse-grained model, studied the adsorption of patchy particles in a polyelectrolyte brush. Substantial adsorbed amounts were reported that increased with increasing particle dipole moment. In many cases a preference was found for the particle to adsorb to the edge of the polyelectrolyte brush.

The second explanation, worked out by Biesheuvel *et al* [12, 18, 19], is based on an effect called charge regulation. As the charges on the protein surface are generally pH-dependent, their degree of dissociation will also be influenced by the local electrostatic potential. The strong electrostatic potential in a polyelectrolyte brush might well be enough to change the net charge of the protein from like-charged to oppositely charged to the brush segments. De Vos *et al* [12 (chapter 6)] compared the results of a model which includes these charge regulation effects to experimental results on BSA adsorption to a planar PAA

brush. As they found good qualitative agreement between the model predictions and the experimental adsorbed amounts (above and below the IEP) it was concluded that charge adaptations contribute to the adsorption of proteins on the wrong side of the IEP. To date significant discussions remain because the two explanations have never been integrated into one and the same model.

It is the purpose of this chapter to present, and show results of, a model in which both the effects of patchiness and those of charge regulation are accounted for. For the first time this provides us with a method to make a fair comparison between the two existing explanations. The new model is a significantly improved version of the model used by Leermakers *et al* [16]. Now the protein is modeled as a finite-sized particle (cylinder) covered with both (weak) acidic and basic groups and the polyelectrolyte brush has annealed charges (it is a weak polyacid). In the new model it is possible to independently consider the effect of charge regulation and that of patchiness. Patches are created by placing the chargeable groups on opposite ends of the cylinder. Typically the charge-dipole of the protein-like object is oriented perpendicular to the surface with the most favorable side (positive side) towards the brush (for obvious reasons). We calculate the change in the free energy upon inserting the inclusion into the brush. When this free energy goes down, the protein is attracted to the brush and when it goes up, it is repelled. The key idea is to compute this insertion free energy as a function of the physical-chemical parameters for both homogeneously distributed and patch-wise distributed acid and basic groups on the protein. In this model it is now possible to unravel the relative importance of the two mechanisms and to predict how far above the IEP adsorption remains possible. It is shown that both processes contribute to the adsorption at the wrong side of the IEP and that they have additive effects.

In the next paragraph we will give more detailed information on the model and the approximations used in the theoretical analysis. There are many relevant parameters in this problem and we cannot deal with all of these. In the results and discussion section we focus on a type of case study as a full analysis is outside the scope of the present work. Nevertheless, results are critically compared to experimental data.

Theoretical considerations and model description

To accurately model polymer brushes it is necessary to solve the Edwards (diffusion) equation for polymer chains in inhomogeneous systems [20]

$$\frac{\partial G(\mathbf{r},s\,|\,1,1)}{\partial s}=\left(\frac{1}{6}\nabla^2-u(\mathbf{r})\right)G(\mathbf{r},s\,|\,1,1) \qquad [1]$$

where the Green's function G represents the statistical weight of all possible conformations of polymer chains with segment s' = 1 next to the surface ($\mathbf{r}_z$ = 1) and segment s' = s at coordinate **r**. This quantity is closely related to the chain partition function (that is, when s = N) and hence to the free energy of the system. In Eq. 1 it is necessary to specify the (dimensionless) segment potential $u(\mathbf{r})$. The role of the segment potential is to mimic the excluded-volume interactions as these result from, e.g., molecular crowding effects. This potential also accounts for the solvent quality. Here and below we assume that the solvent quality is good: the Flory-Huggins parameter χ = 0. In this case the bare second virial coefficient $v = 1-2\chi$ is unity [21]. Assuming for a moment that there is only one relevant coordinate, namely the distance to the wall (for which we use the z-coordinate), the segment potential becomes self-consistent when $u(z) = v\varphi(z)$. A polymer chain should connect its free end, irrespectively to the z-position of this (free) end, to the grafting segment by taking N steps in this potential field. The system can realize this by insisting on a parabolic shape of the segment potential, that is $u(z) = A - Bz^2$. A parabolic potential directly leads to the well-known parabolic volume fraction profile for a dense brush where the chains are strongly stretched [21-22].

Brushes composed of polyelectrolyte chains require an important extra term in the dimensionless segment potential, namely $\Psi(z) = e\psi(z)/kT$, where e is the elementary charge, kT is the thermal energy and $\psi(z)$ is the electrostatic potential. To evaluate this electrostatic potential one needs to solve the Poisson equation [23]:

$$\nabla^2\Psi(\mathbf{r})=-\lambda_B q(\mathbf{r}) \qquad [2]$$

Here $q(\mathbf{r})$ is the number distribution of charges (cations add positively and anions negatively to this quantity) and λ_B is the Bjerrum length which in water, around room temperature, is 0.71 nm. We will assume that the dielectric permittivity is equal to that of water throughout the system. The presence of charged segments in the brush introduces an electrostatic contribution to the effective virial coefficient. This contribution is inversely proportional to the concentration of mobile salt ions, φ_s, and a quadratic function of the charge density α in the brush: $v^{el} = \alpha^2/\varphi_s$ [24]. In many cases the bare virial coefficient is negligible compared to the electrostatic contribution. Again assuming that there is one

relevant coordinate, this implies that the electrostatic potential acquires a parabolic profile, that is $\Psi(z) = A - Bz^2$ [25].

Under relevant experimental conditions, the charges of the polyelectrolyte brush may have a permanent, that is a quenched, character, e.g. in the case of sulfonate groups. Alternatively, the charge on the segments may be annealed, as it results from the equilibration with protons, e.g., with carboxyl groups, hydroxyls or secondary amines. Such annealed brushes have various noteworthy properties such as a non-monotonic swelling with increasing ionic strength [26].

Protein molecules are an interesting class of macromolecules composed of amino acids. A high frequency of occurrence of hydrophobic amino acids in the protein molecule cause the molecule to collapse onto itself. Strategically positioned hydrophilic/charged groups force non-trivial conformations on the globule such that the charged groups are on the exterior. These charged amino acids often prevent the complete phase separation of protein and water. Globular proteins differ from a single molecule micelle because usually the proteins are quenched conformationally. Being in the preferred state allows one to model a protein by a near-to-spherical body with fixed shape and fixed distribution of chargeable groups on the outside. Charged amino acids have an annealed character as these can respond to the physical-chemical parameters that they experience in the local environment. Depending on the length of the amino acid chain, the size of the proteins is often in the nm range and the number of charged groups on the protein is relatively low. In such cases the distribution of the charged groups becomes a relevant issue. A non-random distribution, for example, a patched organization of the charges, is likely to be the case and this feature is relevant for its behavior. In the following, our interest is in modeling the interaction of proteins with polyacid brushes. To account for aspects mentioned above, we consider a small cylinder with two charged patches, one on the top and one on the bottom surface. This non-trivial object is studied in the neighborhood of the polyacid brush. For simplicity, we will refer to this object as protein-like inclusion, or as protein. A graphical illustration is shown in Figure 1.

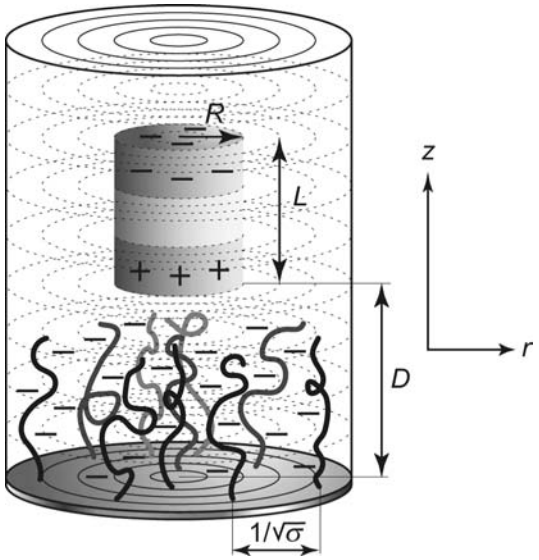

Figure 1. Schematic representation of the coordinate system used in the SF-SCF calculations. Here we show a small protein-like particle (top gray cylinder) with radius R and height L positioned at a distance D from the substrate. The particle is divided into three equally large parts: A top consisting of acidic groups, a neutral middle, and bottom consisting of basic groups. It is also possible to mix the acidic and basic groups at the top and bottom. The two-gradient coordinate system $\mathbf{r} = (z,r)$ *is indicated; layers parallel to the surface are numbered* $z = 1, 2, \ldots, M_z$. *In radial directions the lattice shells are numbered* $r = 1, 2, \ldots, M_r$. *At the surface, a negatively charged polymer brush with grafting density* σ *is present. In the SCF model we assume that the brush chains are laterally mobile along the surface. To avoid adverse effects of the finite size of the computation box, the boundary condition in the radial direction is mirror-like. The size of the polymer chains and that of the inclusion are not on scale.*

The coupled differential equations (Eqs. 1 and 2) highlighted above are solved numerically in a two-gradient coordinate system (Figure 1) to high precision [27]. For such a solution we can evaluate the mean-field free energy of the system, $F(\{n\},V,T) = -kT \ln Q(\{n\},V,T)$, where Q is the canonical partition function and $\{n\}$ is the total number of molecules in the system. Other quantities have their usual meaning. In the calculations we consider a polyelectrolyte brush at fixed ionic strength and pH. In such a system the characteristic function is a partial open free energy given by:

$$F^{(\mathrm{po})} = F - \sum_i \mu_i n_i \qquad [3]$$

In this equation μ is the chemical potential and n is the number of molecules. The summation runs over all molecules i of which not the number, but the bulk concentration is

fixed. In this sum we thus include water and all ions (protons, hydroxyls, sodium, chloride). It is important to mention that the protons that are bound to the acid groups of the brush as well as to the acid groups on the protein-like inclusion must also be included in this sum. The same applies for the hydroxyls that are bound to the basic groups of the protein. Not a part of this sum are the polymer brush chains (their number is fixed) and the protein (there is always one protein-like object in the system) and the solid substrate.

We now refer to the *z*-coordinate of the center of mass of the protein as the distance *D* of the protein to the surface. Systematic variation of *D* gives insight in the insertion free energy, which is computed by

$$\Delta F\left(D\right) = F^{(\mathrm{po})}\left(D\right) - F^{(\mathrm{po})}\left(\infty\right) \qquad [4]$$

where the latter term is calculated for the case that the protein-like inclusion is far from the brush, that is for $D \rightarrow \infty$. One of our interests is in knowing how this insertion free energy is a function of physical-chemical parameters such as the pH and ionic strength. Such results are important to understand why proteins spontaneously insert themselves (adsorb) into the brush even when their charge in the bulk solution has the same sign as the segments of the brush. Below we give some details about the implementation of the abovementioned equations and specify all parameters of the system.

The Scheutjens Fleer self-consistent field approach and parameter setting

All theoretical details of the equations outlined above and in particular how these have been implemented in the lattice model of Scheutjens and Fleer are readily available in the literature [27,28,29]. Hence, we will not repeat this here. It remains necessary, however, to elaborate on the molecular model. In passing we will briefly comment on the main approximations of the theory where appropriate.

The coordinate system is an important ingredient that is taken by the method as an input. It specifies exactly how the local mean-field approximation is implemented and this has direct consequences for the type of inhomogeneities that can develop. The current problem calls for a two-gradient coordinate system which is schematically shown in Figure 1. More specifically we use a cylindrical coordinate system with rotational symmetry. Gradients in segment concentration may develop both in a radial direction, for which we use the *r*-coordinate, and in the direction along the cylinder axis, that is the *z*-direction. The solid phase (substrate) is positioned at negative *z*-values; the surface is at $z = 0$, the first layer accessible for molecules is $z = 1$. The latter layer is where the first segments of the polymer chains are confined to. In principle there are two options for grafting these chains. One can either restrict the lateral mobility, or allow for it. We have chosen for the latter.

The lattice layers parallel to the surface are split up in concentric rings of lattice sites over which the mean-field approximation is applied. This means that we ignore the density gradients in these rings. The system size in the radial direction is set by M_r. This value is set to 20 which is sufficient to allow the perturbations caused by the protein inclusion to relax. The system in the *z*-direction extends to M_z = 112. At this layer mirror-like boundary conditions are implemented. This means that we focus on a pair of interfaces positioned a distance of 224 lattice sites apart. This system size is large enough so that the brush and its inclusion are easily contained. We note however, that for low ionic strength cases the two opposing surfaces have electrostatic interactions and therefore we will avoid very low ionic strength regimes. The segment size, corresponding to the linear size of a lattice site, is taken to be 0.5 nm, which is close to the Bjerrum length of 0.71 nm. Using this length we can relate the dimensionless volume fraction of salt to a molar concentration by multiplying the former by approximately 10.

The molecules. Besides the end-tethered polyacid chains and the rigid inclusion we have monomeric salt ions and a monomeric solvent (representing water). We will discuss all molecular species in order. The polymers are composed of segments type A and have the degree of polymerization of N = 50 segments. The grafting density is fixed in all calculations to σ = 0.02 chains per lattice site. The charge on the segments and how the charge is regulated is discussed below. Adopting the discretization scheme of Scheutjens and Fleer to solve the Edwards equation, implies the subtle change of the chain model from a Gaussian- to a freely-jointed chain. The inclusion has a cylindrical structure with length L = 3 sites in the *z*-direction and R = 2 sites in the r-direction and has no specific interactions with any of the molecular components. The top and bottom surface, however, each contain about 12 surface groups with a weak, that is pH-dependent charge. There are both acid and basic groups. In most of the calculations we have completely separated the charges such that the positive ones are on the face that is closest to the brush, i.e., lowest *z*-value (bottom face) and the negative ones are on the top face. Some more information on the charge regulation is given below. The two mobile ions are monomeric and have a permanent charge +1 for the cation and –1 elementary charge for the anion. The ionic strength in the system is mostly (protons and hydroxyls are included as well) determined by the volume fraction of the salt ions in the bulk, for which we use φ_s. Water is also a monomeric species and comes in three forms: the neutral, the cationic (proton) and the anionic (hydroxyl) form. The pH in the system is set by the fraction of the water molecules that is in the protonated state (in the bulk solution). We note that the fraction of protons in the brush and near the inclusion not only depend on the dissociation in the bulk, but also on the local electrostatic potential.

Charge regulation. In our model, the polymer brush, the two faces on the protein-like inclusion, and the water molecules have annealed charges that depend on pK values, pH, salt concentration as well as local electrostatic potential. The acid groups A in the polymer come in two states, a protonated state which is neutral and a deprotonated state with a negative charge: $A + H_2O \rightleftarrows A^- + H_3O^+$. Assuming carboxylic groups we could have chosen for a low $pK_{a,brush}$ value of 4. As most of the calculations are done for pH 7 or higher, this would imply that the brush is highly charged in all cases (effectively quenched). For this reason we have chosen for a higher value of $pK_{a,brush} = 7$, basically to remain in a regime where the charged brush still can adjust its charge density. The auto-dissociation of water is implemented as $2H_2O \rightleftarrows OH^- + H_3O^+$ with a pK_w of 14. The acid groups on the faces of the protein-like inclusion have a reaction equilibrium similar to the acid groups in the polymers, with a pK_a depending on the system specified below. An equal number of basic groups on the faces of the protein-like inclusion follow the reaction $B + H_2O \rightleftarrows B^+ + OH^-$ with a specified pK_b. Here we have chosen to use a symmetrical system: thus the pK_a for the negative sites is in all cases equal to the pK_b ($pK_b = 14 - pK_a$) of the positive sites. By using this symmetrical approach, the IEP of the protein is always $pH_I = 7$, as at this pH the acidic and basic groups will have exactly the same degree of association resp. dissociation. Varying the $pK_{a/b}$ values of the protein is (for this symmetrical system) a method to increase or decrease the range of pH values for which the protein adjusts its charges. A patched surface is realized by putting the acid and basic groups on different locations on the protein-like inclusion, that is, on the top or bottom faces.

In the results section we will discuss four systems. In the first, the charged groups ($pK_{a/b} = 7$) are mixed on both sides on the cylinder, and as such the charge on the object is not patchy. In the other three systems the positive and negative groups are placed on opposite sides of the cylinder, and the $pK_{a/b}$ value is varied ($pK_{a/b} = 7, 5.5, 4$).

Interaction parameters. In principle there are many Flory-Huggins interaction parameters that may influence the system. Above it was already argued that in the case of the polyelectrolyte brush the electrostatic virial coefficient is dominating over contributions due to the solvent quality and, therefore, we can safely choose athermal conditions for the polymer solvent interactions. For the same reason we neglect specific interactions of the ions with either the protein-like particle or with the polymer brush. Possibly the most significant interaction that affects the protein uptake in the polymer brush is a difference in interaction between the polymer units and the protein-like inclusion and between the water molecules and this object. When the polymer units adsorb preferentially over water on the protein, this would imply an extra driving force for its incorporation into the brush. As we

are in first instance interested in the generic electrostatic driving forces rather than the specific interactions, we deliberately ignore these interactions here. In future studies, however, we definitely should consider this interaction mechanism as well.

Results and discussion

The isolated polyelectrolyte brush

Before we turn our attention to the interaction of the protein-like particle with the polyelectrolyte brush, we first illustrate the effects that the pH and salt concentration have on an unperturbed polyacid brush. These results are of course well known in the literature, but are reproduced for ease of reference.

In Figure 2, we show the average degree of dissociation α of the acid segments as a function of pH. The polyelectrolytes in the brush are anionic and the monomers have a pK_a value of 7. Thus, if the polymer segments would be fully isolated from the others, we would expect the polyelectrolyte chain to be 50% charged at pH 7. For the high salt concentration of φ_s = 0.1, we find that this is indeed the case, however, if the salt concentrations is decreased, the pH at which the polyelectrolyte is 50% charged shifts to higher pH values (for φ_s = 0.0001 to pH 9.4). In other words, because of the dense grafting of the polymer chains the charges in the brush clearly affect each other leading to a suppression of the degree of dissociation. Addition of salt screens this interaction and thus allows the polyelectrolyte to be more fully charged. These observations are in agreement with the experimental results of Currie *et al* [30]. These authors showed by optical reflectometry that in a polymer brush consisting of a weak polyelectrolyte (poly(acrylic acid), σ = 0.125 nm^{-2}, c_{KNO3} = 1 mM) the pH value at which the polyelectrolyte in the brush is 50% charged can be shifted by more than 1.5 pH units with respect to its intrinsic pK_a value.

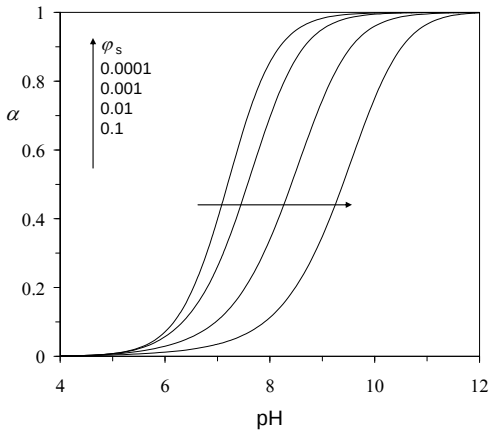

Figure 2. The average degree of dissociation (α) of polyelectrolyte chains in a brush (N = 50, σ = 0.02, pK_a = 7) as a function of pH. The ionic strength is varied by three orders of magnitude as indicated.

This dependence of the degree of dissociation on the pH and the salt concentration will obviously also affect the density profiles of the polymer brush. In Figure 3a we present the polymer volume fraction as a function of distance from the surface (z) for different pH values (at a fixed φ_s = 0.001). Indeed, the effect of the pH is straightforward: the higher the pH, the higher the average degree of dissociation and thus the stronger is the stretching of the polymer chains in the brush. In Figure 3b we quantify the stretching of the polymer in the brush by showing the height (H) of the brush as a function of salt concentration for different pH values. The height is defined here as the first moment (average height) of the polyelectrolyte chain end-points, and is a direct measure for the average degree of stretching. As shown in Figure 3b, the height of the brush is a increasing function of the pH and it is non-monotonic with varying ionic strength. The latter effect is less obvious, yet well known [26]. The ionic strength not only influences the degree of dissociation of the polyelectrolytes, but also affects the interaction between the charges in the brush. At the lowest ionic strength (φ_s = 0.0001), the degree of dissociation is low (see Figure 2) and the brush height will be also rather low. For pH 7, the degree of dissociation is so low (α = 0.035) that the brush height is almost equal to that of a neutral polymer brush of the same grafting density and chain length. An increase in the salt concentration leads to an increase of the charge density in the brush. As the charge is locally compensated by salt ions, there is an increase in the osmotic pressure. This causes an uptake of solvent and thus to a more swollen brush. This regime, where the solvent uptake is driven by the osmotic pressure of the counter ions, is called the osmotic regime. At the highest salt concentration we arrive at

the situation that the salt concentration outside the brush is larger than that inside the brush. In this so-called "salted brush" regime, the brush height decreases with salt concentration because the charges become more and more screened.

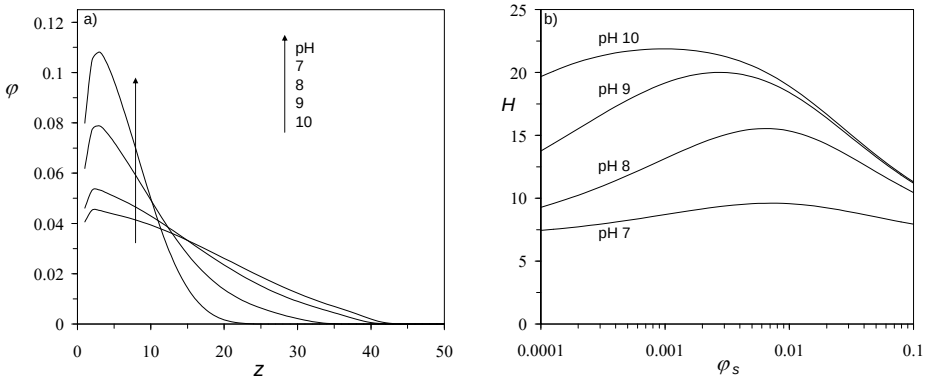

Figure 3. a) The volume fraction of polymer (φ) as a function of layer number (z) (distance to the surface is given by z times 0.5nm) for different pH values as indicated and φ_s = 0.001. b) The height of the brush (H, defined as the average height of the chain ends) as a function of salt concentration for different pH values as indicated.

The isolated protein

As discussed in the theory section, the protein-like particle is modeled as a cylinder with weakly charged groups on both sides of the cylinder. The twelve acidic and twelve basic sites can either be mixed on both sides, or can be placed on opposite sides of the protein-like particle. In this way we can introduce charge anisotropy (patchiness). As the sites are weak acids and bases, the degree of dissociation is determined by their pK values, the pH and the local electrostatic potential. Recall that due to the choice of parameters the proteins have their IEP at pH 7 (in the bulk).

In this investigation we consider four systems mentioned in the theory section at φ_s = 0.001. System 1 has acid and basic groups on both protein faces. Systems 2, 3, and 4 have a patchy configuration with the basic groups on the lower face and the acid groups on the top face with $pK_{a/b}$ = 7, 5.5 and 4, respectively. As we will show, varying the $pK_{a/b}$ values is a way to tune the charge density of the patches. In Figure 4a we show the net charge of the protein as a function of pH for all four systems. As we can see, the four systems have almost identical titration curves. The net protein charge is about 12 (the maximum charge) at low pH, the IEP is as expected exactly pH 7, and at high pH the minimum charge (–12) is reached. For the mixed system (system 1; no patches), the charge per side is simply half

of the net protein charge. For the patchy systems (systems 2, 3, 4) this is no longer the case. In Figure 4b, we give the charge on each face for the patchy systems. The lower the $pK_{a/b}$ value, the higher the charge density on both sides. This difference only disappears at extremely low or high pH at these points the groups are either completely charged or uncharged. Thus, the lower the $pK_{a/b}$, the higher the charge anisotropy.

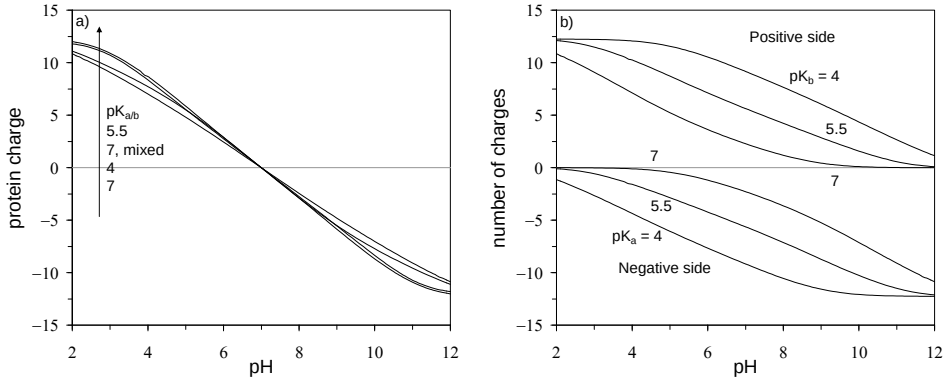

Figure 4. Charge of the protein-like particle (in units e) as a function of pH for different protein properties as indicated, in the bulk solution (φ_s = 0.001). a) The net protein charge. b) The number of charges per face of the protein as a function of pH for systems 2, 3, 4 with pK values as indicated.

Interaction between protein and brush

We use the following approach: we start by investigating the interaction between a protein-like inclusion and the polyacid brush for the case in which the charges are evenly distributed on the protein-like particle. We compare the results to those obtained for different degrees of charge anisotropy.

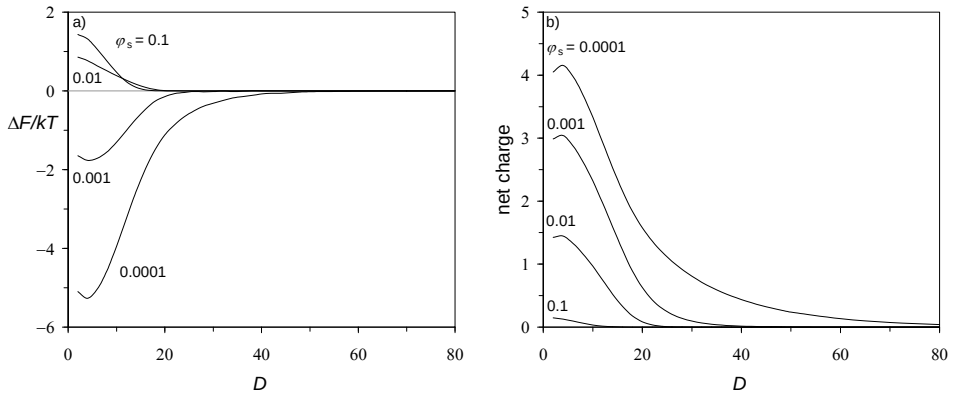

Figure 5. a) The free energy of interaction, in units kT, between protein and polyelectrolyte brush at the IEP of the protein (pH 7) as a function of distance D (in units of lattice size a) of the inclusion to the solid substrate for different salt concentrations as indicated. b) The corresponding net protein charge (in units of elementary charges e).

In Figure 5 we present results for the interaction between a non-patchy protein and a polyacid brush, exactly at the IEP of the particle (pH 7). Again, when the protein is not in contact with the brush, its net charge is equal to 0. However, in contact with the brush the charges are allowed to adjust and the protein becomes positively charged. In Figure 5a we investigate the free energy of interaction ΔF as a function of distance D between the protein and the surface to which the brush is grafted. At a large distance (D = 80), ΔF approaches 0, as there is no interaction between protein and brush, but this changes as the protein is moved towards the polymer brush (going to a lower D). A negative ΔF indicates attraction, which would lead to the uptake of proteins (ad(b)sorption). A positive ΔF indicates repulsion. At low salt concentration (φ_s = 0.001, 0.0001), we find as expected a negative ΔF for all distances D. A minimum in the free energy is found deep inside the brush, where the polymer density is highest. This means that at this distance the electrostatic attraction competes with the osmotic pressure (molecular crowding effects) in the brush. For the lowest salt concentration the minimum in ΔF is about –5 kT, and thus (at this pH and salt concentration) one should anticipate strong protein adsorption. The free energy of interaction, however, depends strongly on the salt concentration. For φ_s = 0.001 the

minimum in the free energy is only about –2 *kT*, and at φ_s = 0.01 and 0.1 the electrostatic attraction is too small to compete with excluded-volume effects and repulsion is found. The onset of the interaction also depends on the salt concentration, the lower φ_s, the further away from the interface that we find a non-zero ΔF. When we compare Figure 5a with Figure 3a, we see that a measurable change in free energy coincides with entering the brush.

As the protein in Figure 5 is non-patchy and neutral in the bulk, the only explanation for the observed attraction at low salt concentration is charge regulation. In Figure 5b we show how the net charge of the protein changes upon insertion into the brush. As expected, the deeper the protein is inserted into the negatively charged brush, the larger its positive charge. Again, the onset and the extent of the charge regulation are determined by the salt concentration. The lower the salt concentration, the higher *D* for which the charge is already affected, and the more the charge is changed. Apparently, the protein-like inclusion already start its charge adjustments in the diffuse layer on top of the brush. The strong salt dependence found in Figure 5a has a counterpart in the charge regulation: higher salt concentrations not only reduce the electrostatic interaction, but also reduce the amount of charge regulation that takes place. It is concluded that charge regulation can be an important factor for the uptake of proteins in a charged brush.

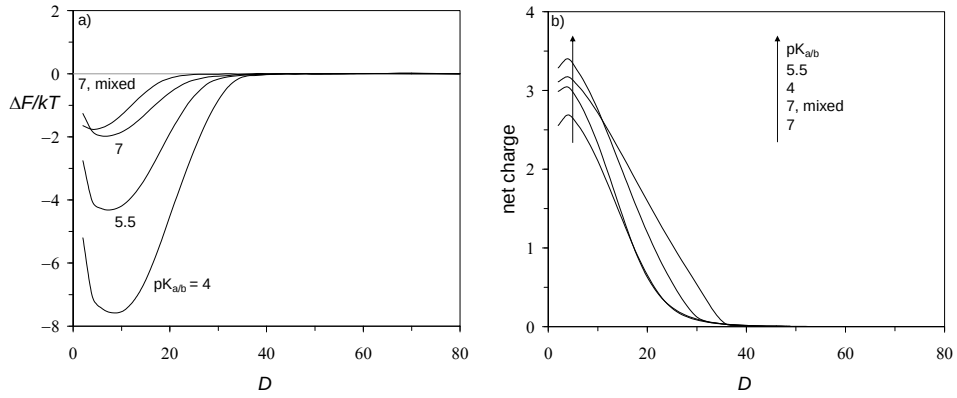

Figure 6. a) Free energy of interaction in units of kT between protein and brush at the IEP (pH 7, φ_s = 0.001) as a function of distance D, in units a, for different degrees of charge anisotropy as indicated. b) The corresponding net protein charge, in units e.

Let us next consider the effect of charge anisotropy (patchiness). In Figure 6, we investigate the four systems that differ with respect to the level of this anisotropy, at the IEP of the protein (pH 7, φ_s = 0.001). It is important to recall that in these conditions the net

charge of the protein outside of the brush is the same in all cases, but that the two sides of the protein (the patches) have very different charge densities. For the mixed system, the charge density at both sides is zero, for the other systems the charge density at each side depends on the $pK_{a/b}$ as shown in Figure 4a (at pH 7: $pK_{a/b}$ = 7, 0.7 charges/nm^{-2}, $pK_{a/b}$ = 5.5, 1.8 charges/nm^{-2} $pK_{a/b}$ = 4, 3.0 charges/nm^{-2}). Note that for all of these systems the charge density is rather high, we believe that only few types of protein exist that have patches with such high charge densities at the IEP and at low salt concentrations. These high charge densities were chosen as Leermakers *et al* [16] already showed that high electrostatic potentials are necessary to achieve a strong contribution of patchiness to ΔF.

Focusing first on the comparison of the free energy of interaction (Figure 6a), it is noticed that this quantity is a strong function of the charge anisotropy. For all systems we find attraction between brush and protein, but this attraction is higher when the protein has a higher charge on each face. In addition the minimum in the interaction free energy slightly shifts with increasing degree of charge anisotropy: for the mixed system, the minimum is found at D = 4, whereas for $pK_{a/b}$ = 4, it is at D = 8. In the mixed system, the minimum in the free energy is found at the location where the charge regulation is strongest: at the highest density of polyelectrolyte chains. For the patchy proteins, the most favorable position for the positive patch is where most negatively charged groups are, that is deep in the brush, whereas the negative patch prefers a position with a low chain density. For that reason the minimum shifts towards the edge of the polymer brush. With increasing brush grafting density (results not shown) this effect becomes stronger and eventually the minimum in the free energy of interaction is found at the edge of the polyacid brush. For the least patchy protein ($pK_{a/b}$ = 7) we find only a small change of ΔF with respect to that of the non-patchy protein. As argued above, high charge densities are necessary to achieve a strong effect on ΔF.

To be sure that the changes in ΔF in Figure 6a can be attributed purely to changes in the amount of charge anisotropy, it is not enough that for all the systems the net protein charge outside of the brush is identical. The protein charge inside the brush also needs to be (approximately) the same. That this is the case, is shown in Figure 6b. For all four systems, at a given value of D, the net protein charge is nearly the same, the small differences that are observed cannot explain the large differences in ΔF observed in Figure 6a. Thus, we conclude that patchiness indeed can be an important factor for the uptake of proteins and that charge regulation and a non-homogeneous charge distributions on the protein surface will both contribute to the uptake of proteins. Apparently, the two effects are additive as together they give the largest free energies of interaction.

Interaction as a function of pH

Let us next consider how the pH influences the protein uptake, and focus on the range of pH values above the IEP of the protein. The key interest of course is to know up to what pH above the IEP adsorption is still expected. Predictions are of interest as these can directly be compared to experimental results [12]. Let us again start with system 1 where the charges on both faces are mixed for a low ionic strength case ($\varphi_s = 0.0001$). Indeed, for the low ionic strength limit we expect the largest effects. In Figure 7 we show the free energy of interaction as a function of D, for a number of different pH values. Above the IEP the interaction curves are more complicated than below this pH. Repulsion is expected at large distances, because like charges repel each other. When attraction occurs, we must attribute these to charge regulation effects. This situation is analogues to the asymmetric situation of two negatively charged (regulating) surfaces, one strongly charged and one weakly charged. For such a system experiments showed long range repulsion and short range attraction [31].

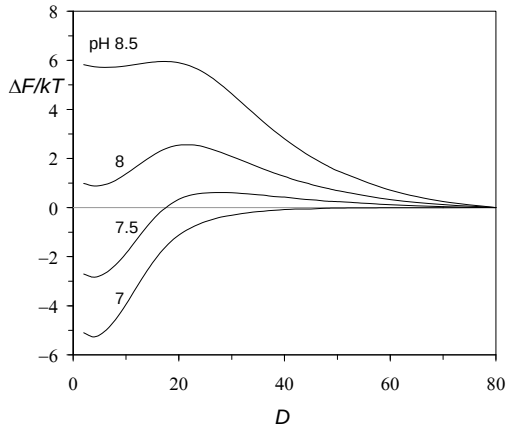

Figure 7. Free energy of interaction in units of kT between a non-patchy protein ($pK_{a/b} = 7$, mixed) and the brush as a function of distance D in units a for different pH values as indicated ($\varphi_s = 0.0001$).

Inspection of Figure 7 proves that with increasing pH, the interaction between the protein, which is negatively charged in the bulk, and the negatively charged brush are attractive at small values of D, but repulsive at large D. Somewhere between pH 7.5 and 8, the brush switches from being an adsorbing medium to one that depletes the protein. The pH value at which the transition occurs is called the critical pH point (pH_c). Interestingly, for pH 7.5, the attraction is only found in the dense parts of the polymer brush: at higher D values we find repulsion. We argue that only in the dense part of the brush, the charge of

the protein is sufficiently adjusted (this costs free energy) from negative to positive to be able to profit enough from the electrostatic attraction. At the distal parts of the interaction curve the brush density and thus the negative electrostatic potential is significantly lower. As a result also the charge on the protein has not reached the values necessary for the attraction. This does not mean that the effective charge of the protein is negative as we will show below.

The free energy barrier, which for pH 7.5 is slightly less than 1 *kT*, has a small effect on the adsorption kinetics. When this barrier grows, that is, when the pH is increased, it may seriously slow down the adsorption rate. Indeed, de Vos *et al* [12 (chapter 6)] found that the initial adsorption rate for the protein BSA (IEP ~pH 5.3 [32] (no fatty acids)) to a PAA brush is much lower above the IEP (pH 6), than at a pH just below the IEP (pH 5).

To more precisely determine the pH_c, ΔF was computed for many pH values for a fixed value of D (D = 8). The results of this 'measurement' are shown in Figure 8a. For the lowest salt concentration (φ_s = 0.0001), we find that pH_c = 7.9. Thus, protein adsorption would be expected up to 0.9 pH units above the IEP. With increasing salt concentration the pH_c decreases, for φ_s = 0.001 the pH_c has reduced to 7.35, and for φ_s = 0.01 and φ_s = 0.1 no adsorption above the IEP is found. This effect of the salt concentration is in line with the experimental results of de Vos *et al* [12 (chapter 6)]. They found for BSA adsorption to a PAA brush, that an increase in the salt concentration leads to a lower pH_c (pH_c = 7 for 1 mM $NaNO_3$, pH_c = 6.5 for 10 mM $NaNO_3$, pH_c = 6 for 30 mM $NaNO_3$, pH_c = 5.3 for 100 mM $NaNO_3$.).

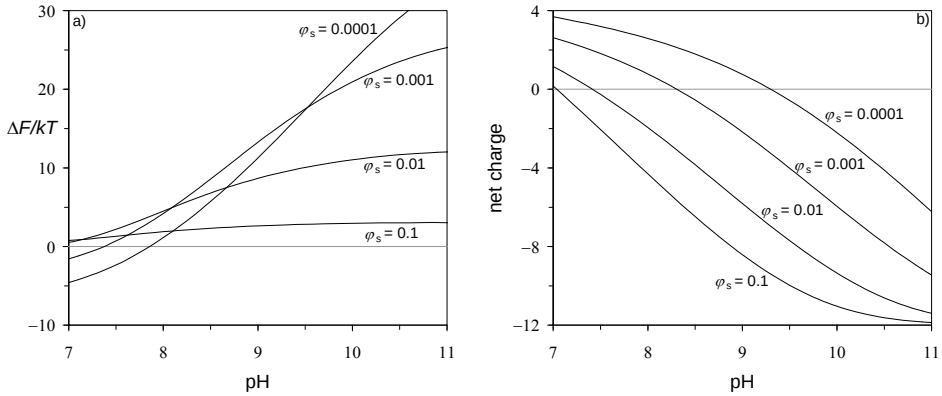

Figure 8. The value of the free energy of interaction in units kT for a non-patchy protein ($pK_{a/b}$ =7, mixed) located at D = 8 and a brush as a function of pH for different salt concentrations as indicated. b) The net protein charge (in units e) when it is at D = 8 for the same ionic strengths as used in panel a.

In Figure 8b we present the charge of the protein that is positioned at D = 8 as a function of pH. As can be seen, the net protein charge may become positive over a significant range of pH values, while outside the brush it is negative for all pH values above 7 (see Figure 3a). Thus, the net charge of the protein has indeed been reversed from negative outside of the brush to positive inside the brush. The degree of charge regulation is strongly dependent on the salt concentration. The pH where the protein switches its charge may be called the pH_0. It is noticed that $pH_0 > pH_c$. This means that in all cases a significant charge regulation is necessary to reach the pH_c. Thus, although the protein has reversed its net charge, we can have situations where repulsion still prevails. This is only partly due to the high excluded-volume interactions (molecular crowding) in the brush.

Reference calculations with the same polyacid brush and for a protein with quenched charges (calculations not presented), proved that for low salt concentrations, a small positive charge on the protein (> 0.5) can overcome the excluded-volume interactions. The fundamental reason why $pH_0 > pH_c$ is that there is a free energy cost related to the charge adjustments of the protein. As such, for charge regulation to lead to attraction, the energy gain resulting from the net positively charged protein being placed in a negatively charged brush must be larger than the energy penalty for charge adjustment. The existence of such an energy penalty in protein adsorption was already discussed by de Vos *et al* [12 (chapter 6)].

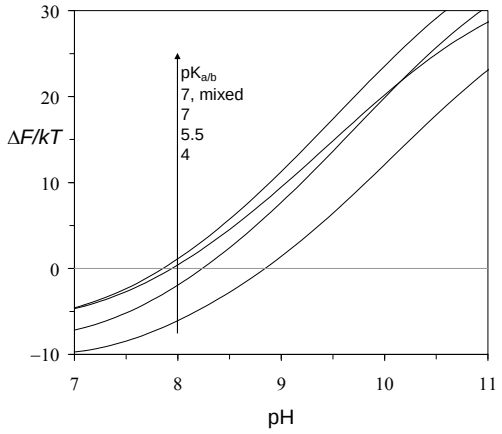

Figure 9. Free energy of interaction in units kT between protein and brush as a function of pH for different degrees of charge anisotropy as indicated (D = 8, φ_s = 0.0001).

Let us finally consider the role of patchiness on the pH dependence of protein uptake. In Figure 9, we show the free energy of interaction for different systems (protein located at D = 8) as a function of pH. Focusing again on the shift of the pH_c, we find that by increasing the value of the pK's one can increase pH_c by one pH unit. Again, the net charge of the protein does not depend much on the pK values used. This is true outside the brush (Figure 4a) but also when the protein is at D = 8 (result not shown). The differences seen in Figure 9, can be attributed to the effect of patchiness.

This result is consistent with the result of Figure 6a where the lowering of the free energy of interaction with increasing $pK_{a/b}$ values was reported. For the highest degree of charge anisotropy, attraction is found up to 1.8 pH units above the IEP. This is twice the value found for a protein with a homogeneous charge distribution. This again shows that effects of charge regulation and protein anisotropy are additive. A protein with weak charges will adsorb on the wrong side of the IEP, but if the protein also has distinct patches, adsorption of the protein in the brush will be possible further from the IEP. For the lowest degree of patchiness ($pK_{a/b}$ = 7) only a very small change in the pH_c is found with respect to that of the non-patchy protein. Clearly, high charge densities are necessary for patchiness to have a strong effect on the pH_c.

Distinguishing between charge regulation and patchiness

Above we have shown that patchiness and charge regulation have additive effects that are of the same magnitude. This makes it hard to determine, for a given protein, whether only one- or both effects caused adsorption at the wrong side of the IEP. The difficulty arises because both effects are electrostatic in nature and hence are affected similarly by, for example, the salt concentration. In this section we elaborate on approaches that can be used to distinguish between charge regulation and patchiness.

One significant difference between patchiness and charge regulation is their effect on the overall charge in the brush. The adsorption of a patchy particle (with fixed charges) to an oppositely charged brush will add to the amount of negative charges in the brush. On the other hand, charge regulation will decrease the overall negative charge in the brush. By measuring the zeta-potential of the brush with, for example, electrophoresis (for SPBs) or streaming potential measurements (for planar brushes) such a difference could be quantified.

A method to quantify the charge regulation is to measure the uptake from or release of protons to the bulk solution, i.e, by measuring pH changes. De Vos *et al* [12 (chapter 6)] used this approach for the bulk complexation of BSA and PAA and found that BSA indeed

reverses its charges upon complexation above its IEP. This approach can also be used with SPBs to quantify the charge regulation for adsorption of proteins to a polyelectrolyte brush.

An alternative is to focus on protein properties. All proteins have weak charges (hence have an IEP), and therefore charge regulation will always play a role. How important charge regulation is, can be estimated from information on the number of charges of the protein as a function of pH. When around the IEP of the protein minor pH changes lead to large changes in the net charge, one can expect that a high electrostatic potential in the brush will also lead to correspondingly large shifts in the net charge. From our work, we estimate that at low salt concentrations, the shift in the net charge will correspond to the shift resulting from changing the pH by 1.5 to 2.5 pH units. For patchiness, we need to quantify the degree of charge anisotropy. This is possible, as the structure of many proteins is known. Not only the size of these patches, but as was shown by Leermakers *et al* [16] and in the previous section, also the charge density on these patches is important. More specifically at least 1 charge per nm^2 is needed for a strong contribution.

As an example we implement this approach for BSA. For this protein, the net charge shifts from approximately –6 at pH 6, to +10 at pH 4.5 [33], indicating that upon adsorption in a negatively charged brush charge regulation is likely to occur with significant effect. In the work of Seyrek *et al* [34] images of the charge distribution on BSA are shown at the relevant pH of 6.5. These images show that BSA is indeed patchy, but that the positively charged patch does not have a high charge density. The rather uniform charge distribution of BSA (investigated at pH 5.8) is also confirmed by Carter and Ho [32]. Therefore, we expect that for BSA adsorption above the IEP, both patchiness and charge regulation will contribute, but that charge regulation will be most relevant.

Conclusions

In this chapter we have presented a model in which we combine two effects that influence the uptake of a protein to a polyelectrolyte brush on the wrong side of the IEP, that is when the protein in the bulk has the same charge sign as the polyelectrolyte brush. Both effects have previously been used, in separate models, to explain this phenomenon. The first effect, patchiness, is based on the fact that not too far from its IEP a net negatively charged protein may still have distinct positively charged patches. Typically, the positive charges gain more energy from interacting with the negative brush than the negative charges loose, especially when the charge densities and electrostatic potentials are high (Poisson-Boltzmann regime). Hence, an inhomogeneous charge distribution on the protein can explain the uptake at the wrong side of the IEP. The second effect, charge regulation, is based on the ability of weakly charged (pH dependent) amino acids to adjust their charge to the local electrostatic potential. In short, charge regulation allows the protein in the brush to change its net charge from like-charged (outside the brush) to oppositely charged (inside the brush). As opposite charges attract, this effect will assist the uptake of proteins at the wrong side of the IEP. Our model calculation confirm that each of the effects separately can explain protein uptake above the IEP, but the more likely scenario is that both factors contribute. We have shown that the two mechanisms have additive effects, which we demonstrate by calculating the free energy of interaction between a protein-like particle and a polyelectrolyte brush using a two-gradient self-consistent field model. We investigated four different systems in which the net charge of the protein is conserved, but with very different degrees of patchiness. For a non-patchy protein we find a significant attraction at the IEP and the attraction remains up to 0.9 pH units above the IEP. Introducing two faces on the protein with different charge densities leads to a stronger attraction at the IEP, and this attraction remains up to 1.8 pH units above the IEP for the highest charge density on the faces. Still, for patchiness to have a strong effect, the patches need to have high charge densities.

As all proteins have weak charges (hence have an IEP), we expect charge regulation to be an important driving force for adsorption at the wrong side of the IEP for all types of protein. Many proteins have a significant inhomogeneous charge distribution, but only in a few cases do these patches reach the high charge densities that are necessary for a strong contribution of patchiness. As such, patchiness will generally only contribute to a small degree to adsorption on the wrong side of the IEP.

References

1. Norde, W.; Zoungrana, T. *Biotechnol. Appl. Biochem.* **1998**, *28*, 133.
2. Zhao, X.S.; Bao, X.Y.; Guo, W.P.; Lee, F.Y. *Materials Today* **2006**, *9*, 32.
3. Caruso, F.; Schüler, C. *Langmuir* **2000**, *16*, 9595.
4. Xia, J.; Mattison, K.; Romano, V.; Dubin, P.L.; Muhoberac, B.B. *Biopolymers* **1997**, *41*, 359.
5. Oh, J.K.; Drumright, R.; Siegwart, D.J.; Matyjaszewski, K. *Prog. Polym. Sci.* **2008**, *33*, 448.
6. Harada, A.; Kataoka, K. *Macromolecules* **1998**, *31*, 288.
7. Lindhoud, S.; de Vries, R.; Schweins, R.; Cohen Stuart, M.A.; Norde, W. *Soft Matter* **2009**, *5*, 242.
8. Wittemann, A.; Haupt, B.; Ballauff, M. *Phys. Chem. Chem. Phys.* **2003**, *5*, 1671.
9. Wittemann, A.; Ballauff, M. *Phys. Chem. Chem. Phys.* **2006**, *8*, 5269.
10. Guo, X.; Ballauff, M. *Langmuir* **2000**, *16*, 8719.
11. Norde, W.; Giacomelli, C.E. *J. Biotechnology* **2000**, *79*, 259.
12. de Vos, W.M.; Biesheuvel, P.M.; de Keizer, A.; Kleijn, J.M.; Cohen Stuart, M.A. *Langmuir* **2008**, *24*, 6575.
13. Rosenfeldt, S.; Witteman, A.; Ballauff, M.; Breininger, E.; Bolze, J.; Dingenouts, N. *Physical review E* **2004**, *70*, 061403.
14. Wittemann, A.; Ballauff, M. *Analytical chemistry* **2004**, *76*, 2813.
15. Neuman, T.; Haupt, B.; Ballauff, M. *Macromolecular Bioscience* **2004**, *4*, 13.
16. Leermakers, F.A.M.; Ballauff, M.; Borisov, O.V. *Langmuir* **2007**, *23*, 3937.
17. Hu, Y.Y.; Cao, D.P. *Langmuir* **2009**, *25*, 4965.
18. Biesheuvel, P.M.; Wittemann, A. *J. Phys. Chem. B* **2005,** *109*, 4209.
19. Biesheuvel, P.M.; Leermakers, F.A.M.; Cohen Stuart, M.A. *Physical Rev.E* **2006**, *73*, 011802.
20. Edwards, S.F. *Proc. Phys. Soc.* **1965**, *85*, 613.
21. Zhulina, E.B.; Priamitsyn, V.A.; Borisov, O.V. *Polymer Science USSR* **1989**, *31*, 205.
22. Milner, S.T.; Witten, T.A.; Cates, M.E. *Macromolecules* **1988**, *21*, 2610.
23. Lyklema, J. *Fundamentals of interface and colloid science Volume I: Fundamentals 1991*, Academic Press, London.
24. Israels, R.; Scheutjens, J.M.H.M.; Fleer G.J., *Macromolecules* **1993,** *26*, 5405.
25. Zhulina, E.B.; Borisov, O.V. *J. Chem. Phys*. **1997**, *107*, 5952.
26. Zhulina, E.B.; Birshtein, T.M.; Borisov, O.V. *Macromolecules* **1995**, *28*, 1491.
27. Scheutjens, J.M.H.M.; Fleer, G.J. *J. Phys. Chem.* **1979**, *83*, 1619
28. Zhulina, E.B.; Leermakers, F.A.M. *Biophysical J.* **2007**, *93*, 1421.
29. Wijmans, C. M.; Scheutjens J. M.H.M.; Zhulina E.B. *Macromolecules* **1992**, *25*, 2657.
30. Currie, E. P. K.; Sieval, A. B.; Avena, M.; Zuilhof, H.; Sudhölter, E. J. R.; Cohen Stuart, M. A. *Langmuir* **1999**, *15*, 7116.
31. Giesbers, M.; Kleijn, J. M.; Cohen Stuart, M. A. *J. Colloid Interface Sci.* **2002**, *248*, 88.
32. Carter, D.C.; Ho, J.X. *Adv. Protein. Chem.* **1994**, *45*, 153.
33. Tanford, C.; Swanso, S.A.; Shore, W.S. *J. Am. Chem. Soc.* **1955**, *77*, 6414.
34. Seyrek, E.; Dubin, P.L.; Tribet, C.; Gamble E. A. *Biomacromolecules* **2003**, *4*, 273.

Part 3: Brushes and Polydispersity

Chapter 8

Modeling the structure of a polydisperse polymer brush.

Abstract

Numerical self-consistent field theory is used to study the structural characteristics of a polydisperse polymer brush. We consider the relevant case of a Schulz-Zimm distribution and find that even a small degree of polydispersity completely destroys the parabolic density profile. The first moment (average height) of the brush increases with polydispersity, while the average stretching in the brush decreases. The density profiles of separate chain length fractions in a single polydisperse brush are also strongly influenced by polydispersity. Short chains are found to be compressed close to the grafting interface, whereas longer chains have a characteristic flowerlike distribution. These longer chains stretch strongly (stem) when surrounded by smaller chains and decrease their stretching (crown) when only surrounded by longer chains. In line with approximate analytical models, our numerical exact results show that the polymer chains in the brush have localized end-point positions (no fluctuations) in strong contrast to the anomalously large fluctuations in the end-point positions of the homodisperse brush. Despite these effects, the scaling of average height with grafting density and number average chain length is unaffected by polydispersity. Many results that we have presented can be understood qualitatively from the bidisperse brush.

A manuscript based on this chapter was published as:
De Vos, W.M.; Leermakers F.A.M. *Polymer* **2009**, *50*, 305-316.

Introduction

Polymer brushes, densely packed arrays of polymer chains end-attached to an interface, have been the subject of many experimental and theoretical investigations in the past 30 years [1,2,3]. There are however significant differences between the theoretical and experimental investigations of polymer brushes. One is that most theories assume strong stretching of the polymer chains in the brush, while it is hard for an experimentalist to achieve densities high enough for this strong stretching [4]. Another significant difference is the polydispersity. While it is practically impossible for an experimentalist to produce a perfectly homodisperse polymer brush, almost no theoretical work has been done on the effect of polydispersity with a realistic size distribution.

Polydispersity in polymer brushes has already received some attention from the modeling point of view. In particular there has been some interest in the modeling of the simplest form of polydispersity, a brush containing two chemically identical fractions with polymers of different length. Approximate analytical self-consistent field theory has been developed by Milner, Witten, and Cates (MWC) [5] and by Birshtein *et al* [6]. In these analytical theories one typically assumes the complete segregation of end-points of the long and short polymer fraction. Although it is known that end-points do segregate, such assumption should be the outcome of the analysis rather than the input. Another assumption is that the local stretching of a chain is determined only by the local chain density. A key result of this approach is the prediction that the density profile of the short fraction is unaffected by length and content of long chains (at fixed grafting density). Both sets of authors also predict that the mixing of long and short chains increases the entropy of a brush. Comparing their models to Monte Carlo (MC) simulations revealed differences, mainly attributed to some overlap of end-points of the long and short fraction [7]. For a uniform distribution of chain lengths as described by MWC the calculated density profile compares well to MC simulations.

To our knowledge, there exists just one analytical SCF study wherein no *a priori* assumption is made on the position of end points. Klushin and Skvortsov [8] used an ingenious trick to extract information for a polydisperse brush from the known properties of a homodisperse one. The start of their analysis is the analytical SCF theory of the homodisperse brush, i.e. the brush described by the strong stretching approximation. For very long chains we know that the results are accurate and that for finite chain length there are shortcomings because of fluctuations of chain conformations beyond those accounted for in the most-likely trajectories. The second step in the analysis is to assign a plane inside the brush and analyze the lengths of all chain parts that reside outside this plane. This population of chain parts consists of short ones that are less strongly stretched and have

their free ends not far from the assigned plane, and longer ones that are more stretched because the free chain end is further from the assigned plane. As a result there exists a full set of lengths with corresponding grafting densities (as evaluated from this reference plane). The third step is to freeze the plane and take this plane as the grafting surface of the polydisperse distribution of chain lengths found in step two. Of this polydisperse brush all properties are known. The overall profile, for example, is parabolic, and the local stretching is the same as that in the homodisperse reference brush. The resulting chain length distributions consist of many long chains and few shorter chains and thus, these authors could consider only very small degrees of polydispersities. One of the main predictions is that the end-point fluctuations decrease with increasing polydispersity. They also predict for low polydispersities, independent of the chain length distribution, that the height H of a polymer brush increases with polydispersity, i.e. increases with the weight average molar mass over the number average mass (M_w/M_n), as $\delta H = (M_w/M_n - 1)^{1/2}$ Currently, it is unknown whether this law also applies to more realistic polymer length distributions.

Dan and Tirrell [9] have investigated bidisperse brushes using a numerical SCF (nSCF) model very similar to the model used below. In this numerical approach these authors also could account for the fact that the end-point distributions of the long and short chains overlap to some extent. They performed a thorough study varying the fraction and the difference in length of the long and short polymer end-grafted chains. They found that the longer chains stretch significantly more than the shorter ones near the grafting interface and that the density profile of the short chain is influenced by the length and content of long ones. Indeed, this complication is the reason for the extremely low attention of the polymer brush community for the effects of polydispersity. There is a lack of rigorous approaches to this problem. As a result the current situation is rather unsatisfactory. On the one hand polydispersity is an inherent aspect of any experimental system but the modeling community ignores this aspect as much as possible.

Results from neutron reflection have been compared extensively to nSCF models (using predictions for homodisperse polymers in a number of papers [10,11]) and are found to compare well. At this stage we might wonder why such good correspondence was found. One possible reason for this is that a small polydispersity does not destroy the expected scaling behavior of the height with the average chain length and overall grafting density. Much less is known about brushes with deliberate polydispersity. Currie et al [12] investigated a bidisperse polymer brush with a combination of nSCF theory and neutron reflection while Kritikos and Terzis [13] investigated both a bidisperse and a tridisperse brush with the same combination of theory and experiments. In both investigations it was

found that the different chain length fractions segregate in height and that the long chains stretch stronger when surrounded by smaller chains.

As stated above, almost no theoretical work has been done on the effect of a realistic form of polydispersity on a polymer brush. We found only a single work by Terzis *et al* [14] who investigated using an SCF model a polymer brush with a realistic size distribution in contact with a polymer melt of chemically equivalent chains. They show that increasing the polydispersity leads to improved miscibility between the brush and the polymer melt. This is a strong indication that polydispersity can have very pronounced effects on the properties of a polymer brush.

In this chapter we investigate the effect of polydispersity on a polymer brush in a good solvent, again using an nSCF model. For the polydispersity we use the Schulz-Zimm distribution, a realistic size distribution often used to describe polymer polydispersities. We investigate the effect on the overall brush density profiles and on the structure of a polydisperse brush by studying the density profiles and end-point distributions of single fractions in the polydisperse brush. We also present a very simple analytical model for polydispersity based on the Alexander and de Gennes box model.

Theory

Numerical self-consistent field theory

There exists a strong analogy between the path followed by a Brownian particle and the conformation of a (Gaussian) polymer chain. As a result, there exists a diffusion-like equation to describe such a polymer system. Polymers with excluded volume have perturbed (non-Gaussian) conformations and, on a mean-field level, one can treat this problem by considering a diffusion problem in an external potential field. Then, in self-consistent field theory the potential is chosen to be a function of the volume fraction (dimensionless concentration) of polymer and the potential assumes the property of self-consistency. This scheme was invented by Edwards and the corresponding diffusion equation carries his name. The Edwards diffusion equation needs to be solved in a particular geometry by specifying the initial and boundary conditions [15]. Exact analytical solutions, especially for situations that the polymer molecules are strongly interacting are not available, only analytical approximations exist.

Numerical solutions for the case that polymers are end-grafted can be generated only after choices have been made about the discretization scheme. Here we follow the approach of Scheutjens and Fleer (SF-SCF) [16], wherein the polymer segment size matches the cell size of the spatial coordinates. In this scheme the conformations of the polymers are

described by freely jointed chains, which have the property of finite extensibility. This means that no polymer chain that is attached with the first segment to the wall can have its N^{th} segment more than N lattice sites away from the surface. The discrete version of the Edwards equation reduces to a set of recurrence equations, also known as propagators.

The propagator formalism can be set-up extremely efficient such that the number of computations for the whole set of polymer chains is comparable to the evaluation of the volume fraction of the largest chain in the distribution [17]. As such an efficient scheme has not been discussed in the literature for end-grafted chains, we discuss the details of this in Appendix A. Apart from this technical issue, there is no additional difficulty as compared to the evaluation of properties of homodisperse brushes. Details of this [10,18] can easily be found in the literature and we do not go into more detail here, apart from mentioning that the inter-chain excluded-volume effects are accounted for the by segment potentials, which in the absence of specific interactions are given by $u(z) = -\ln(1-\varphi(z))$, where z is the distance in units of lattice sites away from the grafting surface, and φ is the volume fraction of segments. For not too high volume fractions and good solvents we thus find $u(z) \approx \varphi(z)$.

For homodisperse brushes it can be shown that the potentials, $u(z)$, are essentially parabolic ($u(z) = A - Bz^2$) and thus that the volume fraction profiles are parabolic. In polydisperse cases polymers with different molecular weight are present. This complicates the issue and strong deviations from this parabolic law are expected. In summary, the key input that is needed for the execution of the SF-SCF method is to feed the formalism with a distribution of chain lengths (degrees of polymerization). As the chain length must remain finite one also has to define the upper limit of the size distribution by choosing an appropriate maximum chain length. In the parameter settings section we will go into details.

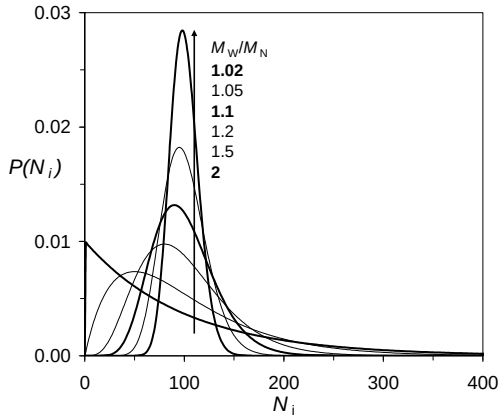

Figure 1. Schulz-Zimm distribution for different polydispersities, the probability for length N_i, $P(N_i)$ is plotted (see Eq. 1).

Polymer length distribution

A function commonly used to represent polymer molecular weight distributions is the so called Schulz-Zimm distribution [19,20]:

$$P(x, N_i) = \frac{x^{x+1}}{\Gamma(x+1)} \frac{N_i^{x-1}}{N_n^x} \exp\left(-\frac{xN_i}{N_n} \right) \qquad [1]$$

In which $P(N_i)$ is the probability of chains with degree of polymerization N_i, N_n is the number average degree of polymerization and x defines the broadness of the distribution. $\Gamma(x+1)$ is the so called gamma function which for integer values of x is equal to $x!$. A nice feature of this distribution is that the parameter x is directly related to the polydispersity:

$$\frac{M_w}{M_n} = \frac{N_w}{N_n} = \frac{x+1}{x} \qquad [2]$$

In Figure 1 we show the Schulz-Zimm distribution for a number of polydispersities used throughout this chapter. As can be seen the distribution is almost symmetrical at low values of the polydispersities, but with increasing polydispersities the distribution shifts to a larger frequency of small chains. At the highest polydispersity given in Figure 1 (M_w/M_n = 2) the maximum in the distribution occurs at the lowest chain lengths and there is a continuous decrease of the occurrence of chains with increasing chain length. This implies that the number of molecules of length $N_i = 1$ is in fact is larger than any particular polymer length.

Here we follow the strategy presented in Appendix A to number the chains by an index i and assume that chain i has a length $N = i$, so that we can interchange notation. The overall grafting density σ is defined as the number of chains per unit area. The grafting density per chain length therefore is given by $\sigma_i = P(x,N_i)\ \sigma$ and the largest chains are given by N_I.

Parameter settings

When varying the polydispersity, we have implemented that the number average degree of polymerization, the overall grafting density and the overall mass are always preserved. Unless specified otherwise we have considered the Schultz-Zimm distribution with a maximum chain length of N_I = 1000. All interaction parameters are taken zero, so the polymer segments have no specific affinity with the surface and the solvent is athermal. In some of the calculations we consider a special distribution where only two chain lengths are used (bidisperse brush). In that case, the chain lengths and the grafting densities are specified separately.

In the lattice model one typically uses dimensionless quantities, i.e. concentrations are expressed in volume fractions and the distances are expressed in lattice units. For conversion to real concentrations and actual distances it is necessary to choose a segment length (equal to the lattice spacing). A reasonable value for this parameter is b = 0.5 nm. The chains are grafted to a solid surface and the solvent is monomeric. The system volume is chosen large enough so that the outer boundary is well above the brush height H.

Results

Bidisperse brushes

The exact solutions of the SCF equations for the general case of a polydisperse mixture is not available and therefore we now turn our attention to the numerical SCF method of Scheutjens and Fleer [16]. The simplest form of polydispersity is a mixture of two polymer fractions with different lengths and equal grafting densities. This system has already been addressed by a number of studies [5,6,9,12,13,21]. We take a somewhat different approach than already performed studies, instead of changing the length (or grafting density) of one polymer fraction while keeping the other chain length fraction constant we change both chain fractions, which have identical grafting densities, simultaneously. As one chain length fraction becomes longer and the other chain length fraction becomes equally shorter, the average chain length, total mass and grafting density are thus conserved. This has the advantage that all changes in the overall brush density profile can be attributed completely to polydispersity and not to any other change in parameters. This for instance allows us to, for the first time, investigate the effect of bidispersity on the average stretching of the chains in the brush. Another difference with earlier studies is that we not only investigate cases were there is a large difference between the long chain fraction and the short chain fraction, but also cases were the chain length fractions differ only a few monomers in length. We present our results in Figure 2 which shows the change in the overall volume fraction profiles of such bidisperse brush upon an increasing disparity between the lengths of the two fractions. In this graph we conserved both the total grafting density and the total mass.

In Figure 2a we demonstrate how the increasing differences between the two polymer fractions influence the overall brush profile. Indeed, for small differences, the profile does not deviate much from that of a parabolic profile of a monodisperse brush. For larger differences, however, the profile resembles that of two parabola one on top of the other, and the height of the brush as judged from the fact that the overall volume fraction extends to larger z-values increases with increasing chain length difference.

In Figure 2b we show the volume fraction profiles of the two separate fractions as well. In this graph the profile of the smaller chain is dotted, and the profile for the longer chain is the solid line. As the grafted amount is fixed $\sigma_1 N_1 + \sigma_2 N_2 = \sigma(N_1+N_2)/2 = 10$, the integral of the two profiles is conserved. Important is that even though the total brush density is not influenced much by small differences, the separate contributions are strongly affected by small length differences. A length difference of 10 monomers (N_1 = 95 and N_2 = 105) is enough to reduce the volume fraction of the long polymer close to the grafting interface by 25%. The concentration of the short fraction increases by a similar amount. The shape of the density profile of the short polymer resembles a parabolic profile in all cases. The profile of the long chains shows a flat region when surrounded by much small chains and after that an increase and then a parabolic-like decrease. This profile indicates a strong stretching of the longer chains when surrounded by much of the smaller chains. Such result was already shown by Dan and Tirrell [9]. This is however a rather qualitative result. To exactly determine how much more the long chain stretches compared to the short chain at a certain position in the brush one can calculate the local stretching as a function of z. Results of such a calculation that confirm the qualitative prediction are given in Appendix B.

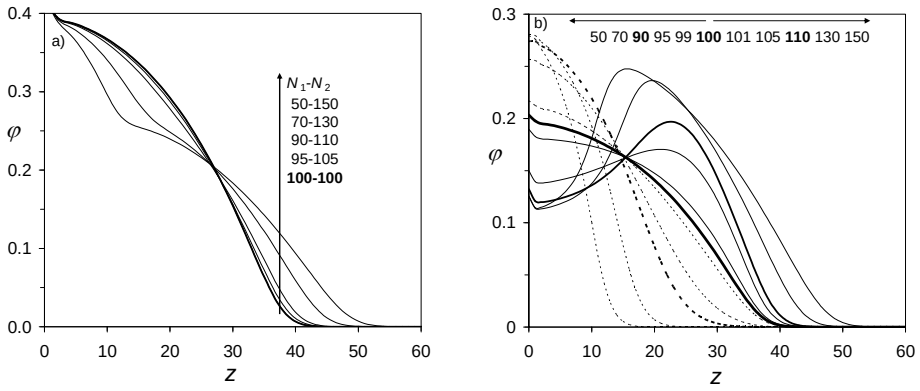

Figure 2. a) Overall volume fraction profiles of a brush containing two fractions, one fraction increases in length and the other decreases an equal amount. $\sigma_{long} = \sigma_{short} = 0.05$. $N_n = 100$. b) The corresponding volume fraction profiles of the separate fractions. The short ones are dotted and the long ones are drawn by a continuous line.

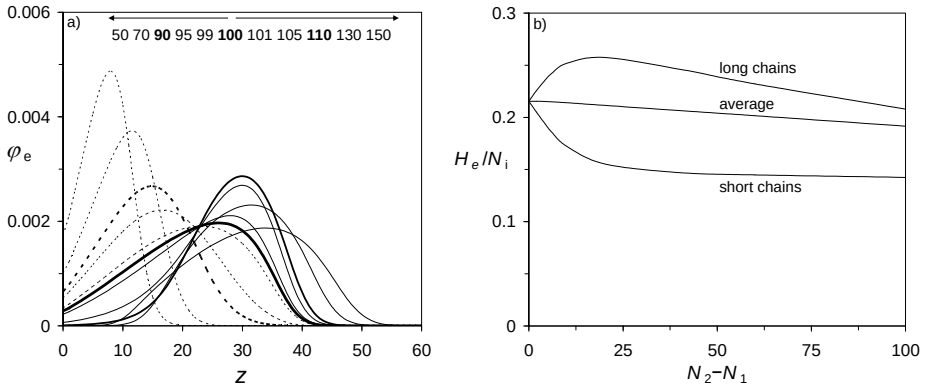

Figure 3. a) End point density profiles $\varphi_e(z)$ of brushes containing two fractions, one fraction increases in length (solid lines) and the other decreases (dotted lines) an equal amount corresponding to the results discussed in Figure 2. b) The average height increase per monomer H_e/N_i as a function of the difference between the lengths of the long and short chains. The height is measured as the first moment of the end-point distribution. Curves for the long and the short chains are given as well as the average between these two.

The end-point distribution $\varphi_e(z)$ (see Appendix A Eq. A4) plays an important role in polymer brush theory (see also Appendix B, Eq. A7). The interesting issue here is that for the homopolymer brush the end-points are distributed throughout the brush. Indeed, the end-point distribution grows approximately linearly with the distance from the grafting surface and only at the periphery of the brush the end-point distribution suddenly drops to zero. Such wide distribution of the end-points, manifests anomalously large fluctuations present in the homopolymer brush. The end-point fluctuations are proportional to the chain length. With this in mind it is appropriate to investigates how the end-points are distributed in the polydisperse brush, and we will begin this investigation by looking at these distributions in the bidisperse brush.

In Figure 3a we elaborate on the end-point distribution of the separate fractions in the same bimodal brushes already discussed in Figure 2. As could be anticipated from the overall profiles, with increasing length difference of the two fractions, we observe a clear increase in the segregation of chain ends. A difference of 20 segments (N_1 = 90 and N_2 = 110) is enough to reduce the volume fraction of end-points of the long fraction to almost zero close to grafting interface. As expected the segregation is strongest for the largest difference in length. Indeed, the region where one finds many end-points of the short chains is depleted with the end points of larger ones. The inverse is true of course as well, but this

is less of a surprise. Clearly, the fluctuations of end points of chains of a particular length are strongly suppressed. Below, we will return to this in more detail.

We can use the end-point distribution to evaluate the average stretching of the chain as a whole. This is done by defining the height H_e of the chain by the first moment over the end-point distribution and normalizing this height by the degree of polymerization N_i. The first moment (or average height) of fraction *i* of component *x* is given by

$$H_{x,i} = \sum_{z=1}^{z=N_i} z\varphi_{x,i}(z) \Big/ \sum_{z=1}^{z=N_i} \varphi_{x,i}(z) \qquad [3]$$

The normalized average stretching H_e/N_i (the average stretching per monomer) is shown in Figure 3b for both the short and the long fraction. For the long fraction the average stretching increases when going to small length differences and then decreases again for larger length differences. The total average stretching is determined by two parts of the brush, the part in which small chains are present and the part where they are not present. In the first part the chains of the long fraction stretch stronger (this decreases the conformation entropy), to allow more segments in the part of the brush where no short ones are present (increasing the conformation entropy). In the second part the chains of the long fraction stretch less strong as the polymer density in the outer region is relatively low. This causes the maximum in average stretching. The stretching of the short chains, however, decreases monotonically to a plateau value with increasing length differences.

More importantly the average stretching of the chains, which is also plotted in Figure 3b decreases slightly with increasing size difference. This very clearly points to the driving force for the large changes in the individual profiles. With increasing size difference there is more freedom (compared to a monodisperse brush) to distribute the stretching of the chains as favorable as possible (reducing the entropy losses of the strongly stretched chains). We recall that even though the average stretching is reduced, we find, completely in line with earlier investigations of bimodal brushes [9], that with increasing differences between the long and the short fraction, the height of the brush increases.

Polydisperse brushes with a realistic size distribution

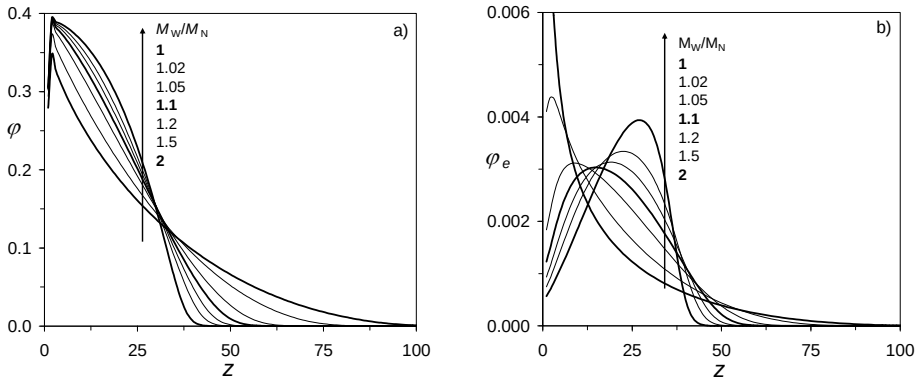

Figure 4. a) Overall volume fraction φ(z) profile for brushes with increasing polydispersity as indicated. N_n = 100, σ = 0.01, polydispersity with Schulz-Zimm distribution. Cutoff chain length N_I = 1000. b) The corresponding overall distribution of end points $\varphi_e(z)$.

Predictions for the structure of polymer brushes with an experimentally relevant chain length polydispersity are not found in the literature. This is remarkable as the effects of polydispersity are both large and non-trivial. We will attempt to rationalize the results for polydisperse brushes from the knowledge collected from the analysis of the bidisperse brush.

The first result is, once again, the overall volume fraction profiles of polydisperse brushes. In Figure 4a we show a set of such graphs for systems with increasing, but still very low, levels of polydispersity. For comparison the homodisperse brush is also presented (most concave, the so-called parabolic-profile). As explained in the Theory section, we have chosen for the Schulz-Zimm distribution, a size distribution commonly used to describe experimental samples. As can be seen in Figure 4a, polydispersity has a strong effect on these profiles, even for polydispersities considered low from a synthetic point of view. Upon going from a polydispersity of unity (homodisperse brush) to a polydispersity of M_w/M_n = 1.1, the profile changes from a convex to a linear profile. At higher polydispersities the profile becomes completely concave. Furthermore, the height of the brush, as judged from the distance away from the surface where the volume fraction of the polymer units remains above a detection limit, increases significantly with increasing polydispersity. At a polydispersity of 1.1 the height of the brush (defined as the distance where the polymer concentration drops below 1% of the highest achieved density) increases

with regard to the homodisperse brush by ~30%. At a polydispersity of 2 the increase is about 120%. This increase in height is depicted in Figure 5 and is discussed there.

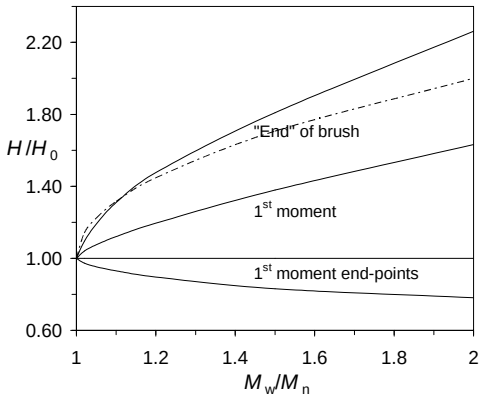

Figure 5. The height (H) of a brush (N_n = 100, σ = 0.01) relative to the height of a corresponding monodisperse brush (H_0) as a function of polydispersity. The various definitions of the heights are discussed in the text. The dotted line is the prediction for the end of brush by Klushin et al [8].

In Figure 4b we show the overall end-point distributions of the brushes presented in Figure 4a. As explained above, in a homodisperse brush there exists a maximum in end-point distribution at the edge of the brush. With increasing polydispersity this maximum moves closer and closer to the grafting interface, even though the overall height of the brush increases. The shift of the maximum of the end-point distribution towards the surface and the gradual growth of the overall brush height are typical polydispersity effects that can be traced to the details of the polymer length distribution. As shown in Figure 1, the Schulz–Zimm distribution increases the number of small chains and has fewer large chains, with increasing levels of polydispersity. This causes the increase of chains ends close to the grafting interface. As in the bidisperse brush, we can deduce the average stretching of the chains in the polymer brush by the average positions of the end points. The average height (first moment) of the end-points is shown in Figure 5.

In Figure 5 the relative height is shown as a function of polydispersity. Here we use three different definitions of the brush height. The first, “end” of brush, is defined as the distance where the polymer concentration drops below 1% of the highest achieved density, and is intended to describe the height where the brush ends. As can be seen, the effect of polydispersity on this is large, the brush height more than doubles when comparing a monodisperse brush with a brush of $M_w/M_n = 2$. However, this definition of the brush

height is rather arbitrary, changing the above discussed 1% to a different value, such as 0.1%, has a large effect. (The lower this percentage, the stronger the height increases with increasing polydispersity).

The arbitrary choice for the end of brush definition also makes it hard to compare these results to the prediction of Klushin *et al* [8] (see introduction), even more so as their definition for the end of a brush is different from the one we use. In aSCF theory the end of a brush is defined as the height were the density goes to zero, a well defined point in aSCF theory as only the most probable conformation of a chain is taken into account. In nSCF theory all possible conformations are taken into account which makes it impossible to use the aSCF definition as this would always give the contour length of the longest polymer (There is always a very slight possibility that this chain is completely stretched, thus the density goes to zero at the contour length). Still, we can say that the prediction of Klushin *et al* compares well with our (arbitrary) definition. Indeed, the prediction shows a strong increase in height for low polydispersities and a lower more linear increase in height for higher polydispersities, very similar to our calculated end of brush and also similar to our other definition of the height, that is, the first moment over the overall volume fraction profile.

The first moment, or average height (see Eq. 3), is a far more useful definition of brush height, and is also shown in Figure 5. Wijmans *et al* [18] used this definition of height to compare aSCF and nSCF polymer brush theory. The definition is not arbitrary and has the large advantage that it can be experimentally determined by reflection techniques such a neutron reflection and ellipsometry. This average height of the brush is also strongly influenced by polydispersity. At a polydispersity $M_w/M_n = 1.1$ of the brush height increases 12% compared to a monodisperse brush, at a polydispersity of $M_w/M_n = 2$ the height has increased 60%. Measuring the average height as a function of polydispersity could be a method to prove the huge effects of polydispersity on polymer brushes as demonstrated in this chapter.

The final definition of height used in Figure 5 is the first moment of the end-points. As was discussed for the bidisperse brushes, the first moment of end-points is directly related to the average stretching. Thus, in Figure 5 we observe that the average stretching at $M_w/M_n = 1.1$ is 7% lower compared to that of the monodisperse brush. For $M_w/M_n = 2$, the average stretching is even 22% lower. This reduction of stretching was earlier also observed for bimodal brushes as discussed above and can be explained in exactly the same way. With increasing polydispersity there is more freedom (compared to a monodisperse brush) to distribute the stretching of the chains as favorable as possible.

In this chapter we only show results for polydispersities up to a value of $M_w/M_n = 2$ as calculated with just a single distribution function (Schulz-Zimm). In a realistic macromolecular system however, the polydispersity might be much higher and/or the distribution function might be different. We have also investigated higher polydispersities (results not shown, up to $M_w/M_n = 10$) and find that the trends reported here for polydispersities between $M_w/M_n = 1$ to $M_w/M_n = 2$ continue. Thus, with increasing polydispersity the height of the brush increases while the average stretching decreases. For these high polydispersities the shape of the density profile is similar to the concave profile that was found for $M_w/M_n = 2$ (Figure 4), the higher the polydispersity the more concave the profile becomes. Furthermore, we have also investigated two other distribution functions (Gaussian distribution and uniform distribution). We found for these distributions exactly the same trends as a function of polydispersity as for the Schulz-Zimm distribution although for a given polydispersity there are small differences in the brush density profiles of the different distributions. We believe that the question of the distribution function will become more relevant when good experiments on the effects of polydispersity become available, and can be compared to the model results.

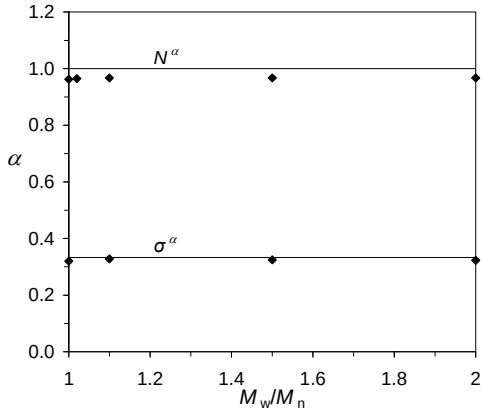

Figure 6. Brush scaling exponents α for polymer length (N_n^{α}) and grafting density (σ^{α}) as a function of polydispersity. The lines are the theoretical values for the monodisperse brush, the points are calculations.

In the above section we predicted a large effect of polydispersity on the height and the density profile of a brush. No experimental evidence exists of these large effects. Indeed, it would be interesting to set up such experiments. Most experimental studies investigating polymer brushes have focused on investigating height as a function of the average degree of

polymerization (N_n) and the grafting density (σ) [23,24]. Results have then be compared to the scaling prediction from Alexander and de Gennes [25,26]: $H \sim N_n\sigma^{1/3}$. This scaling law was derived from a so-called box model (in which all polymers are assumed to stretch exactly the same amount) but is also found for more sophisticated models like aSCF and nSCF [1,18]. The experimental results were found to be in agreement with this scaling law although polydisperse brushes were used. It is therefore interesting to look at the effect that polydispersity has on the exponents for the Alexander and de Gennes scaling law. In Figure 6 we show the results of the determination of these exponents for different polydispersities. The exponents were determined by fitting the average height of a number of average polymer lengths (N_n = 100, 200, 400, 800) and a number of overall grafting densities (σ = 0.05, 0.1, 0.2, 0.4). As can be seen in Figure 6, the scaling exponents are almost independent of the polydispersity. This is a surprising finding if we take into account the large effects that polydispersity has on the brush density profile. The scaling exponent for N_n is for all polydispersities slightly lower than the predicted exponent (α = 1). We believe this is due to the slight depletion interaction between the polymer and the wall, which slightly increases the average height. As this effect is relatively large for small N_n, the scaling exponent is slightly smaller than 1. The scaling exponent for σ (α = 1/3) is almost exactly the same as the predicted exponent. These results compare well to the fact that experimental results in which polydisperse polymer brushes were found to be consistent with scaling exponents as predicted for monodisperse brushes.

The internal structure of a polydisperse brush with a realistic size distribution.

Up till now we have focused on the effect of polydispersity on the brush as a whole. However, as observed with the bidisperse brush, the effects on the internal structure of the brush were even more drastic than the changes on the overall density profile. To get similar information for the internal structure of a polydisperse brush, we focus on one case, namely the polydispersity M_w/M_n = 1.1. Even for such relatively low degree of polydispersity there is a problem in presenting the data because the grafting density for different chain length fractions is very different. Therefore, the density profiles shown in Figure 7 have been normalized by $\sigma_i N_i$, the total amount of each fraction, to adjust for these large differences in mass of the different fractions. As a result, all the distributions in Figure 7 have the same integral. As anticipated, we observe strong similarities with the effects that were discussed for the bidisperse brush. Again, there is a segregation of the different polymer chains based on length. Of course, the shortest chains are located the closest to the surface and the longer ones are further away from the surface. However, they do not assume the ‘normal’

distributions as in the equivalent homopolymer brush cases. Indeed, the short chains appear more compressed and the longer ones assume the characteristic flower-like conformation with a stem (with homogeneous density profile, indicated the strong stretching) and a crown (with increasing density profile, indicating less strong stretching).

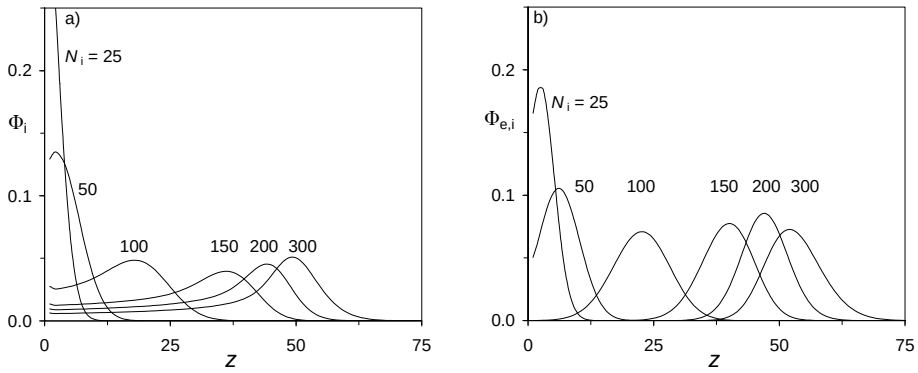

Figure 7. a) Normalized brush density profiles, $\Phi_i = \varphi_i / \sigma_i N_i$ for a selection of single chain length fractions (N_i as indicated) in a polydisperse (M_w/M_n = 1.1) brush. b) Normalized end-point distribution profiles $\Phi_{e,i} = N_n(\varphi_i / \sigma_i N_i)$ for a selection of single chain length fractions (N_i as indicated) in a polydisperse (M_w/M_n = 1.1) brush.

In Figure 7b we show that the end points of different lengths are completely segregated based on chain length. The same normalization is used as in Figure 7a, however the end-point distributions were also multiplied by N_n to give the same scale as in Figure 7a. One remarkable observation form Figure 7b is that the different chain lengths show very similar width of the end-point distribution, indicating that the fluctuations become independent of the chain length. This is a remarkable results especially when we recall the result for the homodisperse brush which features anomalously large fluctuations. Grouping chains of different lengths into "bins" and thus reducing the number of chain fractions to the number of bins has corresponding effects on the fluctuations of end-points in each bin. The fluctuations than scale with the bin size. Thus, reducing the polydispersity to just one bin (monodisperse case) we retrieve the fluctuations to be of order *N*.

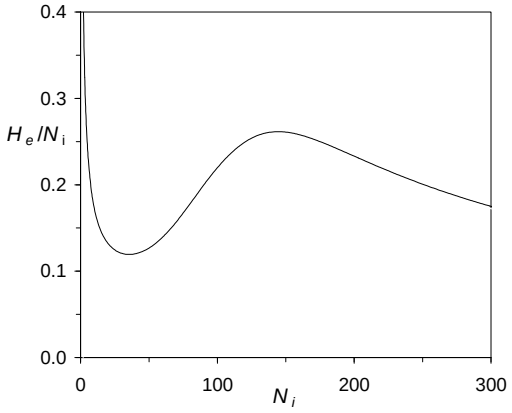

Figure 8. Average normalized chain stretching H_e/N_i as a function of fraction degree of polymerization.

In Figure 8 we show the average stretching of the different fractions in a polydisperse polymer brush. Large differences in stretching are found for the different fractions, the fraction with length $N_i = 150$ stretches almost twice as much as the fraction with $N_i = 50$. Long chains tend to have a stronger stretching than short chains up to a certain length. In the brush it is favorable for the longer chains to stretch further and for the short chains to fill this ”gap”. This has already been observed in a bidisperse brush with two chemical identical polymers of different lengths (see above), the shorter chains are pressed towards the wall, whereas the longer polymers stretch stronger away from the wall. For the longer lengths however, stretching decreases as these chains reach the outer part of the brush where the polymer density is lower. It is also seen that the shortest chains (smaller than $N_i = 40$) have an increased stretching compared to $N_i = 50$. We attribute this to slight depletion interaction between the polymer chain and the wall causing a slightly stronger stretching. This effect is in principle rather small, however, it is large enough to influence the average stretching of these short polymers.

A box model for polydispersity: a stack of boxes.

From the numerical SCF calculations presented above, we have gained detailed insight in the effect of polydispersity on a polymer brush. Polydispersity strongly affects the density profile, the brush height, leads to segregation of end-points, but does not affect the scaling exponents of average height with the degree of polymerization and the grafting density. An interesting question is then if one could use some outcomes of our nSCF model as input to create a much simpler model describing the effects of polydispersity. Alexander and de Gennes used a box-model [25,26] as a simple description for a polymer brush. In that model all end-points are assumed to be in the same plane above the grafting interface and thus all polymers are assumed to stretch exactly the same amount. For the description of a polydisperse brush we propose a stack of boxes (SOB) model. This model is worked out in Appendix C, but a short explanation is given here.

In the SOB model we assume that all end-points of polymers *with the same length* are in the same plane above the grafting interface. However, as we take into account polymers of different lengths we use a stack of boxes, with a number of boxes equal to the number of different chain length fractions. The first box (at the grafting interface) contains al chain length fractions. The second box contains all chain length fractions except the smallest. The third contains all chain length fractions except the smallest two etc. This continues to the last box which only contains the longest chain length fraction. Thus, every box has its own local grafting density determined by the number of chains in all the chain length fractions included in that box. Each box also has a local chain length, which is equal to the length of the smallest chain length fraction in that box minus all the chain lengths of lower boxes. In this way, the sum of all local chain lengths (of all boxes) is the length of the longest fraction. As every box has a local chain length and a local grafting density, we can calculate for every box properties such as its height, its density and its position z. In this model the local chain stretching is *only* determined by the local chain density and we ignore that in reality the local chain stretching is *also* determined by the chain length N. This model is worked out in Appendix C. The results of this model for the same parameter settings as Figure 4, are shown in Figure 9.

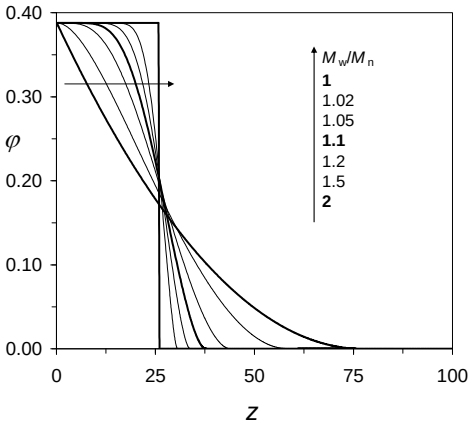

Figure 9. Overall volume fraction φ(z) profile for brushes with increasing polydispersity as indicated as calculated using a SOB model. N_n = 100, σ = 0.1, polydispersity with Schulz-Zimm distribution.

When comparing the results of the stack of boxes model with the results of the nSCF calculations we see that the SOB model gives qualitatively the same results. The density profile shifts with increasing polydispersity from the box profile, to a more parabolic profile, at higher polydispersity to a more linear decrease and at the highest polydispersity to a completely concave profile, resembling an exponential decrease.

In Figure 10 we make a more quantitative comparison between the SOB model and the nSCF model, by showing the calculated relative heights as a function of polydispersity. The SOB model predicts, in agreement with the nSCF model, al large increase in first moment, or average height, as a function of polydispersity. However, especially at low polydispersity this relative increase in height is underestimated. An explanation for this is presented in the same picture, the SOB model overestimates the decrease in average stretching, compared to the nSCF model thus leading to a lower average height. As discussed, with increased polydispersity there is more freedom (compared to a monodisperse brush) to distribute the stretching of the chains as favorable as possible. However, in the box-model the increase of polydispersity provides the brush with an extra form of freedom, namely the distribution of free ends through the entire brush. In a monodisperse brush, as described by the box-model, all free-end are assumed to be in the same plane. With increasing polydispersity the free-ends are spread throughout the brush, which leads to a strong reduction in stretching. In the nSCF model, the free-ends are already spread throughout the whole brush in the monodisperse case. Therefore, the nSCF model shows a much lower reduction is stretching than the SOB model.

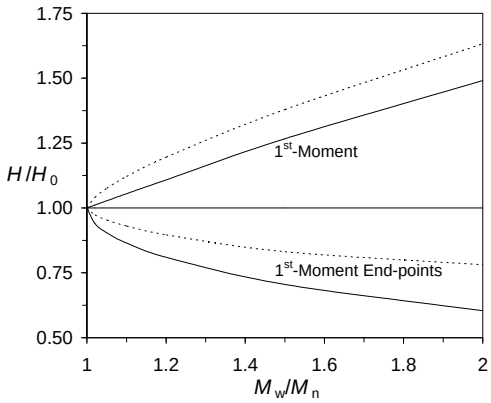

Figure 10. The height (H), as measured by the first moment over the overall volume fraction (1st-Moment) and that of the end-points (1st-Moment End-points), of a brush (N_n = 100, σ = 0.01) relative to the height of a corresponding monodisperse brush (H_0) as a function of polydispersity. Continuous lines as calculated from the SOB model, dotted lines from nSCF (same as Figure 5).

The SOB model gives qualitatively the same results as the nSCF model and as such well describes the trends of polydispersity. As box models can be easily extended to investigate particle adsorption in polymer brushes (for example [22]) we believe that the SOB model could well be used to investigate the effect of polydispersity on the adsorption in polymer brushes.

Conclusions

A detailed investigation for a polymer brush is given on the effect of polydispersity with a realistic size distribution. The numerical SCF model results show that polydispersity strongly affects the density profile of a brush and that with increasing polydispersity the density profile changes from parabolic to linear to concave, the concave resembling an exponential decrease in density. Also, the average height of the brush increases with increasing polydispersity. Going from the monodisperse case to $M_w/M_n = 1.1$ increases the average height with 12%, going to $M_w/M_n = 2$ increases the average height by 60%. We believe that such an effect could well be experimentally determined if one would have corresponding polymer brushes with a significant difference in polydispersity. The average stretching of the brush is found to decrease with increasing polydispersity. With increasing polydispersity there is more freedom (compared to a monodisperse brush) to distribute the stretching of the chains as favorable as possible. Despite these large effects of polydispersity, the exponent with which the average height scales with the grafting density and the degree of polymerization of the brush is unaffected by polydispersity.

The internal structure of the brush is even more radically influenced by polydispersity. A schematic depiction of our proposed structure of a polydisperse brush is given in Figure 11. There is a segregation of the different polymer chains based on length. Short chains are compressed close to the grafting interface while the longer ones assume a characteristic flower-like conformation with a stem (strong stretching) when surrounded by smaller chains and a crown (less strong stretching) when surrounded by longer chains. The longest chains have the same conformation with the stem when surrounded by smaller chains and the crown at the end of the brush. The end points of different lengths are completely segregated based on chain length. Different chain lengths show very similar end-point fluctuations, indicating that the fluctuations become independent of the chain length. This is a remarkable result especially when we recall the result for the homodisperse brush which features anomalously large fluctuations. The chains in the polydisperse brush have anomalously small fluctuations.

Most of the effects observed for polydisperse brushes can also be observed and understood when looking at the simplest form of polydispersity: bidispersity. With increased bidispersity we also observe an increase in average height, a decrease in average stretching , the compression of the short chain fraction, and the flowerlike distribution for the long chain fraction.

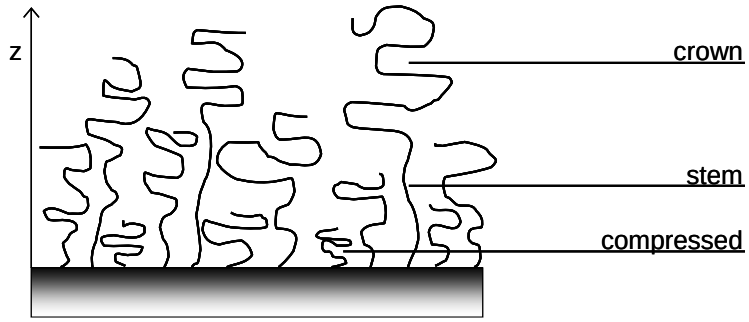

Figure 11. Schematic representation of stretching in a polydisperse polymer brush. Short chains stretch less than longer chains (compressed). Long chains stretch strongly (stem) when surrounded by smaller chains and decrease their stretching (crown) when only surrounded by longer chains. The longest chains stretch to the end of the brush.

The results of a much simpler model based on the well-known concept of the box-model compare well to the nSCF model, although the reduced average stretching as a function of increased polydispersity is somewhat overestimated. This model, in which we describe a polydisperse brush as a stack of boxes, might prove useful when investigating the uptake of particles in a polydisperse brush.

References

1. Currie, E.P.K.; Norde, W.; Cohen Stuart, M.A. *Adv. Colloid Interface Sci.***2003,** *100-102,* 205.
2. Zhao, B.; Brittain, W.J. *Prog. Polym. Sci.* **2000,** *25,* 677.
3. Birschtein, T.M.; Amoskov, V.M. *Polymer Science Ser. C* **2000,** *42,* 172.
4. Milner, S.T. *Science* **1991,** *251,* 905.
5. Milner, S.T.; Witten, T.A.; Cates, M.E. *Macromolecules* **1989,** *22,* 853.
6. Birschtein, T.M.; Liatskaya, Y.V.; Zhulina, E.B. *Polymer* **1990,** *31,* 2185.
7. Lai, P.-K.; Zhulina, E.B. *Macromolecules* **1992,** *25,* 5201.
8. Klushin, L.I.; Skvortsov, A.M. *Macromolecules* **1992,** *25,* 3443.
9. Dan, N.; Tirrell, M. *Macromolecules* **1993,** *26,* 6467.
10. Currie, E.P.K.; Wagenmaker, M.; Cohen Stuart, M.A.; van Well, A.A. *Physica B* **2000,** *283,* 17.
11. Karim, A.; Satija, S.K.; Douglas, J.F.; Ankner, J.F.; Fetters, L.J. *Phys. Rev. Letters* **1994,** *73,* 3407.
12. Currie, E.P.K.; Wagemaker, M.; Cohen Stuart, M.A.; van Well, A.A. *Macromolecules* **1999**, *32*, 9041.
13. Kritikos, G.; Terzis, A.F. *Polymer* **2005,** *46,* 8355.
14. Terzis, A.F.; Theodorou D.N.; Stroeks A. *Macromolecules* **2000,** *33,* 1385.
15. Edwards, S.F. *Proc. Phys. Soc.* **1965**, *85*, 613.
16. Scheutjens, J. M. H. M.; Fleer, G. J. *J. Phys. Chem* **1979**, *83*, 1619.
17. Roefs, S.P.F.M.; Scheutjens, J.M.H.M.; Leermakers, F.A.M. *Macromolecules* **1994,** *27,* 4810.
18. Wijmans, C.M.; Scheutjens, J.M.H.M.; Zhulina, E.B. *Macromolecules* **1992,** *25,* 2657.
19. Schulz, G.V. *Z. Physik. Chem.* **1939,** *B43,* 25.
20. Zimm, B.H. *J. Chem. Phys.* **1948,** *16,* 1099.
21. Terzis, A.F. *Polymer* **2002,** *43,* 2435.
22. Biesheuvel, P.M.; Wittemann, A. *J. Phys. Chem. B* **2005,** *109,* 4209.
23. Currie, E.P.K.; Leermakers, F.A.M.; Cohen Stuart, M.A.; Fleer, G.J. *Macromolecules* **1999,** *32,* 487.
24. Bianco-Peled, H.; Dori, Y.; Schneider, J.; Sung, L.-P.; Satija, S.; Tirell, M. *Langmuir* **2001,** *17,* 6931.
25. Alexander, S. *J. Phys. (Paris)* **1977,** *38,* 983.
26. de Gennes, P.G. *Macromolecules* **1980,** *13,* 1069.
27. Zhulina, E.B.; Priamitsyn, V.A.; Borisov, O.V. *Polymer Science USSR* **1989,** *31,* 205.
28. Milner, S.T.; Witten, T.A.; Cates, M.E. *Macromolecules* **1988,** *21,* 2610.

Appendix A. The SF-SCF formalism for end-grafted polydisperse polymer systems

Here we follow the approach of Roefs [17]. Polymer chains of type i =1, …, I have a degree of polymerization N_i, ranked in increasing values of the chain lengths. This means that N_I is the largest one. For simplicity we will assume that chain i has a degree of polymerization equal to the chain ranking number, i.e. $N_i = i$, so that there exists one normalization per length. For given polydispersity the probability P_i of a chain i is known. Let the overall grafting density be given by σ, then the grafting density of a chain of type i is given by $\sigma_i = P_i \sigma$. Each chain has segment ranking numbers s = 1, …, N_i, where it is understood that segment s = 1 is positioned at the first non-grafted segment just next to the surface, i.e. at z = 1. Here we assume that all polymers are composed of the same segment type and that just one segment potential exists, given by $u(z)$. This segment potential is used in the Boltzmann weight $G(z) = \exp -u(z)/k_BT$. We split up the formalism in a forward and a backward propagator. The forward starts with segment number 1 with the endpoint distribution $G(z,1) = G(z)\ \delta(z,1)$, where $\delta(z,1) = 1$ when z = 1 and zero otherwise. The recurrence relation reads for a 6-choice cubic lattice

$$G(z,s) = G(z)\left[G(z-1,s-1) + 4G(z,s-1) + G(z+1,s-1)\right]/6 = G(z)\left\langle G(z,s-1)\right\rangle \qquad [A1]$$

Which defines the angular brackets as a three layer average. Eq. A1 is performed for each coordinate z and all segments up to $s = N_I$. Let us, for purposes of normalization obtain the single chain partition function Q_i for chain i:

$$Q_i = \sum_{z=1}^{N_i} G(z, N_i) \qquad [A2]$$

Using this single chain partition function we can find the normalization C_i for chain i:

$$C_i = \frac{\sigma_i}{Q_i} \qquad [A3]$$

It is understood that when a particular chain length j is absent $C_j = 0$.

From Eqs. A1 and A3 we now can already identify the volume fraction profile of all chain ends, which we denote by $\varphi_{e,i}(z)$:

$$\varphi_{e,i}(z) = C_i G_i(z,i) \qquad [A4]$$

To evaluate also the distribution of the other segments we need a backward propagator. This propagator is somewhat more complicated because we are going to add contributions

for all chain lengths in this operation together. For this the end-point distribution $G(z,s \mid N \geq s)$ is introduced, which is the total statistical weight of all conformations that start with free end and arrive at segment *s* at coordinate *z*. Obviously, only the chains that are longer or equal than *s* can contribute to this end-point distribution and this is expressed behind the vertical bar. We start the propagator by the end of the longest chains, i.e. $s = N_I$ and write $G(z,N_I \mid N \geq N_I) = C_{N_I} G(z)$ for all *z* (there is no constraint). The backward equivalent of Eq. A1 is

$$G(z,s \mid N \geq s) = G(z)\langle G(z,s+1 \mid N \geq s+1)\rangle + C_N G(z) \qquad \text{[A5]}$$

which is performed N_I times. The overall volume fraction profile is now easily computed by

$$\varphi(z) = \sum_{s=1}^{N_I} \frac{G(z,s \mid N \geq s) G(z,s)}{G(z)} \qquad \text{[A6]}$$

To compute volume fraction profiles for a sub-fraction of the chains one can use the classical method by computing the volume fraction of each chain length separately.

Appendix B. Local chain stretching

In analytical brush theory for monodisperse brushes, as developed by Zhulina, Priamitsyn and Borisov [27] and Milner Witten and Cates [28], local chain stretching plays an important role. This is exemplified in the analytical description for the free energy of a polymer brush [18]

$$\frac{A}{LkT} = \frac{3}{2b^3} \int_0^H dz' \varphi_e(z',N) \int_0^{z'} dz E(z,z',N) + \frac{1}{b} \int_0^H f[\varphi(z)] dz \qquad \text{[A7]}$$

Here *A/kT* is the dimensionless free energy, *L* is the total surface area, *b* is the segment size (equal to the lattice spacing). The second term of this equation accounts for the free energy of mixing of the grafted chains with other molecules in the system. $f[\varphi(z)]$ being the free energy density of mixing, which depends on $\varphi(z)$. However, we focus on the first term of this equation, which represents the contribution from the elastic chain stretching in the brush layer. In this term $E(z,z',N)$ gives the local stretching of a chain at a give distance from the grafting interface z and for a give position of the end-point z' ($z' > z$). Thus, the stretching function $E(z,z',N)$ determines the position of every segment for a given end-point position. For homodisperse brushes the stretching function is given by

$$E(z,z',N) = \frac{\pi}{2N} (z'^2 - z^2)^{1/2} \qquad \text{[A8]}$$

As can be seen, this function leads to a parabolic profile. When depicting this stretching function, it is convenient to plot $E(z,z',N)^2$ as a function of z^2.

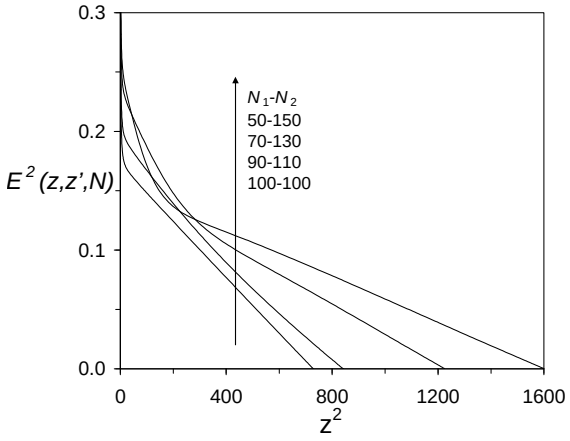

Figure 12. The squared local chain stretching for a given end-point position $E^2(z,z',N)$ for the long chain in bidisperse polymer brushes as described in Figure 2 as a function of the squared distance.

The local stretching can also be determined in numerical SCF calculations. For this we rank the chain segments $s = 1, \ldots, N_i$, where segment $s = 1$ is positioned at the first non-grafted segment just next to the surface, i.e. at $z = 1$. We then calculate the density profile for a given rank number and given end-point position and chain fraction $\varphi_i(z,s \mid z',N_i)$. From this we can calculate the first moment (or average height) of the given segment s

$$< z >_s = \sum_{z=1}^{z=N_i} z\varphi_i(z,s \mid z',N_i) \Big/ \sum_{z=1}^{z=N_i} \varphi_i(z,s \mid z',N_i) \qquad \text{[A9]}$$

For given z' and N_i, we can plot $<z>_s$ as a function of s, and compute $\delta < z >_s / \delta s$ and thus

$$E(z,z',N_i) = E(< z >_s, z',N_i) = \frac{\delta < z >_s}{\delta s}\Big|_{<z>_s} = \frac{< z >_s - < z >_{s-1}}{1}\Big|_{<z>_s} \qquad \text{[A10]}$$

In Figure 12 we show the squared stretching function as determined by nSCF for a monodisperse brush and three corresponding bi-disperse brushes. As can be seen, the squared local stretching for a monodisperse brush indeed gives a linear profile (except close to the wall because of the small depletion interaction between the grafting interface and the polymer chains). Extrapolating this linear profile to z = 0 gives a squared local stretching of 0.18, identical to what one can calculate from the analytical Eq. A8 ($N = 100$, $z' = 27$).

For bidisperse brushes the squared local chain stretching (of the long chain fraction) shows a linear dependence until at a certain z the slope changes. The distance *z* were the kink is observed depends on the length of the small chain fraction; the longer the small chain fraction the further away the kink is. The larger the difference between the long and the short chain, the more pronounced the kink is. The observation that the squared stretching function of the long chain in a polydisperse brush consists of two linear parts with different slope, could be very useful when developing analytical theory for bi- and polydisperse brushes.

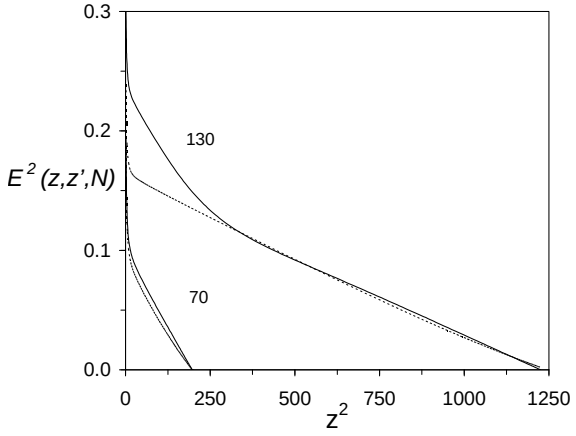

Figure 13. The squared local chain stretching for a given end-point position $E^2(z,z',N)$ as a function of the squared distance, for a long and a short chain (N_1 = 70, N_2 = 130) in a bidisperse brush ($\sigma_1 = \sigma_2 = 0.05$, continuous lines) and corresponding monodisperse brushes (N = 70, σ = 0.1 and N = 130, σ = 0.05, dotted lines).

In Figure 13, the local chain stretching of a long and a short chain in the same bidisperse brush are compared. This shows very clearly that close to the grafting interface the long polymer is stretched much more strongly than the short polymer. At *z* = 7, the local chain stretching of the long chains is twice that of the short chains. The squared local stretching of the short chain follows a linear profile, as such its density profile will be parabolic. There is only a slight difference between the local stretching of the short chain in the bidisperse brush and a corresponding monodisperse brush (dotted line). This is unexpected as in Figure 2b we have seen that the short chain fraction becomes more compressed. This stretching function, however, is only for all chains with a given end-point position *z* = 14, which is close to the end of the short chain fraction density profile. In the bidisperse brush most short chains are compressed, however the few who stretch to *z* = 14

stretch somewhat more than they would in a monodisperse brush. Because of the compression of other chains they are somewhat pushed out of the area with a higher chain density leading to a slight increase in stretching. When we compare the squared local stretching of the long chain in the bidisperse brush with the squared local stretching of its corresponding monodisperse brush, there is a large difference when in the bidisperse brush the long chain is surrounded by short chains, above the short chain fraction the stretching functions are very similar.

Appendix C. A Quasi-analytical Box-Model for the Polydisperse polymer brush: the stack of boxes model

The simplest model for a homodisperse polymer brush is one in which one assumes that all the polymers in the brush have the same stretching and thus that all end-points are at the same distance from the grafting interface. This so called box model was first used by Alexander and de Gennes [25,26] and yielded for uncharged polymers brushes to simple scaling laws for, e.g. the brush height. Using a Gaussian model, one can write a free energy $F(\mathrm{H}) = E - TS$ as being composed interaction part $E \sim v\sigma N^2 / H$, where v is the second virial coefficient (which is unity in good solvent, and will be omitted here), and a loss of entropy $-TS \sim H / N^2$ that originates from the (homogeneous) stretching of the chains. Optimization of the free energy with respect to the height H gives the well-known result

$$H \sim N\sigma^{1/3} \qquad \text{[A11]}$$

Although the assumption of equal stretching of all polymers is a serious oversimplifications, the same scaling law was also found for more sophisticated models like aSCF and nSCF [1,18]. Advantages of using box-models is that they are simple and can easily be extended, e.g., to investigate adsorption in polymer brushes [22].

A polydisperse brush can not be described by a model that uses just one single box, as one would need to assume that polymers of different length stretch to the same height, and thus that short chains are extremely extended and long ones are then compressed. One can however describe a polydisperse brush by a stack of boxes. One simplistic generalization is found when there are as many boxes as there are chain length fractions. The first box (at the grafting interface) contains al chain length fractions. The second box contains all chain length fractions except the smallest. The third contains all chain length fractions except the smallest two etc. This continues to the last box which only contains the longest chain length fraction. Thus, every box has its own local grafting density determined by the number of chains in all the chain length fractions included in that box. Each box also has a local chain length, which is equal to the length of the smallest chain length fraction in that box minus all the chain lengths of lower boxes. In this way, the sum of all local chain lengths (of all boxes) is the length of the longest fraction. As every box has a local chain length and a local grafting density, we can calculate for every box its height by implementation of A11. If every chain length fraction has a width of one monomer (and thus all boxes have a local chain length of one) the height of the total brush is then given by.

$$H \sim \sum_{N=1}^{N_J} \left(\sigma - \sum_{i=1}^{N} \sigma_i \right)^{1/3} \qquad \text{[A12]}$$

In this approach we thus assume that all polymers of the same length stretch exactly the same amount and that the local stretching of a single polymer is only determined by local polymer volume fraction and not by the stretching of the remainder of the chain. Note that these assumptions are very similar to the assumptions made by Milner *et al* and Birshtein *et al* [5,6] as they assume complete segregation of end-points. For a system with many different polymer lengths, this assumption leads to extremely narrow distributions of end-points of polymers with the same height and thus almost the same stretching. Also, in refs. 5 and 6, the point of view is taken that the stretching of the fraction of small polymers is not influenced by the large ones, i.e., that the local stretching is only determined by the local volume fraction. From Eq. A12, it is possible to extract the local polymer volume fraction by dividing the local "grafting density" by the local height increment. Results of the model are shown in Figures 9 and 10.

Chapter 9

Interaction of particles with a polydisperse brush: a self-consistent field analysis.

Abstract

Two complementary theoretical approaches are used to study the effect of polydispersity on (anti)fouling properties of a neutral polymer brush. Polydispersity is described using the Schulz-Zimm distribution. The Scheutjens-Fleer self-consistent field (SF-SCF) formalism is used to consider the interaction between a single particle and a polydisperse brush with grafting density σ, focusing on the influence of the polydispersity index. The larger the polydispersity, the easier it is for a small particle (with radius $R \sim 1/(2\sqrt{\sigma})$) to penetrate the brush. Hence, the monodisperse brush is better suited to protect a surface against the adsorption of small particles compared to a corresponding polydisperse brush. The brush grafting density, however, remains the most important parameter for tuning the brush antifouling properties against small particles. For large particles (modeled as a flat wall) an opposite effect of polydispersity is found: it is harder to compress a polydisperse brush than a corresponding monodisperse brush and thus a polydisperse brush is better suited to protect the surface against adsorption of large particles. A less-detailed approach, based on the stacking of Alexander-de Gennes boxes, is used to study the adsorption of many particles into a polydisperse brush. Consistent with the single-particle data generated by the SF-SCF theory, for weak attraction between the particles and the brush the absolute adsorbed amount remains low, but increases strongly as a function of polydispersity (from M_w/M_n = 1-2 by a factor of 2-4). Obviously, at higher attraction between the particles and the brush the adsorption increases, but a less strong dependence on the polydispersity index is observed.

A manuscript based on this chapter was published as:

De Vos, W.M.; Leermakers F.A.M.; de Keizer A.; Kleijn J.M. and Cohen Stuart M. A. *Macromolecules* **2009**, *42*, 5881.

Introduction

Polymer brushes have been widely investigated over the past 30 years, for example, because of their role as particle stabilizers and their antifouling properties [1, 2, 3, 4, 5]. In this chapter we will focus on how particles can partition into a brush. Brushes are dense layers of polymer chains end-attached to a surface. The chains are stretched in order to reduce their excluded-volume interactions. When a particle, such as a protein, is inserted into a brush, the extra excluded-volume interactions force the polymer chains to increase their stretching causing the free energy to go up. As a reaction to this, the brush tends to push out the inserted particle. Thus, as long as there is no additional attraction between the polymer chains and the particle, the brush is potentially well suited to prevent fouling of the surface.

Antifouling properties have been investigated both experimentally [6-9] and theoretically [8-13]. Interestingly, there appears to be a remarkable disparity between theoretical and experimental investigations. In theoretical studies, the polymer brush is invariably assumed to be monodisperse, i.e., all chains have the same length. In contrast, in all experimental investigations brushes are to a significant extent polydisperse, as polydispersity is unavoidable in the production of polymer brushes.

In a recent paper de Vos and Leermakers [14 (chapter 8)] modeled polymer brushes composed of chains with a Schulz-Zimm length distribution, using a numerical self-consistent field theory implementing the discretization scheme of Scheutjens and Fleer (SF-SCF). In that paper it was proven that even a relatively small degree of polydispersity suffices to completely destroy the parabolic density profile that is characteristic for the monodisperse brush. Increasing the polydispersity at fixed grafting density increases the average height of the brush, but decreases the average stretching. The internal structure of the brush is strongly affected by polydispersity as well. Short chains are found to be compressed close to the grafting interface, whereas longer chains have a characteristic flowerlike conformation. These longer chains stretch strongly (forming a stem) when surrounded by smaller ones and decrease their stretching (forming a crown) as the density increases in the outer part of the brush. The distribution of the free ends, i.e. the end-point distribution, reflects the fluctuations in the conformations of the chains. For a monodisperse brush these fluctuations are anomalously large (proportional to the chain length) as can be concluded from the fact that the end points distribute throughout the brush. In the polydisperse brush, on the other hand, the fluctuations per chain length fraction are strongly suppressed: the distribution of ends are narrow and the width does not depend on the length of the chain. This means that the fluctuations are small. These results might indicate that the monodisperse brush has a limited relevance for practical situations. However, when the

distributions of the free ends in the polydisperse case are added together, they cover the whole brush, similarly as in the monodisperse brush. The latter may explain why the monodisperse brush has been so successfully applied to experimental situations. Nevertheless, to date there is, as far as we are aware, no knowledge about the effects of polydispersity on the (anti) fouling performance of a brush.

At the turn of the century a theoretical approach to investigate the interaction between a polymer brush and a single particle was devised by Steels *et al* [13]. They used a 2-gradient numerical self-consistent field theory (also using the SF-SCF approximations) to investigate the changes in the brush density profile upon the insertion of a cylindrical object (with length L and radius R; see Figure 1). They were able to compute the interaction (free) energy between such a particle and the brush as a function of the position of the particle above the grafting surface, for different grafting densities, and particle sizes. The authors showed that the size of the particle is very important for the way it interacts with the polymer brush. While a relatively small particle (compared to the distance between the grafted chains) is able to penetrate the brush layer, a larger particle can only compress the polymer chains in the brush.

We extend the study of Steels *et al* [13] to account for the polydispersity of the polymer chains that form the brush, and use numerical self-consistent field theory to determine the interaction energy between a single particle and a polydisperse brush. For the polydispersity, the relevant case of the Schulz-Zimm distribution is used. We consider (i) a very small particle penetrating the brush and (ii) a large particle compressing the brush. For both limits we investigate (a) systems where only excluded-volume interaction are important, (b) systems with a weak attraction between the brush and a particle, and (c) systems with a large attraction between the brush and a particle. We note that in the intermediate (mesoscopic) regime of particle sizes, the details of how the polydispersity of the grafted chains is handled (the grafting position is quenched or annealed) is important. In this chapter, however, such details are avoided mostly for computational reasons.

In practice one is interested in the number of particles per unit area that accumulate into the brush at a given particle concentration in the (bulk) solution. Such information typically is collected in adsorption isotherms. Of course, when there is sufficient repulsion, the adsorption is negligible (or in fact negative), but when attractive interactions are turned on, the adsorption can grow to relatively large values. The SF-SCF approach can account for many details of how the polymer chains accommodate a single particle. In addition, the method allows for the evaluation of the free energy of interaction of a particle with the brush (as mentioned above). This insertion free energy can be used in a Boltzmann equation to estimate the distribution of the particles in the brush. Integrating over this distribution

leads to the Henri coefficient (initial rise of the adsorption at very low levels of loading) of the adsorption isotherm. For large adsorbed amounts, however, one has to consider how multiple particles disturb the brush. This problem is currently out of reach for molecularly detailed SCF models. To circumvent this problem and estimate the adsorption isotherms we will use a less rigorous SCF approach known as the Alexander-de Gennes box model, which we extend to account for polydispersity in a reasonable way. A similar box model, in the absence of particles, has been applied to the polydisperse brush in ref. [14 (chapter 8)]. Using this model we will investigate how polydispersity of the brush influences the adsorption of multiple small particles.

In both the SCF method and in the Alexander-de Gennes box model we can identify the transition point that separates the adsorption from the depletion regime. So, in first order we can bring both approaches together so that they complement each other. However, as the two methods treat the particle-insertion problem on a different level of detail, it is hard to match them accurately. It is not the goal of this chapter to determine what values for the pertinent parameters in each approach should be used to describe a particular experimental system. Instead we will focus on how polydispersity of the brush influences the uptake or repulsion of particles. In other words, we are here interested in predicting (measurable) trends rather than to make a quantitative comparison to experiments.

Theory

Many details of the SCF theories used below can be found in the literature [13,14 (chapter 8)]. Here we will only briefly discuss the main points, focus on the approximations, and mention the parameters that are used. The mathematical details are deferred to Appendices. In this section we first will discuss the polymer size distribution, pay some attention to the SF-SCF model and finally discuss the stack of boxes model.

Polymer length distribution

A function commonly used to represent polymer molecular weight distributions, is the so-called Schulz-Zimm distribution [15,16]:

$$P(x, N_i) = \frac{x^{x+1}}{\Gamma(x+1)} \frac{N_i^{x-1}}{N_n^x} \exp\left(-\frac{xN_i}{N_n} \right) \qquad [1]$$

In which $P(x, N_i)$ is the probability of chains with degree of polymerization N_i, N_n is the number-average degree of polymerization, and x defines the broadness of the distribution. $\Gamma(x+1)$ is the gamma function, which for integer values of x is equal to $x!$. A nice feature of this distribution is that the parameter x is directly related to the polydispersity index:

$$\frac{M_w}{M_n} = \frac{N_w}{N_n} = \frac{x+1}{x} \qquad [2]$$

Here M_n is the number-average molecular weight and M_w is the weight-average molecular weight (both in g/mol). The polydispersity index, M_w/M_n, is the most commonly used measure for polydispersity. The Schulz-Zimm distribution is almost symmetrical at low values of the polydispersity (similar to the Gaussian distribution), but with increasing polydispersity the distribution shifts to a higher frequency of small chains. In this way the distribution can be used to describe very high polydispersities.

Numerical Self-Consistent Field Theory

We make use of a numerical self-consistent field (SCF) model with the discretization strategy of Scheutjens and Fleer (SF-SCF). In all calculations an impenetrable surface is present onto which a polymer brush is grafted. The combination of this surface with the brush is called the substrate. Information on the length distribution used for the chains has been given above. The properties of the polydisperse polymer brush have been discussed at length in ref. [14 (chapter 8)]. Here we consider how particles interact with such a brush. The focus is on two limiting cases.

In case *one* we focus on the interaction of small particles with the brush. When the interacting particle is small compared to the relevant properties of the brush, such as the grafting density σ (inverse of the area per molecule) and the chain lengths, one has to account for the fact that the polymer chains can escape from, or are attracted towards the space of confinement (the space between the substrate and the interacting particle). Such relaxation effects can be accounted for by using a cylindrical coordinate system (2-gradient SCF). When doing so it is necessary to compute relevant density gradients perpendicular to the substrate as well as in a radial direction (see Figure 1). In this geometry the particle is modeled as a small cylinder with length L and radius R, and has its long axis along the long axis of the coordinate system (see Figure 1 for a schematic illustration).

In case *two* we will consider very large particles interacting with the brush. The radius of the particle is assumed to be much larger than the spacing between the polymer chains and much larger than the length of the polymers. In this limit it is reasonable to ignore the finite size of the interacting particle and consider a polymer brush compressed by a solid wall representing the particle. This problem is conveniently solved using a classical 1-gradient SCF model and using a flat geometry.

Generic aspects of SF-SCF theory

In general, we are not primarily interested in the conformation of a particular polymer chain in the brush. Instead, the focus is on the average conformations of a large set of polymer chains, resulting, for example, in density profiles. These average conformations can be found by solving the Edwards diffusion equation for the set of polymer chains. Here it is important to mention that for a brush the first segment of each chain is forced to be next to an impenetrable surface S (this is implemented as a constraint). As exact analytical results are not available for this problem, we need some numerical scheme. Details of this scheme are found in the Appendix. Polymer chains with length (degree of polymerization) N_i are referred to by the letter i. The number of chains per unit area of this type, σ_i, are taken from the distribution mentioned above, where the overall grafting density σ is an input parameter. The polymer chains assume non-Gaussian characteristics because they experience a segment potential $u(\mathbf{r})$ (here $\mathbf{r} = (z,r)$ in the case of the 2-gradient SCF calculations and $\mathbf{r} = z$ for the 1-gradient SCF case). For homopolymers, with united segments A, and grafting density $\sigma > 1/N$, it is well known that the SF-SCF method predicts a parabolic potential profile $u(z) = A - Bz^2$, in which A and B are constants. In good solvents the volume fraction profile $\varphi(z)$ will then also be parabolic. For polydisperse systems, on the other hand, this is no longer the case. In the segment potential we account primarily for short-range interactions with a monomeric solvent (W). Using the Flory-Huggins parameters, which are dimensionless exchange interaction energies, we limit ourselves to $\chi_{AW} \equiv \chi \leq 0.5$. The (dimensionless) second virial coefficient v is directly linked to the quality of the solvent, i.e. $v = 1 - 2\chi$. The interactions with the solid substrate are taken to be athermal for all components in the system. The interactions with the particle (P) is one of the main parameters that will be varied below. For attraction the adsorption parameter $\chi_P \equiv \chi_{AP} - \chi_{WP} < 0$. For repulsion $\chi_P > 0$. Also included in the segment potential is a Lagrange field $u'(\mathbf{r})$ which assures the incompressibility condition (all lattice sites must either be occupied by polymer segments or solvent molecules, or are part of the particle).

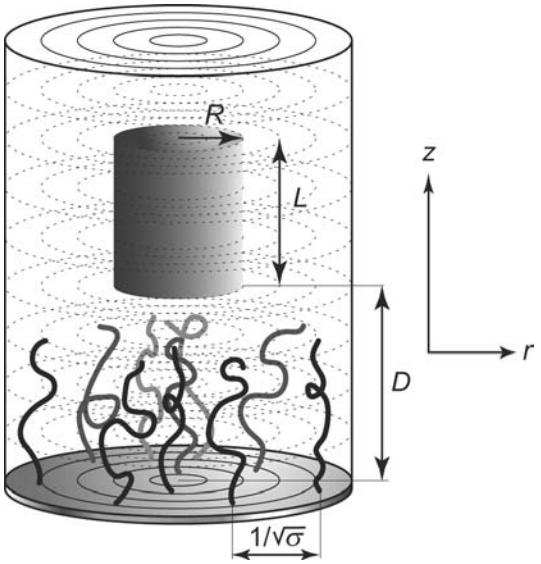

Figure 1. Schematic representation of the coordinate system used in the SF-SCF calculations. Here we show a small particle (top gray cylinder) with radius R and height L positioned at a distance D from the substrate. The two-gradient coordinate system (z,r) is indicated; layers parallel to the surface are numbered z = 1, 2, …, M_z. In radial directions the lattice shells are numbered r = 1, 2, …, M_r. At the surface, a polymer brush with grafting density σ is present. In the SCF model we assume that the brush chains are laterally mobile along the surface. To avoid adverse effects of the finite size of the computation box, the boundary condition in the radial direction is mirror-like.

Polymers near interfaces experience an entropy loss, simply because the chains cannot penetrate the solid particle P or surface S. In a lattice model the entropy loss is easily estimated. This loss is a function of the *a priori* probability λ_1 for a segment to go from one layer to a next one. Here we use a (cubic) lattice where λ_1 =1/6 and the entropy loss per segment-segment bond next to a flat surface amounts to $\Delta S = k_B \ln(1-\lambda_1) \approx -k_B\lambda_1$. There exists a critical (dimensionless) adsorption energy χ_P^{cr} below which adsorption takes place and above which the polymers avoid the surface (particle). For a flat surface and for long chains the critical adsorption energy is equal, but opposite to $T\Delta S / k_B T = \Delta S / k_B$. As a segment next to the surface has λ_1, contacts with the surface, exchange with the solvent gives and energy effect of $\lambda_1\chi_P$. This implies that $\chi_P^{cr} \approx -1$ (recall that the Flory-Huggins parameter is made dimensionless by dividing by k_BT).

The results of the SCF calculations are essentially two-fold. On the one hand there are the measurable volume fraction profiles. These profiles give insight in how the chains accommodate the particle in the brush or deal with the confinement. More importantly for

the results, we can evaluate the free energy of interaction. This quantity is computed directly as a function of the volume fraction and the segment potential profiles. Details are given in Appendix A.

Small particle in brush: 2-gradient SCF

We refer once again to Figure 1 where a schematic drawing is given of the calculation 'box' for the 2-gradient SCF calculations. The use of two gradients allows for the fact that in the case of repulsion the chains that are confined underneath the particle can escape to the unconfined regions and inversely, in the case of attraction that the chains that are outside the confined region can be drawn towards this space. It then becomes important to decide if the grafting points have a fixed position (quenched) or that the chains can move with the grafting point along the surface (annealed). In the latter case, redistribution of the chains is likely to result in an extra decrease of the free energy.

To check the importance of this effect we have compared the free energies of interaction between the particle and a bidisperse brush, for mobile chains and fixed chains (evenly distributed along the surface). We found that for a small particle, there is only a very small difference between the interaction with the fixed and the mobile brush (for M_r = 20). As the annealed grafting condition also solves the issue of which chain lengths to graft in the central region, i.e., near (z,r) = (1,1), we have chosen to model the mobile brush. As long as the particle is far from the surface, each surface site (1,r) has the same probability to have a chain of length N_i grafted to it. Only when the particle is in close proximity of the brush, or when it is inserted deep into the brush, the local grafting length distribution may slightly differ from the overall grafting density distribution.

Large particle in brush: 1-gradient SCF

In this case a polydisperse brush on a solid surface is confined by a second flat surface, P. Only one relevant coordinate is present in the system, namely the distance z from the substrate surface. When the position $z = D$ of the second surface exceeds the lengths of the longest chains, the brush is unperturbed. This is the reference state for the free energy of interaction. In this case all quantities are normalized per unit surface area, i.e. per lattice site area. As the chains cannot avoid the gap between the particle P and the substrate S, the issue of lateral mobility of the chains does not occur here. Obviously, results from this approach are identical to results that we could get from the 2-gradient approach, with a particle that spans the whole box.

"Stack of Alexander-de Gennes Boxes" model

In ref. 14 (chapter 8), we proposed an extension of the classical box model to describe polydisperse brushes. In this extension the idea is to use a stack of boxes. The box model is the simplest model for a monodisperse polymer brush as one assumes that all the polymers in the brush have the same stretching, and thus that all end-points are at the same distance from the grafting interface. This model was first used by Alexander and de Gennes [17,18] and yielded for uncharged polymer brushes simple scaling laws for, e.g., the brush height. In Appendix B we present more details of this model, which can be used to study adsorption of an ensemble of particles into a polymer brush.

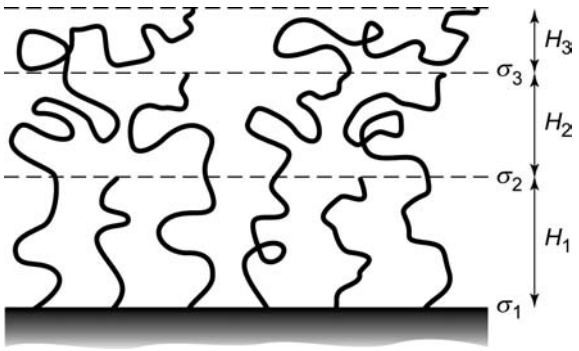

Figure 2. Schematic depiction of a brush in a stack-of-boxes model. Here σ_i represents the grafting density and H_i the height of box i. Small chains reach to height H_1, intermediate chains reach to height $H_1 + H_2$ and the longest chains reach to height $H_1 + H_2 + H_3$. Each layer can be described by a separate box model, with a certain grafting density and chain length, to calculate properties such as the brush height, polymer density or even the amount of adsorbed particles.

A polydisperse brush cannot be described by a model that uses just one single box, as one would need to assume that polymers of different length stretch to the same height, and thus that short chains are extremely extended and long ones are compressed. One can, however, describe a polydisperse brush, in a reasonable fashion, using a stack of boxes. A schematic depiction of this model is shown in Figure 2. The number of boxes equals the number of chain length fractions that is chosen for the modeling (in Figure 2 this number is three). The box directly adjacent to the grafting surface contains all chains. The polymers of the smallest chain length fraction have their endpoints at the top of this box (at distance H_1 from the surface). As a result, the second box contains polymers of all chain length fractions except the smallest one. The third box contains polymers of all chain length fractions except the smallest two, etc. This continues to the last box which only contains

polymers of the longest chain length fraction. Thus, every box has its own local grafting density, which is given by the total number of chains (per unit area) included in that box. Each box also has its own local chain length, which equals the length of the polymers of the smallest chain length fraction in that box, minus the length of the polymers that ended in the box below. In this way, the sum of the chain lengths of all boxes is the length of the longest polymer fraction.

The stack of boxes model (SoB) describes, for a given polymer length distribution, the local grafting density and local chain length for every box. To get more relevant information such as the height, polymer density or even adsorption in such a box a local model is needed. The local model gives the local stretching of the chains and evaluates the adsorption of particles onto these chains while both the solvent and the particles can exchange with the bulk. The local model that we use is a box model based on a simple free energy description of a monodisperse brush, combined with a Langmuir-type model to describe adsorption of particles. The idea is that particles adsorb onto sites that are specified along the polymer chains. This is described in detail in Appendix B.

Parameter settings

In the SF-SCF calculations, we keep the number average degree of polymerization, the overall grafting density and the overall mass constant when varying the polydispersity. Unless specified otherwise, we have used the Schulz-Zimm distribution with a maximum chain length of $N_{\mathrm{I}} = 1000$. The overall grafting density σ is fixed at an experimentally relevant value of $\sigma = 0.05$ chains per surface lattice site. (Common experimental values are between 0.01 and 0.3 polymer chains per nm^2 [2-4]). The cylindrical coordinate system has a finite size in the radial direction of $M_{\mathrm{r}} = 20$ and a size of $M_{\mathrm{z}} = 100$ lattice sites above the surface, which is well above the height of the brush. To describe a small particle, we use an object with a radius of $R = 2$ and a height of $L = 3$ lattice sites. We refer to these numbers as (R x L). As the chosen grafting density is 0.05, the particle diameter ($2R$) is slightly smaller than the distance between two grafting points ($R \approx 1/(2\sqrt{\sigma})$). To be able to compare the free energy of interaction for the large particle (obtained in the 1-gradient coordinate system) with that of the small particle, we multiply the interaction energy obtained for the large particle (which is in k_BT per lattice site) with the surface area of the small particle (thus by πR^2) .

The interaction between the particle and polymer segments in the brush is described by the parameter χ_{P} and the interaction of the polymer segments with the solvent is given by χ. For this investigation we chose three different sets of values for these parameters. The first set reflects only excluded-volume interactions ($\chi_{\mathrm{P}} = 0$, $\chi = 0$), the second a small attraction

between brush and particle in combination with a lower solubility for the polymer chains and the particle (χ_P = –1, χ = 0.5), and the third a strong attraction between brush and particle, also with a lower solubility for the polymer chains and the particle (χ_P = –2.5, χ = 0.5). In the results and discussion section, we will more fully discuss this choice of parameters.

For the SoB model we use a brush with N_n = 100 and σ = 0.1. This brush is in contact with a solution containing particles with size respective to the solvent molecules of N_p = 4 and a bulk volume fraction of Φ_P = 0.001. The particle size is small compared to the particle used in the SF-SCF model for computational reasons; to compensate we also use a higher grafting density than in the SF-SCF model. The (reduced) attraction parameter U is varied between U = 0 and U = –5 to investigate a broad range of attractions. As a rough method to compare the attraction parameter χ_P of the SF-SCF model to the attraction parameter U of the SoB model, we use $U = \chi_P - \chi_P^{cr}$, to which we will come back in the results and discussion section.

Results and discussion

Investigation of brush and interaction parameters

In Figure 3 we show the key prediction of ref. 14 (chapter 8), namely that the polymer volume fraction profile of a brush is strongly dependent on the polydispersity index. Only for a monodisperse brush the volume fraction profile has an almost parabolic shape: $\varphi(z) \sim \varphi_{max} - Bz^2$, were φ_{max} and B are constants, i.e. it is a concave function. Already for $M_w/M_n = 1.1$ the volume fraction drops almost linearly with the distance to the grafting surface. The profile becomes convex at higher polydispersities. With increasing polydispersity the height above the surface where polymer segments are detected, increases. The average stretching of the chains (not shown) decreases with increasing polydispersity index.

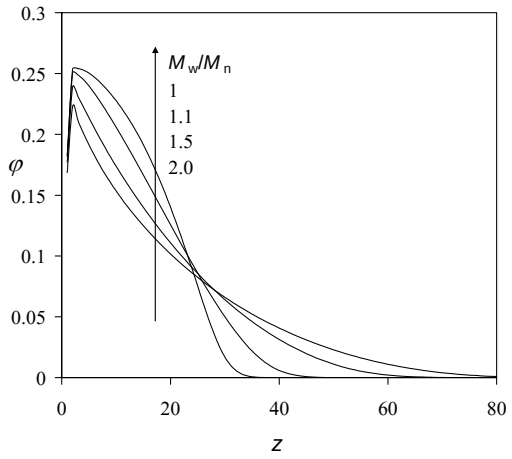

Figure 3. Brush density (φ) as a function of distance from the grafting interface (z) for different polydispersity indices as indicated ($N_n = 100$, $\sigma = 0.05$).

To investigate the interaction of a polymer brush with a particle, we use the approach by Steels *et al* [13]. They used the SF-SCF approach in which a single particle is moved from outside the brush to a certain distance from the interface (*D)* into the brush. The resulting change in free energy is called the free energy of interaction (ΔF). In Figure 4 we show the interaction between a monodisperse brush and a large particle for various values of the polymer-particle interaction strength. This graph clearly illustrates the significance of the critical adsorption energy. At $\chi_P \approx -1$, the entropy loss of the polymer chains touching the particle is matched by the energy gained by adsorption. Thus, above $\chi_P \approx -1$ we only find repulsion, while below $\chi_P \approx -1$ we find attraction for a certain range of *D*.

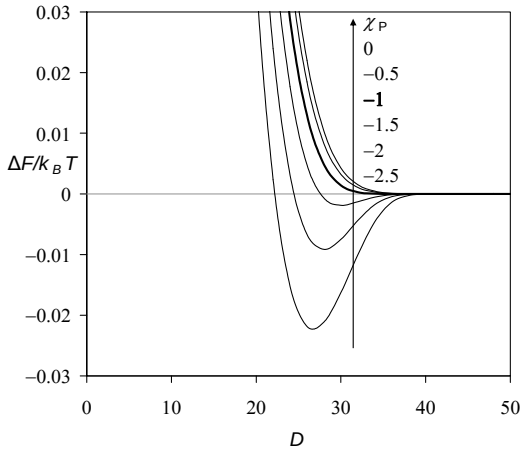

Figure 4. Free energy of interaction (ΔF is given per lattice site) of a large object (a flat wall spanning the whole box) with a polymer brush (σ = 0.05, N = 100) for different values of χ_P as indicated, as a function of distance (D) of the object from the grafting surface as computed using the 1-gradient numerical SCF theory. χ = 0.

We want to investigate the effect that polydispersity has on particle-brush interaction for different values of χ_P. From the results of Figure 4 we have chosen the following three sets interaction parameters. In the first case we want to focus on excluded-volume interactions only and thus χ_P = 0 and χ = 0. In the second case we investigate a system in which we have a small attraction between the particle and the brush. For this we chose χ_P = −1 and χ = 0.5. In this way the total adsorption energy is slightly more negative than the critical value and thus a small attraction is expected. In addition, we argue that a reduced solvent quality of the polymer chains (χ = 0.5) is realistic, as a less soluble polymer chain is more likely to be attracted to a particle than a polymer chain in a good solvent. In the third and last case we have chosen χ_P = −2.5 and χ = 0.5, thus leading to a situation where the particle is strongly attracted to the polymer brush.

Interaction of a polydisperse brush with a small particle

In Figure 5 we show the free energy of interaction between a polymer brush and a small particle (2x3 lattice sites) for different degrees of polydispersity in the first scenario, i.e. the particle has no attractive interactions with the brush. The size of the particle is such that it resembles the interaction of a polymer brush with a small protein. As is observed in Figure 5, at a height of D > 50, ΔF is zero (except for the largest polydispersity index) showing that there is no interaction between the brush and the particle. When the particle is

moved inside the brush (going to lower distance) the particle comes into contact with the brush and ΔF increases. This repulsion is due to the excluded-volume interactions: when the brush is deformed due to insertion of an object, the brush responds with a restoring force. We observe that the higher the polydispersity index, the further away from the surface nonzero ΔF values are found. This is to be expected as the height of the brush increases with polydispersity. On the other hand, we find that ΔF deeper inside the brush is higher for the monodisperse brush than for the polydisperse brushes. The free energy of interaction depends on the local brush density. As increasing polydispersity leads to an increasing brush height, the brush density near the grafting interface decreases. Because of this lower brush density, ΔF is also lower close to the grafting interface. Thus, the higher the polydispersity, the easier it is for a small particle to penetrate the denser parts of the polymer brush and thus to reach the grafting interface. Polymer brushes are often used as barriers that prevent fouling agents from reaching a surface. The harder it is for the fouling agent to reach the surface, the better the antifouling properties. Hence, we may formulate our first conclusion, namely that the more monodisperse the brush, the better the antifouling properties against small particles.

Now that we have shown that the polydispersity can influence the antifouling properties of a polymer brush, it is interesting to compare this effect to that of the grafting density. The brush grafting density is commonly seen as the most important parameter for the antifouling properties of a brush [1-5]. The larger the grafting density, the higher the energy barrier that must be overcome by a particle to reach the surface. We calculated, using the parameter settings of Figure 5, the free energy of interaction for a number of different grafting densities (not shown). For a monodisperse brush with $\sigma = 0.1$ we find that the maximum ΔF becomes approximately 8 $k_B T$, and for $\sigma = 0.2$ we even find a maximum ΔF of approximately 16 $k_B T$. As the effect of the grafting density on the energy barrier is stronger than the effect of polydispersity, it is clear that the grafting density is the more important tuning parameter for antifouling properties against small particles. Still, for all these grafting densities the maximum ΔF decreases when the polydispersity increases.

In some cases, fouling agents such as proteins have a slight attraction to the polymers in the brush. For such a case, we present in Figure 6 the predictions for the free energy of interaction between a small particle and a polymer brush. As the particle is inserted into the brush there is an attraction and a minimum in ΔF appears around $D = 14$. Deeper inside the brush the attraction turns into repulsion. This non-monotonic dependence of ΔF on the position of the particle is a result of the balance between attraction of the polymer chains to the particle and repulsion from the excluded-volume interactions (brush confinement). At low brush densities (at the brush periphery) attraction dominates, but deeper in the brush

where the brush density is higher, repulsion dominates. Although the polydispersity hardly effects the depth of the minimum in the free energy, it has a clear effect on the interaction profile. We find that the higher the polydispersity index, the larger the range of D in the brush where attraction is observed. This is because of the fact that for increasing polydispersity the polymer mass is spread over a larger volume and thus the average brush density decreases. For a broader chain length distribution, the interaction between brush and particle starts further away from the grafting interface, but also the brush density remains low enough for excluded-volume interactions to remain negligible. Only deep in the brush, repulsion due to excluded-volume interactions is dominant. This suggests that, if there is a slight attraction between the brush polymers and, for example, small proteins, the adsorbed amount increases with polydispersity, as there is a larger part of the brush in which attraction dominates. Thus, also if there is a weak attraction between the polymers and the particle, the monodisperse brush is expected to have better antifouling properties than the polydisperse brush.

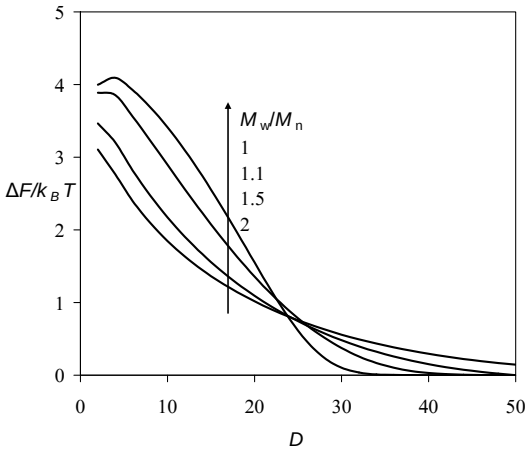

Figure 5. The free energy of interaction (ΔF) of a small object (2x3) in a polymer brush (σ = 0.05, N_n = 100) as a function of distance (D) from the grafting interface, calculated using 2-gradient numerical SCF theory (χ_P = 0, χ = 0).

In Figure 7 we present the free energy of interaction for the case that there is a strong attraction between the particle and the brush. Now, we find that attraction dominates over the whole interaction range. The higher the polydispersity, the further away from the interface (larger D) attraction is found. In Figure 7 the curves cross over between D = 10 and D =20: far away from the interface, the attraction is larger for larger polydispersities, while close to the interface, a larger polydispersity results in a less negative ΔF. Thus, the

attraction depends on the local brush density, a higher polymer density gives a more negative ΔF. Obviously, such a brush is completely unsuitable for antifouling purposes. Instead, it might be used to store or immobilize particles. Indeed, polymer brushes with strong interaction with proteins have been investigated for their use as protein carriers [20,21 (chapter 6)]. Note that here we only consider the case of an isolated particle in the brush. When many particles are simultaneously allowed to adsorb into the brush, one can anticipate that this would lead to strong changes in the density profile of the brush (such as swelling of the brush because of the insertion of the extra volume, or a collapse of the brush because of strong attraction between the polymer chains and the particles). If there is a strong attraction between polymer and protein, one would not expect a large effect of the polydispersity on the adsorbed amount. This quantity will depend mainly on the total amount of polymer in the brush and not so much on the way that it is distributed.

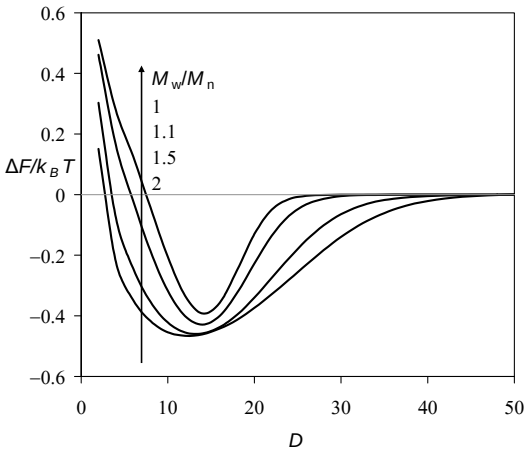

Figure 6. The free energy of interaction of a small object (2x3) in a polymer brush (σ = 0.05, N_n = 100) as a function of distance (D) from the grafting interface, as calculated by 2-gradient numerical SCF theory ($\chi_P = -1$, $\chi = 0.5$).

As stated before, the problem of adsorption of many particles is currently out of reach for molecularly realistic SF-SCF models. We can, however, use the results of our model to predict the adsorption for low bulk particle concentration. In this regime (the so-called Henry regime) the adsorption is considered to be so low that the brush is unperturbed by this adsorption. This implies that the particle density in the brush, φ_p, is only determined by the bulk volume fraction of particles, Φ_p, and the energy of interaction:

$$\varphi_p(D) = \Phi_p \exp\left(\frac{-\Delta F(D)}{k_B T}\right) \qquad [3]$$

Using Eq. (3) we thus find that the particle profile inside the brush is not homogeneous. For example, close to the surface there may be a depletion of particles with respect to the bulk value, whereas on the brush periphery the adsorption is positive (Figure 6). Clearly, for a polydisperse brush there is a larger region with positive adsorption of particles compared to the monodisperse brush (Figure 6 and 7).

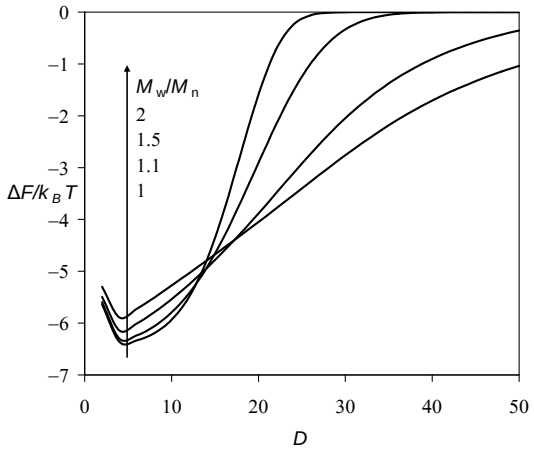

Figure 7. The free energy of interaction of a small object (2x3) in a polymer brush (σ = 0.05, N_n = 100) as a function of distance (D) from the grafting interface, as calculated by 2-gradient numerical SCF theory (χ_P = −2.5, χ = 0.5).

The interaction of a polydisperse brush with a large particle

As stated earlier, there is large difference between a small particle and a large particle interacting with a brush. A small particle (such as a globular protein) can easily penetrate a brush, as the brush polymers can surround the particle. Thus, interaction with the particle in the polymer brush mainly depends on the local brush density. A large particle (such as a bacterium or a colloidal probe for atomic force microscopy (AFM)) cannot penetrate into a brush, it can only compress it. To investigate the interaction of a polydisperse brush with a large particle, we replaced the latter by a flat hard wall. Just as with the small particle, this wall is moved from far above the brush to a distance *D* from the grafting interface, and the difference in free energy is calculated. In Figure 8 results of such calculations are shown.

The free energy of interaction is normalized to the surface area of the small particle to facilitate comparison. In Figure 8 only excluded-volume interactions are taken into account (compare with Figure 5). As can be seen, the interaction energy shows a very strong increase when the particle approaches the grafting interface. The closer the particle wall comes to the grafting surface, the more the polymer brush is compressed. The interaction energy is much larger than for a small particle, simply because the chains cannot escape from the confined region. Polydispersity has a large influence on the interaction energy: at every height we find that the higher the polydispersity, the higher the interaction energy. In other words, it is harder to compress a polydisperse brush than a monodisperse brush. Thus, for the case that there is no attraction between the brush chains and the particles, polydispersity helps to prevent adsorption of large particles (e.g., when there is some long-range interaction between the interface and the particle).

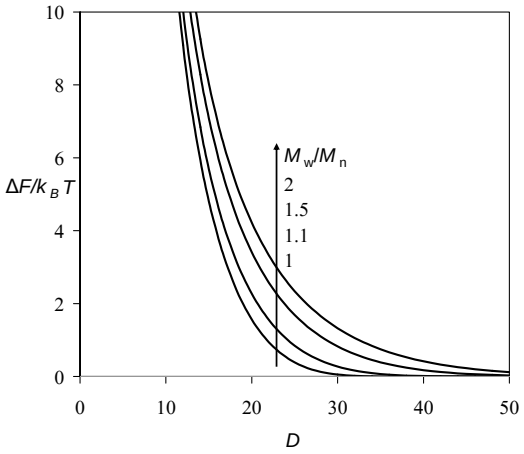

Figure 8. The free energy of interaction (ΔF) of a large object (a flat wall spanning the whole box) on a polymer brush (σ = 0.05, N = 100) as a function of distance (D) from the grafting interface, as calculated by 1-gradient numerical SCF (χ_P = 0, χ = 0). For comparison with Figure 5, ΔF has been multiplied by lower surface area of the small particle (4π).

At this stage it is useful to explain why a polydisperse brush is harder to compress than a monodisperse brush. De Vos and Leermakers [14, (chapter 8)] found for an unperturbed brush that with increasing polydispersity there is more freedom (compared to a monodisperse brush) to distribute the stretching of the chains. One consequence of this is that the average stretching (defined as the height increase per monomer) is lower for a polydisperse brush than for a monodisperse brush. For example, the average stretching of a brush with a polydispersity M_w/M_n = 2 was found to be 22% lower than that of a

monodisperse brush. The relevance for compression of the brush is evident. The entropy loss as a result of compression is higher for a polydisperse brush. This results in a higher free energy of interaction for the polydisperse brush with a large object than for the monodisperse brush.

In Figure 9 we examine the case in which there is a small attraction between the large particle and the chains in the polymer brush. Similar to Figure 6, which shows comparable results for a small particle, we observe an attraction between brush and particle in the region where the brush density is low. Also, with increasing compression of the brush the repulsion ultimately exceeds the attraction. Again, this behavior is the result of a balance of forces: the closer the particle is moved to the grafting interface the higher the compression, but also, up to saturation, the higher the number of possible contacts between brush polymers and the particle. This results in a minimum of ΔF as a function of D. The polydispersity determines the position and depth of this minimum. With increasing polydispersity, the minimum moves further away from the grafting interface and the depth of the minimum slightly decreases. A more significant effect of polydispersity, however, is the change in the range of D where we find attraction between the brush and the particle. We find that the higher the polydispersity, the larger this range.

The same effect of polydispersity is observed in Figure 10, which shows the interaction energy between the large object and the brush when there is a strong attraction ($\chi_P = -2.5$). Because of this strong attraction, the minima in the free energy are much larger than in Figure 9, but the trend is the same: an increase in polydispersity leads to a shift of the minimum in the free energy further away from the grafting interface and the depth of this minimum slightly decreases. A more pronounced effect is that the range of D in which attraction is found increases with increasing polydispersity. As was observed in Figure 8, repulsion because of compression increases with increasing polydispersity. Therefore, the monodisperse brush can be compressed more than the polydisperse brushes, resulting in more contacts between the brush and the particle and thus a slightly deeper free energy minimum at a lower height. Although this effect is not so large, it does show that for the protection of a surface against fouling by large particles, a polydisperse brush is the better choice.

Experimentally the role of polydispersity in the interaction of particles with a brush has not yet been addressed. Colloidal probe AFM is potentially suited to measure the interaction between a large particle and a polymer brush and could thus be used to verify some of our predictions. As an alternative one could use the surface force apparatus (SFA) to measure the interaction between a polymer brush and a planar surface or between two

polymer brushes. For such experiments, however, it is necessary that one has a method to produce polymer brushes with different polydispersities while N and σ are retained.

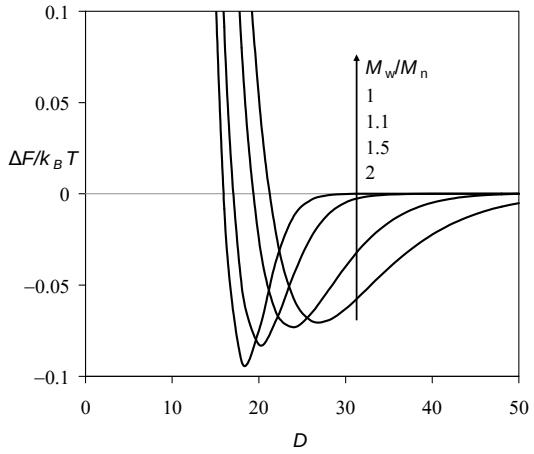

Figure 9. The free energy of interaction of a large object on a polymer brush (σ = 0.05, N_n = 100) as a function of distance (D) from the grafting interface, as calculated by 1-gradient nSCF theory (χ_P = −1, χ = 0.5).

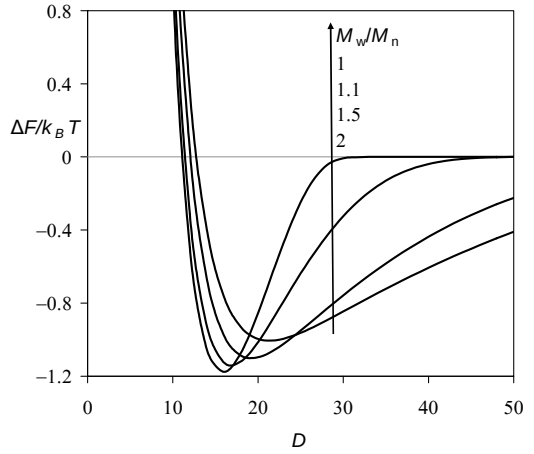

Figure 10. The free energy of interaction of a large object on a polymer brush (σ = 0.05, N_n = 100) as a function of distance (D) from the grafting interface, as calculated by 1-gradient nSCF theory (χ_P = −2.5, χ = 0.5).

Adsorption of many particles in the polydisperse brush

In Figures 5-7 it was shown that the interaction energy between a brush and a single small particle is influenced by polydispersity. Therefore, it is also interesting to investigate how the interaction with many particles depends on the polydispersity. We will now focus on the adsorbed amount of particles in the brush and how this depends on the polydispersity. This is of relevance as adsorption of small particles to a brush (in this context called secondary adsorption) is a problem for its antifouling properties, but also because polymer brushes may be employed to accommodate or immobilize particles (such as proteins, especially enzymes) rather than prevent fouling [20,21 (chapter 6)].

As explained in the theory section, we use an elaborate box model to quantify particle adsorption into a polydisperse brush (see also Appendix B). A similar, but slightly different box model has been advanced before to study adsorption into a polymer brush, and qualitative agreement with experimental results was reported [8]. Here, the focus is on a polydisperse brush. This feature is implemented by using not a single box but rather a stack of boxes (SoB) to describe the brush. Even though such a SoB model does not accurately describe the brush density profile for a given polydispersity, it reasonably well describes the trends observed for brush density profiles as a function of polydispersity (as shown in Figure 3).

To be able to compare the outcome of the SoB model with the results of the SCF calculations, it is helpful to explain the relation between the SoB model interaction parameter U and the SCF interaction parameter χ_P. We have already discussed that for low particle concentrations, the adsorption can be directly calculated from ΔF (Eq. 3). Here ΔF is the result of a balance between the attraction between particle and polymer segments on the one hand and the excluded volume interactions on the other. In the SoB model the adsorption is the result of exactly the same balance of interactions. For the SCF model, it is only above the critical adsorption energy ($\chi_P^{cr} \approx -1$) that ΔF can become negative (see Figure 4) at low polymer densities. In the SoB model we do not take into account the entropy loss of the polymer chain upon contact with a particle and thus the interaction energy can become positive at low polymer densities for $U > 0$. Hence, we can propose that $U = \chi_P - \chi_P^{cr}$ as a first order approximation.

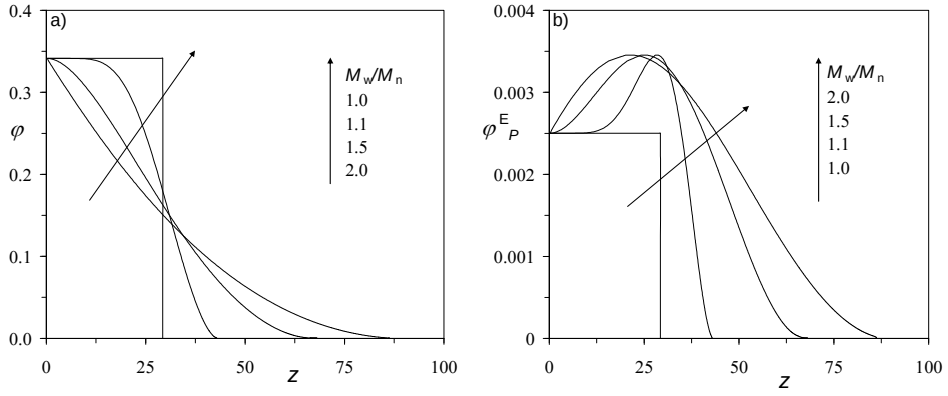

Figure 11. Density profile of a polymer brush (σ = 0.1, N_n = 100) in contact with a particle solution (N_P = 4, U = –1, Φ_P = 0.001) for different polydispersities as indicated, calculated with the SoB model. a) Polymer density (φ). b) Excess particle density ($\varphi_p^E = \varphi_p + \alpha\varphi - \Phi_p$).

In Figure 11, we show results of the SoB model for the specific case of a brush (σ = *0.1*, N_n = 100) in contact with a particle solution (N_P = 4, U = –1, Φ_P = 0.001). In Figure 11a we present the polymer density profile for a number of polydispersities. Comparison with Figure 3 proves that the SoB model reproduces trends of the more detailed SF-SCF model: there is a clear increase in brush height and the change of the profile evolves towards the convex shape with increasing polydispersity indices. In Figure 11b we give the corresponding excess particle density profile that results from the adsorption of the particles inside the brush. Clearly, the differences in the polymer density profiles for the different polydispersities lead to large variations in the particle uptake into the brush. For the monodisperse brush (as described by the SoB model), the polymer density is equal throughout the whole brush, and thus the particle density is also equal throughout the brush. However, for polydisperse brushes there is a maximum in the particle density at a certain height in the brush. The higher the polydispersity, the broader this maximum. It results from the non-monotonic relation between the particle density and the polymer segment density in the brush. For low polymer densities, the adsorption increases because the number of binding sites increases. At higher polymer densities, however, the adsorption levels off due to volume exclusion. Both of these effects have already been discussed in the context of the SF-SCF calculations. Indeed, the single-particle insertion model has a relevance for the adsorption profile.

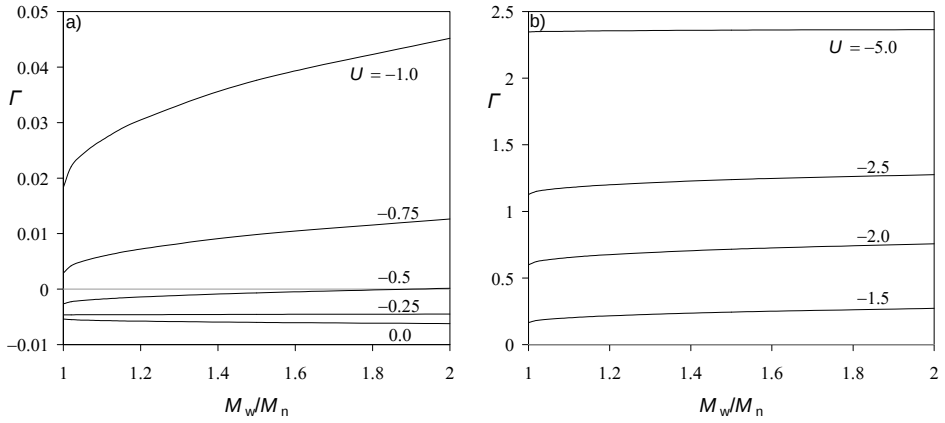

Figure 12. The adsorbed amount (Γ), in number of particles per surface area, of small particles (N_p = 4, Φ_P = 0.001) in a polymer brush (N_n = 100, σ = 0.1) as a function of polydispersity and for a number of different adsorption energies (U) as indicated. Calculated with the stack of boxes model. a) low U values b) high U values.

It is expected that the changes in the density profiles of the particles as a function of polydispersity, will also lead to changes in the total adsorbed amount. In Figure 12 we show the adsorbed amount as a function of the polydispersity index for a number of adsorption energies. The adsorbed amount is defined here as the excess (more than the bulk concentration) number of particles per surface lattice site. For the lowest adsorption energies (Figure 12a, U = 0, U = –0.25), the adsorption is negative. Thus, the density of particles is lower in the brush than it is in bulk solution. This is because of the excluded volume effects of the brush. As a function of polydispersity the negative adsorption remains fairly constant. Interestingly, this is different for the somewhat higher adsorption energies (U = –0.5, –0.75, and –1.0). In the case that U = –0.5, the negative adsorption at low polydispersities turns into positive adsorption at high polydispersities. Admittedly, in the absolute sense there is just a little change in binding, but the switch in sign is of interest from a theoretical point of view. In the case that U = –0.75 or –1.0, the adsorption is low for all polydispersity indices, but the relative changes are large; i.e., over the range M_w/M_n = 1 to 2 the adsorption changes by a factor of respectively 4.4 and 2.5. This increase can be well understood by considering the results of Figure 11. The interaction between brush and particle is so weak that the particles are pushed out of the denser region of the brush. This is very similar to the observations made in Figure 6 where we found that, for a small attraction between brush and particle, attraction is only found in the outer part of the brush where the polymer density is not so high. For the polydisperse brush, the brush density is

spread out over a larger height, thus increasing the volume where we find a net attraction between the brush and the particle, which results in larger adsorbed amounts.

At higher (more negative) values for U (Figure 11b) we find that the polydispersity has only a limited effect on the adsorption. The increase in adsorption between $M_w/M_n = 1$ and 2 changes from about 60% for $U = -1.5$ to only about 1% for $U = -5$. For these high adsorption energies, there is only a very limited effect of the excluded-volume interactions. Therefore, adsorption does not really depend anymore on how the polymer is distributed in the brush, but mainly on the amount of available adsorption sites (hence total amount of polymer in the brush).

In this investigation, we have kept the input parameters of the box model relatively simple. It should be noted that with the same method it is possible to do more system-specific investigations. For example, the effect of solvent quality can be investigated by adding an interaction parameter to describe the interaction between solvent and polymers. The effect of charge can be investigated by using a (salt dependent) interaction parameter to describe repulsion between the particles (as has been done in ref. 8). In addition, it is possible to introduce an interaction parameter that describes interaction between polymer segments. By changing that parameter upon adsorption of a particle to attraction, it is possible that the brush collapses due to particle adsorption.

Conclusions

Using a numerical self-consistent field approach, we have investigated the effects of polydispersity of a polymer brush on its interaction with particles. It is found that with increasing polydispersity it becomes easier for a small particle ($R = 1/(2\sqrt{\sigma})$, size comparable to a globular protein) to penetrate into the brush. When there is a small attraction between the particle and the polymer segments, we find that the particle has a net attraction to the brush only if the brush density is not too high. Since with increasing polydispersity the polymer chains are distributed over a large volume (lowering the average brush density), the particle is able to adsorb in a much larger part of the brush. From this we can conclude that a monodisperse brush is better suited to protect an interface against the adsorption of small particles than a polydisperse one. Still, when we compare this effect of polydispersity to the effect of the brush grafting density on brush particle interactions, we find that the grafting density is the more important parameter for tuning the antifouling properties of a brush.

The effect of polydispersity is very different for a large particle ($R \rightarrow \infty$, comparable to an AFM colloidal probe or bacteria). We find that it is harder to compress a polydisperse brush than a monodisperse one. As the polydisperse brush can distribute its segments over a

larger volume compared to the monodisperse brush, compression of such a brush results in a larger loss of entropy and thus more resistance against compression. This also means that when there is an attraction between the particle and the polymer segments, the most favorable interaction is found for the monodisperse brush. The found differences in this interaction are, however, only small. From the above we predict that a polydisperse brush is more suited to prevent the adsorption of large particles to an interface. This prediction might well be tested with SFA or AFM force measurements if one would be able to prepare a set of polymer brushes differing only in polydispersity.

A complementary model, which involves an extension of the Alexander-de Gennes box-model towards the stacking of boxes, is used to calculate the total adsorbed amount of small particles to a polymer brush as a function of polydispersity. For a weak attraction between polymer chains and particles, the adsorbed amount increases relatively strong with increased polydispersity, although the absolute adsorbed amount remains low. This again leads to the conclusion that monodisperse polymer brushes are better suited to prevent the adsorption of small particles than corresponding polydisperse brushes. For strong attraction between particles and polymer the effect of polydispersity on the adsorbed amount is very limited as the dominating factor in the adsorption becomes the total amount of polymer (the number of adsorption sites) and not the way in which the polymer is distributed.

References

1. Milner, S.T. *Science* **1991,** *251,* 905.
2. Currie, E.P.K.; Norde, W.; Cohen Stuart, M.A. *Adv. Colloid Interface Sci.***2003,** *100-102,* 205.
3. Zhao, B.; Brittain, W.J. *Prog. Polym. Sci.* **2000,** *25,* 677.
4. Advincula, R.C.; Brittain, W.J.; Caster, K.C.; Rühe, J. *Polymer Brushes,* **2004,** Wiley-VHC, Weinheim.
5. Halperin, A.; Leckband, D.E. *C. R. Acad. Sci. Paris* **2000,** *serie IV,* 1171.
6. Mori Y.; Nagaoka S.; Takiuchi H.; Kikuchi T.; Noguchi N.; Tanzawa H.; Noishiki Y. *Trans. Am. Soc. Artif. Intern. Organs* **1982**, *28,* 459.
7. Efremova, N.V.; Sheth, S.R.; Leckband, D.E. *Langmuir* **2001,** *17,* 7628.
8. Currie, E.P.K.; van der Gucht, J.; Borisov, O.V.; Cohen Stuart, M.A. *Pure appl. Chem.* **1999,** *71,* 1227.
9. McPherson, T.; Kidane, A.; Szleifer, I.; Park, K. *Langmuir* **1998**, *14,* 176.
10. Jeon, S.I.; Lee, J.H.; Andrade, J.D.; de Gennes, P.G. *J. Colloid Interface Sci.***1991,** *142,* 149.
11. Szleifer, I.; Carignano, M.A. *Macromelucular rapid communications* **2000,** *21,* 423.
12. Halperin, A.; Fragneto, G.; Schollier, A.; Sferrazza, M. *Langmuir* **2007,** *23,* 10603.
13. Steels, B.M.; Koska, J.; Haynes, C.A. *Journal of chromatography B* **2000,** *743,* 41.
14. de Vos, W.M.; Leermakers, F.A.M. *Polymer,* **2009**, *50,* 305.
15. Schulz, G.V. *Z. Physik. Chem.* **1939**, *B43,* ***25.***
16. Zimm, B.H. *J. Chem. Phys.* **1948,** *16,* 1099.
17. Alexander, S. *J. Phys. (Paris)* **1977,** *38,* 983.
18. de Gennes, P.G. *J. Phys. (Paris)* **1976,** *37,* 1443.
19. S.P.F.M. Roefs, J.M.H.M. Scheutjens; F.A.M. Leermakers *Macromolecules* 1994, *27,* 4810.
20. Wittemann, A.; Ballauff, M. *Phys. Chem. Chem. Phys.* **2006**, *8,* 5269.
21. de Vos, W.M.; Biesheuvel, P.M.; de Keizer, A.; Kleijn, J.M.; Cohen Stuart, M.A. *Langmuir* **2008,** *24,* 6575.

Appendix A. SF-SCF model for polydisperse brushes in 1-gradient and 2-gradient applications

In the present systems we reserve i = 0 to refer to the monomeric solvent (segment type W), while i = 1, 2, …, I refers to polymer chains of different length, where chain i has length N_i. The grafting surface is denoted by the letter S and the particle by P. For a given SCF calculation the positions of S and P are fully specified and fixed. In the coordinate system **r** = (z,r) (see Figure 1) we thus have fixed the volume fractions of both S and P to unity at coordinates where the surface and the particle exists and zero otherwise. The remainder of the sites **r** = **r'** is available for the solvent molecules and the polymers segments.

Basically, in the SCF method the free energy F (more specifically, the Helmholtz energy) is optimized. This free energy can be expressed as a function of the volume fraction and potential profiles. The solvent is the only component that is in equilibrium with a reservoir. For this problem the relevant thermodynamic potential is given by

$$F^{po} = F - n_W \mu_W \qquad [A1]$$

where n_W is the number of solvent molecules and μ_W the corresponding chemical potential, and F^{po} is the partial open free energy. As in the bulk, i.e. far above the brush, the volume fraction of solvent is unity; the chemical potential of the solvent can conveniently be fixed to zero, hence $F^{po} = F$. Now, the free energy of a polydisperse brush is given by

$$\frac{F}{kT} = -\sum_{i>0} \sigma_i \ln Q_i - \sum_{\mathbf{r}'} \varphi(\mathbf{r}) u(\mathbf{r}) - \sum_{\mathbf{r}'} \varphi_W(\mathbf{r}) u_W(\mathbf{r}) + \sum_{\mathbf{r}'} \left[\varphi(\mathbf{r}') \chi \langle \varphi_W(\mathbf{r}') \rangle + \varphi(\mathbf{r}') \chi_P \langle \varphi_P(\mathbf{r}') \rangle \right] \qquad [A2]$$

In this equation, Q_i is the single-chain partition function, which can be computed once the segment potentials are known (i.e. the result of the propagator procedure discussed briefly below). In Eq. A2 the angular brackets imply a local averaging of the quantity over all neighboring lattice sites weighted by the a priori step probabilities to move to such site (which depend on the geometry). Note that there is a constraint imposed on Eq. A2 that at all coordinates

$$\varphi + \varphi_W = 1 \qquad [A3]$$

Optimization of the free energy (Eq. A2) with this constraint leads to the well known self-consistent field equations, which may be expressed by

$$u\left[\varphi(\mathbf{r})\right] \Leftrightarrow \varphi\left[u(\mathbf{r})\right] \qquad [A4]$$

In words this equation says that the segment potentials are found from the volume fraction profiles (left hand side of Eq. A4) and the segment volume fractions are computed from the segment potentials (right hand side of Eq. A4). For the mathematical details we refer to the literature [14, 19]. Here it suffices to mention that for given segment potentials there exists an efficient propagator scheme to compute the single-chain partition functions on the one hand and the volume fraction profile for polydisperse brushes on the other hand. This propagator scheme implements a Markov approximation for the polymer chains (freely jointed chain model). It evaluates the statistical weights of all possible and allowed chain conformations and sums the result properly. In the segment potentials the short-range interactions are parameterized by Flory-Huggins parameters and the use of local volume fractions implies the Bragg-Williams mean-field approximation.

The optimal free energy (Eq. A2), that is the self-consistent field solution or the fixed point of Eq. A4, is found numerically with a precision of at least 7 significant digits. It is clear that this free energy is a function of the distance of the particle from the surface, i.e. $F = F(D)$. The free energy of interaction is found by subtracting the value of the free energy for very large distance of the particle from the surface, i.e.,

$$F^{\text{int}}(D) = F(D) - F(\infty) \qquad \text{[A5]}$$

These calculations can be done for a 2-gradient geometry. In this case the interaction free energy directly represents the work needed to insert the particle to a position D. Alternatively, when we consider a large particle interacting with the brush, we use 1-gradient SCF calculations. Usually, the free energy of interaction is then normalized per unit surface area, i.e. per area of a lattice site. However, in this chapter we have multiplied this by the cross-section area of the small particle πR^2 for ease of comparison of the 1-gradient SCF with the 2-gradient SCF calculations.

Appendix B. A quasi analytical box model for adsorption

A stack-of-boxes theory has been used to describe the adsorption of particles in a polydisperse brush. This theory requires as input a description of each individual box. The sub-model that gives this information is discussed here in a condensed form, in *chapter 4* the model is described in more detail. In this sub-model we do not have to worry about polydispersity, since in each box all chains are equally long, having N segments. The grafting density is σ. We assume athermal interactions except for the interaction parameter between the particles and the polymer. For each contact (and exchange with the a solvent molecule) this interaction energy is given by U (in units of k_BT). Here we assume, according to the quasi-chemical approach, that a particle is either fully adsorbed (all

particle segments in contact with a polymer segment) or that the particle is not adsorbed (no contact with polymer segments). The particles adsorb onto the polymer chains in a Langmuir-type way. Hence, the maximum adsorption is linked to the total amount of polymer per unit area. We do not take into account any adsorption of particles on the surface. Besides the adsorption energy U, the grafting density σ and the chain length N, the volume fraction of particles in the bulk Φ_p is an input quantity. Typically, in a Langmuir model one assumes that the solvent molecule is of the same size as the adsorbing species. Here we take a slightly more general model and allow for a size ratio given by N_p (which is the number of times that the particle is larger than the solvent). The outcome of the calculations is the brush height H, the amount of particle segments per unit area θ and, related to this, the adsorption Γ. There are two incompressibility constraints. In the bulk the volume fraction of particles and solvent must add up to unity:

$$\Phi_p + \Phi_s = 1 \qquad \text{[B1]}$$

and in the brush we have

$$\frac{\theta}{H} + \varphi_s + \varphi = 1 \qquad \text{[B2]}$$

where $\varphi = \sigma N / H$ is the volume fraction of polymer in the box.

The starting point for the box model is the free energy G per chain (in units of k_BT).

$$G = F^{elastic} + F^{adsorption} + F^{mixing} \qquad \text{[B3]}$$

The first term in Eq. B3 gives the dimensionless free energy of stretching of the polymer chains in the brush. Here we use the Gaussian chain model and write

$$F^{elastic} = \frac{3}{2}\frac{H^2}{N} \qquad \text{[B4]}$$

The second contribution to the free energy stems from the adsorption process. Here we introduce the fraction α of polymer covered by the particles. The fraction of polymer in contact with the solvent is thus given by $1-\alpha$. The total dimensionless adsorption energy per polymer chain for a given fractional coverage is given by

$$F^{adsorption} = \alpha UN \qquad \text{[B5]}$$

Hence, the maximum adsorption energy is found for $\alpha = 1$ and this is limited by the total amount of polymer in the brush.

In the box model we need to account for the dimensionless mixing entropy. In this model we have two contributions, one related to the adsorption process and the other related to the exchange of particles an solvent with the bulk.

$$F^{mixing} = N\left[\frac{\alpha}{N_p}\ln\frac{\alpha}{\varphi_p} + (1-\alpha)\ln\frac{1-\alpha}{1-\varphi_p}\right] + \frac{H}{\sigma}\left[\frac{\varphi_p}{N_p}\ln\frac{\varphi_p}{\Phi_p} + \varphi_s\ln\frac{\varphi_s}{\Phi_s}\right] \qquad \text{[B6]}$$

The first part of this equation describes the mixing entropy along the polymer chain, it is multiplied by N to give the free energy per polymer chain. The second term describes the exchange of the solvent and particles in bulk, with solvent and free (unadsorbed) particles in the polymer brush. The free particle volume fraction in the brush is given by φ_p This second term is multiplied by H/σ, which gives the volume of the brush per polymer chain.

Optimization of the total free energy (Eq. B3) with respect α gives a Langmuir-type equation:

$$\frac{\alpha}{(1-\alpha)^{N_p}} = \frac{\varphi_p}{\left(1-\varphi_p\right)^{N_p}} e^{-UN_p} \qquad \text{[B7]}$$

which specifies the relation between α and φ_p. Similarly, there exists a relation between bulk volume fractions and corresponding quantities in the brush for those components that are free to exchange. Here the size ratio between solvent and particles appears as well

$$\frac{\varphi_p}{\Phi_p} = \left(\frac{\varphi_s}{\Phi_s}\right)^{N_p} \qquad \text{[B8]}$$

Eq. B8 thus shows that the volume fractions of φ_p and φ_s are coupled.

Next, we need to optimize the free energy G with respect to H. We do this numerically, in short as follows. For a given value of H, we know the volume fraction of polymer φ. Using the compressibility relations (B1,B2), we are left with two equations (B7 and B8) with two unknowns, namely α and φ_s. After solving these equations, we can evaluate G. We continue changing H until G is optimized. This is routinely done up to 5 significant digits.

The excess particle density is found by

$$\varphi_p^E = \varphi_p + \alpha\varphi - \Phi_p \qquad \text{[B9]}$$

while the excess adsorbed amount (in particles per surface area) is found by

$$\Gamma = \frac{H\varphi_p^E}{N_p} \qquad \text{[B10]}$$

Part 4: Sacrificial Layers

Chapter 10

Thin polymer films as sacrificial layers for easier cleaning.

Abstract

We propose a new approach for the removal of fouling agents from an interface. The interface is pre-coated with a polymer layer of a few nanometers thick which can be removed by a simple trigger such as a change in pH or salt concentration. When fouling agents adsorb on the interface, they can be removed by simply desorbing (sacrificing) the polymer coating. We show a proof of principle of this concept by investigating two different types of sacrificial layers. The first system consists of a silica interface that is pre-coated with a polyelectrolyte multilayer consisting of poly(allylamine) hydrochloride (PAH) and poly(acrylic acid) PAA. The top layer of the polyelectrolyte multilayer is the positively charged PAH and on top of that silica particles are adsorbed. We investigated the release of silica particles resulting from a pH drop (leading to desorption of the multilayer), as a function of the number of polyelectrolyte layers in the multilayer. Four layers are already enough to significantly enhance the desorption of the silica particles (70% removal). With fourteen layers (total adsorbed amount of polymer approximately 6 mg/m^2) the silica particles are completely removed.

The second system consists of a weak poly(acrylic acid) brush (PAA), coated with an extra layer of PAA (the PAA chains are connected to a small polystyrene (PS) block). At low pH, the polyelectrolytes are uncharged, and the double polyelectrolyte layer is stable. However, when the pH is increased, the polyelectrolytes become charged and the extra polyelectrolyte layer is removed, including any attached fouling agents. For this system, we show proof of principle of the sacrificial layer approach, by measuring the hydrodynamic force, necessary to remove PS particles (radius 3 μm) from a PAA brush. We show that the hydrodynamic force for removal is two orders of magnitude lower for the sacrificial layer system (PAA brush plus extra layer of PS-PAA), than for the PAA brush alone.

A manuscript based on this chapter is in preparation.

Introduction

Over the years much research has been dedicated to making cleaning easier. This has brought forward a number of very different approaches. The oldest approach is to use surfactants [1,2], amphiphilic molecules that can significantly reduce the attractive interaction between a surface and a fouling agent. Another approach is to use self-cleaning surfaces such as ultra-hydrophobic coatings [3,4]. These coatings are so hydrophobic that water will form almost spherical droplets that "roll off" the (tilted) surface taking with it any dust or dirt particles. A third approach is to prevent the fouling of surfaces by using antifouling layers. The polymer brush [5,6] is the best known example of such a layer, where the steric hindrance from the polymers in the brush prevents fouling agents such as proteins to reach the interface [5,6].

What all these approaches have in common is that, although they have been proven to work very well for a large number of fouling agents, non of them is universally applicable. This means that for every system there are fouling agents for which they are unsuitable. Surfactants work extremely well to remove hydrophobic fouling agents but are much less effective in removing hydrophilic objects, especially from hydrophilic surfaces. For example, the polymer poly(ethylene oxide) (PEO) adsorbs cooperatively with the surfactant SDS to a silica surface [7]; nonionic surfactants can remove PEO from a silica surface, but this happens only if the PEO chain is short [8]. The ultrahydrophobic surfaces work well for the removal of larger particles, but will never work for hydrophobic particles in the nanometer range, or for protein molecules, because there objects are smaller than the roughness that the ultra-hydrophobicity depends on. Brushes, often made of PEO chains, are very suited to prevent the adsorption of proteins but silica particles are found to adsorb in large adsorbed amounts to these brushes [9].

In this chapter we present a new approach to cleaning surfaces: the use of a sacrificial layer of a few nanometers thick. A surface can be pre-coated with a thin polymer layer that can be desorbed from the surface by a simple trigger, such as a change in pH or in salt concentration. Any fouling agent that is adsorbed to the interface can then be removed by desorbing (or sacrificing) the polymer layer. This approach has a great advantage: as no direct contact between the interface and the fouling agent needs to be broken, it has the potential to work for any fouling agent. Limitations, however, are that a specific trigger is necessary to remove the sacrificial layer, and that after every cleaning step, the surface has to be re-coated. On a macroscopic scale this kind of approach is already commonly used in, for example, consumer electronics. View screens in mobile phones etc. are protected by a thin sheet of plastic called a tear-off. When the consumer buys the product, any grease or dust on the view screen can simply be removed by peeling of the tear-off. However, as far

as we know this concept has never been studied before using molecular ‘tear off’ layers that are only a few nanometers thick.

Here we consider two systems that would both be well suited as sacrificial layers. The first is a system of polyelectrolyte multilayers [10,11]. By subsequent adsorption of two oppositely charged polyelectrolytes one forms a dense polymer layer at the surface. The thickness of the layer can be tuned simply by the number of adsorption steps, while by choosing the right polyelectrolytes one can provide a trigger such as a change in pH or salt concentration that leads to the destruction of the layer [12]. An extra benefit might be that the polyelectrolytes that are released into solution upon destruction of the layer could well act as so-called anti-redeposition agents: by adsorbing to the released fouling agents they might prevent possible re-adsorption of the fouling agents. We schematically show this approach in Figure 1. We use polyelectrolyte multilayers in combination with silica particles to give a “proof of principle” of the use of such multilayers as sacrificial layers.

The second system that we investigate consists of a weak polyelectrolyte brush that has been coated with an extra layer of the same weak polyelectrolyte. The polyelectrolyte in the coating is connected to a short hydrophobic block because of the preparation method. This system is stable at a pH at which the polyelectrolyte is uncharged. Changing the pH so that the polyelectrolyte becomes charged, leads to the removal of the extra layer, including any attached fouling agents. This approach is schematically shown in Figure 2. To investigate how well this system is suited to remove fouling agents, we measure the hydrodynamic force necessary to remove 50% of previously attached PS particles (radius 3 μm). This so-called critical removal force is a measure for the adhesive force between the particle and the interface [13,14].

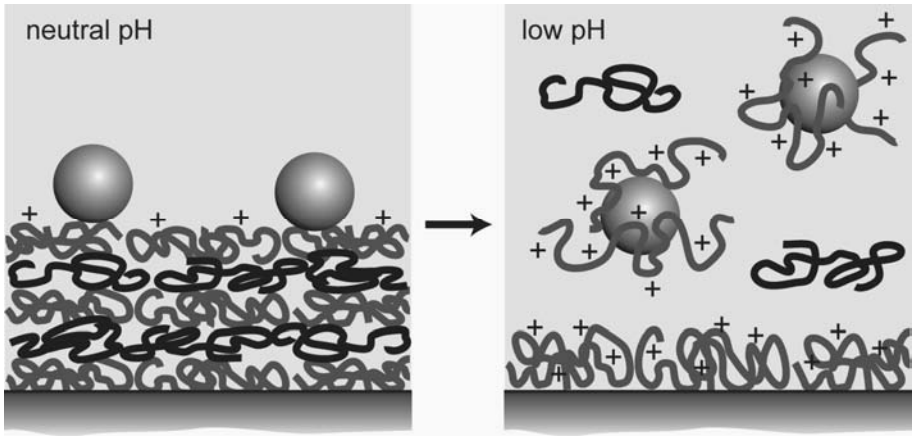

Figure 1. Schematic depiction of the potential application of a polyelectrolyte multilayer as a sacrificial layer. Fouling agents are adsorbed to the multilayer but upon change of the pH, the layer desorbs, taking with it the adsorbed fouling agents. Released polyelectrolytes cover the particles and prevent re-adsorption of the fouling agents.

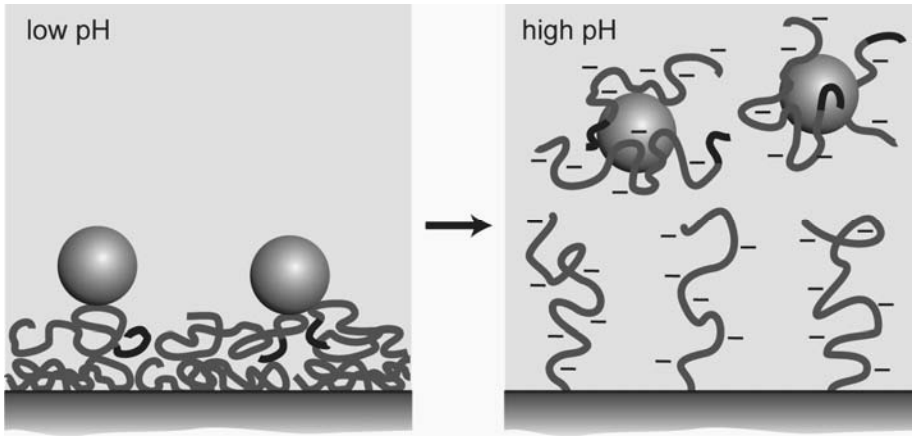

Figure 2. Schematic representation of the approach to use as a sacrificial layer, a weak polyelectrolyte brush (anionic in this Figure) coated with an extra layer of the same weak polyelectrolyte. At low pH the polymers are uncharged and the layer is stable, at high pH the polyelectrolytes are charged and the extra polyelectrolyte layer, including adsorbed fouling agents, desorb from the interface.

Materials and methods

Polyelectrolyte multilayers

The adsorption and desorption of polymers and particles was followed with fixed-angle optical reflectometry using an impinging jet flow-cell. A detailed description of the reflectometer setup is provided by Dijt *et al* [15]. It contains a He-Ne laser (monochromatic light, λ=632.8 nm) with linearly polarized light. Change in polarization is measured by simultaneously detecting the parallel (R_p) and the perpendicular (R_s) reflectance and dividing R_p by R_s to give signal S. Before each measurement, the system was calibrated by flushing with solvent to get a stable baseline (S_0) signal. The measurement is started by introducing a polymer solution into the cell. The change in signal is measured ($\Delta S = S - S_0$) with a sample time of 2 s. The adsorbed amount (Γ) can be calculated from: $\Gamma = Q(\Delta S/S_0)$. Here Q is a sensitivity factor, which depends on the angle of incidence of the laser (θ), the refractive indices (n), the thicknesses (d) of the layers on the silicon wafer, and the refractive index increment (dn/dc) of the adsorbate. To calculate the Q-factor the following values where used: $\theta = 71^\circ$, $n_{silica} = 1.46$, $\tilde{n}_{silicon,} = (3.85, 0.02)$, $n_{H2O} = 1.33$, $dn/dc_{PAH} = 0.21$, $dn/dc_{PAA} = 0.16$, $d_{silica} = 50$ nm, $d_{adsorbed\ layer} = 5$ nm. This leads to somewhat different Q-factors for the different polymers. For the sake of simplicity we have used the average of these Q-factors (30 mg/m^2) for all our experiments. The silica substrates were prepared in the following way. First, a silicon wafer was put into an oven at 1000°C for one hour to create on top of the silicon, a silica layer of approximately 50 nm thick. The wafer was cut into strips (4 cm x 1 cm), rinsed with alcohol and water, and further cleaned using a plasma-cleaner (10 minutes). The surfaces were carefully stored in water until use. Poly(allylamine) hydrochloride (PAH_{748}), 70 kg/mol, and Ludox particles (Ludox SM, radius approximately 9 nm) were ordered from Sigma-Aldrich. Poly(acrylic acid) (PAA_{163}) 11.7 kg/mol, $M_w/M_n = 1.07$ was ordered from Polymer Source Inc. Montreal/Canada. All water used was demineralized using a Barnstead Easypure UV and had a typical resistance of 18.3 MΩ/cm.

A polyelectrolyte layer on a polyelectrolyte brush

The second sacrificial layer system consists of a PAA brush, coated with an extra layer of PS-PAA. These layers can be produced by using Langmuir-Schaeffer transfer. This technique was first used by Currie *et al* [16] to produce PAA brushes. A short summary of the technique is given here. First a PS_{40}-PAA_{270} solution (60% 1,4-dioxane, 40% toluene) is carefully applied to the air-water interface of a Langmuir trough using a syringe. The pH in the water phase is slightly acidic (pH 4) so that the PAA is mostly uncharged. After

evaporation of the solvent, the surface area of the trough is changed to get the desired grafting density (here σ = 0.2 nm^{-2}). A PS surface (made according to the procedure of Maas *et al* [17]) is then horizontally dipped through the air-water interface, transferring the PS-PAA to the PS interface. It was shown by de Vos *et al* [18 (chapter 6)] that for Langmuir-Schaeffer transfer of PS-PAA to a PS surface the transfer ratio is 1, so that the grafting density of PS-PAA at the air-water interface is equal to the grafting density at the solid interface after transfer. After drying, the surface is put in an oven at 100°C for 5 minutes to facilitate mixing (interdiffusion) of the chains of the PS surface and the PS block of the diblock copolymer. To produce another layer of PS-PAA on top of the PAA brush, we simply repeat the dipping procedure, without the heating step.

Flow cell

To test the effect of the sacrificial layers (system 2), we use a flow-cell [13, 14] to determine a measure for the adhesive forces between a fouling agent (Polystyrene (PS) particles, radius 3um) and a surface coated with and without the sacrificial layer. A schematic representation of such a flow-cell setup is shown in Figure 3. In the flow-cell, solution flows between two surfaces. The surfaces have been pretreated with a particle suspension containing PS particles with a radius of 3 μm. These particles can be observed using an optical microscope. The flowing of solvent exerts a certain force on these particles, that depends on the particle size and the solvent flow speed. The hydrodynamic force (F) acting on a sphere on a flat surface because of simple shear flow is given by [19]

$$F = 10.2\pi R^2\tau \quad \text{(N)} \qquad \tau = \frac{6\eta Q}{rh^2} \quad \text{(N/m}^2\text{)} \qquad [1]$$

Here R is the particle radius (m), and τ the shear stress at the cell wall; Q is the flow rate (m^3/s), h is the separation distance between the surfaces (m), r is the width of the plates (m), and η the viscosity of the solution (Ns/m^2). During a measurement, the force on the particles is gradually increased by either increasing the flow rate Q, or decreasing the separation distance h. After each increase in force, the number of particles still attached to the interface is determined by use of the optical microscope. The force necessary to detach 50% of the particles that were originally attached is used as a measure for the adhesive forces between particles and interface.

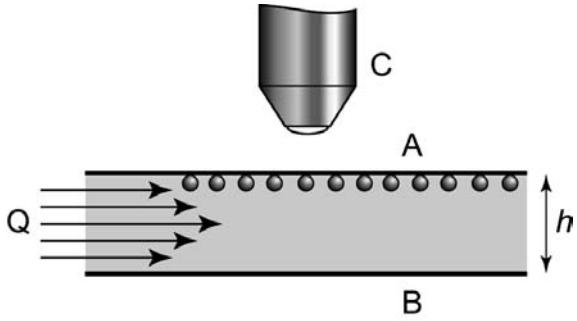

Figure 3. Schematic representation of the flow cell setup. A. Glass surface coated with the PAA brush or sacrificial layer. B. Silica surface. C. Optical microscope. h. Distance between surfaces, tuneable between 0.5 mm and 2.8 mm. Q. Flow rate. The spheres represent the PS particles (R = 3μm), not drawn to scale.

Results and discussion

System 1: polyelectrolyte multilayers

To study the adsorption and desorption of the sacrificial layer and the fouling agents, we use optical fixed angle reflectometry. With this technique we can measure in real time the adsorbed amount, while applying different solutions to the interface. In Figure 4a we show a typical reflectometer experiment, in which we explore the properties of the system without the sacrificial layer. The measurements starts with a baseline, in which a pH 6, 1mM $NaNO_3$ solvent solution is applied to the interface. The adsorption begins (+) when we apply a solution containing the cationic polymer (0.1 g/l PAH, pH 6, 1mM $NaNO_3$). When a stable adsorption maximum is reached, we switch back to the solvent solution (S). Then we apply a solution containing our model fouling agent (L, 0.1 g/l Ludox, pH 6, 1mM $NaNO_3$), the model fouling agents, so-called Ludox particles, are tiny (radius ~ 9 nm) spherical silica particles. As can be seen, these particles lead to a large increase in the signal. When rinsed with a pH 1 solution the adsorbed amount decreases but an adsorption remains of about 1.5 mg/m^2. Here we note that the increase in adsorbed amount that we observe when applying solvent (S) for the second time is not due to real adsorption, it is an optical effect that is the result of large changes in the pH and salt concentration.

For the polyelectrolyte multilayer we use the combination of poly(allylamine) (PAH_{748}) and poly(acrylic acid) (PAA_{163}). PAH is a strongly charged cationic polyelectrolyte, while PAA is a weakly charged anionic polyelectrolyte. This combination of polyelectrolytes has been studied by Shiratori *et al* [20] and at pH 6 the resulting multilayer is known to show a linear growth pattern (thus every adsorption step gives the same increase of the layer

thickness). Such a linear growth is associated with a polyelectrolyte multilayer of which the polymer chains are not mobile [11]. In Figure 4b we show the growth and the destruction of this polyelectrolyte multilayer. Here we again start with a baseline (solvent solution), but then subsequently adsorb the cationic polyelectrolyte (+) and the anionic polyelectrolyte (–). As expected the multilayer formation follows a typical layer-by-layer deposition, in which each adsorption step leads to a similar adsorbed amount. Still we see that after a number of adsorption steps the adsorbed amount does increase somewhat per adsorption step, which is attributed to an increase in the surface roughness. Upon exposing the surface to a solution with a pH of 1, the layer desorbs almost completely within a few seconds. After the solution is rinsed with solvent (S), we see that a small adsorbed amount remains, which was expected, as we know that the cationic polyelectrolyte PAH remains adsorbed to silica even at pH 1 (Figure 4a). Still, a part of the PAH has desorbed, which we can show by exposing the surface again to a PAH solution. As can be seen, this leads to another adsorption that reaches a plateau value exactly at the same adsorbed amount that was obtained for the first adsorption step.

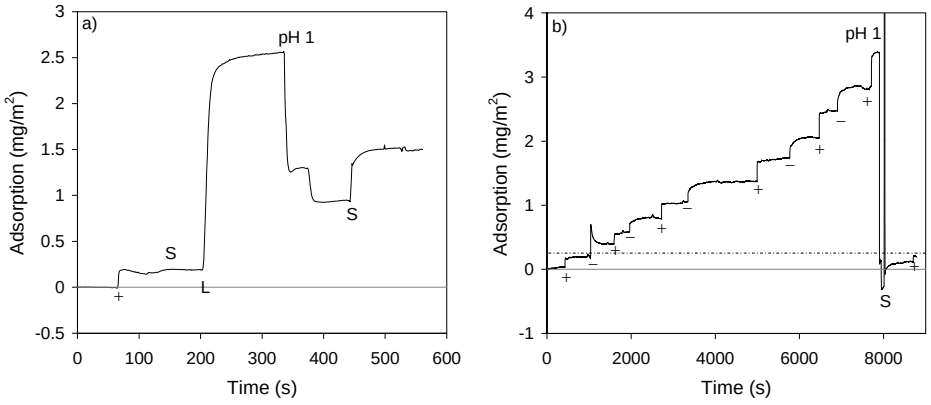

Figure 4. Adsorption and desorption as studied by optical reflectometry of a) PAH (+, 0.1 g/l, pH 6, 1mM $NaNO_3$) and Ludox particles (0.1 g/l, pH 6, 1mM $NaNO_3$) b) PAH (+) and PAA (–, PAA, pH 6, 1mM $NaNO_3$). S denotes the exposure of the surface to the solvent solution (pH 6, 1mM $NaNO_3$), and pH 1 denotes exposure to a 0.1 HNO_3 solution.

Thus, subsequent adsorption of PAH and PAA provides us with a polyelectrolyte multilayer that can be easily desorbed by changing to a pH of 1. Also we have a fouling agent for which we know that at pH 1 a significant adsorption to the surface remains. In Figure 5a we combine the polyelectrolyte multilayer with the fouling agent to investigate the effect of the multilayer as a sacrificial layer. As in Figure 4b, we build up the polyelectrolyte multilayer by subsequent adsorption of PAH (+) and PAA (–). We end with

a layer of PAH and on top of that adsorb the Ludox particles (L). Note that the adsorbed amount of Ludox particles is slightly larger than in Figure 4a, probably because of the increased roughness of the layer. When we now desorb the multilayer by applying a pH 1 solution to the surface, the multilayer including all the Ludox particles completely desorbs. After exposure to a PAH solution, the adsorbed amount indeed returns to exactly the adsorbed amount that was observed after the first PAH adsorption step (the dotted line). Thus, Figure 5a provides us with direct evidence that the sacrificial layer method works. Without the polyelectrolyte multilayer, there is a large residual adsorption of Ludox particles after rinsing with pH 1, however, with the sacrificial polyelectrolyte multilayer the residual adsorption is reduced to zero.

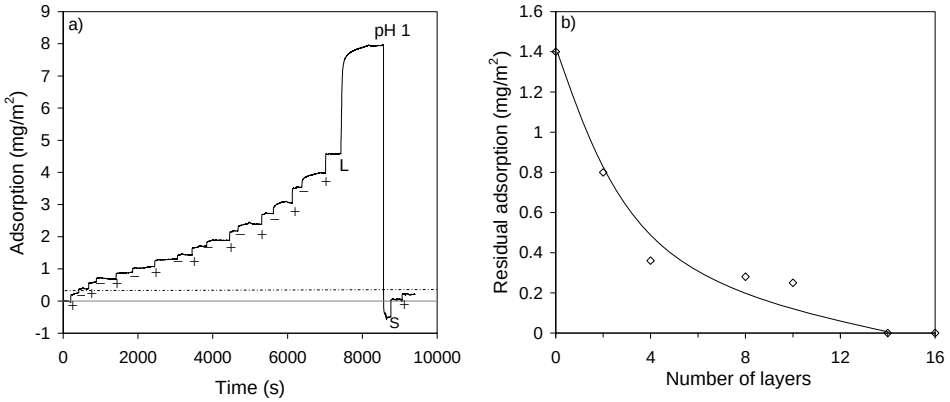

Figure 5. a) The adsorption and desorption of PAH (+), PAA (–) and Ludox particles (L) (all 0.1 g/l, pH 6, 1mM $NaNO_3$). S denotes the exposure of the surface to the solvent solution (pH 6, 1mM $NaNO_3$), and pH 1 denotes exposure to a 0.1 HNO_3 solution. b) The residual adsorption of Ludox particles after desorption of the sacrificial polyelectrolyte multilayer as a function of the number of layers (PAA and PAH).

In Figure 5b we show how the residual adsorption of the Ludox particles depends on the number of PAH and PAA layers in the polyelectrolyte multilayer. We find that a minimum of 14 layers (thus 7 PAH and 7 PAA layers) is necessary to achieve a residual adsorption of 0. Still only a few layers (4) is already enough to significantly reduce the residual adsorption (approximately 70% reduction).

What is the reason that a substantial thickness of the polyelectrolyte multilayer is necessary to achieve complete removal of the fouling particles? One reason might be that the polymers in the polyelectrolyte multilayers mix to a certain extent. As such, there could be a small amount of polymer chains that bridge the complete layer, thus are connected to the silica surface and to the silica particles. The larger the number of layers, the smaller the

number of bridging chains will be. Another possibility is that the residual adsorption stems from redeposition. Upon release of the polymer layer including the silica particles, it is possible that the particle diffuses back to the interface and re-adsorbs. With a thicker polymer layer, there is more material in the layer that can act as an anti-redeposition agent, the released PAH can cover the silica particle so that the particle becomes positively charged, preventing the adsorption to the also positively charged PAH covered silica surface. Understanding the effects resulting in the residual adsorption is important, as this might lead to the design of sacrificial layers that provide complete cleaning with even lower adsorbed amounts of polymer.

As discussed above, a polyelectrolyte multilayer consisting of PAA and PAH shows (at pH 6 and low salt) a linear growth pattern. Such a growth pattern is always associated with a low mobility of chains in the polyelectrolyte multilayer. A different growth pattern can be achieved by using different polyelectrolytes. Kovačević *et al* [21] showed that with the combination of PAA and Poly(N-methyl-2-vinyl pyridinium) (P2MVP), the growth pattern is exponential. Thus, with every adsorption step, the increase in layer thickness is approximately twice that of the previous adsorption step. Such exponential growth is attributed to a high mobility of the polyelectrolyte in the multilayer [11]. The advantage of such growth is that a thick multilayer can be achieved with only a few adsorption steps. Here, we test if the multilayer consisting of P2MVP and PAA is also suitable for use as a sacrificial layer. Just as the PAH-PAA system, this system can be desorbed by changing to a pH of 1, while at that pH P2MVP will not desorb from a silica surface, or from silica particles (experiments not shown). In Figure 6 we show the results of a reflectometry experiment in which we test the P2MVP and PAA multilayer as a sacrificial layer. We clearly see the exponential growth: with every adsorption step, the adsorbed amount is much larger than the previous adsorption step. Thus, much less adsorption steps are necessary to get a thick polyelectrolyte multilayer. However, as we can see in Figure 6, this type of polyelectrolyte multilayer does not behave as a good sacrificial layer. The adsorption of Ludox particles to the layer is very large (20 mg/m^2) compared to the Ludox adsorption for the PAH-PAA system (3.5 mg/m^2). Even more important is, that when we switch to a pH of 1, a large residual adsorbed amount remains. We believe that because of the high mobility of polyelectrolyte chains in this multilayer, the silica particles can penetrate the polyelectrolyte multilayer, resulting in the large adsorbed amount. Upon changing pH, the negative polymer (PAA) is released from the layer, but a network consisting of P2MVP and silica particles remains attached to the surface. Clearly, polyelectrolyte multilayers that allow mixing with the fouling agent are unsuitable to function as a sacrificial layer.

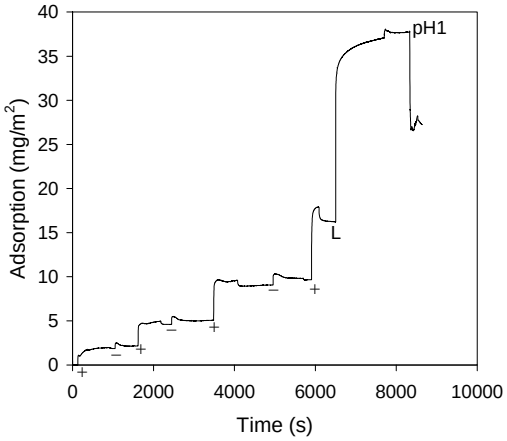

Figure 6. a) The adsorption and desorption of P2MVP (+), PAA (–) and Ludox particles (L) (all 0.1 g/l, pH 6, 1mM $NaNO_3$). S denotes the exposure of the surface to the solvent solution (pH 6, 1mM $NaNO_3$), and pH 1 denotes exposure to a 0.1 M HNO_3 solution.

System 2: a polyelectrolyte brush coated with a polyelectrolyte layer

A second system, that we believe could be used as a sacrificial layer consists of a PAA brush coated with a layer of PS-PAA as schematically depicted in Figure 2. To show that this system can indeed function as a sacrificial layer, we have investigated the dry layer thicknesses of the proposed system. In this way we can determine if, after the right trigger is given, the PS-PAA layer is indeed removed from the surface. The layer thickness is investigated using ellipsometry and the results are shown in Figure 6.

The dry layer thickness of the PAA brush (N = 270, σ = 0.2 nm^{-2}) is approximately 8 nm. By horizontal dipping (Langmuir-Schaeffer transfer) of that surface through an air-water interface that is covered with a layer of PS_{40}-PAA_{270}, the extra layer of PS-PAA is added. This transfer leads to an increase in thickness of again approximately 8 nm, indicating complete transfer of the PS-PAA layer. Rinsing the layer with a 1 mM HNO_3 (pH 3) solution does not lead to a significant decrease in the layer thickness. In contrast, rinsing with a 0.1 mM NaOH (pH 10) solution, does lead to a decrease of the layer thickness of approximately 8 nm, showing that the second layer of PS-PAA is removed from the surface. Clearly, the layer is stable as long as the PAA remains uncharged (pH 3), however when the pH increases and PAA becomes charged then the second PS-PAA layer is removed from the surface. Thus, we have a layer that can be removed by a simple pH trigger, exactly what we want for a sacrificial layer.

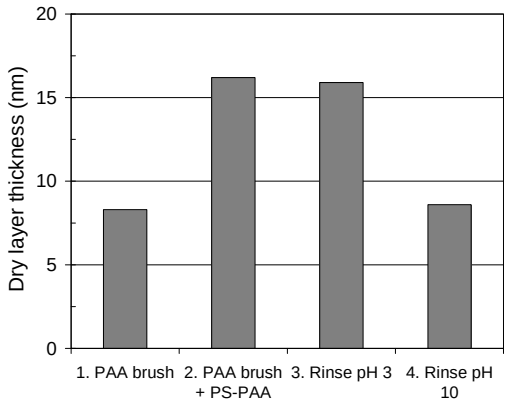

Figure 6. The dry layer thickness (nm) as measured by ellipsometry of a layer on a PS surface: 1. PAA brush (N = 270, σ = 0.2 nm^{-2}) 2. as 1 but with extra layer of PS_{40}-PAA_{270} (σ = 0.2 nm^{-2}) 3. as 2, after rinsing in pH 3 (1 mM HNO_3) solution. 4. as in 3, after rinsing in a pH 10 (0.1 mM NaOH) solution.

To investigate if this sacrificial layer assists in the removal of fouling agents, we have measured for this and other surfaces the so called critical removal force (CRF) for polystyrene particles (radius 3 μm). We define the CRF as the hydrodynamic force necessary to detach 50% of the originally attached particles from the surface. The CRF is a measure for the adhesive force between the surface and the particles [13,14]. By comparing the CRF of the PS particles to a PAA brush with and without the extra layer of PS-PAA, we can investigate the effect of the sacrificial layer. In a typical experiment to determine the CRF, a solution containing the PS particles (10 g/l, pH 3) is applied to an interface for 20 minutes. Then, the attached particles are exposed to a laminar flow. During the experiment the flow speed is gradually increased and after each increase we determine the number of particles still attached to the interface. Typically, there is a rather sharp decrease in the number of particles in a small range of forces. In Figure 8a we show the results of a typical measurement. In this case the PS particles attached were adsorbed to a PAA brush-coated surface and exposed to a laminar flow of a solution containing surfactants (SDS, 1 g/l, pH 3). As can be seen, with increasing force, the number of particles on the surface decreases and the CRF is determined to be approximately $2*10^{-11}$ N. In 8b we compare the critical removal force for a number of systems. For PS particles attached to a PAA brush (one layer) at pH 10, the particles are so firmly attached that the CRF is so high that we cannot measure it with this setup. The same holds for the system were the extra layer of polyelectrolyte is added on top of the PAA brush at pH 3. Hence, we know that for these systems the CRF is at least equal to the maximum force that can be reached with this setup,

namely $2*10^{-9}$ N. However, if we change the pH to pH 10 for the sacrificial layer system, the CRF shows an enormous decrease. This effect must be related to the sacrificial nature of the added polyelectrolyte layer. We find that the CRF decreases at least 2 orders of magnitude. The sacrificial layer even works for this system just as well as the addition of surfactants to only the PAA brush.

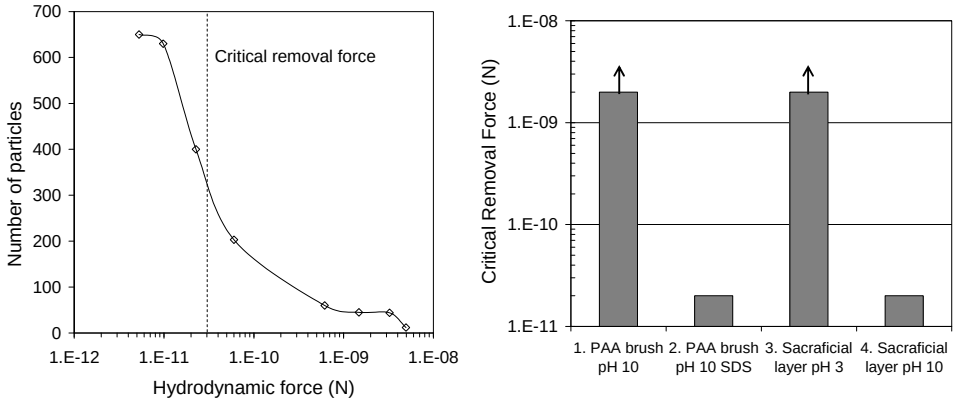

Figure 8a. Determination of the critical removal force using the flow cell approach. The number of particles (PS, radius 3 μm) still attached to an interface is shown as a function of force exerted on the particle by a laminar flow (pH 10, 25 mM SDS). The critical removal force is the hydrodynamic force at which 50% of the particles originally attached to the interface has been detached. b) An overview of critical removal forces for PS particles (radius 3 μm) as measured for a number of systems as indicated. 1. PAA brush (N = 270, σ = 0.2 nm^{-2}) at pH 10 (0.1 mM NaOH). 2. As 1, with SDS (25 mM). 3. PAA brush (N = 270, σ = 0.2 nm^{-2}), covered with a layer of $PS_{40}PAA_{270}$ (σ = 0.2 nm^{-2}) at pH 3 (1 mM HNO_3). 4. As in 3, at pH 10 (0.1 mM NaOH). Arrows indicate that CRF is larger than can be reached with this setup.

Conclusions

In this chapter we present a novel approach for cleaning surfaces that we call the sacrificial layer approach. Two different systems are investigated as sacrificial layers. The first system features as sacrificial layer, a polyelectrolyte multilayer consisting of PAH and PAA. When such a layer is built up on a positively charged surface (a silica surface with adsorbed PAH) with a fouling agent being adsorbed on top of the layer, the fouling agent can simply be removed by desorbing (sacrificing) the polyelectrolyte multilayer. For complete removal of the fouling agent a thickness of at least 14 layers is found to be necessary, although 4 layers already lead to a significant removal (approximately 70%). A polyelectrolyte multilayer built from P2MVP and PAA is found not to be effective as a sacrificial layer. The reason is probably that this multilayer has a high mobility of polyelectrolyte chains that allows mixing with the fouling agents.

A different system investigated as a sacrificial layer, is a PAA brush coated with a layer of PS-PAA. At low pH this layer is stable, but at high pH the increased negative charge of the PAA leads to desorption of the PS-PAA layer, including any attached fouling agents. With the sacrificial PS-PAA layer, the hydrodynamic force necessary to detach a PS particles from the PAA brush is two orders of magnitude lower than without the sacrificial layer.

Thus, for two different systems we have shown that the sacrificial layer approach is effective. Additional research will be necessary to investigate if the sacrificial layer may be universally applicable. In addition, there might be many other systems very suitable as sacrificial layers.

References

1. Holmberg, K.; Jönsson, B.; Kronberg, B.; Lindman, B. *Surfactants and polymers in aqueous solution* **2002,** Wiley, West Sussex.
2. Farn, R. J. *Chemistry and technology of surfactants* **2006**, Wiley-Blackwell, Oxford.
3. Fürstner, R.; Barthlott, W.; Neinhuis, C.; Walzel, P. *Langmuir* **2005,** *21,* 956.
4. Parkin, I.P.; Palgrave, R.G. *J. Mater. Chem.* **2005**, 15, 1689.
5. Currie, E.P.K.; Norde, W.; Cohen Stuart, M.A. *Adv. Colloid Interface Sci.***2003,** *100-102,* 205.
6. Halperin, A. *Langmuir* **1999,** *15,* 2525.
7. Cosgrove, T.; Mears, S.J.; Obey, T.; Thompson, L.; Wesley, R.D. *Coll. Surf. A* **1999,** *149,* 329.
8. Postmus, B.R.; Leermakers, F.A.M.; Koopal, L.K.; Cohen Stuart, M.A. *Langmuir* **2007,** *23,* 5532.
9. Gage, R.A.; Currie, E.P.K.; Cohen Stuart, M.A. *Macromolecules* **2001,** *34,* 5078.
10. Decher, G. *Science* **1997,** *277,* 1232.
11. von Klitzing, R. *Phys. Chem. Chem. Phys.* **2006,** *8,* 5012.
12. Lynn, D.M. *Adv. Mater*. **2007,** *19,* 4118.
13. Janex, M.L.; Chaplain, V.; Counord, J.L.; Audebert, R. *Colloid Polym. Sci.* **1997,** *275,* 352.
14. Freitas, A.M.; Sharma, M.M. *Langmuir* **1999,** *15,* 2466.
15. Dijt, J.C.; Cohen Stuart, M.A.; Hofman, J.E.; Fleer, G.J. *Colloids and Surfaces* **1990,** *51,* 141.
16. Currie, E.P.K.; Sieval, A.B.; Avena, M.; Zuilhof, H.; Sudhölter, E.J.R.; Cohen Stuart, M.A. *Langmuir* **1999,** *15,* 7116.
17. Maas, J.H.; Cohen Stuart, M.A.; Sieval, A.B.; Zuilhof, H.; Sudhölter, E.J.R. *Thin Solid Films* **2003,** *426,* 135.
18. de Vos, W.M.; Biesheuvel, P.M.; de Keizer, A.; Kleijn, J.M.; Cohen Stuart, M.A. *Langmuir* **2008,** *24,* 6575.
19. Goldman, A.J.; Cox, R.G.; Brenner, H. *Chem. Eng. Sci.* **1967,** *22,* 653.
20. Shiratori, S.S.; Rubner, M.F. *Macromolecules* **2000,** *33,* 4213.
21. Kovačević, D.; van der Burgh, S.; De Keizer, A.; Cohen Stuart, M.A. *J. Phys. Chem. B* **2003,** *107,* 7998.

Chapter 11

General discussion: designing a polymer brush.

Introduction

Since de Gennes [1] introduced the term ‘brush’ for a dense layer of end-attached polymer chains on a surface, the understanding of this system has increased substantially. This is the result of many investigations over the past 30 years [2-9, this thesis], which have shown an especially strong correlation between experimental and theoretical work. Many properties of the polymer brush have been investigated. For example, it is now very well understood how the density profile of a polymer brush depends on its grafting density, on the polymer chain length, and on the interaction between polymer and solvent [2,3,9]. In addition, the effects of more exceptional properties of the system, such as extremely high grafting densities [10], strong attraction between polymer chains and the interface [11,12], and polydispersity [Chapter 8] have now been addressed. And last but not least, the effects of charge in the system is now well documented by experiments and theoretical modeling [9].

Many investigations have also focused on understanding the properties that make the polymer brush so suitable for applications. Thus, the brush has been studied for particle stabilization [14], for friction reduction [15], as a protein carrier [16, Chapter 6], and especially for its role as antifouling layer [2, 4, 8, Chapter 3]. Here we will focus on the latter two applications, in which the brush directly interacts with particles, since this is the principal theme of this thesis. Clearly, the interaction between a polymer brush and a particle is determined by more parameters than only the typical brush parameters that have been mentioned above. There is, for example, the particle size that plays a role, but also the interactions between the polymer chains and the particle, and the interactions between the particle and the surface are of importance. Overall, the effects of these parameters are now more or less understood due to the many experimental and theoretical investigations on brush-particle interactions [2, 8, 17, Chapters 4-7].

With the current insight in brushes as well as in brush-particle interactions, we argue that one can now relatively easily *design* a brush specifically for a direct application. In this general discussion we review how to proceed with such a design process for a system in which we want to prevent adsorption (antifouling) and, for the opposite case, a system in which we want to stimulate adsorption (protein carrier). In Chapter 1 (and references

therein) several good methods to produce polymer brushes have been described, including which brush parameters can or cannot be controlled in each of these preparation methods. In this chapter we therefore only discuss the optimal polymer brush for either antifouling or accumulation purposes, and not how such a brush should be produced.

Designing a brush for antifouling applications.

A polymer brush can act as a barrier for particles (fouling materials) to reach an interface and adsorb there [2, 4, 8]. This barrier action stems from the very high excluded volume inside a polymer brush. Penetration of the brush by a particle leads to a deformation of the brush and thus to a local increase in the osmotic pressure which will force the particle out of the brush and restore the brush equilibrium. It is important to realize that the particles cannot only adsorb to the solid surface, but they might also adsorb in or on the outside of the polymer brush. In Figure 1 we show these three possible ways in which particles can accumulate at a surface containing a polymer brush [2]. Primary adsorption implies that a particle penetrates the polymer brush to adsorb to the solid surface (the substrate or grafting surface). Secondary adsorption denotes that the particle adsorbs on top of the polymer brush, while in ternary adsorption the particle also adsorbs to the polymer chains, but now inside the brush.

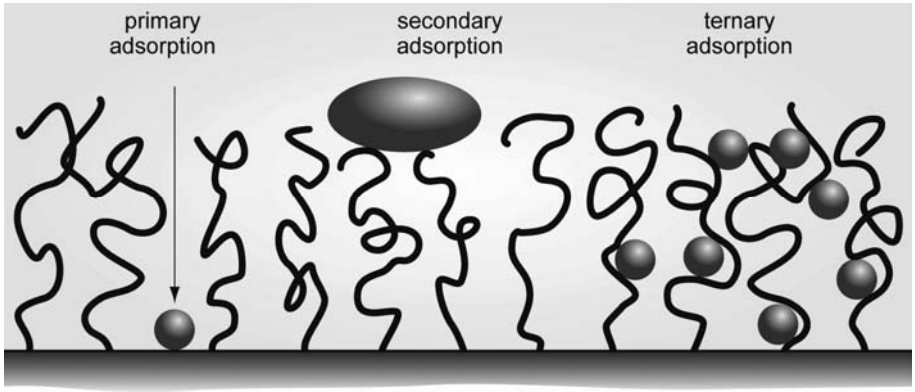

Figure 1. Schematic depiction of the three different modes of particle adsorption to a polymer brush. Figure adapted from Currie et al [2].

In case particles are attracted to the polymer chains, the polymer brush could thus also be a part of the problem. Especially as a polymer brush strongly increases the surface area to which particles can attach, covering a surface with a polymer brush could actually lead to a strong increase in the adsorption [16, 18, Chapter 6]. This is of course only the case if the

affinity between polymer chain and particle is large enough to give a net attraction. This immediately shows that when designing a polymer brush for antifouling purposes, the most important choice is the chemistry of the polymer chains that form the brush. It is essential that these chains have no attractive interaction with the fouling particles. For example, PEO brushes are amply used brushes to prevent the adsorption of proteins to an interface [2, 4], but these same brushes allow for very high adsorbed amounts of silica particles to an interface [18] and would thus be completely unsuitable as antifouling agents against these particles.

Obviously, it is very difficult to find a polymer that has no interaction with any of the fouling particles if the brush is used to protect against a mixture of fouling materials. This is the case when using brushes for applications in for example biological systems (e.g. blood, milk), or waste water treatment. Therefore, we will discuss the design parameters of the brush not only for the scenario that the particles have no affinity for the polymer chains, but also for the scenario that particles do have this affinity.

In the case that there is no affinity between the fouling particles and the polymer chains in the brush, the most important mode of adsorption is primary adsorption. The brush must thus be designed to prevent the particle from reaching the interface. The main tuning parameter is then the grafting density with respect to the size of the particle. Ideally, the grafting density should be so high that the smallest contour of the particle is larger than the distance between two grafted chains. Beyond that density, the particle will have to compress the polymer chains to get close to the grafting surface, and it will have to deform the brush substantially to adsorb to it. This is so unfavorable that primary adsorption is strongly reduced. If, because of the production method one is using, it is not possible to reach this grafting density, the polydispersity of the brush chains also becomes a factor. Increasing the polydispersity lowers the energy barrier for the particle to reach the interface [Chapter 9], and thus the polydispersity should be as low as possible.

Without adsorption of particles to the polymers that form the brush, it is still possible that the particles will accumulate in or on top of the brush because of long range attraction to the substrate. For example, this could be an electrostatic attraction, or (for large particles) van der Waals interaction. In this case the polymer brush, apart from being dense, also needs to reach so far into the solution that at its edge this attraction is strongly reduced. Consequently, the height of the brush, which is for a large part determined by the polymer chain length, is then an important parameter. For example, bacteria could not be repelled from a glass surface by a short dense PEO brush (N = 12, σ = 2.3 nm^{-2}), but a longer and sparser polymer brush (N = 222, σ = 0.2 nm^{-2}) reduced the adsorption significantly [19], a result attributed to van der Waals forces between the bacteria and the substrate.

Hence in order to prevent fouling when there is no affinity between the fouling material and the polymer chains, the brush needs to be dense enough to prevent primary adsorption and thick (high) enough to suppress long range interactions. A low polydispersity is favorable for achieving the high density. For the case that the fouling particles can also adsorb to the polymer chains, these same design rules hold as primary adsorption still needs to be prevented. In addition, the best way to reduce ternary adsorption (adsorption in the brush) is by increasing the grafting density. For ternary adsorption there is a balance between the energy gained by adsorption and the energy lost due to the high excluded volume in the brush. By increasing the brush density the particles can be "pushed out of the brush". A low polydispersity enhances this effect. Hence, for high enough grafting densities, fouling particles will be unable to adsorb in the brush and will only attach to the edge of the brush were the polymer density is low. How high the grafting density must be, depends again on the size of the object, but also on the affinity between particle and polymer chains.

This leaves us with the adsorption of fouling agents on top of the polymer brush (secondary adsorption) as a result of attraction between particle and polymer. This mode of adsorption is almost impossible to prevent. We illustrate this by showing the interaction between a large particle and a polymer brush for different grafting densities in Figure 2. Here a negative free energy of interaction (ΔF) denotes attraction.

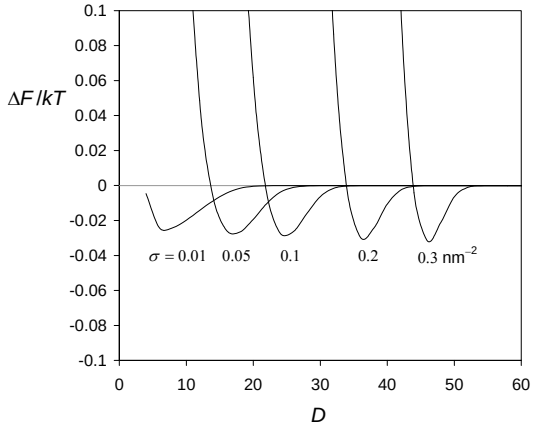

Figure 2. Free energy of interaction (ΔF) per amount of surface area between a polymer brush (number of segments per chain N = 100) and a large particle (radius R = ∞) as a function of distance from the grafting interface (D) for different grafting densities as indicated. As calculated by 2-gradient numerical SCF theory (Flory-Huggings parameter for particle-brush interaction $\chi_P = -1$, for brush-solvent interaction $\chi = 0.5$). See Chapter 9 for more information.

As shown in Figure 2, we find attraction (negative ΔF) between brush and particle for a broad range of grafting densities. The minimum in the free energy per lattice site is only small (~0.03 kT) but for large particles (> 1 um^2) the adhesive energy would be tens of kTs. The grafting density, which is so important to reduce primary and ternary adsorption, has hardly any effect on the attraction between a polymer brush and a large particle (and thus on the secondary adsorption). An even more interesting finding is that the small effect that we do find is opposite to the effect of the grafting density on the primary and ternary adsorption. For secondary adsorption, a higher grafting density leads to a (slightly) more negative ΔF and thus to a somewhat stronger adsorption. This is because the most favorable position of the particle is at the edge of the (undisturbed) brush, as this is the location for which no energy is used to compress or stretch the brush chains. A higher grafting density leads to a higher polymer density at the edge of the brush and hence to slightly stronger attraction. Other brush parameters such as the chain length will also not counteract this secondary adsorption, although a more polydisperse polymer brush is predicted to give less attraction than a corresponding monodisperse brush [Chapter 9].

So, although secondary adsorption cannot be prevented, one can try to keep it as low as possible. For a particle that is very large with respect to the grafting density, the best way to do this is to lower the grafting density as much as possible. In addition, one should use a brush as polydisperse as possible. For a small particle these adjustments are however counterproductive as they would lead, as argued, to less secondary adsorption, but they would also promote primary and ternary adsorption.

Dealing with secondary adsorption

In the previous section we argued that, if the fouling agent is significantly attracted to the polymer chains in the brush, secondary adsorption cannot be prevented. Here we propose to combine polymer brushes with systems designed for cleaning to tackle this problem. The polymer brush could for example work very well together with surfactants. In Chapter 5 we showed that the combination of an anionic surfactant and a PEO polymer brush could prevent attractive interaction between the brush and a silica particle. We propose that a more universal approach would be the combination of a PEO brush with a nonionic surfactant. Such nonionic surfactants, especially the ones whose hydrophilic parts also consist of EO groups, are well known to be able to desorb adsorbed PEO chains from solid interfaces (by competitive adsorption, if the polymer chain is not too long [20]. For a system with large particles and a surface covered with a PEO polymer brush the only possible interaction with the interface would be with PEO, exactly the interaction that we

know can be broken by nonionic surfactants. As such, this system would have the potential to suppress fouling by any particle.

Another interesting solution would be to produce polymer brushes that can also act as sacrificial layers [Chapter 10]. If the brush gets fouled because of secondary adsorption, it could simply be removed (sacrificed) to get rid of the fouling, after which a new brush layer can be produced. An especially promising system for this is the zipper brush system as proposed in Chapter 3. With the zipper brush approach, dense brushes can be made by adsorption and these can also be removed by applying a trigger such as a change in the pH.

Designing a brush as a protein carrier

Polyelectrolyte brushes are now being investigated for applications as protein carriers [15, Chapters 6,7]. In line with the previous section, we discuss here how we believe that such a brush should be designed. The ideal protein carrier has a large capacity to store proteins, releases the protein molecules upon a simple trigger such as a change in pH or salt concentration, and is completely stable at the pH at which it is used. Such carriers have already been realized by coating colloidal particles with a polyelectrolyte brush [15], so-called spherical polyelectrolyte brushes (SPBs). The polyelectrolyte properties are necessary to ensure that the attraction between the brush chains and the protein is large enough to overcome the high excluded volume interactions in the brush. The amount of protein that can adsorb depends strongly on the amount of polymer in the brush. In Chapter 6 we found that over a range of grafting densities (0.05 nm^{-2} to 0.3 nm^{-2}) the amount of protein adsorption keeps increasing, although this trend will undoubtedly stop somewhere at a higher grafting density. The adsorbed amount increases linearly with the chain length, and this makes the chain length the ideal tuning parameter for the amount of adsorbed protein.

The weakness of the current generation of SPBs is that the particles loose their colloidal stability when oppositely charged proteins adsorb to the brush. The oppositely charged proteins neutralize the charge in the brush to a large extent, thus creating an almost neutral particle. Without the charge which gave the stabilization the particles aggregate. However, proteins are also found to adsorb to like-charged polymer brushes (at the wrong side of the iso-electric point of the protein). In that case the adsorption does not lead to neutralization of the polyelectrolyte brush, and the particle dispersion remains stable. As adsorption above the iso-electric point is only found a few (about 1.5) pH units above the iso-electric point [Chapter 6], the pH range in which the particles are stable and also carry proteins is severely limited. To some extent one could widen this pH range by choosing a polyelectrolyte that has some (chemical) affinity to the protein. However, to strongly

increase the pH range in which they can be applied we suggest to incorporate an extra built-in stabilization mechanism into the "next generation" of SPBs protein carriers. One way would be to graft diblock copolymers on the particle. Such diblock copolymers should consist of a polyelectrolyte part for the storage of the proteins, and a neutral polymer (such as PEO) for the particle stabilization. This idea is schematically shown in Figure 3.

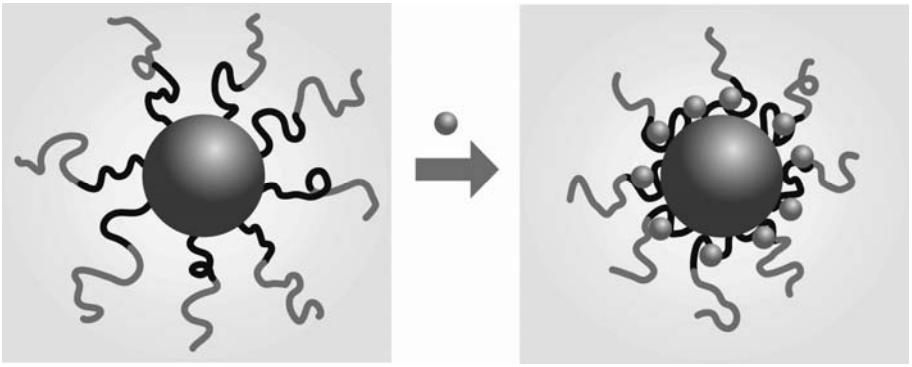

Figure 3. Schematic depiction of a particle covered with a brush consisting of a polyelectrolyte block (dark line) and a neutral (water soluble) polymer block (grey line). Upon the addition of oppositely charged protein molecules (grey spheres), the polyelectrolyte block complexes with the protein, forming a net neutral phase. The neutral polymer block stabilizes this particle.

Summary

In this chapter we have discussed design parameters for polymer brushes, both for antifouling applications and for applications as protein carriers. For antifouling purposes, it is very important that the fouling agents do not adsorb on the polymer chains. Thus, the choice of polymer is extremely important. If there is no such adsorption, the design of the brush is quite straightforward: the grafting density of the brush must be high enough that fouling particles cannot reach the surface, while the height of the brush, mostly determined by the polymer chain length, must be large enough to screen long distance interactions with the substrate. A low polydispersity helps in preventing the fouling agents to reach the surface.

In the case that some fouling materials can adsorb to the polymer chains, the design parameters depend strongly on the size of the fouling particles with respect to the grafting density. Small particles might be able to adsorb to polymer chains in the brush, so called ternary adsorption. A high grafting density is necessary to prevent this mode of adsorption. The adsorption of particles at the edge of the brush, so called secondary adsorption, cannot be prevented. For large particles (significantly larger than the distance between two grafted chains), however, secondary adsorption can be suppressed somewhat. Here a low grafting density and a high polydispersity are desirable. In addition, as secondary adsorption cannot be prevented by changing the properties of the brush, we suggest that the brush could be combined with surfactants or with a sacrificial layer approach to allow for removal of the particles adsorbed on top of the protective brush.

For applications as a protein carrier, the brush polymer is preferably a polyelectrolyte for the adsorption to be strong enough to overcome excluded volume interactions, and allow for large adsorbed amounts. The polymer chain length should be as high as possible, to allow for the highest adsorbed amounts. We propose that neutral polymer chains, connected to the ends of the polyelectrolyte chains could stabilize brush coated particles that complex with oppositely charged proteins.

References

1. de Gennes, P.G. *Scaling Concepts in Polymer Physics* **1979**, Cornell University Press, Ithica, N.Y.
2. Currie, E.P.K.; Norde, W.; Cohen Stuart, M.A. *Adv. Colloid Interface Sci.***2003,** *100-102,* 205.
3. Milner, S.T. *Science* **1991**, 251, 905.
4. Halperin, A.; Leckband, D.E. *C. R. Acad. Sci. Paris* **2000,** serie IV,1171.
5. Zhao, B.; Brittain, W.*J. Prog. Polym. Sci.* **2000,** *25,* 677.
6. Advincula, R.C.; Brittain, W.J.; Caster, K.C.; Rühe, J. *Polymer Brushes,* **2004,** Wiley-VHC, Weinheim.
7. Szleifer, I.; Carignano, M.A. *Advances in chemical physics, volume XCIV* **1996,** 165.
8. Halperin, A. *Langmuir* **1999,** *15,* 2525.
9. Birschtein, T.M.; Amoskov, V.M. *Polymer Science Ser. C* **2000,** *42,* 172.
10. Rühe, J.; Ballauff, M.; Biesalski, M.; Dziezok, P.; Gröhn, F.; Johannsmann, D.; Houbenov, N.; Hugenberg, N.; Konradi, R.; Minko, S.; Motornov, M.; Netz, R.R.; Schmidt, M.; Seidel, C.; Stamm, M.; Stephan, T.; Usov, D.; Zhang, H. *Adv. Polym. Sci.* **2004,** *165,* 79.
11. Tsujii, Y.; Ohno, K.; Yamamoto, S.; Goto, A.; Fukuda, T. *Adv. polym. Sci.* **2006,** *197,* 1.
12. Chakrabarti, A. *J. Chem. Phys.* **1994,** *100,* 631.
13. Szleifer, I. *Biophysical J.* **1997**, *72,* 595.
14. Napper, D.H. *Polymeric stabilisation of colloidal particles* **1983**, Academic press, London.
15. Klein, J. *Annu. Rev. Mater. Sci.* **1996,** *26,* 581.
16. Wittemann, A.; Ballauff, M. *Phys. Chem. Chem. Phys.* **2006,** *8,* 5269.
17. Steels, B.M.; Koska, J.; Haynes, C.A. *Journal of chromatography B* **2000,** *743,* 41.
18. Gage, R.A.; Currie, E.P.K.; Cohen Stuart, M.A. *Macromolecules* **2001,** *34,* 5078.
19. Roosjen, A.; van der Mei, H.C.; Busscher, H.J.; Norde, W. *Langmuir* **2004,** *20,* 10949.
20. Postmus, B.R.; Leermakers, F.A.M.; Koopal, L.K.; Cohen Stuart M. A. *Langmuir* **2007**, *23,* 5532.

Summary

This thesis presents a broad study on the topic of polymer brushes with an emphasis on the interaction between *brushes and particles*. Polymer brushes are dense layers of polymer chains end-attached to an interface that stretch out into the surrounding solution. An important application of these brushes is to protect an interface from unwanted adsorption (antifouling). Because of their high excluded volume, brushes can act as a barriers that prevent fouling particles from reaching the interface. Other applications for the polymer brush include the stabilization of particles in solution, the decrease of friction between two interfaces, and the uptake (immobilization) of enzymes. This thesis can be divided into four parts. In Part 1, we investigate the production of polymer brushes, while in Part 2, the most central part of this thesis, we investigate the interaction between polymer brushes and particles, directly connected to the applications antifouling and protein immobilization. Part 3 investigates the effects on the structure and the antifouling properties of a polymer brush when not all chains in the brush are of the same chain length (polydispersity). In Part 4, an alternative to the polymer brush is suggested to be used for antifouling applications. We will now describe these four parts in more detail.

Part 1 of the thesis (Making Brushes: C*hapters 2 and 3*) focuses on two different techniques to produce polymer brushes. The first technique (C*hapter 2*) is a method to produce poly(ethylene oxide) (PEO) brushes by Langmuir-Blodgett (LB) transfer. A monolayer of a diblock copolymer consisting of polystyrene (PS) and PEO is spread on the water surface to form a PEO brush at the air-water interface. Here the hydrophobic PS block acts as an anchor block, keeping the PEO chains attached to the air-water interface. The grafting density of the formed PEO brush is completely controlled by tuning the size of the interface. By then dipping a polystyrene surface through the air-water interface, the PEO brush is transferred to the polystyrene surface, strongly attached by the hydrophobic interaction between the PS surface and the PS block. Over the years this technique has been used to produce PEO brushes in seven different studies. In all of these investigations, it was assumed that the transfer ratio upon LB dipping equals unity, thus the grafting density on the solid substrate is the same as the grafting density at the air-water interface. In our investigation we find that this assumption is not valid. By ellipsometry we find that for PS_{36}-PEO_{148}, PS_{36}-PEO_{370}, and PS_{38}-PEO_{770} the transfer ratios are respectively 94%, 57% and 19%. Thus, the longer the PEO chain the lower the transfer ratio. We attribute this reduced transfer ratio to a competition for the PS surface between the PEO block and the PS block. We shortly review the papers in which this technique was previously used and discuss their main results in the light of this new information. Furthermore, we show that

by using Langmuir-Schaeffer (horizontal) dipping, much higher mass transfers can be reached than with the LB method.

In *Chapter 3*, we present a new method to produce polymer brushes called the zipper brush approach. By adsorbing a diblock copolymer with one charged block and one neutral block to an oppositely charged polyelectrolyte brush, a neutral polymer brush is formed on top of an almost neutral layer of complexed polyelectrolytes. This neutral brush can be adsorbed in minutes and desorbed in seconds to restore the original polyelectrolyte brush. These characteristics are shown by fixed-angle optical reflectometry for the system of poly(N-methyl-2-vinyl pyridinium)-block-poly(ethylene oxide) (P2MVP-PEO) adsorbed to a poly(acrylic acid) (PAA) brush. After the diblock copolymer has adsorbed (at pH 6), the charges of the PAA brush are almost completely compensated by the charges of the P2MVP block. A nice feature of the zipper brush is that the grafting density of the formed neutral brush can be controlled by the chain length and grafting density of the PAA brush, and by the chain length of P2MVP block. As the P2MVP blocks used in this study are much smaller than the PAA chains in the brush, the grafting density of the PEO brushes are found to be a multiplication of that of the PAA brush, and much higher grafting densities (up to 1.59 chains per nm^2) can be obtained than have previously been reported for polymer brushes prepared by adsorption. We show that by using a diblock copolymer with a different chemistry (poly(N,N-dimethyl amino ethyl methacrylate-PEO) (PDMAEMA-PEO)), we can change the conditions (pH, salt) at which the diblock copolymer adsorbs or desorbs. With diblock copolymers with a chemically different water-soluble neutral chain, in principle all kind of different neutral brushes can be prepared.

Part 2 of this thesis (Brushes and Particles: *Chapters 4 to 7*) focuses on the central theme: the interaction between brushes and particles. *Chapter 4*, in which we present a simple model to describe particle adsorption in a polymer brush, acts as an introductory chapter to this part. The presented box-model combines a simple free energy description of a monodisperse brush, with a Langmuir-type model to describe adsorption of particles. When there is no attraction between the particles and the polymer chains that form the brush, the brush acts as a barrier for the particles to reach the grafting interface. For the situation that there is an attraction between brush chains and the particle: they are found to adsorb. A maximum in the adsorbed amount is then predicted as a function of grafting density, while this amount is predicted to be linearly dependent on the chain length. These model predictions are in full agreement with the results of experiments and more sophisticated models.

In *Chapter 5* we investigate the adsorption of the anionic surfactants sodium dodecyl sulphate (SDS) and sodium dodecyl benzene sulphonate (SDBS) in poly(ethylene oxide)

(PEO) brushes. We show that just as in solution there is a critical association concentration (CAC) for the surfactants at which adsorption in the PEO brush starts. At low brush density the adsorption per PEO monomer is equal to the adsorption of these surfactants in bulk solution. However, with increasing brush density the number of adsorbed surfactant molecules per PEO monomer decreases rapidly. This decrease is explained in terms of excluded volume interactions plus electrostatic repulsion between the negatively charged surfactant micelles. Experimentally, a plateau value in the total adsorption is observed as a function of grafting density. Quantitative agreement was found with the results of an analytical self-consistent field (aSCF) model. Both experiments and model calculations show that the adsorption scales directly with the polymerization degree of the polymers in the brush. They also show that an increase in the ionic strength leads to an increase in the adsorbed amount, which is explained as being due to a decrease in the electrostatic penalty for the adsorption of the SDS micelles. The adsorption of SDS micelles changes the interactions of the PEO brush with a silica particle. This is illustrated by atomic force microscopy (AFM) measurements of the pull-off force of a silica particle from a PEO brush: at high enough PEO densities, the addition of SDS leads to a very strong reduction in the force necessary to detach the colloidal silica particle from the PEO brush. We attribute this effect to the large amount of negative charge incorporated in the PEO brush because of SDS adsorption.

In *Chapters 6 and 7*, the interaction between a polyelectrolyte brush and protein molecules is studied. We focus on the interesting experimental finding that a net negatively charged protein can adsorb to a negatively charged polyelectrolyte brush. At the moment two competing explanations exist for this phenomenon called adsorption on the “wrong” side of the iso-electric point (IEP) of the protein. One explanation is based on charge regulation. The idea is that a protein can reverse its charge when it is in the presence of the high electrostatic potential of the brush and then can be inserted. The other explanation relies on the charge anisotropy (patchiness) of proteins, that is, that the molecules carry positively charged and negatively charged patches. The positively charged patches gain more energy from interacting with the negative brush than the negative charged patches loose, especially when the charge densities and electrostatic potentials are high, thus providing a net attraction.

In *Chapter 6*, we investigate one specific system: the adsorption of bovine serum albumin (BSA) in a planar poly(acrylic acid) (PAA) brush layer. The investigation is performed using fixed-angle optical reflectometry. The influence of polymer length, grafting density, and salt concentration is studied as a function of pH. The results are compared with predictions of an analytical polyelectrolyte brush model, which incorporates

charge regulation and excluded volume interactions. A maximum in adsorption is found near the IEP of the protein. At the maximum, BSA accumulates in a PAA brush to at least 30 volume percent. Substantial adsorption indeed continues above the IEP, up to a critical pH value. This critical pH value decreases with increasing ionic strength. The adsorbed amount increases strongly with both increasing PAA chain length and increasing grafting density. Experimental data compare well with the analytical model without having to include a non-homogeneous charge distribution on the protein surface. Specifically for this protein, we conclude that charge regulation is the main driving force for adsorption above the IEP, and that the effect of patchiness is less important.

In *Chapter 7*, we take a more general approach to the discussion on which is the main driving force for adsorption above the IEP: charge regulation or patchiness. We present a model in which both effects are included. We confirm that both charge anisotropy and charge regulation can be responsible for protein uptake at the "wrong" side of the iso-electric point (IEP) and conclude that the respective effects are additive. Indeed, taking both effects into account results in a stronger attraction between a PE brush and a protein at the IEP, and the attraction is found further above the IEP than the individual effects would have made possible. As both effects are based on properties typical for proteins, we argue that for most proteins both effects will contribute to the adsorption of proteins in like-charged polyelectrolyte brushes. Still, for a protein that does not contain highly charged patches, like BSA (at relevant pH), we expect that charge regulation is the dominant effect.

Part 3 of this thesis (Brushes and Polydispersity, *Chapters 8 and 9*) treats the effect of polydispersity on the structure of the brush and on brush-particle interactions using numerical self-consistent field theory. For the polydispersity, we consider the relevant case of a Schulz-Zimm distribution. On the structure (*Chapter 8*), we find that even a small degree of polydispersity completely destroys the parabolic density profile. The first moment (average height) of the brush increases with polydispersity, while the average stretching in the brush decreases. The density profiles of separate chain length fractions in a single polydisperse brush are also strongly influenced by polydispersity. Short chains are found to be compressed close to the grafting interface, whereas longer chains have a characteristic flowerlike distribution. These longer chains stretch strongly (stem) when surrounded by smaller chains and decrease their stretching (crown) when only surrounded by longer chains. In line with approximate analytical models, our numerical results show that the polymer chains in the brush have localized end-point positions (no fluctuations) in strong contrast to the anomalously large fluctuations in the end-point positions of the homodisperse brush. Despite these effects, the scaling of the average height with grafting density and number average chain length is unaffected by polydispersity.

In *Chapter 9*, we investigate the effect of polydispersity on the (anti)fouling properties of a neutral polymer brush. We consider the interaction between a single particle and a polydisperse brush with grafting density σ. The larger the polydispersity, the easier it is for a small particle (with radius $R \sim 1/(2\sqrt{\sigma})$) to penetrate the brush. Hence, the monodisperse brush is better suited to protect a surface against adsorption of small particles compared to a corresponding polydisperse brush. The brush grafting density, however, remains the most important parameter for tuning the antifouling properties of the brush against small particles. For large particles (modeled as a flat wall) an opposite effect of polydispersity is found: it is harder to compress a polydisperse brush than a corresponding monodisperse brush and thus a polydisperse brush is better suited to protect the surface against adsorption of large particles. A complementary approach, based on the stacking of Alexander-de Gennes boxes, is used to study the adsorption of many particles into a polydisperse brush. Consistent with the single-particle data generated by the self-consistent field theory, for weak attraction between the particles and the brush the absolute adsorbed amount remains low, but increases strongly as a function of polydispersity (from $M_w/M_n = 1$ to 2 by a factor of 2-4). Obviously, at higher attraction between the particles and the brush the adsorption increases, but a weak dependence on polydispersity is observed.

In **Part 4** of this thesis (Sacrificial Layers, *Chapter 10*), we propose a new approach for the removal of fouling agents from an interface. The interface is pre-coated with a polymer layer of a few nanometers thick which can be removed by a simple trigger such as a change in pH or salt concentration. When fouling agents adsorb onto the interface, they can be removed by simply desorbing (sacrificing) the polymer coating. We show a proof of principle of this concept by investigating two different types of sacrificial layers. The first system consists of a silica interface that is pre-coated with a polyelectrolyte multilayer consisting of poly(allyl amine) hydrochloride (PAH) and poly(acrylic acid) PAA. The top layer of the polyelectrolyte multilayer is the positively charged PAH and on top of that silica particles are adsorbed. We investigate the release of silica particles resulting from a pH drop (leading to desorption of the multilayer), as a function of the number of polyelectrolyte layers in the multilayer. Four layers are already enough to significantly enhance the desorption of the silica particles (70% removal). With fourteen layers (total adsorbed amount of polymer approximately 6 mg/m^2) the silica particles are completely removed.

The second system consists of a weak poly(acrylic acid) brush (PAA), coated with an extra layer of PAA (the PAA chains are connected to a small polystyrene (PS) block). At low pH the polyelectrolytes are uncharged, and the double polyelectrolyte layer is stable. However, when the pH is increased, the polyelectrolytes become charged and the extra

layer is removed, including any attached fouling material. For this system we show proof of principle of the sacrificial layer approach by measuring the hydrodynamic force, necessary to remove PS particles (radius 3 μm) from a PAA brush. We show that the hydrodynamic force for removal is two orders of magnitude lower for the sacrificial layer system (PAA brush plus extra layer of PS-PAA), than for the PAA brush alone.

The results in this thesis provide insight in properties of polymer brushes in relation to their interaction with particles. This contributes to the rational design of polymer brushes for specific applications, as elaborated in the *general discussion.*

Samenvatting

Het centrale thema in dit proefschrift is de zogenaamde polymeerborstel in water. Zoals de naam al zegt, is dit systeem opgebouwd uit polymeren, zeer lange moleculen die bestaan uit veel meestal identieke korte schakels. Om van die polymeren nu een polymeerborstel te maken, moet men de polymeren aan een van hun uiteinden vast maken op een oppervlak, en wel zo dat de polymeren dicht tegen elkaar aan zitten. In Figuur 1a laten we in een cartoon zien wat er gebeurt als de polymeren niet dicht genoeg tegen elkaar aan zitten. In dat geval hebben de polymeren geen contact met elkaar (ze voelen elkaar niet) en daarom vormen ze een zogenaamde polymeerkluwen, een ijle structuur gedomineerd door de willekeurige bewegingen van het polymeer. Wanneer we echter de polymeerketens veel dichter bij elkaar plaatsen, zoals in Figuur 1b, dan beginnen de polymeren elkaar in de weg te zitten. Door de drukte zoekt het polymeer de ruimte om weer zoveel mogelijk vrij te kunnen bewegen. De enige plaats waar die ruimte te vinden is omhoog, weg van het oppervlakte. Een polymeerborstel is dus een systeem waarbij polymeren die vastgezet zijn aan een oppervlakte, elkaar zoveel in de weg zitten dat de polymeren wel moeten strekken.

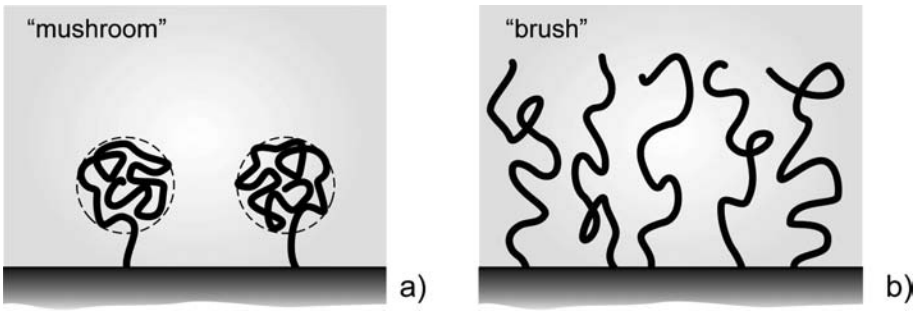

Figuur 1. Een schematische voorstelling van a) polymeren die ver van elkaar op een oppervlakte vast zijn gezet b) een polymeerborstel.

De belangrijkste toepassing van polymeerborstels is dat ze een oppervlak kunnen beschermen tegen vervuiling. Dit heeft heel veel te maken met de reden dat de polymeerketens in de borstels strekken: doordat het zo druk is in de borstel. Een deeltje dat in de borstel wil komen, moet ruimte maken voor zichzelf door de polymeren aan de kant te duwen. Hierdoor worden de polymeren dan weer nog dichter op elkaar gedrukt, dit is ongunstig en leid tot een tegenkracht: de polymeren duwen het deeltje de borstel weer uit, waardoor het oppervlakte schoon blijft.

De eerste uitdaging is dan natuurlijk om polymeerborstels te maken. In **Deel 1** van dit proefschrift bekijken we twee verschillende manieren dit te doen. In *Hoofdstuk 2* onderzoeken we een al bestaande methode om borstels te maken. In deze methode maakt men de polymeerborstel eerst op een water oppervlak alvorens het over te brengen op een vast oppervlak (zie hoofdstuk 1, plaatje 3d). Het voordeel hiervan is dat doordat men het wateroppervlak makkelijk groter en kleiner kan maken, men heel nauwkeurig kan bepalen hoe dicht de polymeren tegen elkaar aan zitten alvorens de borstel over te brengen op het vaste oppervlak. Wij vinden echter dat gedurende de overdracht van het water oppervlakte naar het vaste oppervlakte er een gedeelte van de polymeren verdwijnen. Dit was nog niet bekend van deze methode en werpt een heel nieuw licht op de resultaten van eerder werk waarbij de borstels volgens deze methode werden geproduceerd.

In *Hoofdstuk 3* beschrijven we een nieuwe manier om polymeerborstels te maken. In deze methode beginnen we met een oppervlak met daarop al een polymeer borstel. Speciaal aan deze borstel is echter dat hij geladen is. Deze geladen borstel brengen we dan in contact met een polymeer dat uit twee delen bestaat, een niet elektrisch geladen gedeelte en een gedeelte dat tegengesteld geladen is aan de polymeren in de borstel. Doordat polymeren met een tegengestelde elektrische lading elkaar sterk aantrekken, zullen ze complexeren. Het niet complexerende, ongeladen deel van het dubbele polymeer vormt dan een nieuwe ongeladen polymeerborstel bovenop een dichte laag van de gecomplexeerde geladen polymeren (zie hoofdstuk 3, figuur 1). Het voordeel van deze methode is, dat op een relatief simpele manier hele dichte ongeladen polymeerborstels gemaakt kunnen worden.

In **Deel 2** onderzoeken we de interactie tussen polymeerborstels en deeltjes. Eerder in dit hoofdstuk beschreven we al dat polymeerborstels vaak gebruikt worden om vuildeeltjes weg te houden van een oppervlakte. Echter de mogelijkheid bestaat ook dat als een deeltje sterk genoeg tot de polymeren in de borstel wordt aangetrokken dat een deeltje toch aan die polymeren kan plakken (adsorberen). In *hoofdstuk 4* wordt een simpel model beschreven om die adsorptie van deeltjes in de borstel te onderzoeken. Onderzocht wordt bijvoorbeeld hoe de grootte van het deeltje en de attractie tussen het deeltje en de polymeren in de borstel, bepalen of het deeltje kan adsorberen in de borstel of juist wordt weggehouden.

In *Hoofdstukken 6 en 7* kijken we naar een geheel andere toepassing van de polymeerborstel. De borstel wordt niet onderzocht om deeltjes weg te houden van het oppervlak, maar juist graag om deeltjes (in dit geval eiwitten) op te slaan in de polymeerborstel (zie Hoofdstuk 1, Figuur 2d). Dit zou belangrijk kunnen zijn voor het stabiel houden van de eiwitten in oplossing. Het is mogelijk om eiwitten in een borstel op te slaan zolang het eiwit en de polymeerketens in de borstel elkaar sterk aantrekken. Hiervoor wordt weer een geladen polymeerborstel gebruikt. Zolang het eiwit en de borstel

tegengesteld geladen zijn dan zal het eiwit heel sterk plakken aan de geladen polymeren in de borstel. Maar, het is zelfs ook mogelijk dat eiwitten die in oplossing dezelfde lading hebben als de polymeerketens, en daarom juist afgestoten zouden moeten worden, toch kunnen plakken. Dit heeft te maken met de mogelijkheid die het eiwit heeft om zijn lading aan te passen, wanneer het eiwit in de buurt van de geladen polymeerborstel komt dan verandert hij zijn lading van gelijk naar tegengesteld geladen, waardoor toch attractie ontstaat.

In het **Deel 3** van dit proefschrift onderzoeken we een meer fundamentele vraag over de polymeerborstel: hoe gedraagt een polymeerborstel zich als niet alle polymeerketens even lang zijn. De vraag is relevant omdat eigenlijk in alle theoretische onderzoeken naar polymeerborstels men voor het gemak aanneemt dat alle polymeerketens even lang zijn. Dit terwijl in experimenteel onderzoek men eigenlijk altijd werkt met ketens die niet allemaal even lang zijn. Wij laten zien dat de verdeling van ketenlengten in een polymeerborstel (de zogenaamde polydispersiteit) wel degelijk invloed heeft op de eigenschappen van de borstel. In *Hoofdstuk 8* wordt de invloed van de polydispersiteit op de structuur van de borstel onderzocht en laten we zien dat de lange ketens anders gestrekt zijn dan de korte ketens (zie Hoofdstuk 8, Figuur 11). In *Hoofdstuk 9* wordt onderzocht hoe polydispersiteit de interactie met tussen borstels en deeltjes beïnvloed.

In **Deel 4** van het proefschrift wordt een alternatief voor de polymeer borstel voorgesteld om oppervlaktes schoon te houden. Het idee is als volgt: er wordt een dun laagje polymeer op een oppervlak aangebracht waarvan bekend is dat het laagje gemakkelijk verwijdert kan worden door te spoelen met bijvoorbeeld een zure oplossing, of een oplossing met veel zout erin. Op het moment dat het oppervlakte dan vies wordt, dan kunnen het makkelijk schoongemaakt worden door het polymeer laagje, inclusief het daarop plakkende vuil weg te spoelen. We noemen deze laagjes dat ook opofferings laagjes. In *Hoofdstuk 10* laten we voor twee verschillende systemen zien dat dit concept werkt.

In de *General discussion* wordt tenslotte ingegaan op de vraag hoe men het beste een polymeerborstel zou kunnen ontwerpen voor specifieke toepassingen zoals het beschermen van oppervlaktes en het opslaan van eiwitten.

Dankwoord

Beste lezer, laat ik u als eerste hartelijk danken. U heeft net de moeite genomen om dit boekje door te lezen (of misschien door te bladeren, of in elk geval open te slaan) en dat doet me goed, dit boekje dient gelezen (of opengeslagen) te worden. Hartelijk dank dus daarvoor. Maar u bent niet de enige die ik hier graag wil bedanken. Ik heb veel hulp gehad bij de totstandkoming van mijn proefschrift. Sommigen hielpen door actieve samenwerking, maar anderen ook puur door bijvoorbeeld het creëren van de gezellige sfeer op de leerstoelgroep, voor het zorgen voor voldoende afleiding buiten het werk om en vooral toch ook voor aanhoren van het vele geklaag (en de opschepperij) over mijn project. Een aantal van deze mensen wil ik nu graag bij naam noemen:

Arie en Mieke, wij overlegden bijna elk week over mijn project en die gesprekken heb ik altijd als heel nuttig en prettig ervaren. Vooral ook bij het schrijven van de artikelen en van dit boekje heb ik enorm veel aan jullie input gehad. Arie, jij functioneerde een beetje als de eerste drempel voor al mijn wilde ideeën, pas wanneer ik jou kon overtuigen dat het een goed plan was, dan ging ik er zelf ook in geloven. Mieke jij bent een tovenaar met woorden, soms wist je door in mijn tekst een paar woorden te verplaatsen of toe te voegen een hele alinea om te toveren van complex en onbegrijpelijk naar iets wat duidelijk en goed te lezen was. Beiden ontzettend bedankt voor de prettige samenwerking.

Martien, je bent een inspirerend persoon om mee samen te werken. Een halve zin en een slecht getekend grafiekje zijn voor jou altijd al voldoende om exact te weten over welk stukje onderzoek het gaat en waar de mogelijke kansen en oplossingen liggen. Door je drukke agenda was je niet altijd even direct bij mijn onderzoek betrokken maar vaak was jij het wel die bij de afronding van een stuk werk de laatste puzzelstukjes wist in te vullen.

Alle stukken theoretisch werk in dit proefschrift hebben alleen tot stand kunnen komen door mijn samenwerking met twee theoretici: Frans en Maarten. Frans, door jouw enorme kennis en creativiteit hebben we veel mooie resultaten geboekt en heb ik ontzettend veel geleerd. Jouw enorme enthousiasme maakte die samenwerking ook nog eens ontzettend leuk. Maarten, het was een mooi moment toen wij als kamergenoten erachter kwamen dat jij net een model had ontwikkeld wat de experimenten die ik net had uitgevoerd wel mooi zou kunnen beschrijven. Twee uur later waren de eerste plotjes al uitgerekend. Ik ben elke keer weer onder de indruk van de snelheid waarmee je werkt en het gemak waarmee je nieuwe concepten kunt oppikken en uitwerken.

Geert, ik vond het een eer om jouw MSc project te mogen begeleiden. Jouw mooie experimentele werk vormde de basis voor hoofdstuk 3.

I would like to thank Unilever Research & Development, Port Sunlight, for funding and supporting this work. Furthermore, I would like to thank Tony Mckee from Unilever R&D for the good contact over the years. I was extremely happy with the confidence and freedom that you entrusted me with during this project and also with the more practical input that you provided. I enjoyed working together.

Wouter bedankt voor de lessen in borstels maken en je zinnige commentaar op mijn tweede hoofdstuk. Gert, de prachtige figuren die je voor me gemaakt hebt maken het boekje helemaal af. Remco, bedankt voor alle hulp met de reflectometer. Ronald bedankt voor de computer en netwerk ondersteuning. Wim bedankt voor de hulp met de pH-stat titraties.

Ondanks de soms diepe dalen waar ook ik als AIO doorheen moest, is er toch nooit zelfs maar een moment geweest dat ik ‘s ochtends geen zin had om naar mijn werk te gaan. Dat komt simpelweg omdat Fysko veel meer is dan alleen het project waar je aan werkt. De gezelligheid tijdens de pauzes, de leuke discussies tijdens de werkbespreking en de leuke uitjes, borrels en feestjes hebben veel voor me betekend de afgelopen jaren. Daarvoor wil ik dan ook graag al mijn collega’s bedanken. Aernout, jij was een geweldig gezellige kamergenoot met wie je ook nog een goed gesprek kon voeren. Het was prachtig om af en toe stukjes mee te krijgen van de creatieve chaos die jouw brein is. Ilja, Bart, Bas en Diane, een borrelcommissie vol gezellige mensen was precies wat Fysko nodig had. Joris en Bas, bedankt voor de extreem efficiënte manier waarop we samen de AIO-reis naar Zweden en Denemarken georganiseerd hebben. Bas, ook nog bedankt voor je hulp als paranimf. Verder wil ik nog Pascal, Erika, Renate, Richard, Wout, Wouter, Henk, Marat, Yansen, Olga, Erwin, Petja, Astrid, Luben, Guido, Kathelijne, Yun, Paulina en Agatha bedanken voor de gezelligheid en de saamhorigheid die je alleen met je mede-AIO’s (en Postdocs) kunt hebben. Josie, Anita, Mara, Rhoda, Anneke en Bert, hartelijk dank voor het draaiende houden van de leerstoelgroep.

Maar ook al mijn vrienden en familieleden wil ik graag hartelijk danken voor de steun gedurende de afgelopen jaren. Geerten en Gijs, ik zal de ongedwongen en ongecompliceerde gezelligheid van ons huis missen. Yvonne, onze relatie hield geen stand, maar we hebben wel heel veel lol gehad samen. Bedankt ook voor je steun de eerste jaren van mijn promotietijd. Geachte jaarclubgenoten, bedankt voor de gezellige weekenden, verjaardagen en trouwerijen. Leden der H.M.I.D.H.D. de Zwevelpin, BRAND!!! Mijn nieuwe familieleden Teuntje, Peter, Simon en Corinne, bedankt voor de prettige opname in de familie. Jan, Ellinor, Eliza en Julia, bedankt dat jullie zo’n leuk en schattig gezinnetje vormen. Zus, ik ben je heel dankbaar dat je me op een voor mij zo bijzonder dag bij wilde staan als paranimf. Pap, bedankt voor je steun, zorgen en liefde, niet alleen gedurende de afgelopen jaren, maar al mijn hele leven lang.

Lieve Saskia, ik heb zwaar op jouw schouders gesteund de afgelopen twee jaar. Terwijl ik zeer vermoeid was zorgde je voor me, toen het wat beter ging hielp je me en zelfs terwijl jij ook druk bezig was met het afronden van je eigen boekje wist je nog de tijd te vinden om de layout van mijn leesversie te verzorgen. Wat de toekomst ons gaat brengen weet ik niet, maar ik weet wel het belangrijkste, dat we die toekomst samen zullen gaan beleven.

Wiebe

List of publications

This Thesis:

- De Vos, W.M.; de Keizer A.; Cohen Stuart M.A. and Kleijn J.M. *In preparation.* Thin polymer films as sacrificial layers for easier cleaning. (Chapter 10)
- De Vos, W.M.; de Keizer A.; Cohen Stuart M.A. and Kleijn J.M. *Submitted.* Zipper Brushes: Ultra dense brushes by adsorption. (Chapter 3)
- De Vos, W.M.; Leermakers F.A.M.; de Keizer A.; Cohen Stuart M.A. and Kleijn J.M. *Accepted in Langmuir*. Field theoretical analysis of driving forces for the uptake of proteins by like charged polyelectrolyte brushes: effects of charge regulation and patchiness. (Chapter 7)
- De Vos, W.M.; Biesheuvel, P.M.; de Keizer A.; Kleijn J.M. and Cohen Stuart M. A. *Accepted in Langmuir*. Adsorption of anionic surfactants in a non-ionic polymer brush: Experiments, comparison with mean-field theory and implications for brush-particle interaction. (Chapter 5)
- De Vos, W.M.; Leermakers F.A.M.; de Keizer A.; Kleijn J.M. and Cohen Stuart M. A. *Macromolecules* **2009**, *42*, 5881. Interaction of Particles with a Polydisperse Brush: A Self-Consistent Field Analysis. (Chapter 9)
- De Vos, W.M.; Kleijn J.M.; de Keizer A.; and Cohen Stuart M. A. *Angew. Chem. Int. Ed.* **2009**, *48*, 5369. Ultra dense polymer brushes by adsorption. (Chapter 3)
- De Vos, W.M.; de Keizer A.; Kleijn J.M. and Cohen Stuart M. A. *Langmuir* **2009**, *25*, 4490. The production of PEO polymer brushes via Langmuir-Blodgett and Langmuir-Schaeffer methods: incomplete transfer and its consequences. (Chapter 2)
- De Vos, W. M. and Leermakers F.A.M. *Polymer*, **2009**, *50*, 305. Modeling the structure of a polydisperse brush. (Chapter 8)
- De Vos, W.M.; Biesheuvel, P.M.; de Keizer, A.; Kleijn, J.M.; Cohen Stuart, M.A.; *Langmuir* **2008**, *24*, 6575. Adsorption of the protein bovine serum albumin in a planar poly(acrylic acid) brush layer as measured by optical reflectometry. (Chapter 6)

Other work:

- Biesheuvel, P.M.; de Vos, W.M.; Amoskov, V.M.; *Macromolecules* **2008,** *41*, 6254. Semianalytical continuum model for nondilute neutral and charged brushes including finite stretching.
- Voets, I.K.; de Vos, W.M.; Hofs, B, de Keizer A.; Cohen Stuart M.A.; Steitz R.; Lott D. *J. Phys. Chem. B.* **2008**, *112*, 6937. Internal structure of a thin film of mixed polymeric micelles on a solid/liquid interface.
- Cohen Stuart, M.A.; de Vos, W.M.; Leermakers, F.A.M. *Langmuir* **2006**, *22*, 1722. Why surfaces modified by flexible polymers often have a finite contact angle for good solvents.
- Yildirim Z.; Mendes E.; Picken S.J.; Paraschiv I.; Zuilhof H.; de Vos W.M.; Sudholter E.J.R.; Marcelis A.T.M. *Molecular crystals and liquid crystals* **2005**, 439, 2103. Binary phase diagram of triphenylene derivatives: The role of hydrogen bonds.
- Vermonden, T.; de Vos, W.M.; Marcelis, A.T.M.; Sudhölter E.J.R. *European Journal of Inorganic Chemistry* **2004**, *14*, 2847. 3-d water-soluble reversible neodymium(III) and lanthanum(III) coordination polymers.

Levensloop

Wiebe Matthijs de Vos werd op 22 maart van het jaar 1980 geboren te Amsterdam. Hij groeide op in nabijgelegen plaatsje Diemen en behaalde in 1998 zijn VWO diploma aan het Pieter Nieuwland College te Amsterdam. Vervolgens begon hij zijn studie Moleculaire Wetenschappen aan de Wageningen Universiteit. In het studiejaar 2001-2002 maakte Wiebe deel uit van het bestuur van studentenvereniging SSR-W als penningmeester vereniging. Vervolgens werkte hij bij de leerstoelgroep Organische Chemie aan zijn eerste afstudeervak, waarbij hij onderzoek deed aan wateroplosbare coördinatiepolymeren met Neodymium ionen. Tijdens zijn tweede afstudeervak deed hij bij de vakgroep Fysische chemie en kolloïdkunde onderzoek naar de adsorptie van polyelectroliet micellen, en de mogelijke vuilafstotende werking van de daardoor gevormde polymeerlaag. Voor zijn stage vertrok Wiebe naar Engeland alwaar hij bij het Unilever R&D laboratorium in Port Sunlight onderzoek deed bij de afdeling wasmiddelen. In oktober 2004 begon hij aan zijn promotieonderzoek bij de leerstoelgroep Fysische chemie en kolloïdkunde. Het werk beschreven in dit proefschrift is hiervan het resultaat.

Overview of completed training activities.

Courses

Molecular Modeling, Wageningen, 2005.

Physical Chemistry Winterschool, Han-sur-Lesse (Belgium), 2005.

RPK Polymer Physics, Utrecht, 2005.

Polyamphi Summer school, Chodova Plana (Czeck Republic), 2005.

Polyamphi Summer school, Biezenmortel, 2007.

Conferences and Colloquia

Autumn Meeting on Macroscopic Physical Chemistry, Schiermonnikoog, 2004.

Student Conference, Biezenmortel, 2005*.

Autumn Meeting on Macroscopic Physical Chemistry, Schiermonnikoog, 2005.

Dutch Polymer Days, Lunteren 2006.

Bunsen Colloquium, Bayreuth (Germany), 2006.

Dutch Polymer Days, Lunteren, 2007*.

Student Conference, Ven (Sweden), 2007*.

ECIS, Geneva (Switzerland), 2007^{+}.

Dutch Polymer Days, Lunteren, 2008*.

ECIS, Cracow (Poland) 2008*.

Dutch Polymer Days, Lunteren, 2009*.

Colloquium Laboratory of Biosensors and Bioelectronics, Zürich (Switserland), 2009*.

ICSCS, New York (USA), 2009*.

Gordon Research Conference, Waterville ME (USA), 2009^{+}.

*=oral contribution, $^{+}$= poster

Other meetings and activities

Writing project proposal, 2004.

Group meetings 2005-2009.

Group colloquia 2005-2009.

Excursion BASF, Ludwigshafen (Germany), 2006.

PhD-study trip Sweden and Denmark, 2007.

Cover Image: Concept by Teuntje Lindhoud. Photography by Saskia Lindhoud.

Graphics: Gert Buurman is acknowledged as the artist for the figures on page 3, 4, 6, 8, 38, 63, 137, 193, 195, 222, 225, 236, 241, and 251.

Printing: Ponsen en Looijen b.v., Ede